Comparative investigation of erythemal ultraviolet radiation in the tropics and mid-latitudes

A thesis submitted to the University of Manchester for the degree of Doctor of Philosophy
in the Faculty of Engineering and Physical Sciences

2010

SUMAMAN BUNTOUNG

SCHOOL OF EARTH, ATMOSPHERIC AND ENVIRONMENTAL SCIENCES

List of Contents

Word count: 43,427

List of Tables

List of Figures

List of Abbreviations

AAOD	Aerosol Absorption Optical Depth
AERONET	Aerosol Robotic Network
AI	Aerosol Index
AOD	Aerosol Optical Depth
ARF	Angular Response Function
ATLAS	Atmospheric Laboratory for Applications and Science
BCC	Basal Cell Carcinoma
CFC	Chlorofluorocarbon
CIE	Commission Internationale de l'Eclairage
CM	Cutaneous Melanoma
DISORT	Discrete Ordinate Radiative Transfer
DNA	Deoxyribonucleic Acid
DOAS	Differential Optical Absorption Spectroscopy
DU	Dobson Unit
EOS	Earth Observing System
FOV	Field of View
FWHM	Full Width at Half Maximum
GES DISC	Goddard Earth Sciences Data and Information Services Centre
GOME	Global Ozone Monitoring Experiment
HDF	Hierarchical Data Format
HPA	Health Protection Agency
LER	Lambertain Equivalent Reflectivity
MLER	Minimum Lambertian Equivalent Reflectivity
MODIS	Moderate Resolution Imaging Spectroradiometer
NASA	National Aeronautics and Space Administration
NIST	National Institute of Standards and Technology
NOAA	National Oceanic and Atmospheric Administration
OMAERO	OMI/Aura Multi-wavelength Aerosol Optical Depth
OMAERUV	OMI/Aura Near-UV Aerosol Optical Depth
OMAERUVd	Level-3 OMI Near-UV Aerosol Optical Depth
OMI	Ozone Monitoring Instrument
OMUVB	Level-2 OMI Surface UV irradiance and Erythemal Dose
OMUVBd	Level-3 OMI Surface UV irradiance and Erythemal Dose
PMT	Photomultiplier Tube
PSC	Polar Stratospheric Cloud
QA	Quality Assurance
QASUME	Quality Assurance of Solar UV Measurements in Europe
QC	Quality Control
SBUV	Solar Backscatter Ultraviolet
SCC	Squamous Cell Carcinoma
SSA	Single Scattering Albedo
TOMS	Total Ozone Mapping Spectrometer
UV	Ultraviolet

Abstract

Ultraviolet (UV) radiation has several effects on human health as well as other biological and chemical systems. The radiation can be weighted with the erythemal action spectrum and then converted to the dimensionless UV Index, which is designed to indicate the detrimental "*sunburning power*" of the radiation for public heath purposes. A global view of the erythemally weighted irradiance from the Ozone Monitoring Instrument (OMI) on board the Aura spacecraft has been available since July, 2004. However, ground-based validation and correction of the satellite data are still required. In this thesis, the erythemal dose rates at local solar noon taken from the satellite were compared to ground-based data measured by spectroradiometers or broadband radiometers in two different climate areas: the Tropics and midlatitudes. This seeks to redress the lack of data and satellite validation for the Tropics, and also allows comparison with previous work in midlatitudes. The validation results show that the satellite data overestimates the ground-based data by 9%-32% at the cleanest site, with a much higher discrepancy at polluted sites. Using a radiative transfer model confirmed that the positive bias in the satellite data was mainly caused by aerosol absorption that is not taken into account in the satellite retrieval algorithm. Therefore, two empirical methods were introduced in order to correct the OMI UV data for absorbing aerosols under clear sky conditions. These methods required aerosol optical depth and aerosol single scattering, or aerosol absorption optical depth, as input parameters. The methods improved the OMI UV data by up to 30% depending on site and input data source. For cloudy conditions aerosol data is usually not available either from ground-based or satellite-based measurements; however, the effect of cloud is usually far greater than that of aerosol, and some of the aerosol effect (scattering) is intrinsically included in the cloud correction. A further empirical model for cloudy conditions was derived to reduce bias of the OMI UV data with respect to ground-based data. The method only requires the OMI UV data as an input. The cloudy model reduced the bias by about 13%-30% depending on site, and gave similar results even when used with clear sky data. Since ground-based data is sparse, the final goal of the work was to produce a corrected map of UV index for the whole of Thailand, based only on data available from satellite, which gives full regional coverage. Issues with availability and quality of satellite data meant that the best results were achieved by using only the cloudy sky correction, for all conditions. The resulting daily noontime UV Index maps of Thailand were assessed against ground-based data for independent years. The corrected UV Index was within ±2 compared with ground-based data for all sites, compared to discrepancies of up to 4 UV Index for uncorrected data.

Declaration

that no portion of the work referred to in the thesis has been submitted in support of an application for another degree or qualification of this or any other university or other institute of learning.

Copyright

i. The author of this thesis (including any appendices and/or schedules to this thesis) owns certain copyright or related rights in it (the "Copyright") and s/he has given The University of Manchester certain rights to use such Copyright, including for administrative purposes.

ii. Copies of this thesis, either in full or in extracts and whether in hard or electronic copy, may be made **only** in accordance with the Copyright, Designs and Patents Act 1988 (as amended) and regulations issued under it or, where appropriate, in accordance with licensing agreements which the University has from time to time. This page must from part of any such copies made.

iii. The ownership of certain Copyright, patents, designs, trade marks and other intellectual property (the "Intellectual Property") and any reproductions of copyright works in the thesis, for example graphs and tables ("Reproductions"), which may be described in this thesis, may not be owned by the author and may be owned by third parties. Such Intellectual Property and Reproductions cannot and must not be made available for use without the prior written permission of the owner(s) of the relevant Intellectual property and/or Reproductions.

iv. Further information on the conditions under which disclosure, publication and commercialisation of this thesis, the Copyright and any Intellectual Property and/or Reproductions described in it may take place is available in the University IP Policy (see http://www.campus.manchester.ac.uk/medialibrary/policies/intellectual-property.pdf), in any relevant Thesis restriction declarations deposited in the University Library, The University Library's regulations (see http://www.manchester.ac.uk/library/aboutus/regulations) and in The University's policy on presentation of Theses.

Acknowledgements

First and foremost I would acknowledge my supervisor, Dr. Ann Webb, for providing expert and valuable guidance throughout my study. She gave me all the support I needed during my time in the University of Manchester.

I wish to thank my advisor, Professor Martin Gallagher, who gave me useful suggestions and feedbacks during my first and second year Ph.D.

My thanks also go to Dr. Andrew Smedley, Dr. Richard Kift and Mr. Peter Kelly who are members of Radiation group in the Centre for Atmospheric Science, the University of Manchester, for their help and support with their knowledge and skills.

I would like to thank Dr. Serm Janjai and members of the Laboratory of Tropical Atmospheric Physics at Silpakorn University, Thailand, and Andy Pearson at Health Protection Agency, UK for providing the ground-based data. I am also grateful to the OMI Aura science teams for their efforts in producing the OMI satellite data.

This thesis would not have been possible without financial support from the Royal Thai Government for which I also thank.

Last, but by no means least, I would like to thank my family and friends for their support and encouragement throughout my study.

Chapter 1 – Introduction

1.1 General Overviews

Solar ultraviolet (UV) irradiance may produce a variety of effects, many of them detrimental, on human health, terrestrial and aquatic ecosystems. In this thesis, the erythemal irradiance affecting human skin is taken as the focus. It refers to the spectral UV irradiance weighted by the erythema action spectrum defined by Commission Internationale de l'Eclairage (CIE), or in layman's terms the "*sunburning power*" of the radiation. It is becoming increasingly difficult to ignore the knowledge of its variability in space and time.

The amount of UV irradiance can be measured directly by ground-based instruments and calculated by using model calculations, for instance, radiative transfer models and empirical models. The model outputs are limited by the knowledge of the atmospheric conditions being modelled, i.e. the availability of relevant input data. Since ground-based measurements have been installed at limited sites, covering a small fraction of the earth's surface, satellite UV estimation techniques based on radiative transfer models and reflectivity measurements are a promising advance since they can in principle provide UV irradiance on the global basis. However, satellite data represents average conditions over large areas, and it is based on model calculations including some assumptions that are sometimes unrealistic. Thus, the validation of satellite data with ground-based data is required. Recent validations of satellite retrievals have been concentrated mostly in regions of midlatitudes and high latitudes, where there are the most ground-based instruments. Far too little attention has been paid to Tropical sites. Therefore, this thesis examines erythemal irradiance retrieved from Ozone Monitoring Instrument (OMI) in the Tropics with respect to local ground-based measurements, and compares the results to similar validation techniques at midlatitudes.

1.2 The Purposes of This Work

The final goal of this work is to provide a method of using satellite retrieved UV irradiance to provide public health information on erythemal irradiance in the

Tropics, specifically in Thailand. To that end, the satellite data must first be validated against ground-based measurements. This validation is undertaken both for sites in the Tropical and midlatitudes.

The objectives in achieving this goal are:

- To identify the differences between erythemal irradiance at local solar noon retrieved from OMI and measured from ground-based instruments.
- To present new methodologies of estimating the erythemal irradiance using both satellite and ground-based data. The methods will be tested by application in the midlatitudes and the Tropics.
- To investigate and compare the success of the improvements to the basic OMI retrievals in the two different climates.
- To provide data for public use, for example, erythemal irradiance or UV Index maps, based on the empirically improved satellite retrievals.

1.3 Outline of Structure

In the following chapter, it begins by laying out the background and literature review. In Chapter 3, sites and instrumentation used in this research are described. In Chapter 4, comparisons between satellite and ground-based data for clear sky and all sky conditions have been investigated. Chapters 5 and 6 introduce methodologies to improve satellite estimates for clear sky and cloudy sky conditions. The results of the further extension to generate UV maps for Thailand are shown in Chapter 7. The final conclusion is presented in Chapter 8.

Chapter 2 – Background and Literature Review

2.1 Solar Ultraviolet Radiation

Solar radiation is electromagnetic radiation emitted by the sun. The emission spectrum of equivalent blackbody temperature of the sun at 5900 K is represented in Figure 2.1, compared with the spectrum of solar irradiance at the top of the atmosphere and ground surface. The majority of solar radiation, with a wavelength more than 300 nm, is emitted from the sun's photosphere whereas the radiation with a wavelength less than 300 nm is emitted from the sun's chromosphere. Solar radiation whose wavelength is shorter than 50 nm is radiated from the corona. In the earth's atmosphere, wavelengths shorter than 300 nm are mainly absorbed by ozone and molecular oxygen and wavelengths higher than 700 nm are absorbed by water vapour and carbon dioxide, to give the spectrum at the surface shown in Figure 2.1. [*Salby*, 1996]

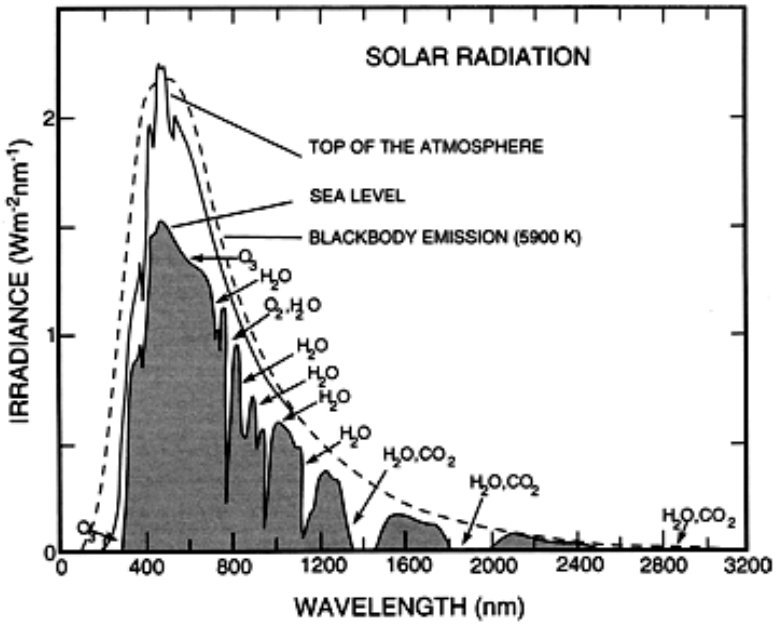

Figure 2.1 The spectrum of a black body at 5900 K (dashed), the spectrum of solar irradiance at the top of the atmosphere (solid) and at the earth's surface (shaded) [*Salby*, 1996].

It should be noted that there are artificial sources of UV radiation such as high-pressure discharge lamps and welding arcs [*NRPB*, 2002]; however, all naturally occurring UV radiation arriving at the earth's surface is from the sun. Solar UV radiation is only about 5% of the solar radiation at the top of the atmosphere compared to 55% in the visible and 40% in the infrared ranges [*Vardavas and Taylor*, 2007]. It can be subdivided into three categories: UVA (315-400 nm), UVB (280-315 nm) and UVC (200-280 nm) according to CIE, based on physical effects [*Webb*, 2000b]. When the radiation passes through the earth's atmosphere, absorption and scattering processes occur, e.g., absorption by atmospheric gases and aerosols, scattering by aerosols and clouds. Although UVC radiation has the highest photon energy, it is essentially all absorbed by atmospheric oxygen and ozone in the "*Hartley band*". Most of UVB radiation and some of the UVA radiation are also absorbed by atmospheric ozone in the "*Huggins band*", demonstrated in Figure 2.2.

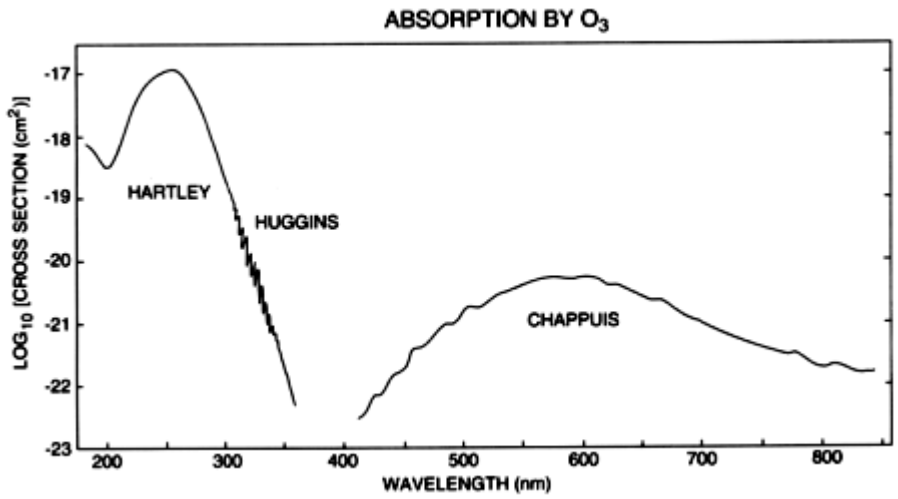

Figure 2.2 Ozone absorption coefficient of UV radiation [*Salby*, 1996].

Much of the interest in solar UV radiation stems from its effects on human health, most often quantified as the erythemal irradiance. Erythema is sunburn and the action spectrum for this effect is defined by CIE [1998], after *McKinlay and Diffey* [1987]. It is this measure of UV radiation with which we will be concerned. The erythemal weighting function is defined by Equation 2.1.

$$\mathrm{CIE}(\lambda) = \begin{cases} 1.0 & \text{for} \quad 250 < \lambda \leq 298\text{nm} \\ 10^{0.094(298-\lambda)} & \text{for} \quad 298 < \lambda \leq 328\text{nm} \\ 10^{0.015(140-\lambda)} & \text{for} \quad 328 < \lambda \leq 400\text{nm} \\ 0.0 & \text{for} \quad \lambda > 400\text{nm} \end{cases} \tag{2.1}$$

where $\mathrm{CIE}(\lambda)$ is the normalised erythemal weighting function or erythema action spectrum, and λ is wavelength (nm).

Erythemal irradiance can be calculated by integrating the product of spectral irradiance and erythema action spectrum over the UVA and the UVB ranges as shown in Equation 2.2.

$$\text{Erythemal Irradiance} = \int_{250}^{400} \mathrm{I}(\lambda)\mathrm{CIE}(\lambda)\mathrm{d}\lambda \tag{2.2}$$

where $\mathrm{I}(\lambda)$ is the spectral irradiance ($\mathrm{W \cdot m^{-2}}$), and $\mathrm{CIE}(\lambda)$ is the erythema action spectrum.

For public awareness, the level of erythemally weighted UV irradiance at the earth's surface is converted to a unitless value called "*UV Index*" or "*UVI*" [*WHO*, 2002]. The UV Index can be calculated by dividing the erythemally weighted UV irradiance ($\mathrm{mW \cdot m^{-2}}$) by 25 $\mathrm{m^2 \cdot mW^{-1}}$. The integer UV Index is further separated into bands based on effects on a fair-skinned person as shown in Figure 2.3. Values less than 2 are defined as low risk whereas over 10 are extreme (rapid sunburn). Maximum values of UV Index are determined mainly by latitude and altitude, e.g., the UV Index value does not exceed about 6 in Southern Ontario, Canada [*Fioletov et al.*, 2004] while it can be up to the value of about 10 or more in the Tropics [*Ilyas et al.*, 1999; *Janjai et al.*, 2009a], and reaches up to 20 at a tropical high altitude station in Andean Altiplano, Argentina [*Cede et al.*, 2002].

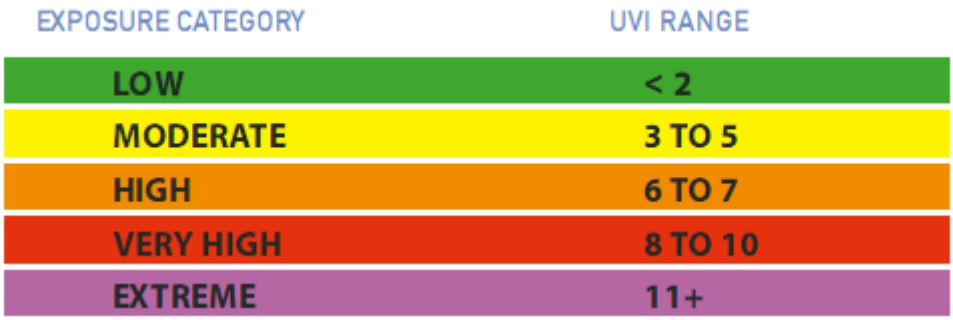

Figure 2.3 UV radiation exposure categories [*WHO*, 2002].

2.2 Factors Influencing Solar UV Radiation

Since solar UV radiation is electromagnetic radiation, when it passes through the earth's atmosphere it can be absorbed, scattered and reflected by the components of the atmosphere such as atmospheric gases, air molecules, clouds, aerosols and ozone. Its intensity at the surface also depends on the solar energy output, some geographical factors such as the solar zenith angle and the sun-earth distance, and finally the albedo of the surface. This section describes the main factors affecting UV radiation reaching the earth's surface.

2.2.1 The Extraterrestrial Solar Spectrum

The total solar output reaching the top of the atmosphere at the mean sun-earth distance is called the "*solar constant*" which is actually variable. The average solar constant measured by several satellites is about 1370 $W \cdot m^{-2}$. Variability in solar output is controlled by two phenomena: the 27-day solar rotation and the 11-year solar cycle. This variability influences the amount of extraterrestrial solar UV radiation. The variation of the total solar extraterrestrial radiation is about 0.1% or 1 $W \cdot m^{-2}$ during each 11-year sunspot cycle, while at UV wavelengths it is a few percent [*Lean et al.*, 1997]. Since increases in solar output result in more ozone production, the UV radiation is absorbed more before arriving at the surface, and surface UV radiation follows the ozone cycle. The total solar output also depends on the distance between the sun and the earth's surface. Because of the eccentricity of the orbit of the earth, the distance between the sun and the earth is smallest on 3 January (perihelion) and largest on 4 July (aphelion) with the difference of about 7%

between extremes. As a result, the incoming solar radiation varies by ±3.5% throughout the year.
[*Iqbal*, 1983; *Salby*, 1996; *WMO*, 2007]

The solar spectrum outside the earth's atmosphere can be obtained by the ground-based Langley plot method [*Bais*, 1997; *Gröbner and Kerr*, 2001] and space-based measurements from satellite instruments onboard, for example, the Atmospheric Laboratory for Applications and Science (ATLAS), the National Oceanic and Atmospheric Administration (NOAA) and the Upper Atmosphere Research Satellite [*Cebula et al.*, 1996; *WMO*, 2007]. The comparison of the solar spectrum from the ground-based Langley plot method and the satellite measurements shows an agreement better than ±3%.

2.2.2 Solar Zenith Angle

The solar zenith angle is the angle measured at the earth's surface between the sun and the local zenith, and depends on latitude, season and time of day. It is the factor most strongly influencing solar radiation intensity causing diurnal, annual and latitudinal variations in the amount of UV irradiance at the earth's surface. When the sun is at a high position in the sky, the radiation travels through less atmosphere, and is absorbed and scattered less, so more UV radiation reaches the earth's surface. On the other hand, the radiation passes through more of the atmosphere when the sun is at a lower position, so less UV radiation reaches the ground. In addition, radiation striking the ground at a larger solar zenith angle is spread out over a larger area, thus significantly reducing irradiance.

Solar zenith angle can be calculated following Equations 2.3 and 2.4 as described by *Iqbal* [1983].

$$\theta_z = \cos^{-1}(\sin\delta\sin\phi + \cos\delta\cos\phi\cos\omega) \qquad (2.3)$$

where θ_z is the solar zenith angle,

ϕ is the geographic latitude,

ω is the hour angle, the angular distance that the earth has rotated in a day. In one day (24 hours) the earth rotates 360°. Therefore, the hour angle is equal to 15° multiplied by the number of hours from local solar noon, and defined by $\omega = 15(12 - \text{hour})$ where hour is the current time of the day.

δ is the solar declination, the angular distance of the sun at local solar noon with respect to the celestial equator plane. It is maximum (23.5°) on the summer/winter solstice and minimum on the equinoxes. The solar declination can be calculated as follows:

$$\begin{aligned}\delta = \frac{180^o}{\pi}(&0.006918 - 0.399912\cos\Gamma + 0.070257\sin\Gamma \\ &- 0.006758\cos 2\Gamma + 0.000907\sin 2\Gamma \\ &- 0.002697\cos 3\Gamma + 0.00148\sin 3\Gamma)\end{aligned} \tag{2.4}$$

where $\Gamma = 2\pi(d_n - 1)/365$ and d_n is the day number of the year.

2.2.3 Altitude

Altitude, is the height of the surface above sea level (a.s.l.), also influences the amount of solar radiation [*Blumthaler et al.*, 1997; *Dubrovský*, 2000; *Pfeifer et al.*, 2006; *Schmucki and Philipona*, 2002; *WMO*, 2007]. At high altitudes, more UV radiation reaches the surface because the radiation passes through less of the atmosphere before it reaches the surface. Also, at high altitudes the surface is often covered with snow, contributing to enhanced UV irradiance with high surface albedo. Thus, the effects of altitude depend on location, through the local surface and the clearness of the atmosphere. The variation with altitude of erythemal radiation measured by Robertson-Berger broadband filter UV radiometer at two sites: Hradec Kralove (50.17°N, 15.83°E, 278 m a.s.l.) and Milesovka (50.55°N, 13.93°E, 827 m a.s.l.) in the Czech Republic, was found to be 4% to 8% per km [*Dubrovský*, 2000]. The wavelength dependency of the altitude effect at Garmisch-Partenkirchen (730 m a.s.l.) and Wank (1730 m a.s.l.) in Germany was also reported by *Blumthaler et al.* [1997]: 9% per km at 370 nm, 11% per km at 320 and 24% per km at 300 nm. The

effect is far more pronounced at short wavelengths, but will depend on the amount of aerosol and ozone in the layer between any two altitudes. For instance, *Herman et al.* [1999b] reported that with every 1 km increase in altitude, the erythemal radiation increases by 10% to 40% in Germany where the low altitude sites considered were relatively polluted and cloud effects were included [*Blumthaler et al.*, 1997; *Schmucki and Philipona*, 2002; *Seckmeyer et al.*, 1997].

2.2.4 Stratospheric Ozone

Ozone (O_3) is a molecule of three oxygen atoms naturally found in the stratosphere where it is produced (see in Equations 2.5 and 2.6). It occurs mainly at altitudes between approximately 25 km and 100 km. Stratospheric ozone is the main component of the atmosphere which strongly absorbs solar UV radiation, especially UVC and UVB and some part of UVA radiation (see in Equations 2.7 and 2.8) [*Liou*, 2002].

$$O_2 + h\nu \rightarrow 2O, \lambda < 242nm \tag{2.5}$$

$$O + O_2 + M \rightarrow O_3 + M \tag{2.6}$$

$$O_3 + h\nu \rightarrow O_2 + O, \lambda < 1100nm \tag{2.7}$$

$$O + O_3 \rightarrow 2O_2 \tag{2.8}$$

where $h\nu$ is solar energy depending on wavelength. M is any third atom or molecule such as N_2 and O_2, and λ is wavelength.

The absorption of UV radiation by ozone depends on wavelength. For example, ozone absorption of the radiation at 320 nm is only 1% of that at 280 nm [*Webb*, 1998]. Figure 2.2 shows the ozone absorption cross section in three bands: Hartley band, Huggins band and Chappuis band, covering the UV and visible wavelengths. We can see that UV radiation is strongly absorbed in the Hartley band and weakly

absorbed in the Huggins band whereas the Chappuis band covers visible wavelengths and is also relatively weak.

The study of atmospheric ozone was first begun in the mid-1920s using the Dobson instrument developed at Oxford University, followed by a network of six instruments in the late-1920s. A big increase in total ozone measurement with about 100 instruments began in the year 1957 during the International Geophysical Year. In the early 1980s, the Brewer spectrometer was also developed to measure total ozone. At present there are more than 200 Brewer spectrometers installed worldwide, and more than 100 Dobson instruments, both contributing to the ground-based network of ozone measurements. Apart from ground-based measurement, total ozone data has been available from satellite measurement since 1979, e.g., Total ozone Mapping Spectrometer (TOMS), Solar Backscatter Ultraviolet (SBUV), Global Ozone Monitoring Experiment (GOME), which can show the pattern of total ozone on a global scale. The data from all these measurements led to the discovery of ozone depletion and determined the basic geographical and annual behaviour of total ozone. They have been also shown that total ozone is strongly correlated to weather patterns [*Kerr*, 2005] and meteorology, e.g., vorticity [*Vaughan and Price*, 1991].

The first discovery of ozone depletion was in the Antarctic in the 1980s by *Farman et al.* [1985]. The ozone at Halley Bay (76°S, 27°W) observed by a Dobson spectrometer had declined from about 300 Dobson Unit (DU) in year 1975 to less than 200 DU in year 1984. The chemical ozone loss in these areas is enabled by the polar vortex during mid-winter and early spring. During the Antarctic winter, it is almost dark, and there are strong winds around the lower stratosphere resulting in low temperatures (less than 190 K) and a pool of trapped air over the continent [*WMO*, 2007]. As a consequence of these low temperatures, Polar Stratospheric Clouds (PSCs) are formed comprising of water vapour and nitric acid [*Pyle*, 2000]. The chemical reaction involving chlorofluorocarbon (CFC) product on the surface of the PSCs is shown in Equation 2.9.

$$HCl(solid) + ClONO_2(gas) \xrightarrow{PSCs} HNO_3(solid) + Cl_2(gas) \qquad (2.9)$$

In early spring, molecular chlorine is photolysed to chlorine atoms by sunlight and the chlorine then acts as a catalyst in destroying ozone. This is illustrated through Equations 2.10 to 2.14 [*Pyle*, 2000]. From these equations, it can be seen that the stratospheric ozone is transformed to oxygen molecules, causing the loss of the stratospheric ozone.

$$ClO + ClO + M \rightarrow Cl_2O_2 + M \qquad (2.10)$$

$$Cl_2O_2 + h\nu \rightarrow Cl + ClO_2 + M \qquad (2.11)$$

$$ClO_2 + M \rightarrow Cl + O_2 + M \qquad (2.12)$$

$$2Cl + 2O_3 \rightarrow 2ClO + 2O_2 \qquad (2.13)$$

Net: $$2O_3 \rightarrow 3O_2 \qquad (2.14)$$

where M is usually N_2 or O_2.

In addition, a cycle of bromine and chlorine oxides [*McElroy et al.*, 1986] can also reduce the polar ozone during winter and spring as shown in Equations 2.15 to 2.18 [*WMO*, 2007].

$$BrO + ClO + h\nu \rightarrow Br + Cl + O_2 \qquad (2.15)$$

$$Br + O_3 \rightarrow BrO + O_2 \qquad (2.16)$$

$$Cl + O_3 \rightarrow ClO + O_2 \qquad (2.17)$$

Net: $$2O_3 \rightarrow 3O_2 \qquad (2.18)$$

The above chemical reactions lead to the so-called ozone hole, whose area defined by total column ozone values less than 220 DU and depth vary from year to year. There has been an increase of the ozone hole area since the early 1990s, with nearly 25 million km^2 in year 2003 [*Newman et al.*, 2004], and a decrease of minimum total ozone from about 200 DU in year 1979 to about 100 DU in year 2000 [*WMO*, 2003]. While the Montreal Protocol [*WMO*, 2007] has reduced chlorine emissions and chlorine loading has begun to respond, there is as yet no sign of a reduction in the annual loss of Antarctic ozone.

The decrease of stratospheric ozone was found not only in the Antarctic, but also in the Arctic [*Sinnhuber et al.*, 2000] and midlatitudes [*Kerr*, 1991; *Siani et al.*, 2002; *Stolarski et al.*, 1992], although not the Tropics [*Ganguly and Iyer*, 2006; *Pyle*, 2000]. The polar and global ozone depletion were reviewed by *WMO* [2003; 2007]. In the Arctic, the decrease of total ozone was not as much as in the Antarctic since the Arctic stratospheric temperatures in winter are not as low as those in the Antarctic and the vortex is not as strong. The total ozone at Ny-Ålesund, Spitsbergen (79°N, 12°E) in March, 2000 was less than the mean total ozone between years 1980 and 1989 by about 100 DU [*Sinnhuber et al.*, 2000]. The stratospheric ozone declined about 6% for southern midlatitudes and about 5% for northern midlatitudes between the years 2002 and 2005, compared with that in the year 1980 [*WMO*, 2007]. During the same period, the global annually averaged stratospheric ozone decreased approximately 3.5%. These values were similar to the value of the years 1997 to 2001 indicating that ozone is no longer decreasing [*WMO*, 2003].

The Antarctic ozone depletion was a major force in defining the Montreal Protocol, agreed in year 1987. The Montreal Protocol and later amendments were designed to reduce production of ozone depleting substances such as CFCs, Halons, Methyl chloroform (CH_3CCl_3) and Methyl bromide (CH_3Br), in order to protect the ozone layer. At the present, it can be seen that the protocol is working with clear evidence of a decrease of ozone depletion substances in the atmosphere [*WMO*, 2007]. Forward modelling predicts that the global ozone layer should be recovered to the same levels of the pre-1980s by about year 2050 [*WMO*, 2007] or year 2068 estimated by *Newman et al.* [2006]. These predictions are, however, dependent on

other factors that might interact with ozone cycle described earlier. For example, climate change (surface warming) gives cooling in the stratosphere, which can decrease chemical reaction rates at midlatitudes, but increase ozone loss at high latitudes (where more PSCs form). Climate change can also change global dynamics which transports ozone from source to sink regions [*Stevenson et al.*, 2005; *Zeng and Pyle*, 2003].

Since the stratospheric ozone is the main absorber protecting the earth's surface from the harmful solar radiation, the decrease in total ozone and the change in vertical ozone profile should lead to an increase in surface UV irradiance as illustrated by various recent studies [*Bartlett and Webb*, 2000; *Garane et al.*, 2005; *Herman et al.*, 1996; *Janjai et al.*, 2009a; *Josefsson*, 2006; *Kerr and McElroy*, 1993; *Madronich et al.*, 1998; *McKenzie et al.*, 1999; *Meleti et al.*, 2009; *Sasaki et al.*, 2002; *Trepte and Winkler*, 2004; *Zerefos et al.*, 2000; *Zerefos*, 2002]. For example, *Kerr and McElroy* [1993] reported the decrease in total ozone from 1989 to 1993 at Toronto as 4.1% per year in winter and 1.8% per year in summer. In contrast, the increase in spectral UV irradiance at 300 nm was 35% per year in winter and 6.7% per year in summer. *Bartlett and Webb* [2000] showed that the decrease in ozone was by 5.9%, while the increase in the ratio of erythemal to UVA (320-400 nm) irradiance was by 4.3% between years 1993 and 1997 at Reading, UK. *Zerefos et al.* [2002] showed that UV irradiance at 305 nm at Thessaloniki increased about 0.40% per year based on the 1990s level which was related to a 0.13% per year ozone decline. *Sasaki et al.* [2002] showed that from years 1990 to 2000 UVB (290-320 nm) irradiance increased 1.22% per year, especially in winter, at Tokai University (Japan), corresponding to the ozone depletion in midlatitudes in 1990s. *Josefsson* [2006] reported that the CIE-weighted (erythemal) irradiance during years 1983-2003 at Norrköping, Sweden was increased by 0.52% per year responding to a total ozone decrease of 0.14% per year. *Janjai et al.* [2009a] showed increases in erythemal irradiance at Chiang Mai, Ubon Ratchathani and Nakhon Pathom, Thailand from years 2001 to 2005, i.e. 1.43% per year all year and 2.66% per year during dry season for Chiang Mai. However, they suggested that this may due to a reduction of cloud cover resulting from a decrease in precipitation. *WMO* [2007] reported that due to the success of the Montreal Protocol, increases in UV radiation observed at some southern hemisphere sites in unpolluted locations have levelled off following a similar observed consistency in

ozone over the past few years. Increase in UV radiation is significantly related to ozone depletion but other factors such as changes in clouds, aerosols and sunshine duration must also be considered. Recent studies show that where ozone changes were small, others factors, e.g., changes in pollution could dominate changes in UV radiation [*Chubarova*, 2008; *Janjai et al.*, 2009a; *McKenzie et al.*, 2007].

2.2.5 Tropospheric Trace Gases

Apart from ozone in the stratosphere, UV radiation can be absorbed by tropospheric trace gases, and through photolysis influence atmospheric chemistry. There are many tropospheric absorbers of UV radiation such as tropospheric ozone, sulphur dioxide (SO_2) and nitrogen dioxides (NO_2) [*Chubarova*, 2006; *Chubarova*, 2008; *WMO*, 2007]. The influence of these gases can be usually detected in polluted areas or during natural hazards, e.g., forest fires, volcanic eruptions. For example, erythemal irradiance at Moscow decreased about 1.5% to 2% due to increase in NO_2 [*Chubarova*, 2008].

2.2.6 Clouds

Clouds, formed of small water droplets or ice crystals [*Calbó et al.*, 2005], scatter (according to Mie scattering) UV radiation without significant absorption. The amount of clouds on average can cover over half of the earth's surface and influence both incoming and outgoing radiation [*Houghton*, 2002]. Clouds have strongly non-linear effects on the amount of UVA and UVB radiation. Clouds can both enhance and reduce UV radiation, depending on their geometrical thickness, composition, height and spatial homogeneity. In addition, clouds may play a role in absorption of UV radiation by other atmospheric compositions such as ozone through increasing the pathlength travelled by radiation. UV radiation can be decreased by about 65% up to 90% under overcast conditions [*den Outer et al.*, 2005; *Németh et al.*, 1996; *Seckmeyer et al.*, 2008]. For broken cloud conditions, the radiation can be enhanced (according to Mie scattering) by about 15%-25% compared to the radiation at clear sky conditions [*Németh et al.*, 1996; *WMO*, 2007]. The average reduction of UV radiation by clouds is less than for visible radiation with 32% for erythemal irradiance against 43% for total solar radiation compared to the clear sky values [*den*

Outer et al., 2005; *Josefsson and Landelius*, 2000]. Similarly, the percentage increase due to broken clouds is 6% for UV radiation compared to 12% for total solar radiation, relative to no clouds near the sun [*Piacentini et al.*, 2003].

Clouds are highly variable in space and time which causes differences when UV irradiances from satellite retrievals and ground-based measurements are compared. This is likely due to the fact that satellites measure over an area, which clouds in the area will be averaged, whereas ground-based measurements refer to an exact point.

2.2.7 Aerosols

Aerosols are tiny solid and liquid particles suspended in the air [*Iqbal*, 1983; *Seinfeld and Pandis*, 2006]. There are both natural and anthropogenic aerosols such as desert dust, biomass burning aerosols and organic carbon significantly affecting solar radiation, as reviewed in *WMO* [2007]. Aerosols have both direct and indirect effects on solar radiation [*IPCC*, 2007]. The direct effect is that they can both absorb and scatter (according to Mie theory) solar radiation resulting in a change to the radiative balance of the earth-atmosphere system. As a result, they cause warming where there is absorption, and reduce solar radiation at the earth's surface. An indirect effect of aerosols is that they can change the microphysical properties of cloud in ways that depend on particle size, chemical composition, and ambient environment [*IPCC*, 2007]. This can induce changes of cloud height, cloud lifetime and cloud albedo, for example, and hence alter the cloud (and therefore planetary) albedo. Effects of aerosols on UV radiation depend on their optical properties and the number of particles. Normally, the optical properties of aerosols are presented in terms of aerosol optical depth, which is a parameter that indicates how much radiation is reduced by aerosols; aerosol single scattering albedo which is the ratio of aerosol scattering to attenuation by both absorption and scattering processes; and phase function which determines the amounts of forward and backward scattering. These parameters are wavelength dependent.

The understanding of the aerosol properties and their effect on UV radiation has been a challenge often due to paucity of aerosol data. Recent studies showed that aerosol has a measurable impact on UV irradiance, i.e. it can reduce the surface UV

irradiance [*di Sarra et al.*, 2002; *Erlick and Frederick*, 1998; *Esteve et al.*, 2009; *Krzyscin and Puchalski*, 1998]. For example, *Krzyscin and Puchalski* [1998] suggested that aerosol optical depth at Belsk, Poland (52°N, 21°E) varying from 0.1 to 0.7 can change erythemal daily doses by 20%-30%. The reduction of erythemal irradiance per unit aerosol optical depth at 415 nm can be up to 50%-55% as illustrated in *di Sarra et al.* [2002]. *Balis et al.* [2004] showed that the surface UV irradiance at 305 nm may change about 10%-25% for different aerosol optical depth and aerosol type. At the same aerosol optical depth, the erythemal irradiance decreased less than 20% under high aerosol single scattering albedo (0.94), while the decrease was about 25%-30% at lower aerosol single scattering albedo (0.87) [*Chubarova*, 2009]. *Acosta and Evans* [2000] showed that erythemal irradiance in downtown areas of the Mexico City were lower than the values in the suburban regions by 20% (or up to 40% on polluted days). During biomass burning in northern region of India, *Latha et al.* [2004] and *Badarinath et al.* [2009] suggested that every 0.1 increase in aerosol optical depth measured at 500 nm can reduced 0.01 $W \cdot m^{-2}$ of erythemal irradiance. *Kalashnikova et al.* [2007] show that smoke aerosols over Darwin, Australia, reduced the surface UV irradiance (290-300 nm) by as much as 40%-50% near active fires. The smoke aerosols reduced the UV irradiance (290-300 nm) by 15%-25% for the area far from the fires. Apart from reduction of the surface UV radiation due to aerosol, *Wenny et al.* [2001] showed that erythemal irradiance can increase up to 4% during low aerosol optical depth periods.

Since the properties of aerosol are difficult to determine, this can be a problem of UV estimation using satellites especially for polluted areas [*Arola et al.*, 2009; *Buchard et al.*, 2008; *Ialongo et al.*, 2008; *Kazadzis et al.*, 2009b; *Meloni et al.*, 2005; *Tanskanen et al.*, 2006], an issue discussed further in Section 2.4.5.

2.2.8 Surface Albedo

The earth's surface can absorb, reflect or scatter UV radiation reaching it, and in the case of water transmit to some depth. Consequently, it can enhance UV radiation especially with high reflecting surfaces such as snow, sand and ice [*Kalliskota et al.*, 2000; *Renaud et al.*, 2000; *Reuder et al.*, 2007; *WMO*, 2007]. The proportion of reflecting and scattering indicated by surface albedo depends on surface types. For

instance, the UVB surface albedo values for various surface types were published, e.g., snow: up to 0.90, dry beach sand: 0.02-0.15, vegetated surfaces (grass): 0.01-0.05, building materials: 0.02-0.10, water: 0.05-0.08 [*Blumthaler and Ambach*, 1988; *Chadyšienė and Girgždys*, 2008; *Corrêa and Ceballos*, 2008; *Godar*, 2005]. Since snow is highly reflective, it increases UV radiation both on a horizontal surface, following further backscattering by the atmosphere, and for other surfaces by direct reflection onto the surface. *Renaud et al.* [2000] showed that erythemal irradiance at snow covered surfaces on a cloudless day can increase by 15% to 25% while on a cloudy day it can increase by up to 80% due to multiple reflections between the surface and cloud layer. A practical problem when UV radiation is estimated by using satellite data is that snow can be classified as cloud since its brightness is similar to that of cloud, and the UV radiation is then underestimated [*Tanskanen et al.*, 2007].

2.3 Effects of UV Radiation

Although UV radiation is the shortest wavelength radiation and the smallest part of solar radiation arriving at the earth's surface, it has the highest energy, with various detrimental effects on human health, terrestrial ecosystems, aquatic ecosystems, biogeochemical cycles, tropospheric composition, air quality and materials damage [*UNEP*, 2006]. However, it is not all negative and there is one well known beneficial effect of exposure to UV radiation, the production of vitamin D which is a necessary hormone for bone health and potentially for many aspects of general health [*Norval et al.*, 2007; *UNEP*, 2006]. Following are some detrimental examples of UV exposure on human health. UV radiation does not penetrate far into the body because most of it is absorbed in the superficial tissue layers. Therefore, much of the harmful UV radiation affects the eyes and skin. In addition, UV also affects the immune system.

2.3.1 Effects on the Eye

The eye can be directly exposed to UV radiation and this may cause acute effects or chronic effects. Exposure to UV radiation can damage many components of eyes such as sunburn at the eyelid, photoconjunctivitis at the conjunctiva, pterygium at

cornea, and anterior subcapsular opacities of the lens [*de Gruijl et al.*, 2003; *Longstreth et al.*, 1998; *Norval et al.*, 2007; *UNEP*, 2006]. *Longstreth et al.* [1998] demonstrated that most of UV radiation (below 300 nm) does not pass beyond the cornea and the rest of UV radiation (below 370 nm) can be absorbed at the lens, thus only the radiation at longer wavelengths than that can reach the retina. As a result, the cause of the lens damage is usually UVA radiation while UVB and UVC wavelengths affect the cornea. The acute effect of receiving UV radiation is photokeratitis which happens after a few hours exposure. This can be characterised by reddening and inflaming of the eyeball, gritty feeling of severe pain, tearing, photophobia (fear of light) and blepharospasm (twitching). This is often found in skier and is known as snow blindness. The chronic effects are pterygium resulting from an outgrowth of the conjunctival tissue over the surface of the cornea, and pinguecula which is a raised opaque mass (usually as a yellowish patch) just adjacent to the cornea [*Longstreth et al.*, 1998]. These result in the loss of transparency. Cataracts are the well known eye damage and a major cause of blindness due to oxidized lens proteins [*Longstreth et al.*, 1998].

A number of epidemiologic publications have reviewed the relationship between UV exposure and its effect on the eye in several countries such as the U.S. [*Taylor et al.*, 1988; *West et al.*, 2005], Australia [*Taylor*, 1980; *Threlfall and English*, 1999], Jordan [*Al-Bdour and Al-Latayfeh*, 2004], and Japan [*Hayashi et al.*, 2003]. For example, a strong correlation between pterygia and surface UV irradiance in Jordan was shown by *Al-Bdour and Al-Latayfeh* [2004]. In a group of Australian Aborigines, cataracts occurred more often in the high annual mean UV level areas [*Taylor*, 1980]. A correlation with regression coefficient of 0.70 between the risk of cortical cataract and the cumulative UVB exposure was found in Chesapeake Bay [*Taylor et al.*, 1988]. Although overall UV exposures relate to eye diseases, the correlations must also account for other factors, such as behavioural, ethnic and environmental differences.

2.3.2 Effects on the Skin

Skin can be directly exposed to UV radiation which can cause not only acute injury (suntan, sunburn, blistering and peeling) but also chronic injury (skin ageing and

skin cancer) in all types of human skin [*de Gruijl et al.*, 2003; *MacKie*, 2000]. The effects of UV radiation on human skin depend on exposure time and human skin types, the latter divided to six groups shown in Table 2.1 [*MacKie*, 2000]. The effects are most often presented with respect to risk for people who have fair skin (Types 1 and 2) that tans poorly and burns frequently. The acute effects on human skin can happen 4-12 hours after exposure to UV radiation and are observed as sunburn – a reddening of the skin and hot or burning sensation. This may be followed by inflammation, blistering and peeling of the skin. The maximum damage can be seen 12-24 hours after excess exposure to the UV radiation, and be diminished over the next 48-72 hours after the exposure.

Table 2.1 Classification of skin types [*MacKie*, 2000].

Skin type classification	Characterisation
Type 1	Fair skinned Caucasians who burn very easily and never tan.
Type 2	Fair skinned Caucasians who burn easily and tan slowly and with difficulty.
Type 3	Medium skinned Caucasians who burn rarely and tan relatively easily.
Type 4	Darker skinned Caucasians who virtually never burn and tan readily.
Type 5	Asian or Indian skin.
Type 6	Afro-Caribbean or Black skin.

Regarding chronic effects, exposure to natural UV radiation can cause photoaging which changes the texture and the elasticity of skin. As a result, damaged skin gets wrinkles and sags. A more serious effect is skin cancer. There are three skin cancer types: basal cell carcinoma (BCC) which appears as a red lump, squamous cell carcinoma (SCC) appearing as a thickened red scaly point, and cutaneous melanoma (CM) which is the most dangerous type of skin cancer appearing as a mole or fleck [*Longstreth et al.*, 1998; *MacKie*, 2000; *Norval et al.*, 2007; *UNEP*, 2006]. The first two skin cancers are often referred to as the non-melanoma skin cancers which are clearly correlated with UV exposure. They usually occur in light-skinned people and on the areas of the body most exposed to sunlight such as face, neck and ear. It is clear that the risk of SCC can be linked to cumulative lifetime exposure to UV radiation. BCC may also be related to a high level of childhood exposure to sunlight.

Unlike BCC and SCC, CM is often found on areas of the body that are infrequently UV exposed.

Epidemiological studies show that increases in skin damage were reported for many countries and this likely related to UV exposure. *Abarca et al.* [2002] showed that ozone depletion, increased terrestrial UVB radiation and sunburn increase were related during 1986-2000 spring period in Southern Chile where ozone loss can be significant. In Manitoba, Canada, the annual percentage change of BCC and SCC increased 2.4%, mainly in people older than 40 years of age from the early 1970s to 2000 [*Demers et al.*, 2005]. Similar increases in skin cancer incidence have been observed elsewhere but are influenced by behaviour [*Veierod et al.*, 2003] and case of travel to low latitudes, not simply local increases in erythemal irradiance, which are often small [*Bentham*, 2001; *Office for National Statistics*, 2003].

2.3.3 Immune System

The skin includes a number of cells from the immune system. The immune system is the body's defence mechanism against foreign substances (antigens), e.g., virus infection, cancers and diseases. When substances enter the body, the immune system will recognise them to be either "*self*" or "*non-self*" entities. However, the immune system needs to be able to classify between self and non-self, and eliminate only the non-self. UV radiation can induce photochemical changes in the skin and potentially alter cell surface proteins (at least three photoreceptors located at or near the skin surface are involved – Deoxyribonucleic acid (DNA), urocanic acid and membrane components) that are used to determine self from non-self entities. Thus UV radiation can act as an immunosuppressive. The absorption of UV radiation at the body surface can affect the function of the skin-mediated part of the immune system that can then cause a weakened immune system, depending on UV doses, wavelengths, and types of immune response. When immunosuppression is induced, the immune system wrongly determines self to non-self or vice versa. Therefore, the immunosuppressive effects of UV radiation can influence the outcome of melanoma and non-melanoma skin cancer, certain infectious diseases, some forms of autoimmunity, and allergy.
[*Longstreth et al.*, 1998; *Norval*, 2000; *Norval et al.*, 2007; *Ullrich*, 2005]

2.4 Methods to Determine UV Irradiance

After the discovery of ozone depletion and concern about the expected increase in UV irradiance, there was much effort to determine UV irradiance at the earth's surface. This can be obtained from several resources: ground-based instruments, radiative transfer models, statistical models and satellite instruments. These methods have both advantages and disadvantages. Ground-based measurement can directly provide UV irradiance at a specific point and for real weather conditions if instruments have good calibrations and specifications. However, instruments can measure UV radiation for a limited area, and do not provide for regional or global coverage. Radiative transfer models calculate UV irradiance based on a model atmosphere with the extraterrestrial solar spectrum and several scattering and absorbing geophysical parameters as input. Statistical models show relationship between surface UV irradiance and one or more parameters such as ozone, solar zenith angle. Both types of model need input data from atmospheric measurements. One solution is to use the satellite retrieved UV irradiance for the entire globe, based on radiative transfer models and other products, e.g. backscattered radiation at several wavelengths which provides atmospheric data such as ozone, aerosols, clouds and surface albedo. However, satellite retrieval data is usually provided once per day from polar orbiting satellites and represents average conditions over large areas. The UV values from satellite retrievals are often different from those from ground-based measurements, showing the retrieval algorithm still needs improvement, as detailed in later chapters. More details on measurement of UV radiation at the surface are given in the following section.

2.4.1 Ground-Based Measurements

In general, there are four main types of ground-based instruments measuring solar UV radiation namely spectroradiometers, broadband radiometers, narrowband multifilter radiometers and dosimeters, having some differences of their systems, characteristics, and purposes of use [*Webb*, 1998; *WMO*, 2007]. In this section, the fundamental systems of these instruments, and benefits and weakness will be described.

2.4.1.1 Spectroradiometers

Spectroradiometers are instruments that are used to measure spectral irradiance. A spectroradiometer includes three essential components: input optics, monochromator(s) and a detector. Input optics collect the incident radiation and direct into the monochromator. The most common input optics are quartz or Teflon cosine response diffusers, providing for a measurement of irradiance. The light is guided from the input optic to the monochromator by either liquid or (quartz) fibre bundles or enters directly into the monochromator which then separates the radiation into each specific wavelength. The monochromator usually consists of gratings (or prisms), with the full width at half maximum (FWHM) recommended to be less than 1 nm. For solar UV measurement, a double monochromator is again advised [*WMO*, 2001]. The monochromator often also includes mirrors to guide the light from the entrance slit to the gratings or prisms and on to the exit slit of the monochromator, where it is incident on a detector. The standard double grating monochromator scans to sample each specific wavelength. The scan time for all wavelength desired can be several minutes depending on wavelength interval, bandwidth, step length and the time spent to measure at each position. Then the light in each wavelength is transformed to electronic signals by the radiation detector that normally is either a Photomultiplier tube (PMT) for high sensitivity, photodiode detector, or a diode array. In the case of recent diode array instruments a single monochromator is used, and straylight and sensitivity characteristics are not as good as those of the double monochromator instruments. The instruments are temperature dependent, especially the PMT, and require well-controlled temperature stabilization. Long-term stability of such spectroradiometers is generally not good and frequent calibration checks are necessary, both for wavelength specification and absolute units of irradiance. The double monochromator instruments tend to be large with high costs, are temperature dependent, and require computer control, a steady power supply and calibration facilities. The accuracy of the spectroradiometer is affected by a number of parameters including wavelength alignment, bandwidth, straylight, angular dependence, temperature dependence, linearity, stability, polarisation, and calibration sources [*Webb et al.,* 1998]. Since it can measure the spectral irradiance with high spectral resolution, the data is versatile with multiple uses, for example,

studying the effects of cloud and aerosol on UV irradiance [*Bais et al.*, 2005; *Bartlett and Webb*, 2000; *Seckmeyer et al.*, 1996].

2.4.1.2 Broadband Radiometers

Broadband radiometers can provide the total irradiance in a wider band (more than 10 nm), the detail depending on the device used. Filters and solid-state detectors are used to tailor the waveband and spectral response of the instruments. For UV measurement, the radiometers are often designed to mimic the erythemal action spectrum [*McKinlay and Diffey*, 1987]. This measurement is instantaneous and can therefore be at far higher temporal resolution than the spectrometers which take time to scan. It is less temperature dependent and more stable compared to spectrophotometers. The broadband radiometer is quite a compact, cheap and simple system, and requires a data logger to collect the voltage signal. For these reasons, this radiometer type is more frequently used for long-term monitoring. However, they still require Quality Control (QC) which is the on-site or internal checks such as regular calibrations, instrument maintenance and routine or temporary data correction, and Quality Assurance (QA) which is the external verification of the on-site QC, resulting data and its related uncertainty. The data are less versatile than the spectral measurements in term of atmospheric or biological research, but provide useful data for climatology and public health applications.

2.4.1.3 Narrowband Multifilter Radiometers

The performance of narrowband instruments is between spectrophotometers and broadband radiometers. Essentially they consist of a series of several wavelength limited broadband meters packaged together. They can measure the radiation in several narrow bands, usually between 2 nm and 10 nm, so have lower spectral resolution than that of spectrophotometers. Therefore, they give more information compared with broadband radiometers and need less maintenance than spectrophotometers. In addition, this instrument, combined with a radiative transfer model, can provide information on temporal change and derived UV spectral data which can be used to determine dose rates for any desired action spectrum. The

instruments have also been used to derive column ozone, and photolysis rates of some atmospheric species [*Dahlback*, 1996; *Gao et al.*, 2001].

2.4.1.4 Dosimeters

All the above physical instruments are used predominantly to measure UV irradiance, that is, on a flat horizontal surface. Dosimeters measure dose, usually based on a biological response, over wavelength and time of radiation received at a specific point. To know the direct dose received by a person, a dosimeter is needed. Polysulphone film [*Davis et al.*, 1976] is the most well known of the dosimeters in human exposure studies [*Parisi and Kimlin*, 2004; *Siani et al.*, 2008], with a response spectrum similar to that for erythema [*Davis et al.*, 1981; *Diffey*, 1997], causing a measurable response at a wavelength of 330 nm. The dosimeter can be used not only in air but also underwater [*Dunne*, 1999]. Photosensitive papers are another type of dosimeter, which change colour when exposured to UV radiation [*Diffey*, 1997]. Uracil thin film [*Gróf et al.*, 1996; *Webb*, 1998] and "*biofilm*" [*Rettberg et al.*, 1999; *Rettberg and Cockell*, 2004] are dosimeters based on DNA damage and require significant post-processing for analysis. The size of dosimeters is smallest compared to other types of physical instrument, so it can be used easily and personally. In addition, it does not need any power supply. As a result, the cost of dosimeters should be lower than other types. However, they need to be calibrated by using broadband radiometers or spectroradiometers, and under the same source spectrum as that for which they will be used [*Webb*, 1995; *Webb*, 2000a]. While approximate, their outputs are compared to the more sophisticated instruments, dosimeters have an important role in determining UV exposures and effects.
[*Di Menno et al.*, 2002; *Webb*, 2000a; *Webb*, 2003; *WHO*, 1992; *WMO*, 2003]

2.4.2 Radiative Transfer Models

A radiative transfer model is a set of mathematical tools, used to calculate spectral intensity (diffuse, direct and global). The model considers absorption, scattering and emission of radiation passing through the atmospheric column. The accuracy of radiative transfer models depends on both the mathematical schemes and the accuracy of input data. There is a variety of radiative transfer models, freely

available, that can be used to estimate spectral UV irradiance reaching the earth's surface such as Libradtran or uvspec model [*Mayer et al.*, 1997; *Mayer and Kylling*, 2005]; the Tropospheric Ultraviolet Visible model [*NCAR (National Center for Atmospheric Research)*, 2006]; the Streamer model [*Key and Schweiger*, 1998]; the System for Transfer of Atmospheric Radiation model [*Ruggaber et al.*, 1994]. These models are different in terms of their accuracy, input data, processing of times and methodologies, but have all been validated against measurements. Although there are several radiative transfer models, the widely accepted uvspec model is the only one that was used in this study. The following provides general information on the uvspec radiative transfer model.

2.4.2.1 The Uvspec Radiative Transfer Model

Libradtran is a library of radiative transfer routines and program produced as a software package [*Mayer and Kylling*, 2005]. It is used for radiative transfer calculations in the earth's atmosphere using the main program called uvspec model. The software package is freely available from http://www.libradtran.org. The program can be run using the command line in UNIX and Windows. In this study, the libradtran version 1.3 was installed under the Windows operating systems. The user, in this case, is recommended to install the Cygnus development suite called Cygwin, a Linux-like environment for Windows, which is one of the "*GNU*" tools available from http://cygwin.com [*Mayer et al.*, 2007].

2.4.2.2 The Uvspec Input and Output

As mentioned above, the uvspec model is invoked from the single command line as

uvspec <input_file> output_file

where *input_file* is an ASCII file varied by users. It contains many options for atmospheric parameters including the molecular atmosphere such as pressure, temperature and ozone, aerosol and cloud [*Mayer and Kylling*, 2005]. A comment is described by using a *#*. An example of the uvspec input file for a clear sky atmosphere is shown below:

```
                                    # Location of atmospheric profile file.
atmosphere_file ../data/atmmod/afglt.dat
                                    # Location of the extraterrestrial
                                    spectrum
solar_file ../data/solar_flux/atlas_plus_modtran
ozone_column  247.                  # Scale ozone column to 247.0 DU
day_of_year 2                       # Correct for Earth-Sun distance
sza 36.81                           # Solar zenith angle
rte_solver disort2                  # Radiative transfer equation solver
deltam  on                          # delta-M scaling on
nstr  6                             # Number of streams
wavelength 291.0 400.0              # Wavelength range (nm)
spline 291.0 400.0 1.0              # Interpolate from first to last in step
quiet.                              #End of the command
```

From the input file, the atmospheric model containing pressure, temperature, ozone and some trace gases profiles are read from *atmospheric_file*. There are six standard atmospheric models provided by libradtran, which can be chosen by users, as follows:

afglt	Tropical
afglms	Midlatitide Summer
afglmw	Midlatitude Winter
afglss	Subarctic Summer
afglsw	Subarctic Winter
afglus	U.S. Standard.

In this study, the atmospheric file, *afglt, afglms* and *afglmw* were selected for Thailand and UK. Likewise, the extraterrestrial solar flux can be read from *solar_file*. There are several extraterrestrial solar flux files which can be chosen in libradtran such as *apm_1nm* referring to ATLAS plus modtran spectrum convolved with a triangular function with FWHM of 1 nm [*Mayer et al.*, 2007] and

atlas_plus_modtran which includes the flux from ATLAS2, ATLAS3 and modtran. The latter is used in this study.

Ozone_column defines total ozone column in DU.

Aerosol properties can be set up and modified with *aerosol_* as can be seen in the example below:

aerosol_vulcan 1 *# Aerosol type above 2km*
aerosol_haze 6 *# Aerosol type below 2km*
aerosol_season 1 *# Summer season*
aerosol_visibility 20.0 *# Visibility in km.*

aerosol_vulcan specifies aerosol situation above 2 km from the earth's surface. It can be separated into four types: background, moderate volcanic, high volcanic and extreme volcanic aerosols. *aerosol_haze* is used to define aerosol type in the lower 2 km of the atmosphere, which contains four types of aerosol (rural, maritime, urban and tropospheric types) for selection. *aerosol_season* is used to specify aerosol profile as spring-summer or fall-winter profiles. *aerosol_visibility* sets a value of visibility in km. Furthermore, in case event that aerosol optical thickness is known, *aerosol_set_tau* can be used to set it as a parameter into the model.

For the output, the program reads the standard input file and then gives a standard output file. For a discrete ordinate radiative transfer (DISORT) solver applied in this work, the output format is presented below.

lamda edir edn eup uavgdir uavgdn uavgup

where *lamda* is wavelength (nm)
edir is direct beam irradiance ($mW \cdot m^{-2}$-nm)
edn is diffuse down irradiance ($mW \cdot m^{-2}$-nm)
eup is diffuse up irradiance ($mW \cdot m^{-2}$-nm)
uavgdir is direct beam contribution to the main intensity ($mW \cdot m^{-2}$-nm)

uavgdn is diffuse downward radiation contribution to the mean intensity ($mW \cdot m^{-2}$-nm)

uavgup is diffuse upward radiation contribution to the mean intensity ($mW \cdot m^{-2}$-nm)

The uvspec model includes three essential steps. Firstly, the standard input data is converted to the optical properties data. Then the radiative transfer equation solver as described above calculates transmittance, reflectance and radiances. Finally, the calculated outputs are post-processed to give absolute values by multiplication with the extraterrestrial solar irradiance, correction of sun-earth distance, and then, if required, convolution with a slit function, or integration over a wavelength region [*Mayer et al.*, 1997; *Mayer and Kylling*, 2005].

2.4.2.3 The Use of Uvspec Model

The uvspec radiative transfer model has been used widely. Many studies used uvspec for estimating surface UV irradiance, based on satellite data inputs, e.g., reflectivity [*Meerkoetter et al.*, 1997; *Verdebout*, 2000; *Wuttke et al.*, 2003] and ozone column [*Janjai et al.*, 2009a]. Many studies estimated clear sky surface UV radiation using uvspec and some input data, e.g., ozone and aerosol optical depth [*Lindfors and Vuilleumier*, 2005; *Mayer et al.*, 1997; *Seckmeyer et al.*, 2008]. In addition, using the radiative transfer model combining with spectral UV irradiance and aerosol optical depth, aerosol single scattering can be estimated [*Arola et al.*, 2005; *Cordero et al.*, 2009; *Ialongo et al.*, 2010; *Kazadzis et al.*, 2009a].

Validation of radiative transfer models can be checked either by comparing results with measurements or with other models of known quality. *Mayer et al.* [1997] found that the differences between measurement and uvspec model values were between -11% and 2% for wavelengths between 295 nm and 400 nm and solar zenith angles up to 80°. The agreement of UV irradiances between measurements and discrete ordinate methods was found within 6% (290-350 nm) [*Wang and Lenoble*, 1994] and 8% (290-320 nm) [*Zeng et al.*, 1994] for cloudless conditions, and 20% (280-320 nm) for cloudy conditions [*Forster et al.*, 1995]. The comparison of UV Index calculated from six radiative transfer models including the uvspec model was

presented by *Koepke et al.* [1998] and the agreement was generally within ±0.5 UV Index. The computed spectral global irradiance calculated from twelve radiative transfer models agreed to between 2% and 5% as shown by *van Weele et al.* [2000] using the same input parameters.

2.4.3 Parameterization Schemes

A parameterisation scheme uses one or more main controlling parameters for a physical process to define a related variable in a simple way. This method uses less input data compared with radiative transfer models and is not complicated compared with other methods. A direct relation between input and output is defined rather than representing the full complexity of the physical scheme (in this case radiative transfer). The scheme is limited by the accuracy of the algorithm and the spatial resolution. Following are several examples of parameterization methods.

One parameterization method was built by *Eck et al.* [1995] to calculate UVB irradiance (290-325 nm) under both clear sky and cloudy sky conditions in Toronto. The input data needed in the model are total ozone column and UV reflectivity from TOMS, solar extraterrestrial irradiance and solar zenith angle. The difference between modelled and measured spectral UVB irradiances was only 4% for a very clear day, but greater in less ideal conditions.

Li et al. [2000] built a model from ozone column, aerosol extinction optical depth, aerosol single scattering, reflectivity at 360 nm and 380 nm from TOMS or visible wavelength from NOAA/Advanced Very High Resolution Radiometer or Geostationary Operational Environmental Satellites. The validation was shown by *Wang et al.* [2000]. UVB (280-320 nm) and erythemal irradiances from the model were compared to the ground-based data measured at several Canadian sites, and the mean differences were found: 0.033 $mW \cdot m^{-2}$ for UVB irradiance, and 3.02 $mW \cdot m^{-2}$ for erythemal irradiances.

Parameterisation of daily UV irradiation was introduced by *Feister et al.* [2002]. This method used daily global and diffuse irradiation and the daily minimum solar zenith angle as input parameters. The results showed overestimation of modelled

values by 15% and 21% for UVA (315-400 nm) and UVB (290-315 nm), respectively.

Fioletov at al. [2003] estimated UV Index at 45 sites in Canada. Their model requires global irradiance, total ozone column and dew point temperature as input parameters. The modelled results generally agreed within 2%-3% compared to ground-based data. In Spain, UV Index was also estimated by using a simple parameterisation scheme presented by *Badosa et al.* [2005]. Solar zenith angle, total ozone column, altitude, aerosol optical depth and single scattering albedo were taken into account in the model. The results showed a bias of 4% when compared with ground-based data.

2.4.4 Empirical Models

Empirical models present relationships between UV irradiance and routinely measured meteorological parameters. This method has been explored by a number of authors as detailed below. It should be remembered that empirical relationships often only apply to the site where they were derived, and they should be used with caution at other locations.

The relation between UV and global radiation has been widely investigated [*Antón et al.*, 2005; *Cañada et al.*, 2000; *Cañada et al.*, 2003; *Feister et al.*, 2002; *Ilyas et al.*, 1999; *Kudish and Evseev*, 2000]. The studies presented either linear relations or multiple regressions between UV and global radiation in different areas such as Penang, Malaysia [*Ilyas et al.*, 1999] and Dead Sea and Beer Sheva, Israel [*Kudish and Evseev*, 2000] and Valencia and Cordoba, Spain [*Cañada et al.*, 2003]. Several attempts have been made to relate UV radiation to other parameters such as relative optical mass, clearness index [*Cañada et al.*, 2000; *Cañada et al.*, 2003], ozone column, reflectivity, aerosol index [*Antón et al.*, 2005] and sunshine duration [*Lindfors and Vuilleumier*, 2005; *Lindfors et al.*, 2003]. The differences between modelled and ground-based UV data can be quite large, e.g., 20% as shown by *Lindfors and Vuilleumier* [2005] and 5-27% as presented by *Antón et al.* [2005].

Apart from UV irradiance, several recent studies have developed empirical models to estimate UV Index by using data such as solar zenith angle and total ozone [*Allaart et al.*, 2004; *Sudhibrabha et al.*, 2004]. The model presented by *Allaart et al.* [2004] showed better performance than the model introduced by *Burrows et al.* [1994] at high solar zenith angles for the data of De Bilt (midlatitudes) and Paramaribo (Tropics). Another empirical model using the data of Thailand was presented by *Sudhibrabha et al.* [2004]. This study found the mean absolute percentage error of the residual of 7.5% compared with ground-based data.

2.4.5 Satellite Retrievals

The advantage of satellite retrievals is providing data with a global view; however, they need good algorithms and input data to calculate UV irradiance. Since the 1970s, satellite retrievals combined with radiative transfer models have been used to derive ozone, trace gases and erythemal irradiances at the earth's surface for the entire globe, initially using TOMS, onboard several satellites; Earth Probe, Meteo-3 and Nimbus-7, during 1978-2005. This has been superseded by OMI onboard the National Aeronautics and Space Administration (NASA) Aura spacecraft since July 2004 to continue monitoring of ozone, trace gases and retrieval of surface UV irradiance [*Levelt et al.*, 2006b; *Tanskanen et al.*, 2006]. The description of the OMI UV algorithm and products will be given later in Chapter 3.

Although satellite retrievals can provide data over a wide geographical distribution, they do so at relatively low spatial resolution, and ground-based validation of satellite data is required in any event. Initial studies compared TOMS UV data with ground-based UV data at several sites in Canada [*Fioletov et al.*, 2002; *Fioletov et al.*, 2004; *McKenzie et al.*, 2001], the U.S. [*DeLuisi et al.*, 2003; *Fioletov et al.*, 2004; *Sabburg et al.*, 2002], Garmisch-Partenkirchen, Germany and Lauder, New Zealand [*McKenzie et al.*, 2001], Ispra (Italy) and Thessaloniki (Greece) [*Arola et al.*, 2005; *Kazantzidis et al.*, 2006; *McKenzie et al.*, 2001], Sodankyla (Finland) and Bilthoven (Netherland) [*Kazantzidis et al.*, 2006], island of Campedusa [*Meloni et al.*, 2005], Ushuaia (Argentina), Palmer (Antarctica) and San Diego (California) [*Cede et al.*, 2004; *Kalliskota et al.*, 2000]. Overall, they found that the TOMS satellite data were generally higher than ground-based data. Biases, for cloud-free

conditions, were in the range of 5%-45%, and this can be larger for cloudy conditions. The differences between satellite data and ground-based data for clean areas (low aerosol) were lower than those for urban areas.

After the Aura spacecraft was launched, comparisons of the OMI based UV data and ground-based data became the focus of attention [*Buchard et al.*, 2008; *Ialongo et al.*, 2008; *Kazadzis et al.*, 2009a; *Tanskanen et al.*, 2007; *Weihs and Simic*, 2006; *Weihs et al.*, 2008]. Many of the studies used UV data from spectrophotometers to estimate ground-based spectral UV dose rates and daily doses for the northern high latitudes and midlatitudes, but several have used broadband measurements for comparison, e.g., *Ialongo et al.* [2008] and *Weihs et al.*, [2008]. The broadband data is often at higher time resolution and thus would allow the effects of rapidly changing conditions to be examined. Overall, results showed overestimation of UV product by OMI when compared with ground-based data; however, for some instances of snow covered surfaces OMI underestimated measurements compared to ground-based instruments as the bright scene from the snow covered surface was misinterpreted as cloud [*Tanskanen et al.*, 2007]. It would appear that the bias mainly results from aerosol absorption which is not accounted for in the satellite UV algorithm and therefore causes the satellite retrieval to overestimate surface UV when significant aerosols are present.

Several studies [*Arola et al.*, 2005; *Arola et al.*, 2009; *Cede et al.*, 2004; *Ialongo et al.*, 2010; *Kazadzis et al.*, 2009a; *Krotkov et al.*, 2005] have introduced various correction procedures to account for aerosol absorption with some success, e.g., the correction method in *Arola et al.* [2009] reduced bias by 5%-20% at midlatitude sites. It should be remembered that aerosols are not the only source of uncertainty in the satellite retrievals. Other sources include problems with defining surface albedo [*Tanskanen et al.*, 2007], cloudiness, and pixel inhomogeneities [*Kazadzis et al.*, 2009b; *Weihs et al.*, 2008]. These factors will be discussed in more detail in later chapters.

Having provided a general background to UV science in terms of radiative transfer, measurements and biological effects, the following chapters will detail efforts to improve satellite UV estimation in the UK and Thailand. The goal is to improve UV

estimation for areas with no ground-based measurement systems and provide a tool for public health applications.

Chapter 3 – Sites and Instrumentation

There are two main sources of UV irradiance data used in this thesis: ground-based measurements and satellite retrievals. This chapter will describe the sites, instruments and techniques used in acquiring the data that is analysed in subsequent chapters. It is separated into three main sections, descriptions of sites and instrumentation of the two different climate areas of concern: the Tropics (Thailand) and the midlatitudes (UK); and then the satellite retrievals.

3.1 Sites and Instrumentation in Thailand

3.1.1 Erythemal UV Irradiance Measuring Sites in Thailand

Thailand is a country in Southeast Asia, covering the latitudes from 5°N to 20°N and longitudes from 97°E to 105°E (see Figure 3.1). The climate of Thailand is classified as tropical wet and dry [*Met Office*, 2007], and characterized by two monsoons: the South-West monsoon (from mid-May to mid-October) causing rain over the whole country and the North-East monsoon (from mid-October to mid-February) which brings cold and dry air from China to northern and north-eastern parts but causes rain along the eastern side of the country. Between the two monsoons (from mid-February to mid-May), is the period April/May when the sun is highest in the sky for the country, and temperatures are greatest. The other period of highest sun coincides with the wet South-West monsoon. The northern part of the country is surrounded by the landmass of Southeast Asia with local industries and traffic, while the southern peninsula is surrounded by the Gulf of Thailand in the east and the Andaman Sea in the west, with resulting cleaner air than the north.

UV irradiance measurement in Thailand is coordinated at the Laboratory of Tropical Atmospheric Physics, Silpakorn University, Thailand, using broadband instruments in several selected parts of the country [*Janjai et al.*, 2009a; *Janjai et al.*, 2010; *Kift et al.*, 2006]. The four UV measurement sites in Thailand used in this study are at Chiang Mai (18.78°N, 98.98°E, 240 m a.s.l.), Ubon Ratchathani (15.25°N, 104.87°E, 122 m a.s.l.), Nakhon Pathom (13.82°N, 100.04°E, 30 m a.s.l.) and Songkhla

(7.20°N, 100.60°E, 4 m a.s.l.), as shown in Figure 3.1. These sites cover the four main climatic regions of Thailand. Chiang Mai is a city in northern Thailand. It has the highest altitude of the four sites with a relatively cool, dry season in winter, and is situated in a natural bowl which tends to trap pollutants. Development within the city drives air pollution to high levels. Nakhon Pathom is a suburb of Bangkok characterised by urban and industrial aerosols with a dry season in winter. Ubon Ratchathani is in the Northeast of Thailand with a dry season in winter, and the industry is of a more agricultural nature than the other two cities. These cities are also influenced by seasonal biomass burning during January to April when rice straw is burnt after harvesting [*Janjai et al.*, 2009b]. Songkhla is in the Southeast of Thailand on the coast of the Gulf of Thailand, which has mild weather and is wet for the whole year. Tourism is the main industry and the aerosols are under a maritime influence.

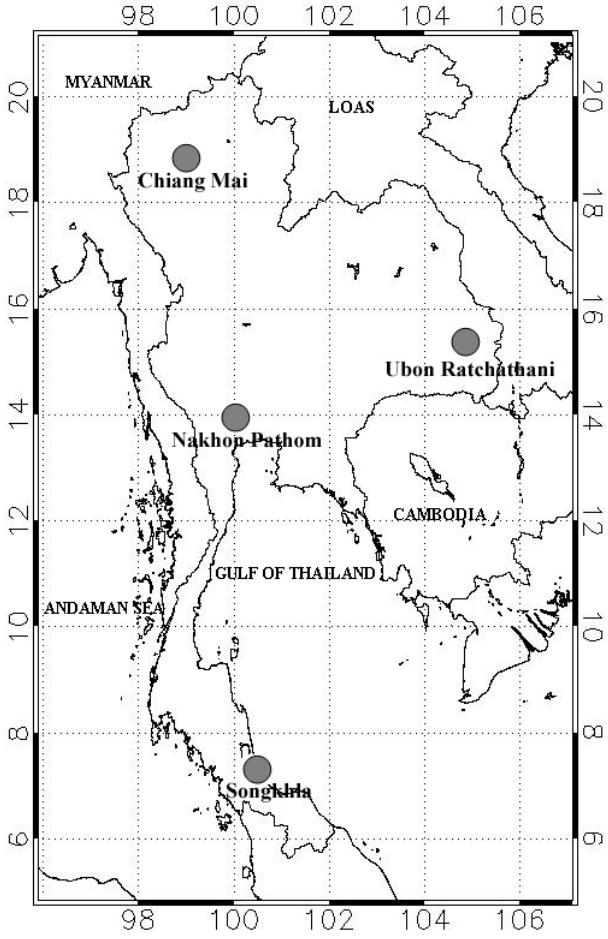

Figure 3.1 The positions of Thailand sites.

The instruments are mounted at a height of about 1.5 m to 2.0 m above the local platform surface, close to the standard height for radiation instruments, allowing for observation and cleaning of the domes. The local platforms are flat roof tops which enable the instruments to be unshaded and with a clear view of the horizon despite local buildings and vegetation.

3.1.2 Broadband Instrument Measuring Erythemal UV Irradiance in Thailand

For long-term outdoor measurement, broadband UV radiometers of Solar Light Company Inc. (Solar Light, Pennsylvania, USA) have been installed at the four sites. The first radiometers were purchased in June, 1997 for Nakhon Pathom, and in November, 1997 for Chiang Mai. After several years two other radiometers were installed at Songkhla in July, 2000 and at Ubon Ratchathani in August, 2000. Another UV-Biometer was purchased in year 2003, for use as a travelling standard for calibration purposes.

3.1.2.1 Specifications

The broadband radiometers installed at the four sites of Thailand are the UV-Biometer (model 501) of the Roberson-Berger type meter [*Morys and Berger*, 1993]. The UV-Biometer is designed to measure erythemally weighted UV irradiance, which means the spectral response of the meter approximates the sunburn (erythema) response of human skin to UV radiation. The radiometer consists of a quartz dome, black glass filter, green glass filter, GaAsP diode, diode insulator, Peltier element, heat conductor, and desiccators, as shown in Figure 3.2.

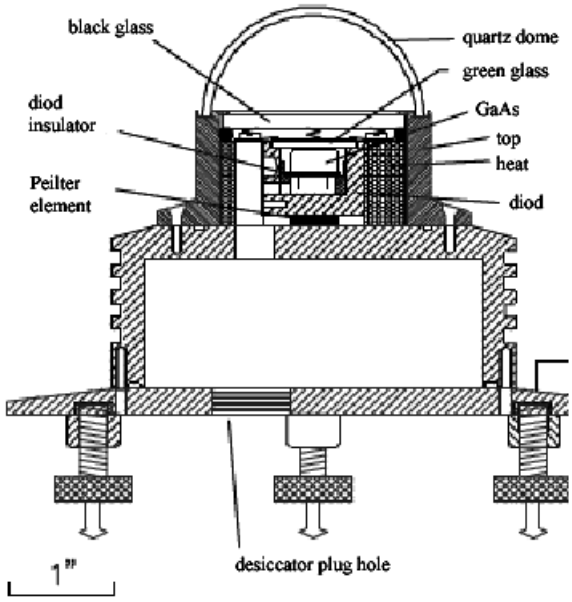

Figure 3.2 Diagram of a UV-Biometer detector [*Morys and Berger*, 1993].

Of the radiation incident on the quartz dome, the visible and infrared radiation is absorbed by the black filter while UV radiation can pass through to the phosphor. The phosphor absorbs the UV light and then re-emits it as green light. The green light from the phosphor passes a green glass filter, which blocks any red light passed by the black filter. The remaining light is detected by a solid state (GaAs) photodiode. The phosphor, green filter and photodiode assembly together is surrounded by a good heat conductor for temperature stabilization. The combination of the phosphor and GaAs responses together provide an instrument that can be used as an erythemal UV sensor since it has a spectral response close to the erythemal action spectrum defined by CIE [*McKinlay and Diffey*, 1987] as seen in Figure 3.3 (the figure of spectral response of the travelling standard UV-Biometer measured in Manchester, 2009, can be seen in Appendix 1, which includes the experimental details). The signal from the photodiode, which is proportional to the erythemal radiation, produces a current and it is transferred to a data recorder.

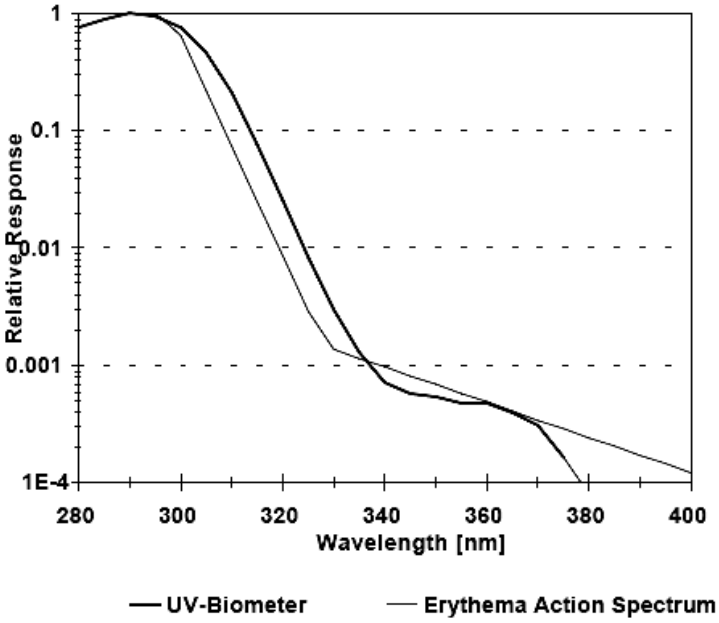

Figure 3.3 Typical Spectral response of the UV-Biometer [*Morys and Berger*, 1993].

The incident radiation on a horizontal surface varies as the cosine of the zenith angle of incidence. This dependency is usually called the "*cosine law*" and ideally the angular response of a radiometer for irradiance should mimic this cosine dependency. However, imperfections of the quartz dome, reflections from the surface of the dome and black filter, non-uniformity of the phosphor and shading of the sensor for high incident angles are causes of deviations in angular response. In general, the angular response of this type of detector is within a 5% error of the ideal cosine response for incident zenith angles less than 60°, and less well matched at larger angles (see Figure 3.4) [*Webb*, 1998]. The experimental details of cosine response for the travelling standard UV-Biometer measured in Manchester, 2009, can be seen in Appendix 1.

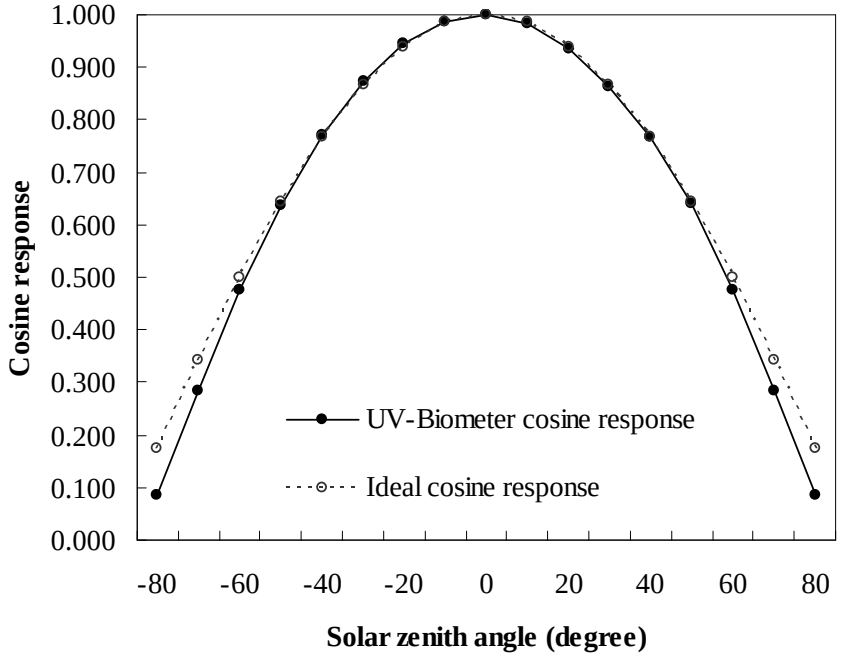

Figure 3.4 The actual cosine response of the UV-Biometer (s/n 5809) measured by the manufacturer compared with the ideal cosine function.

3.1.2.2 Data Acquisition

The electrical signal from the UV-Biometer must be recorded on a suitable data logger. In order to collect data from the instrument, the radiometer at each site is connected to the data logger (DC100) and chart recorder of Yokogawa (Japan) as shown in Figures 3.5 and 3.6. The chart recorders are a backup which are used only when the data loggers fail, and for a quick visual check that data recording is proceeding normally. The data logger is set to sample the voltage output from the radiometer every second and then records the averaged value every ten minutes.

Figure 3.5 A data logger of Yokogawa.

Figure 3.6 A chart recorder of Yokogawa.

These data are sent to the Laboratory of Tropical Atmospheric Physics, Silpakorn University. The voltage signals are then converted to erythemal irradiance by using conversion factors in $V/(W \cdot m^{-2})$ from the manufacturer and field calibrations, and corrected for spectral and cosine errors. The conversion factor is initially provided in calibration information from the manufacturer, but must be checked at regular intervals. In addition, the single conversion factor does not give true erythemal irradiance in all conditions unless the instrument response exactly matches the human erythemal response. Thus the calibration must be adjusted for the interplay of this mismatch with the changing solar spectrum due to changing ozone and solar zenith angle.

To convert the raw data from the data logger to erythemally weighted UV irradiance, Equation 3.1 [*Webb et al.*, 2006] was used to calculate the UV irradiance and apply the spectral response and cosine response functions.

$$E_{CIE} = (U - U_o)Cf(\theta_z, TO_3)Coscor \qquad (3.1)$$

where E_{CIE} is the erythemal effective irradiance,

U and U_o are the raw and dark signals from the detector,

C is the absolute calibration factor,

$f(\theta_z, TO_3)$ is the normalisation spectral response function , and

Coscor is the cosine correction function.

The value of U is collected from the radiometer during day time at the specified measurement time (unit of voltage) while the value of U_o is the value measured at night in the same units (i.e. the dark signal). C is a constant value used for converting the voltage to irradiance ($W \cdot m^{-2}/V$) verified for a specific set of conditions. For instance, for the model 501 UV-Biometer, the condition is at solar zenith of 30°, total ozone column of 270 DU, zero albedo and sea level. The function of $f(\theta_z, TO_3)$ for each site can be determined by using a uvspec radiative transfer model (see Chapter 2) to give a matrix for the differences from these baseline conditions, dependent on solar zenith angle and total ozone following Equation 3.2 [*Webb et al.*, 2006], as shown in Figure 3.7. The limitations of the matrix are: solar zenith angles are in the range of 0° to 90° with 1° step, and total ozone column are in the range of 200-400 DU with 1 DU step.

$$f(\theta_z, TO_3) = \frac{\int CIE(\lambda)E_{rad}(\lambda)d\lambda}{\int SRF(\lambda)E_{rad}(\lambda)d\lambda} \qquad (3.2)$$

where $CIE(\lambda)$ is the CIE erythemal action spectrum [*McKinlay and Diffey*, 1987],

$SRF(\lambda)$ is the response of the radiometer,

$E_{rad}(\lambda)$ is a set of solar spectra calculated with uvspec for different solar zenith angles and total ozone column,

λ is wavelength.

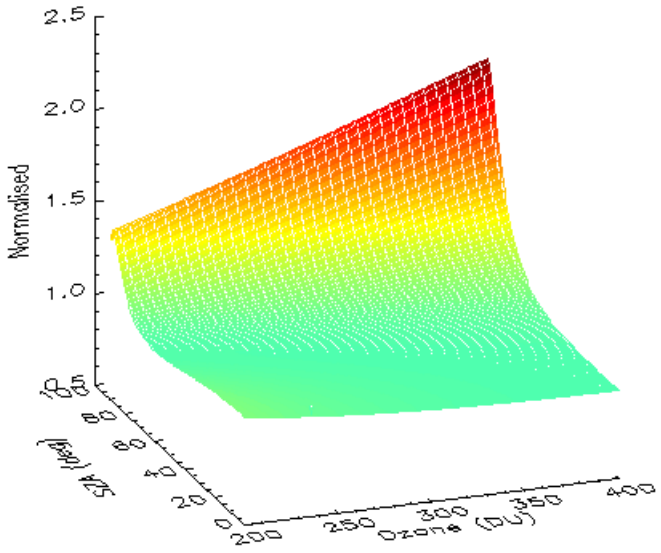

Figure 3.7 The normalisation of spectral response function.

For the cosine error correction (Coscor), since the actual cosine response of the instruments is not the same as the ideal cosine function, this can result in systematic measurement errors. The magnitude of the cosine error depends on the "*state of the sky*" such as zenith angle and cloud cover, which determine the radiance distribution i.e. the pattern of the direct and diffuse components across the hemisphere [*Hülsen and Gröbner*, 2007; *Webb*, 1998].

To correct the cosine error, the following equations have been used [*Hülsen and Gröbner*, 2007].

$$\text{Coscor} = \frac{1}{f_{glo}} \tag{3.3}$$

$$f_{glo} = f_{dir}\frac{E_{dir}}{E_{glo}} + f_{dif}\frac{E_{dif}}{E_{glo}} \tag{3.4}$$

where f_{glo} is the global cosine error and E_{glo} is the global radiation which is the sum of the direct radiation, E_{dir}, and the diffuse radiation, E_{dif}. The values of E_{dir} and E_{dif} can be obtained from measurement or models. f_{dir} is the direct cosine error which is the angular response function (ARF) that can be obtained in a laboratory, and f_{dif} is the diffuse cosine error which can be calculated from the following equation assuming a homogeneous radiance distribution integrated over the whole hemisphere.

$$f_{dif} = 2\int_{0}^{\pi/2} ARF(\theta)\sin(\theta)d\theta \qquad (3.5)$$

where θ is solar zenith angle.

3.1.2.3 Calibrations

A full calibration of the UV-Biometer can be divided into three main steps: spectral response, angular response and absolute calibration (see Appendix 1). The first two steps are performed in a laboratory with standard lamps while the absolute calibration is performed with respect to a standard instrument and the sun as source.

The absolute calibration factor can be obtained by using a reference spectroradiometer. The calibrated detector is placed against the reference spectroradiometer on a roof to measure the radiation from the sun. Then the absolute calibration factor can be calculated from the equation below [*Hülsen and Gröbner*, 2007].

$$C = \frac{E_D}{U_D - U_{offset}} \times \frac{1}{Coscor} \times \frac{1}{f_o} \qquad (3.6)$$

where C is the absolute calibration factor and E_D is the spectrum weighted with the detector spectral response. U_D and U_{offset} are the raw and dark signal measured by the detector. Coscor is the cosine error correction and f_o is the normalization spectral response factor as mentioned above. For details of the calibration of UV-Biometer (s/n 5809) against a double monochromator in Manchester, 2009, see Appendix 1.

Regarding the instruments in Thailand [*Janjai et al.*, 2009a], these UV-Biometers were originally calibrated to National Institute of Standards and Technology (NIST) traceable standards via quartz-halogen lamps by the Solar Light facility in Pennsylvania, USA. By using the fifth UV-Biometer as a travelling standard, the calibration factors at each site have been reviewed annually by an on-site intercomparison between the standard and each site instrument using the method in *Webb et al.* [2006]. Prior to 2003, one site instrument per year was sent to Solar Light for characterisation and recalibration, and then used to check the calibrations at the other sites through intercomparison. The cosine responses showed little change while the spectral responses altered gradually with time causing changes in calibration factors that were within 1.5% over an 8-year period [*Janjai et al.*, 2009a]. The spectral response of the fifth, travelling standard instrument was checked in Thailand in 2008 and both cosine and spectral responses were independently checked in Manchester in 2009: the cosine response showed little change from the original (within the measurement uncertainties ~ 2%), while there had been a small shift in the spectral response at longer UVA wavelengths. However, the spectral response check in 2008 in Thailand showed no significant change in response. So we take the statement of *Janjai et al*. [2009a] that this travelling instrument was stable for the period of concern. Therefore, the original cosine and spectral responses from the manufacturer have been used throughout since any observed changes during recalibration have been small. The estimated overall uncertainty of the radiometer is within ±8% [*Janjai et al.*, 2009a].

3.1.2.4 Maintenance

The quality of data also depends on maintenance of the instruments. The instruments at the four Thai sites are well maintained with daily cleaning of the quartz dome, regular changing of the desiccants and annual field calibrations under clear sky conditions. Additionally, the instruments are transported to the manufacturer periodically to calibrate the angular response, the spectral response and the absolute calibration in the laboratory.

3.2 Sites and Instrumentation in UK

3.2.1 Erythemal UV Irradiance Measuring Sites in UK

The UK is a country at northern midlatitudes, covering the latitudes from 50°N to 60°N and longitudes from 8°W to 2°E. The UK climate is classified as the cold temperate (or maritime, west coast) [*Met Office*, 2007], which has unpredictable weather. It can be sunny, raining, and cloudy in one day. These weather patterns can occur in summer as well as winter. The four seasons of the UK are: spring (March to May), summer (June to August), autumn (September to November) and winter (December to February). The main influence on the climate is from the Atlantic Ocean. The weather in the UK is very variable with large inter-annual differences, and can be under the influence of air masses from both the Arctic and the Tropics, and either continental or maritime in origin.

In this study, there are nine UK sites where UV irradiances are measured; Camborne (50.22°N, 5.32°W, 85 m a.s.l.), Chilton (51.58°N, 1.32°W, 122 m a.s.l.), Glasgow (55.86°N, 4.34°W, 9 m a.s.l.), Kinloss (57.64°N, 3.56°W, 5 m a.s.l.), Leeds (53.85°N, 1.61°W, 164 m a.s.l.), Lerwick (60.14°N, 1.19°W, 79 m a.s.l.), Snowdon (53.07°N, 4.08°W, 1025 m a.s.l.), Manchester (53.47°N, 2.23°W, 43 m a.s.l.) and Reading (51.44°N, 0.94°W, 67 m a.s.l.) as shown in Figure 3.8. The last two sites provide spectral data, while the remainder operate broadband instruments similar to those in Thailand.

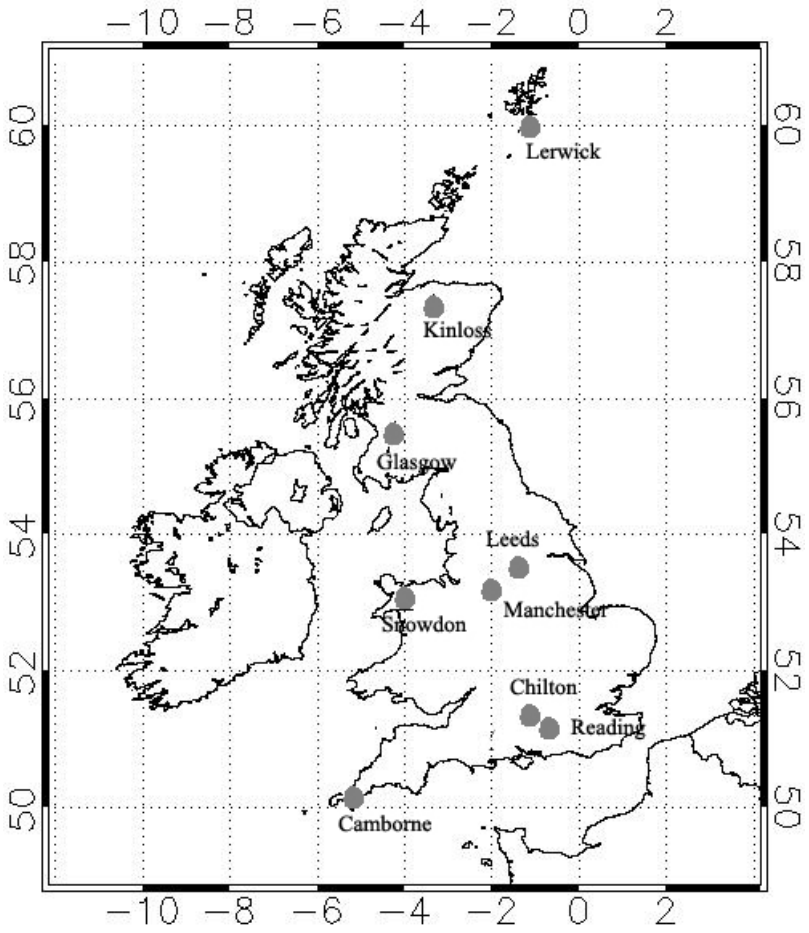

Figure 3.8 The position of nine stations in the UK.

3.2.2 Broadband Instruments

There are seven broadband instruments [*Pearson et al.*, 2006] in UK used in this study. Three of them; Chilton, Leeds and Glasgow, are at Health Protection Agency (HPA) sites, and were installed in 1988. A further three instruments installed at Camborne and Lerwick since 1993, and Kinloss since 1995 are based at UK Meteorological office sites. Another instrument supported by a Welsh Assembly Grant has been on the mountain of Snowdon since 2003. The data collection and analysis, and calibration of all instruments are overseen by HPA.

3.2.2.1 Specifications

These networks have used two versions of broadband instruments; model 500 (RB-500) and model 501 (RB-501) of Robertson-Berger meters. Initially, RB-500 meters were used at the all sites except at Snowdon. Currently, these instruments are still used at Camborne, Kinloss and Lerwick, while they have been replaced by RB-501 meters at Chilton in October, 2004 and at Leeds and Glasgow in May 2005. For Snowdon, a RB-501 meter was installed in 2003. The specifics of the model 501 Roberson-Berger meter have been described above. The RB-500 meter was the earlier version: it used a vacuum photodiode rather than the solid state version, and did not have the same temperature stabilisation [*Pearson et al.*, 2004].

3.2.2.2 Data Acquisition

The erythemal irradiance data from the instruments is converted from analogue to digital data and then transferred to processing computers. The data from these instruments is recorded every 20 seconds and then averaged over five minutes, and then the calibration applied to give irradiances. For Snowdon, since the location of this instrument is on the mountain of Snowdon, the data is limited by the power supply taken from a railway station. Therefore, the data of this site can be recorded only about six months per year from April/March to September/October when the tourist train is operating. For missing data, any small data gap is filled by the average data on either side of the gap, and large data gaps cause rejection of the whole day in climatological data analysis.

3.2.2.3 Calibrations

All these instruments are field calibrated using a standard broadband instrument. Usually, the field calibration is held in July. The standard is calibrated against a double monochromator scanning spectroradiometer which is calibrated against deuterium discharge lamps traceable to the National Physical Laboratory. The overall uncertainty is estimated at 9% for RB-500 and 4% for RB-501, based on uncertainties of national standard, transfer standard, spectral response, temperature response, linearity, angular response and offset [*Pearson et al.*, 2000].

3.2.3 The Bentham Spectroradiometer

The Bentham spectroradiometer model DMc150 is one version of the spectroradiometers manufactured by Bentham Instruments Limited (Reading, UK). It is a double monochromator with the advantage of reduced straylight compared with a single monochromator. There are four basic units of the instrument: input optics, monochromator, detector, and control and logging system (see Figure 3.9). The input optics of DMc150 are usually made from Teflon for UV measurement. The cosine response of the diffuser, measured using a 1000 W quartz halogen lamp, is wavelength independent. The radiation is transferred to the monochromator through the quartz fibre optic cable.

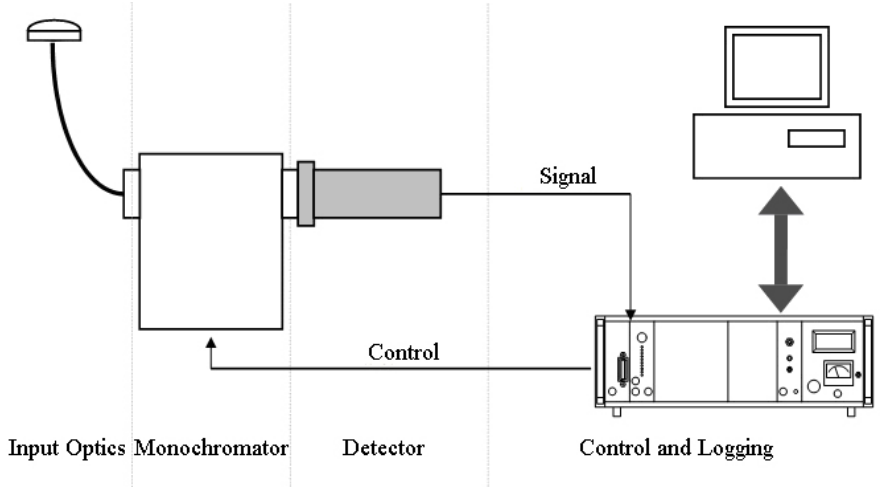

Figure 3.9 Basic components of a spectroradiometer system [*Bentham Instruments Ltd*, 1997].

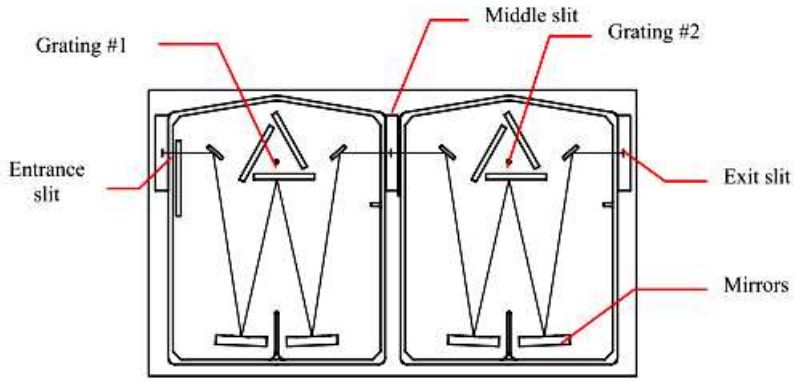

Figure 3.10 Schematic elements of a Double Monochromator [*Bentham Instruments Ltd*, 1997]. The layout of the DMc150 is slightly different, but the basic elements are the same.

The double monochromator (see Figure 3.10) packed in the "*envirobox*" (a temperature stabilisation system) consists of mirrors and 1200 lines/mm gratings with the reciprocal dispersion 2.7 nm per mm. The mirrors are used for directing the radiation from the entrance slit, which reduces straylight. Then the light is separated into its specific wavebands at the first diffraction grating. At the middle slit of the DMc150 double monochromator, there is a filter wheel used for the purpose of limiting the signal at the detector, which is a PMT, and for measuring the dark current. Further dispersion occurs at the second grating and the light is then directed wavelength by wavelength, as the gratings turn, onto the PMT thus building a complete spectrum. The bi-alkali end window PMT is selected for low dark current noise and for low hysteresis. The wavelength dependent electrical signals from the PMT are converted to corresponding irradiance values in units of $mW \cdot m^{-2} \cdot nm^{-1}$ by way of the calibration. A computer is used for controlling and logging the system.

The Bentham instrument has been located in a small building at the University of Reading since August 1999. The input optic mounted on the roof is connected to the double monochromator and the PMT mounted in the envirobox inside the building, by way of the fibre optic cable. Both sections are also connected to the control and logging system as can be seen in Figure 3.11.

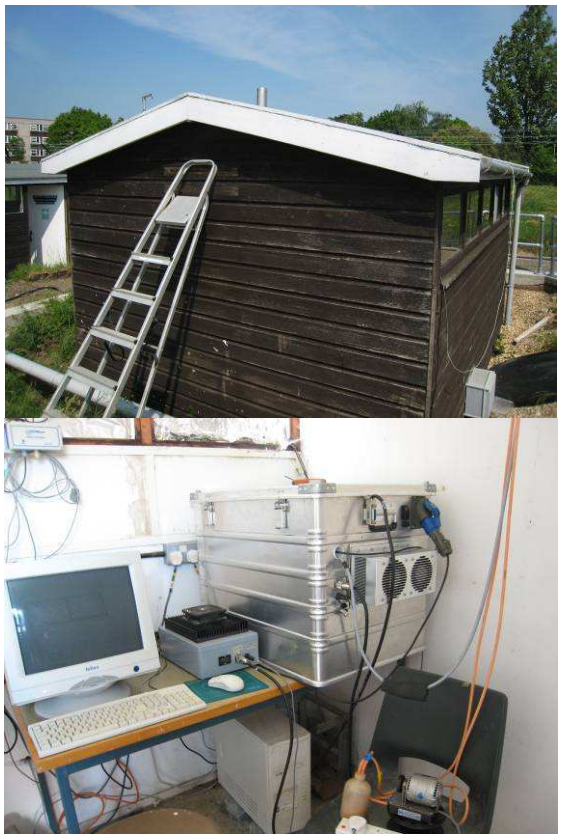

Figure 3.11 The Bentham DMc150 installed at the University of Reading.

Raw data from the Bentham is automatically collected from sunrise to sunset every half an hour. The spectral irradiance is scanned from 290 nm to 500 nm with a step of 0.5 nm, and the spectral calibration file applied. A single scan takes approximately five minutes. Furthermore, SHICrivm software [*Slaper et al.*, 1995] is used for routine QC of the measurements. This package, now widely used, assesses and corrects small wavelength inaccuracies in the spectral data, and then provides spectra as they would appear if measured by an instrument with a triangular slit function of 1 nm FWHM, as well as the wavelength corrected spectra with the instrument's true slit function. Ideally, a spectroradiometer would have an infinitely narrow slit function to truly measure monochromatic light. In practice, this is not possible and there is always a trade off between signal, dispersion and slit function. However, with a rapidly changing signal with wavelength (as in the solar UV) different slit functions will incorporate different amounts of straylight into a pseudo-monochromatic signal. Normalising the slit function effect to a standard function, as SHICrivm does, makes it easier to compare data from different instruments. The

package also makes a number of other quality control checks for shape-errors, spikes and variability, for example, and returns a number of coloured QC flags for each spectrum. The quality controlled data is then available and can be accessed from ftp://o3uvdata.seaes.manchester.ac.uk/. The output data file called as "*level_1*" from the database contains the metadata information, wavelength, and the measured spectral irradiance in unit of $mW \cdot m^{-2} \cdot nm^{-1}$.

The erythemal irradiance from the raw data can be calculated by using Equation 2.2 (see Chapter 2). After that the erythemally weighted UV irradiance at the lowest solar zenith angle of the day is selected to represent the irradiance at local solar noon. Note that the erythemal irradiance at solar local noon from the Bentham DMc150 used in this study is not always exactly at true solar noon value since measurements are made only every 30 minute, but the time difference is no more than 15 minutes.

Calibration of the instrument is required more frequently than for the broadband radiometers since the double monochromators with their moving parts, and the high voltage PMT detectors, are inherently less stable than the simpler radiometers. The wavelength calibration (or check of wavelength alignment of monochromator) should be performed first, and then the irradiance calibration should be checked. The initial method of calibration in the laboratory (see Figure 3.12 with the DMc150 in place of the DTM300) uses a 1000 W FEL tungsten halogen lamp as a primary standard lamp with known spectral output, traceable to NIST, and certificated by Optronics Laboratories, Florida, USA. The output of the lamp is stable and smooth from UV to infrared ranges [*Webb*, 1998].

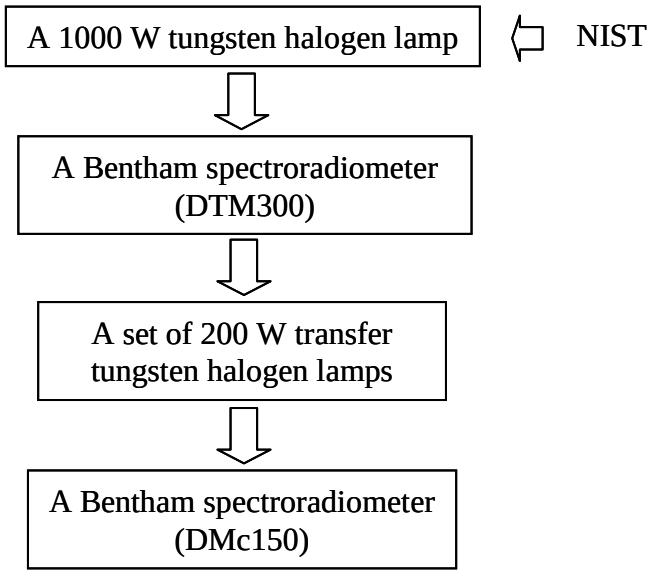

Figure 3.12 The diagram of calibration process for spectrophotometers.

Thereafter the DMc150 is calibrated in the field, at monthly intervals or more frequently if circumstances dictate, using the transfer standards that are themselves calibrated via the DTM300 (Figure 3.12). The uncertainty incurred in the calibration process can be about 1% including uncertainties of alignment and orientation, stability of the detector, statistical noise, nonlinearity and straylight, additional to the 2%-3% uncertainty inherent in a new standard lamp. Since the standard lamp is not field equipment, a set of several 200 W DXW tungsten halogen standard lamps, in fixed mounts that attach uniquely to the input optics, are used as transfer (or travelling) standard lamps. The uncertainty of transfer lamps is approximately 3%-5% with wavelength dependence, including uncertainties due to statistical noise, current regulation of the lamps, and transportation and long-term use of the lamps [*Gröbner et al.*, 2005]. During the monthly calibration checks, changes of less than 2% are deemed to be within the stability and uncertainties of the calibration process and no changes are made to the calibration. From results of the calibration check during 2004-2007, mean changes were considerably less than 2% and only occasional adjustments to the calibration were required. In addition, external quality assurance of the data has come through a series of international intercomparisons (of this instrument or its predecessor, e.g., *Bais et al.* [2001]; *Webb*, [1997] and *Gröbner et al.* [2005]), and more recently on-site comparison with a travelling standard instrument developed within the European Union project Quality Assurance of Solar

UV Measurements in Europe (QASUME). The results showed the deviations of the Bentham at Reading relative to the QASUME reference spectroradiometer were 1% in the UVB (305-315 nm) and 2% in the UVA (above 315 nm) [*Gröbner et al.*, 2006].

3.2.4 Brewer Spectrophotometers

Brewer instruments, of which there are several models, are a type of spectrophotometer originally intended for automatic, total ozone measurements in the UV range by using either direct sunlight or diffuse sky light from the zenith. They can also measure spectral irradiance in a limited wavelength range (dependent on model) by using a quartz dome and Teflon diffuser. Recently, more than 200 of the instruments have been used globally [*Kimlin et al.*, 2003; *Sci-Tec*, 1996; *Tanskanen et al.*, 2007; *WMO*, 2008].

The general system of the instrument consists of three main sections: foreoptics, spectrometers, and a PMT detector as shown in Figure 3.13. For the foreoptics, incoming light is incident at zenith prism (ZP1), which by rotating can direct radiation into the monochromator from different sources: quartz window, calibration lamps or UV diffuser. For zenith angles between 0° and 90°, the sunlight and sky light passes through an inclined quartz window. At zenith angle 180° the spectrometer points to the calibration lamps, and at -90° a Teflon UV diffuser occupies the field of view (FOV) as shown in Figure 3.14. The light from the prism is then passed through several lenses and three control elements (iris diaphragm (IR1), filter wheel#1 (FW1) and filter wheel#2 (FW2) which control intensity for ozone, UV and lamp measurements) to a mirror (SM1). At the mirror, the light is reflected to a moveable grating (GR1) where the light is dispersed. The spectrum is then reflected and focused by the mirror on the plane of cylindrical slit mask (SL1) consisting of six exit slits (EX1). A stepper motor can control the slit mask positions to allow the spectrum to enter one of the six exit slits. In the double monochromator (Mark III) instrument the spectrum is then focused onto another grating (GR2) by another mirror (SM2). Finally, the spectral elements passing through the

spectrometer are amplified by the PMT detector and photon counts (raw counts) are then transmitted to a counter.

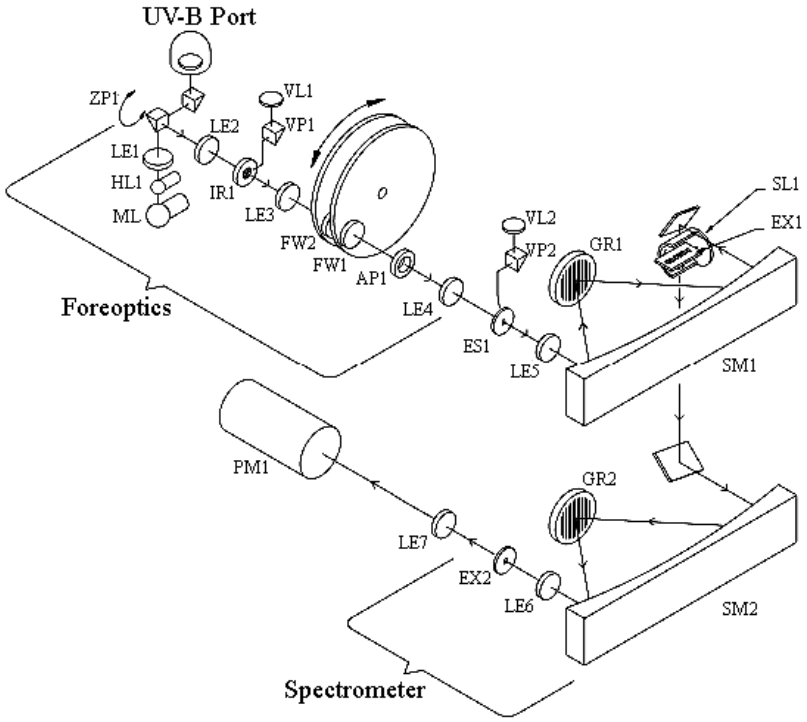

Figure 3.13 Optical Elements of Brewer Spectrophotometer [*Sci-Tec*, 1999].

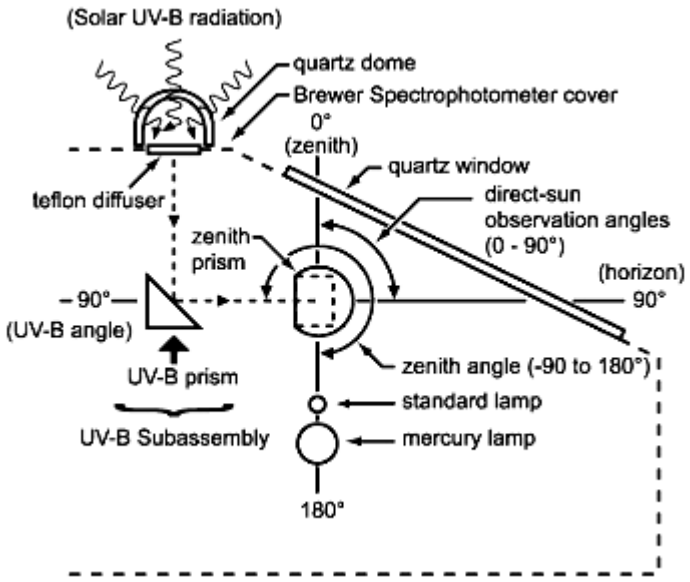

Figure 3.14 Zenith prism targets [*Sci-Tec*, 1999].

The spectrophotometer located on the roof of the Pariser building at the University of Manchester is a Brewer Mark III model (Figure 3.15) which is a double monochromator spectroradiometer, and the spectroradiometer at the University of Reading is a Brewer Mark IV single monochromator (Figure 3.16).

Figure 3.15 The Brewer spectrophotometer (#172) installed at the University of Manchester.

Figure 3.16 The Brewer spectrophotometer (#075) located at the University of Reading.

For ozone measurement at zenith angles between 0° and 90°, the grating (GR1) is fixed to adjust the light onto the slit mask that selects single wavelengths used for total ozone calculation. From the slit mask positions selected, the direct sun is measured at six wavelengths: 303.2 nm, 306.3 nm, 310.1 nm, 313.5 nm, 316.8 nm and 320.1 nm, with resolution of 0.6 nm [*Sci-Tec*, 1995]. The spectral radiation is counted and amplified in term of photon counts by using PMT. Total column ozone can be calculated by using differential absorption of selected wavelengths in the UV range, a process performed by the Brewer software.

To monitor UV irradiance, the spectral UV data can be collected by using the quartz dome and Teflon diffuser for the zenith angle prism of -90°. The slit mask (SL1) is fixed to allow for dark count measurement. The grating (GR1) is moved to enable UV wavelengths to reach the PMT in turn as the wavelength incident on the slit changes with the grating rotation. The software for UV measurement is set to scan from 286.5 nm to 363.0 nm for Mark III and from 290.0 nm to 325.0 nm for Mark IV, in steps of 0.5 nm, which takes about six minutes to complete. The raw counts are converted throughout to counts per second and corrected for instrument dead time. Then the corrected raw counts are divided by the instrument response values and multiplied by the erythema weighting value at each wavelength (see Equation 2.2). The weighted spectrum is then integrated to give the erythemal irradiance. Note that the Brewer UV spectral data do not extend across the full waveband of erythemally effective UV (290-400 nm), although the most erythemally effective wavelengths are measured. However, the erythemal data used in this thesis was corrected automatically for the missing wavelength by the retrieval software of the Brewer spectrometer. The uncertainty incurred by the lack of longer UVA wavelengths is less than 2% for the solar zenith angle less than 70° [*Fioletov et al.*, 2003; *Fioletov et al.*, 2009].

The wavelength calibration of the instruments is performed regularly by using the internal mercury lamp and the sensitivity of the instruments is monitored by using an internal halogen lamp. Regarding the intercomparison of Brewer#075 and #172 in 2005, 2007 and 2009, the UV calibration of the Brewer spectrophotometers was maintained in between the ozone calibration intercomparisons by calibration checks

against a series of 50 W tungsten halogen lamps, which allow any drift in the calibration to be identified. If necessary the UV operation of the Brewer can be calibrated with NIST traceable 1000 W tungsten halogen lamps. The new response files of years 2007 and 2009 were compared with the calibration file of year 2005, and the results for both instruments showed the stability of the systems with the differences within 8% for Brewer#075 and 3% for Brewer#172. The results of ozone data showed the agreement within approximately ±2 DU.

3.3 Overall Uncertainty of Ground-Based Instruments

The broadband radiometer has a typical uncertainty of 7.2% or more. This includes the uncertainty of calibration procedure (~3.1%), the uncertainty of converting from detector weighted irradiance to erythemally weighted irradiance (~1.7%), and the uncertainty of the cosine correction (1.7%-4.3%) [*Hülsen and Gröbner*, 2007]. However, as discussed earlier, the broadband radiometers used in this study have the overall uncertainties within ±9% (i.e., ±8% for the Thai sites, and ±4 to ±9% for the UK sites).

Overall uncertainty in spectral UV data measured by carefully calibrated and maintained Bentham and Brewer spectrometers is usually less than that from broadband radiometers. The uncertainty of UV irradiance measured by Brewer spectrometer is estimated to be within ±6% depending on sites for all known major sources of error such as straylight and cosine error [*Sabburg et al.*, 2002] and within ±5%, measured by Bentham spectrometer [*Webb et al.*, 1999].

3.4 The Ozone Monitoring Instrument

3.4.1 General Information

The Ozone Monitoring Instrument is one of the instruments onboard NASA Earth Observing System (EOS) Aura spacecraft. It was launched on 15 July, 2004 [*Levelt et al.*, 2006a], and from 6 September, 2004 OMI has measured the composition of the earth's atmosphere on a global scale [*Tanskanen*, 2008].

Aura/OMI is a sun synchronous polar orbiting satellite passing near the earth's poles at an altitude of around 705 km above the earth's surface, with an inclination of 98.2° [*Laan et al.*, 2001; *Levelt et al.*, 2006b]. The telescope of OMI provides a large FOV of 114° as can be seen in Figure 3.17. This results in a higher spatial resolution (13 km×24 km at nadir) compared with TOMS and GOME. The resolution can reach up to around 13 km×150 km at the largest swath-angle (57°) [*Levelt et al.*, 2006b]. OMI is a nadir-viewing spectrometer with a 2600 km wide swath that can cover most of global area in a day using a two dimensional charge-coupled device detector. One dimension detects the spectral information and another detects the spatial information. The equator overpass time of the satellite is usually about 1:45 pm local solar time, which can be varied by ±50 minutes, and at high latitudes there are often several overpasses per day [*Tanskanen et al.*, 2007].

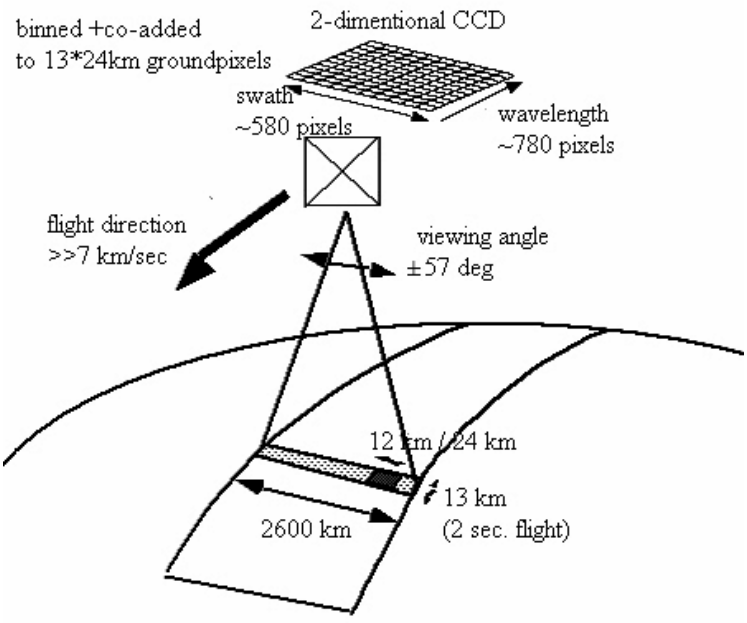

Figure 3.17 OMI measurement principle modified from *Levelt et al.* [2006b].

The instrument contains two spectrometers measuring the earth radiance and solar irradiance spectrum between 270 nm and 500 nm, covering UV and visible ranges. The light entering the telescope and then passing a polarization scrambler is split into two channels: the UV channel (270-365 nm) and the Visible channel (365-500 nm), using a dichroic filter. The UV channel is divided into two sub-channels: UV-1 (270-

310 nm) and UV-2 (310-365 nm) [*Levelt et al.*, 2006b], to reduce an excess of straylight below 290 nm.

OMI requires not only on-ground but also in-flight calibration [*Levelt et al.*, 2006b]. The on-ground calibration provides several parameters, for example, absolute radiance, absolute irradiance, straylight, detector and electronics characteristics. The purpose of the in-flight calibration is for measuring the sun once per day using an internal white light source and light emitting diodes to check the overall performance. More extensive information about the OMI calibration can be also seen in *Laan et al.* [2001] and *Dobber et al.* [2006].

With regard to the science objectives [*Levelt et al.*, 2006a], OMI can provide data on trace gases including Ozone, Nitrogen dioxide, Sulphur dioxide, Formaldehyde (HCHO), Bromineoxide (BrO) and Chlorinedioxide (OClO). Furthermore, OMI can also retrieve aerosol characteristics, cloud top heights and surface UV irradiance. In this thesis, we aim to use the OMI surface UV irradiance and OMI aerosol data.

3.4.2 Surface Ultraviolet Irradiance from OMI

3.4.2.1 OMI Surface UV Algorithm

The OMI UV algorithm is based on the TOMS UV algorithm developed by NASA Goddard Space Flight Centre [*Eck et al.*, 1995; *Krotkov et al.*, 1998; *Krotkov et al.*, 2001; *Tanskanen et al.*, 2006]. However, the OMI UV product has a higher spatial resolution of 13×24 km^2 at nadir. The OMI surface UV algorithm relies on "*TOMRAD*" radiative transfer model [*Dave*, 1964] and input data such as total column ozone from OMI and climatological surface albedo based on TOMS data [*Tanskanen*, 2004]. Firstly, clear sky UV irradiance is calculated by assuming that the atmosphere has no cloud and no aerosols. Then the clear sky irradiance is multiplied by a cloud and nonabsorbing aerosol correction factor (i.e., aerosol scattering which is included in the backscatter measurement) derived from further OMI products, e.g., the measured 360 nm radiance at the overpass time. Note, however, that the backscatter measurements on which this correction is based still do

not fully probe the lower boundary layer and the aerosols therein [*McKenzie et al.*, 2008]. An overview of the OMI UV algorithm is shown in Figure 3.18.

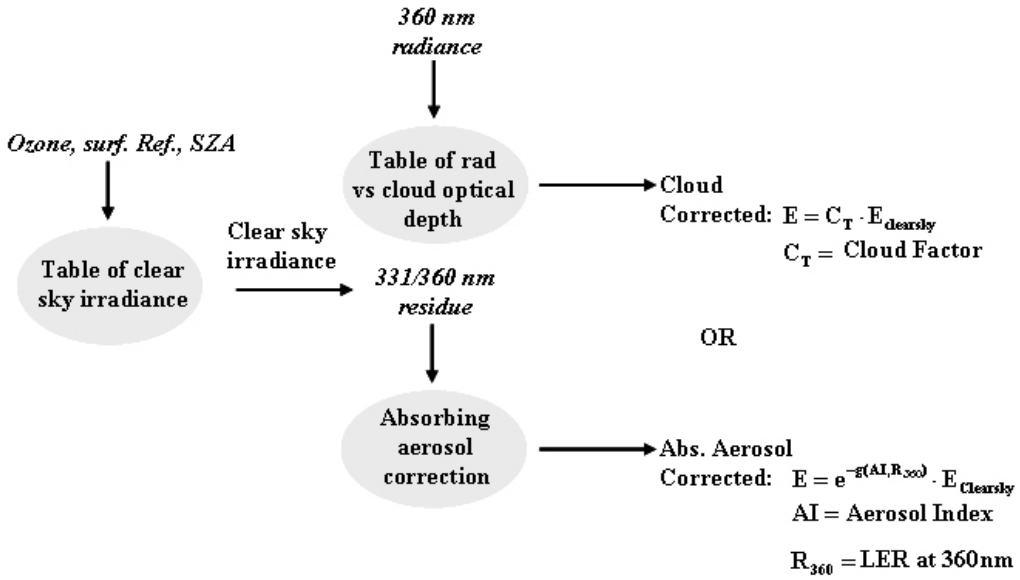

Figure 3.18 OMI UV algorithm overview modified from *Krotkov et al.* [2002b].

In the algorithm, the non-clear sky conditions are distinguished into cloud/nonabsorbing aerosol, and absorbing aerosol. These can be separated by using the two values of Lambertian Equivalent Reflectivity (LER) at 360 nm (see Equation 3.7) [*Krotkov et al.*, 2002a; *Krotkov et al.*, 1998; *Krotkov et al.*, 2001; *Krotkov et al.*, 2002b] and Aerosol Index (AI), (see Equation 3.8) [*Krotkov et al.*, 2002a; *Krotkov et al.*, 2002b].

$$I_{360} = I_o(\theta, \theta_o, P_S) + \frac{R_{360} T_{360}(\theta, \theta_o, P_S)}{1 - R_{360} S_b(P_S)} \qquad (3.7)$$

where I_{360} is the LER radiance at near 360 nm,

I_o is the radiation reaching the instrument from a pure Rayleigh atmosphere with zero surface reflectivity,

θ is the viewing angle,

θ_o is solar zenith angle,

R_{360} is the LER at 360 nm,

T_{360} is the total amount of direct plus diffuse radiation reaching the surface, multiplied by the atmospheric transmission of the diffuse reflected radiation in the direction of the satellite,

P_S is surface pressure, and

S_b is the diffuse reflection of Rayleigh atmosphere illuminated from below by an isotropic source.

$$AI = -100[\log_{10}(I_{331nm}/I_{360nm})_{meas} - \log_{10}(I_{331nm}/I_{360nm})_{calc}] \qquad (3.8)$$

where I is the upwelling radiance at the top of the atmosphere at 331 nm and 360 nm, these being the shortest and longest available wavelengths where gaseous absorption is negligible.

- Clear-Sky UV Irradiance

For a cloud- and aerosol-free atmosphere, the clear sky surface UV irradiance, E_{clear}, is calculated for a Lambertian reflecting surface by using the formula below [*Krotkov et al.*, 1998; *Tanskanen et al.*, 2006]:

$$E_{clear} = \frac{E_o}{d^2}\frac{E_{dir} + E_{diff}}{1 - A_S S_b} \qquad (3.9)$$

where E_{dir} is direct irradiance at the ground for unit solar flux and zero surface reflectivity,

E_{diff} is diffuse irradiance at the ground for unit solar flux and zero surface reflectivity,

d is the sun-earth distance,

E_o is the extraterrestrial solar flux at 1 Astronomical Unit,

A_S is the surface albedo, and

S_b is the fraction of reflected radiation that is in turn backscattered to the surface by the Rayleigh atmosphere.

For the purpose of estimating E_{clear}, the E_{dir}, E_{diff} and S_b in Equation 3.9 were solved from the radiative transfer equation in the UV range (290-400 nm) using the auxiliary equations method [*Dave*, 1964]. This process accounts for all orders of scattering and polarization effects. In addition, a spherical geometry correction is required [*Krotkov et al.*, 2002b]. Therefore, the irradiances at solar zenith angles up to 85° are more correct.

The model was separated for a set of 26 ozone and temperature profiles to calculate the numerical parameters using ozone absorption coefficients based on the laboratory measurements of *Bass and Paur* [1985], and the Rayleigh scattering coefficients based on the work by *Bates* [1984], cited in *Krotkov et al.* [2002b]. The ozone and temperature profiles are based on the Nimbus-7/SBUV instrument measurements above 15 km and on balloon ozonesonde measurements for lower altitudes [*McPeters et al.*, 1998]. The profiles have been generated for three zones: low latitude (15°) covering a range of 225-475 DU, midlatitude (45°) and high latitude (75°) covering a range of 125-575 DU.

To estimate surface albedo (A_S), it is assumed that the albedo is spectrally independent in the UV range. Monthly Minimum Lambertain Equivalent Reflectivity at 360 nm or 380 nm (MLER) retrieved from the Nimbus-7/TOMS during 1978 to 1993 was used. A linear interpolation in space and time method is then used for estimating MLER on a given day for each OMI FOV [*Krotkov et al.*, 2002a; *Tanskanen et al.*, 2003; *Tanskanen*, 2004].

The irradiance values were convoluted using the numerical parameters with a triangular slit function (FWHM=0.55 nm) centred at 305, 310, 324, 380 nm and 22 additional wavelengths to generate lookup tables to calculate E_{clear}. Finally, the surface albedo correction and sun distance correction were applied according to Equation 3.9.

- Correction for absorbing aerosols

Aerosols can absorb both direct and diffuse UV radiation. Additionally, they also attenuate the outgoing diffuse radiation. If the satellite algorithms do not account for absorbing aerosol, overestimation of UV irradiance can result. The situation becomes more complicated in cases where aerosols are located mostly in the atmospheric boundary layer under a cloud layer. However, nonabsorbing and absorbing aerosols can be separated by LER and AI. Absorbing aerosols cause the satellite-derived LER to decrease with decrease in wavelength while nonabsorbing aerosols typically cause the LER to increase with decrease in wavelength [*Krotkov et al.*, 2002a].

In the case that LER<0.15 and AI>0.5, the absorbing aerosol correction factor is applied. Using AI, the correction factor for absorbing aerosol is determined as $e^{-g(AI,R_{360})}$ [*Herman et al.*, 1999a; *Krotkov et al.*, 2002a; *Krotkov et al.*, 1998; *Krotkov et al.*, 2002b; *Tanskanen et al.*, 2006]. Therefore, the UV irradiance (E) in this case can be calculated by using the equation below:

$$E = e^{-g(AI,R_{360})} \cdot E_{Clear} \qquad (3.10).$$

The g factor is a function of aerosol height, observational geometry and aerosol type, which is set to a constant value of 0.25 in the current version of the OMI UV algorithm.

- Cloud/nonabsorbing aerosol correction

For the other conditions, surface UV irradiance (E) can be found by multiplying the cloud correction factor (C_T) [*Krotkov et al.*, 2001] with clear sky UV irradiance as in the equation below:

$$E = C_T \cdot E_{Clear} \qquad (3.11).$$

To estimate the cloud correction, the assumptions are that cloud is homogeneous, the plane-parallel cloud model is embedded into a scattering molecular atmosphere with

known ozone absorption and surface albedo, and cloud optical thickness is spectrally independent. The cloud correction is based on radiative transfer calculations and is generated as lookup tables as functions of cloud optical thickness, surface albedo and solar zenith angle. The cloud optical thickness is obtained by using the 360 nm radiance measured at the overpass time by OMI. Surface albedo is taken from a climatology database [*Tanskanen*, 2004].

3.4.2.2 Data Products

The Level-2 OMI Surface UV irradiance and Erythemal Dose (OMUVB) products are provided in terms of surface spectral UV irradiances at 305 nm, 310 nm, 324 nm, 380 nm, erythemal dose rate both at overpass time and local solar noon, and erythemal daily dose [*Levelt et al.*, 2006b; *Tanskanen et al.*, 2006].

For specified sites, these data can be accessed from http://avdc.gsfc.nasa.gov/. However, this requires a formal request to the OMI team, who will then provide the data for the stations requested. This data product will be used in Chapter 4 to Chapter 6. The data product is written as text files containing the data as shown below:

```
Datetime  : Date and time
MJD2000   : Modified Julian Day 2000
Year      : Year
DOY       : Day Of Year
sec. (UT) : Elapsed time (seconds, UT)
Orbit     : Aura orbit number
CTP       : OMI Cross Track Position (0-59)
Lat.      : CTP center latitude (degree)
Lon.      : CTP center longitude (degree)
Dist.     : Distance between the station and the CTP (km)
SZA       : Solar Zenith Angle (degree)
GPQF      : Ground Pixel Quality Flags (dimensionless)
OMAF      : OMTO3 Algorithm Flags (dimensionless)
OMQF      : OMTO3 Quality Flags (dimensionless)
UVBQF     : Quality Flags on Pixel Level (dimensionless)
CSEDDose  : Clear Sky Erythemal Daily Does (J/m^2)
CSEDRate  : Clear Sky Erythemal Daily Does Rate (W/m^2)
CSIrd305  : Clear Sky Irradiance at 305 nm (W/m^2/nm)
```

```
CSIrd310  : Clear Sky Irradiance at 310 nm (W/m^2/nm)
CSIrd324  : Clear Sky Irradiance at 324 nm (W/m^2/nm)
CSIrd380  : Clear Sky Irradiance at 380 nm (W/m^2/nm)
CldOpt    : Cloud Optical Thickness (dimensionless)
EDDose    : Erythemal Daily Does (J/m^2)
EDRate    : Erythemal Daily Does Rate (W/m^2)
Ird305    : Irradiance at 305 nm (W/m^2/nm)
Ird310    : Irradiance at 310 nm (W/m^2/nm)
Ird324    : Irradiance at 324 nm (W/m^2/nm)
Ird380    : Irradiance at 380 nm (W/m^2/nm)
OPEDRate  : Overpass Erythemal Dose Rate (W/m^2)
OPIrd305  : Overpass Irradiance at 305 nm (W/m^2/nm)
OPIrd310  : Overpass Irradiance at 310 nm (W/m^2/nm)
OPIrd324  : Overpass Irradiance at 324 nm (W/m^2/nm)
OPIrd380  : Overpass Irradiance at 380 nm (W/m^2/nm)
LambEquRef: Lambertian Equivalent Reflectivity at 360 nm
(dimensionless)
SufAlbedo : Surface Albedo at 360 nm (dimensionless)
TerrHgt   : Terrain Height for center co-ordinate of ground
pixel(m).
```

For the global view, the Level-3 OMI Surface UV irradiance and Erythemal Dose (OMUVBd*)* product is now available at http://disc.sci.gsfc.nasa.gov/Aura/OMI/omuvbd_v003.shtml. The OMUVBd data product is written as Hierarchical Data Format (HDF)-EOS5 data files. This product will be described in more detail in Chapter 7.

3.4.2.3 Error of OMI UV Irradiance

Since the OMI UV irradiance is calculated by using the extraterrestrial solar irradiance, clear sky surface UV irradiance, cloud and aerosol correction factors, the errors can be caused by any or all of these factors. In *Krotkov et al.* [2002b], error analysis of OMI UV irradiance was investigated. By comparing three sets (Solar Stellar Irradiance Comparison Experiment, Solar Ultraviolet Spectral Irradiance Monitor and SBUV/2) of extraterrestrial solar irradiance, the differences found are less than ±3% in the UV range. This can be assumed as the absolute uncertainty of ±3%. The error in clear sky irradiance depends on the input data used in the radiative

transfer models. This typically gives an uncertainty of less than 5%. The error for cloud/aerosol correction factors can be significant, in the region of 20% or more. This includes errors in properties of cloud (e.g., cloud shape and cloud altitude, given the assumption of a homogenous, plan parallel cloud layer), ozone, and type of aerosols, which are used in models. In addition, when validating against ground-based observations, there is the issue of temporal and spatial matching.

3.4.3 Aerosol Optical Depth and Aerosol Absorption Optical Depth from OMI

A further two satellite products, not themselves fully incorporated into the OMI UV algorithm, were used in this thesis work. There are two methods used to estimate aerosol optical depth, aerosol absorption optical depth and single scattering albedo for cloud free conditions: the OMI Near-UV Aerosol Optical Depth (OMAERUV) and the OMI Multi-wavelength Aerosol Optical Depth (OMAERO) algorithms. The OMAERUV algorithm uses the relationship between two UV wavelengths (354 and 388 nm) and a set of assumed aerosol models to estimate aerosol index, aerosol extinction and absorption optical depth, as been used in TOMS aerosol algorithm [*Torres et al.*, 1998]. The aerosol models consist of three major aerosol types: desert dust, biomass burning and sulfate-based aerosols, where each aerosol type is represented by seven aerosol models of varying single scattering albedo. Each subtype depends on size distribution and refractive index. The OMAERO algorithm uses up to 19 wavelengths in the 330 nm to 500 nm spectral range, which are independent from Raman scattering and gas absorption attributes [*Torres et al.*, 2002b]. This algorithm is based on four main aerosol models: desert dust, biomass burning, volcanic and weakly absorbing aerosol with several subtypes represented by each models according to their properties (particle size and refractive index). The particle size distributions and refractive index used in the OMI aerosol algorithm are taken from long-term Aerosol Robotic Network (AERONET) ground-based observations. The difference between the two methods is that the OMAERO method is mainly used over the oceans while the OMAERUV method is used over land. The reason for this is that over land the available spectral surface reflectivity database

may not be good enough to apply the multi-wavelength method which relies on spectral surface reflectivity data.

In this study, the OMAERUV aerosol data product was used. This product includes aerosol optical depth, aerosol absorption optical depth at 354, 388 and 500 nm, and UV aerosol index. The data is written as an HDF-EOS5 which can be downloaded from http://avdc.gsfc.nasa.gov/ for the specific sites and from http://disc.sci.gsfc.nasa.gov/Aura/data-holdings/OMI/omaeruv_v003.shtml for the global view (Level-3 OMI Near-UV Aerosol Optical Depth, OMAERUVd).

The overall accuracy of aerosol optical depth retrieved from the OMI product is estimated to be about 30% or more, and the accuracy of the single scattering albedo is 0.1, depending on the main uncertainties such as the aerosol size distribution, refractive index, layer height, the surface reflectivity and the cloud mask. The aerosol absorption optical depth is estimated to have a root mean square error about 0.01 [*OMI Team*, 2009; *Torres et al.*, 2002a; *Torres et al.*, 2002b]. *Ahn et al.* [2008] compared aerosol optical depth and aerosol absorption optical depth retrieved from OMI with that from Aqua/Moderate Resolution Imaging Spectroradiometer (MODIS) and found that the OMI aerosol optical depth values were generally higher than the MODIS values. *Livingston et al.* [2009] also showed that OMAERUV aerosol optical depth retrievals are within 20% of the AERONET values for the nonabsorbing aerosols but are higher for the urban aerosols.

3.4.4 Total Column Ozone from OMI

Total ozone column from OMI is derived from two algorithms [*Kroon et al.*, 2008]: OMI Total Ozone Mapping Spectrometer ("*OMI-TOMS*") and OMI Differential Optical Absorption Spectroscopy ("*OMI-DOAS*") technique developed by the Royal Netherlands Meteorological Institute [*Veefkind et al.*, 2006]. The differences between the two algorithms are described in *Kroon et al.* [2008].

The total column ozone from TOMS and DOAS algorithms are in the OMI Total ozone data products, written as an HDF-EOS5. It can be downloaded from

http://avdc.gsfc.nasa.gov for the specific sites, and from http://disc.sci.gsfc.nasa.gov/Aura/data-holdings/OMI for the global view.

The relative differences of total ozone column from the different methods vary from 0% to 3% depending on latitude and season. The OMI-TOMS total ozone column is slightly lower than that measured from Brewer spectrometers by about 2%. For OMI-DOAS ozone data, the bias is about 1.4% [*Antón et al.*, 2009].

3.4.5 Overall Uncertainty of OMI Data

Several OMI products are used in the following work and each product has its own uncertainty. The smallest uncertainty is in total column ozone and is within 3% when compared to a range of ground-based instruments (which do not themselves agree perfectly). The uncertainty of indirect measurements of UV from OMI data can be much greater (20% or more). According to the comparisons of the OMI UV and ground-based UV at several sites [*Buchard et al.*, 2008; *Ialongo et al.*, 2008; *Kazadzis et al.*, 2009a; *Tanskanen et al.*, 2007], OMI data has been found to generally overestimate UV with respect to ground-based data, e.g., by 20% for erythemal data at the overpass time [*Kazadzis et al.*, 2009a] and up to 50% at sites affected by absorbing aerosols [*Tanskanen et al.*, 2007]. In contrast, the underestimation of the OMI UV data can be found at several sites affected by snow covered surface [*Tanskanen et al.*, 2007], while for clean sites agreement with ground-based measurements is within the measurement errors [*Fioletov et al.*, 2002; *McKenzie et al.*, 2001]. The uncertainty of OMI aerosol optical depth can be about 30% or more dependent on condition. This is borne out by the level of agreement with other measurements (which are themselves imperfect).

Data of the types, and from the sites, described in this chapter are used in the following chapters to assess the success of OMI UV retrievals in the Tropics – a region for which the OMI retrieval has not previously been tested, and for which there are few ground-based measurements. Successful application of the OMI UV algorithm would therefore provide valuable data that is not available by other means.

Chapter 4 – Comparison between OMI and Ground-Based UV Data

In this study, the erythemal irradiance at local solar noon, when the sun is highest in the sky, was used. This is a standard OMI data product available for anywhere on the globe, and represents the expected maximum UV value for the day under stable conditions. The time difference between the OMI UV overpass and ground-based measurements at local solar noon varies more for the UK sites (-1.5 to 2.5 hours) than that for Thai sites (0.5 to 2.5 hours). The OMI algorithm assumes that atmospheric conditions stay constant between the overpass time and noon, in calculating local noontime UV irradiance. This assumption and the time difference can introduce an additional uncertainty into the noon UV data product. This becomes an intrinsic part of the uncertainty in the OMI product. However, the mean ratios at overpass and noon differ by only 2% and the normalised root mean square deviations are also similar (0.16 for Songkhla at overpass and 0.18 at noon, with the other sites showing a corresponding result). For a broad application, e.g., one aimed at public health information, noon UV dose rate is more easily understood and more applicable and thus we use this in the following analysis.

In this chapter, erythemal dose rates at local solar noon retrieved from OMI were compared with those from ground-based measurements at the UK sites (solar noon ±4 minutes) and Thai sites (solar noon ±6 minutes). These sites represent different geographical and environmental conditions from previous studies [*Arola et al.*, 2009; *Buchard et al.*, 2008; *Ialongo et al.*, 2008; *Kazadzis et al.*, 2009a; *Tanskanen et al.*, 2007; *Weihs et al.*, 2008], which focused mainly on comparisons for the northern midlatitudes and high latitudes. The period of the data used for the comparison is from August 2004 to December 2007. The results of the comparison are shown as scatter plots for all sky conditions and the subset of cloudless conditions, and can be evaluated against the one-to-one line with the limitation of ±30% as shown in Figure 4.1. To determine cloudless days, the ground-based UV irradiance (10 minutes averages for Thai data and 5 minutes for UK data) was plotted from sunrise to sunset: days with an uninterrupted smooth bell curve were manually selected as clear days.

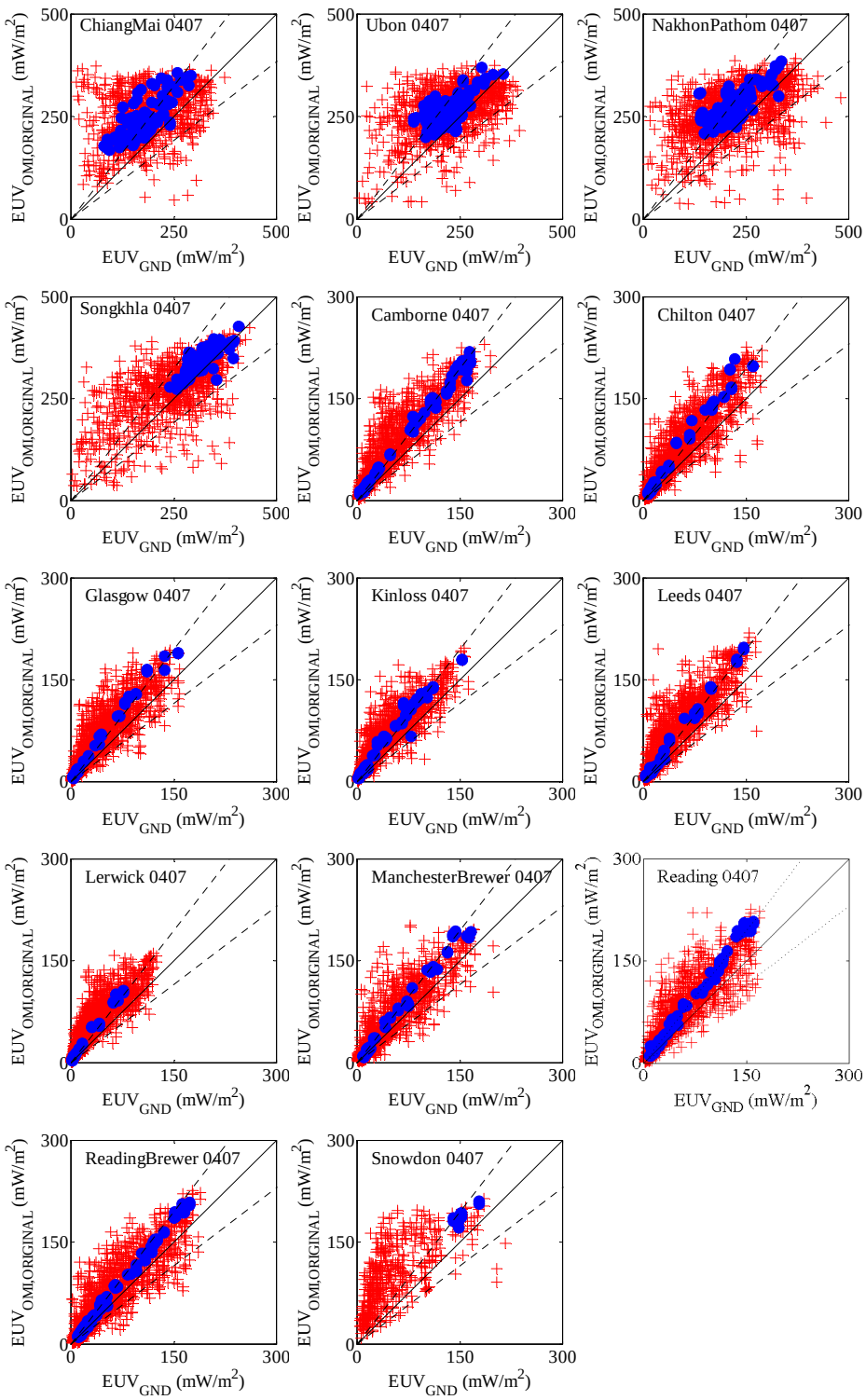

Figure 4.1 Comparison of the OMI erythemal UV irradiances at local solar noon ($EUV_{OMI,ORIGINAL}$) with those measured from ground-based instruments (EUV_{GND}) for all sky conditions (+) and cloudless conditions (•) for the years 2004-2007. The one-to-one line (—) and 30% limits (----) are also shown.

In order to indicate the agreement between the noontime erythemal irradiance retrieved from the OMI and the ground-based measurement, the ratios of the OMI data and the ground-based data were calculated and the distribution of the ratio at each site was plotted as shown in Figure 4.2. Since most of the distributions were not normal, mean and median of the ratio were calculated [*Tanskanen et al.*, 2007]. The percentages of the OMI data that agree within ±10%, ±20% and ±30% of the ground-based data were determined and denoted as $\%W_{10}$, $\%W_{20}$ and $\%W_{30}$, respectively [*Kazadzis et al.*, 2009a; *Tanskanen et al.*, 2007]. Additionally, the agreement between the erythemal irradiance retrieved from OMI (y_i) and ground-based (x_i) sources was calculated in terms of the averaged percentage differences $(\%\text{AvgDiff})$ and the bias $(\%\text{Bias})$ as

$$\%\text{AvgDiff} = \frac{1}{N}\sum_{i=1}^{n}\left(\frac{y_i - x_i}{(x_i + y_i)/2}\right) * 100, \quad \%\text{Bias} = \frac{1}{N}\sum_{i=1}^{n}\left(\frac{y_i - x_i}{x_i}\right) * 100,$$

where N is the number of data taken into account in the comparison [*Siani*, 2007]. All the statistical data described above are shown in Table 4.1 for Thai data and Table 4.2 for UK data.

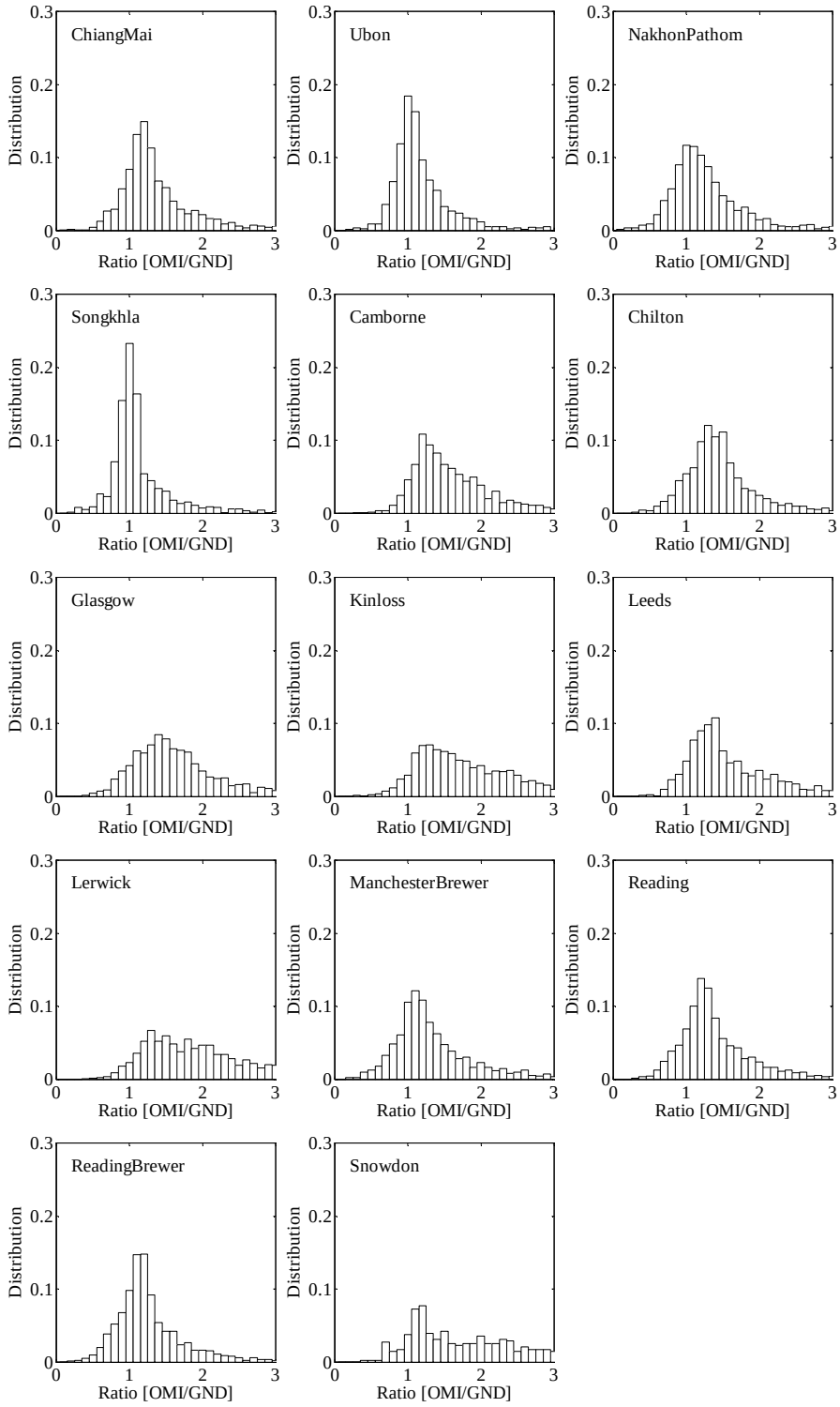

Figure 4.2 Distributions of the ratio of the OMI data and ground-based (GND) data for all sky conditions.

Table 4.1 Statistical analysis of the ratio of the OMI to ground-based data for Thai sites under all sky and cloudless conditions during 2004-2007.

Sites	All sky conditions (Original OMI)								Cloudless conditions (Original OMI)							
	N	Median	Mean	$\%W_{10}$	$\%W_{20}$	$\%W_{30}$	%AvgDiff	%Bias	N	Median	Mean	$\%W_{10}$	$\%W_{20}$	$\%W_{30}$	%AvgDiff	%Bias
Chiang Mai	1158	1.30	1.62	14	30	48	32	62	180	1.30	1.37	1	19	51	30	37
Ubon Ratchathani	1203	1.14	1.32	30	53	67	18	32	178	1.14	1.19	34	67	82	16	18
Nakhon Pathom	1206	1.24	1.44	21	38	52	23	44	108	1.29	1.31	7	34	52	26	31
Songkhla	1094	1.09	1.32	39	62	70	15	32	79	1.09	1.09	52	95	100	8	9

Table 4.2 Statistical analysis of the ratio of the OMI to ground-based data for UK sites under all sky and cloudless conditions during 2004-2007.

Sites	All sky conditions (Original OMI)								Cloudless conditions (Original OMI)							
	N	Median	Mean	$\%W_{10}$	$\%W_{20}$	$\%W_{30}$	%AvgDiff	%Bias	N	Median	Mean	$\%W_{10}$	$\%W_{20}$	$\%W_{30}$	%AvgDiff	%Bias
Camborne	1650	1.59	1.92	7	15	26	51	92	103	1.42	1.54	0	3	21	40	54
Chilton	1697	1.46	1.64	10	19	30	38	64	70	1.52	1.50	0	0	11	40	50
Glasgow	1866	1.63	1.92	8	16	23	50	92	72	1.65	1.71	0	1	4	50	71
Kinloss	1973	1.77	2.06	5	12	20	57	106	83	1.70	1.83	0	5	10	55	83
Leeds	1682	1.52	1.94	8	18	28	49	94	67	1.41	1.50	4	7	21	38	50
Lerwick	2066	1.99	2.34	4	9	14	67	134	39	2.03	2.01	0	0	3	64	101
Manchester	1481	1.27	1.73	17	34	48	31	73	65	1.25	1.23	9	40	66	20	23
Reading (Bentham)	2052	1.34	1.54	12	25	42	33	54	151	1.32	1.32	5	13	43	27	32
Reading (Brewer)	1919	1.23	1.48	17	37	55	25	48	153	1.22	1.21	8	35	89	19	21
Snowdon	480	2.11	2.58	5	14	25	68	158	15	1.25	1.24	0	20	93	21	24

We can see from the results in Figure 4.1 and Tables 4.1 and 4.2 that the noontime erythemally weighted irradiances obtained from OMI generally overestimate those from ground-based measurements, particularly for cloudless conditions. The ratios for the all sky conditions show greater scatter than for the cloudless conditions and include instances of underestimation by OMI. Some of this scatter can be due to changing cloud conditions between overpass time and local solar noon. The bias values for all sky conditions are greater than for the cloudless conditions; for example, the bias values of Reading sites are 54% for all sky conditions and 32% for cloudless conditions. The scatter is greater in cloudy conditions, as expected, but the median values are found to be independent of cloudiness as a few outliers skew the mean values upwards in cloudy conditions, but do not affect the median. The results for the cleaner air site at Songkhla (mean=1.32, median=1.09) are in better agreement than the more urban sites such as Chiang Mai (mean=1.62, median=1.30). Comparing the results from the two regions, the scattergrams in Figure 4.1 show that the data for Thai sites are more scattered than those for the UK, which may result from more variations in cloud type (tropical cumuli) and aerosol loading (biomass burning) in Thailand, but also from the range of time differences between overpass time and local noon allowing more time for conditions to change. The bias values for UK sites are generally higher than for Thai sites. This might be due to the fact that the absolute amount of erythemal irradiance for the UK is lower than for Thailand and the low UV levels can result in large relative differences because of rapid changes in cloudiness [*Arola et al.*, 2009; *Buchard et al.*, 2008]. The ratios between the OMI and ground-based data in this study were in general slightly higher than those from previous studies [*Arola et al.*, 2009; *Kazadzis et al.*, 2009a; *Tanskanen et al.*, 2007]. This may be due to the fact that the noontime data was used in our study while the overpass time data [*Arola et al.*, 2009; *Kazadzis et al.*, 2009a] and daily doses [*Tanskanen et al.*, 2007] were used for the other studies, but different environmental and climatological conditions may also have some bearing on the results.

In order to investigate the effect of aerosol, the uvspec model [*Mayer and Kylling*, 2005] as described in Chapter 2 was run for aerosol free and realistic polluted aerosol cases for clear sky days in the years 2005 and 2006. The data used in this section are from Chiang Mai, Nakhon Pathom, Songkhla, Manchester and Reading,

where there are ground-based measurements that can provide some indication of aerosol properties. The radiative transfer model was set as follows: the standard atmospheric profiles were assumed as midlatitude summer and winter for UK and tropical atmosphere for Thailand. The extraterrestrial solar spectrum was based on *Atlas_Plus_Modtran*. The DISORT was selected as a radiative transfer equation solver with 6 streams [*Chandrasekhar*, 1960]. Total ozone column was taken from Brewer spectrophotometers for Reading and Manchester, and the satellite data from OMI was used for the other sites. Ground albedo was taken from OMI products, at values between 0.03-0.07 for UV wavelengths. Solar zenith angle was matched with that for local solar noon from the OMI UV product. Aerosol type above 2 km was assumed as background type and that below 2 km was assumed as maritime type for Songkhla and urban type for the other sites.

For Reading and Manchester, the daily aerosol optical depth data were taken from Brewer spectroradiometers, based on direct sun measurements. These data are available at ftp://o3uvdata.seaes.manchester.ac.uk/. The aerosol optical depth can be set as a routine Brewer output, calculated as a residual of the ozone and SO_2 measurements. As such it is subject to uncertainties of the order of 1% when evaluated against other methods of AOD measurement (*W. Kumharn*, personal communication). The aerosol optical depth at the two sites shows seasonal variation with a maximum (up to 2.32) in summer and a minimum (less than 0.14) in winter. The mean value (± standard deviation) from years 2003 to 2008 is 0.76±0.08. The aerosol single scattering albedo for these sites is set as a constant value at 0.85. This value was from running the uvspec model for clear sky days of years 2005 and 2006, and varying aerosol single scattering albedo at 0.80, 0.85 and 0.95. The smallest bias between ground-based and uvspec erythemal irradiances occurred when the aerosol single scattering albedo was set at 0.85.

For the three Thai sites, the aerosol optical depth and aerosol single scattering albedo data were taken from AERONET level 1.5 (data available at http://aeronet.gsfc.nasa.gov) [*Holben et al.*, 1998]. The AERONET stations were not installed until late 2006, and this limited the number of clear sky days available for use with our ground-based UV dataset. For this reason we used mean monthly

averaged aerosol optical depth data at 340 nm from the years 2006 to 2008, matched to clear sky UV data from a given month. The standard deviation on the monthly mean aerosol optical depth data is about 40% for each site. For the two inland sites (Chiang Mai and Nakhon Pathom), there is a clear seasonal cycle in aerosol optical depth with maximum (up to 1.2) in February-April due to biomass burning [*Kift et al.*, 2006]. This reduces to 0.3-0.6 for the rest of the year. Songkhla in contrast exhibits very little seasonal cycle, having aerosol optical depth values in the range 0.2 to 0.5 throughout the year. Long-term averaged (years 2006 to 2008) single scattering albedo values at 440 nm (the shortest wavelength available) were used as constant values: 0.89 for urban sites and 0.97 for the maritime site.

The erythemal irradiances calculated from uvspec with and without effects of aerosol, plus OMI UV erythemal irradiance, were plotted against the ground-based data shown in Figure 4.3.

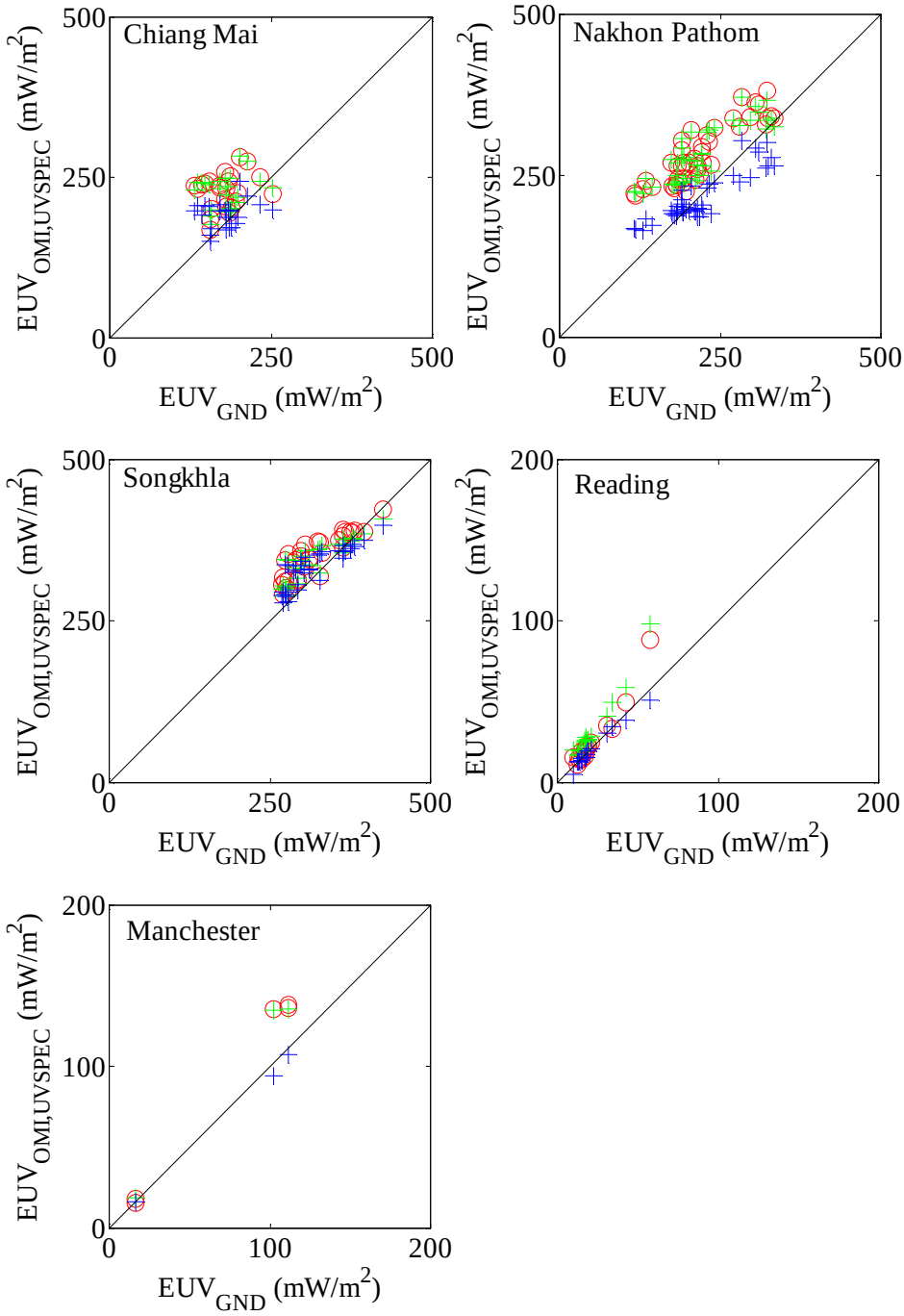

Figure 4.3 Comparison of erythemal UV irradiances retrieved from OMI (o), modelled by uvspec with aerosol (+) and without aerosol (+), and measured by ground-based instruments.

As we can see, the values calculated from the Libradtran model with aerosol were closer to the ground-based values than those without aerosol, particularly for UK sites. This may result from the monthly averaged aerosol optical depth values used

for the Thai sites while the daily values were used for the UK sites. For the cleaner site of Songkhla, the erythemal irradiance calculated from uvspec with and without aerosols are similar, since maritime aerosol absorbs only a small amount of the radiation (SSA=0.97).

This result supports the hypothesis that a large part of the differences between OMI and ground-based data may be attributed to aerosol. Therefore to improve the OMI UV data, a correction for the aerosol absorption should be applied as this is not included in the standard OMI UV algorithm (although aerosol scattering has already been included).

In summary, the noontime erythemal irradiance retrieved from OMI data from years 2004 to 2007 were compared with those measured by ground-based instruments at four Thai sites and nine UK sites. The results showed an overestimation of UV data in the OMI product compared with the ground-based data. The biases between the OMI data and the ground-based data were 9% for cloudless conditions and 32% for all sky conditions at the clean site. These were much higher for the urban sites (37% and 62%, respectively). Most of the biases for the UK data were greater than for Thai data. It should be noted that each data set has an associated uncertainty, described in Chapter 3, which should be considered in the comparison results. Nonetheless, the overall results suggest that aerosol correction is needed to improve the OMI UV data and this will be discussed in more detail in Chapter 5.

Chapter 5 – Improving Satellite Estimates for Clear Skies (Using Aerosol Data)

Aerosols play an important role in the change of UV radiation reaching the earth's surface [*Chou et al.*, 2006]. The effects of aerosol on the UV radiation can occur through both scattering and absorption. Aerosols that absorb the UV radiation can attenuate both direct and diffuse radiation, with an effect greater than nonabsorbing aerosols at the same optical depth. The scattering effect is included in the cloud/nonabsorbing aerosol correction in the OMI UV algorithm while the absorption effect is not. Thus, the overestimation in the OMI UV data when compared to the ground-based data that has been documented in several previous studies is likely attributable to the lack of attention to aerosols in the OMI algorithm. The results shown in Chapter 4 support this hypothesis for the sites in the UK and Thailand. Having identified that the OMI UV product requires a correction to account for absorption by aerosols, a broadly applicable method of performing such a correction and a source of aerosol data is needed.

In this chapter, two empirical methods that can improve the noontime OMI erythemal irradiances for clear sky conditions are introduced. The first method is based on the uvspec radiative transfer calculation, as suggested by *Kazadzis et al.* [2009a]. The uvspec model helps to generate a look up table of the aerosol correction factor as a function of aerosol optical depth and aerosol single scattering albedo. The second method shows the aerosol correction factor as a function of aerosol absorption optical depth, and this follows the method suggested in previous studies [*Arola et al.*, 2005; *Arola et al.*, 2009; *Ialongo et al.*, 2010; *Kazadzis et al.*, 2009a; *Krotkov et al.*, 2005].

It should be noted that all data analysed in this chapter are erythemal irradiance at local solar noon under clear sky conditions.

5.1 The Aerosol Optical Depth Correction

5.1.1 Modelling

Based on the result from the uvspec model in Chapter 4, the erythemal data retrieved from OMI can be brought closer to the ground-based data when aerosols are taken into account (see model results with and without aerosol). In this section, the uvspec model was used to calculate the erythemal irradiance at local solar noon for clear sky days of year 2005 (to match the OMI retrievals) for varying aerosol optical depth (AOD) and aerosol single scattering albedo (SSA). The AOD values were varied from 0.0 to 1.2 with 0.1 step and SSA values were varied between 0.80 and 1.0. The data used for comparison were from four sites: Chiang Mai, Nakhon Pathom, Songkhla and Reading, where AOD and SSA were available as described in Chapter 4. The erythemal irradiances at local solar noon calculated from the uvspec sensitivity study were then plotted against those retrieved from OMI. The plot is separated into two different cases (urban and maritime) as shown in Figure 5.1. The data of Songkhla was used as a reference maritime site while the combined data of the other three sites represented the urban case.

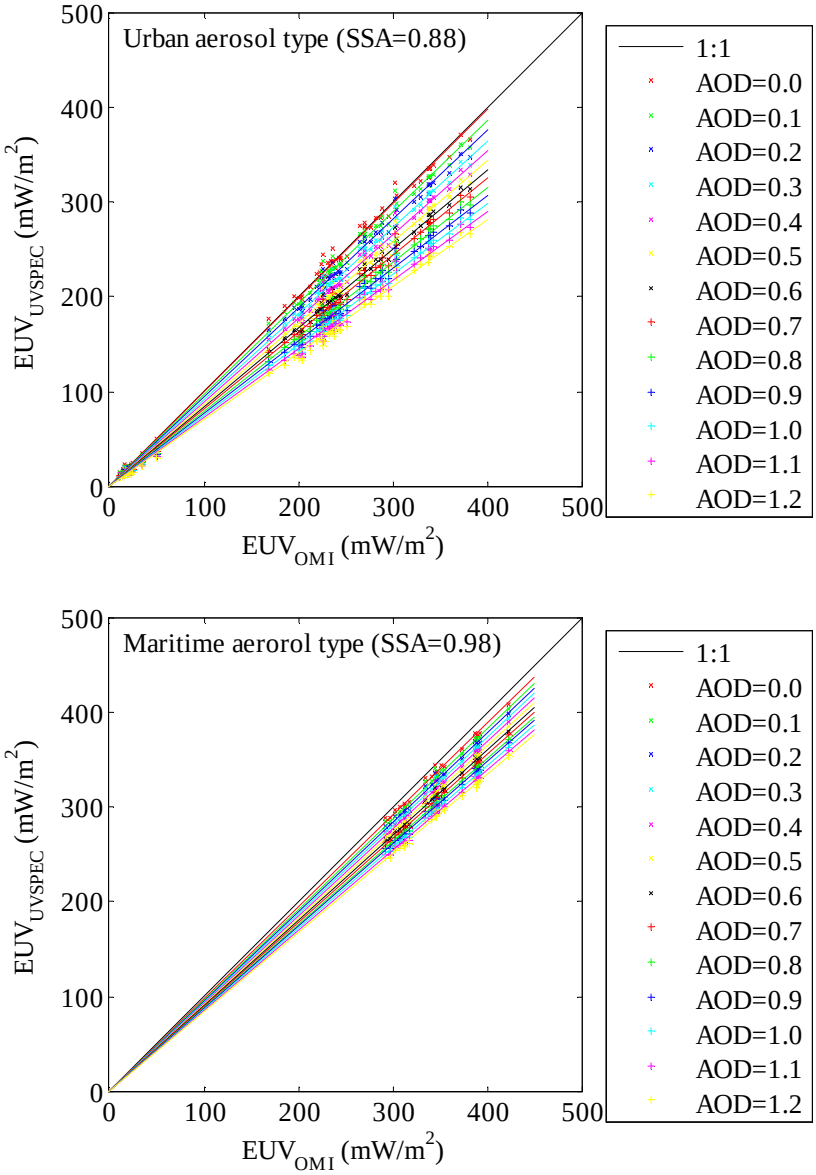

Figure 5.1 Examples of comparisons between the noontime erythemal irradiance from OMI (EUV_{OMI}) and uvspec (EUV_{UVSPEC}) by varying aerosol optical depth between 0.0 and 1.2.

From Figure 5.1, we can see that for the free-aerosol (AOD=0.0, top red line) the uvspec values were close to the OMI values and the uvspec values got progressively less as aerosol increases. At a fixed AOD, the uvspec values were closer to the OMI values when SSA was higher. This is due to the fact that absorbing aerosol is not included in the current OMI surface UV algorithm. From the above results, the erythemal irradiance calculated from the uvspec model can be written as a function of AOD, SSA and the OMI erythemal data as shown below:

$$EUV_{CORR} = F(AOD, SSA) \cdot EUV_{OMI} \quad (5.1)$$

where EUV_{CORR} is the erythemal irradiance at local solar noon corrected in this study, EUV_{OMI} is the original erythemal irradiance at local solar noon retrieved from OMI, and $F(AOD, SSA)$ is an aerosol correction factor.

In order to determine $F(AOD, SSA)$, the slopes of the linear lines at each AOD and SSA (see Figure 5.1) were then obtained. The slopes normalised at AOD=0 were plotted against AOD at each SSA as illustrated in Figure 5.2.

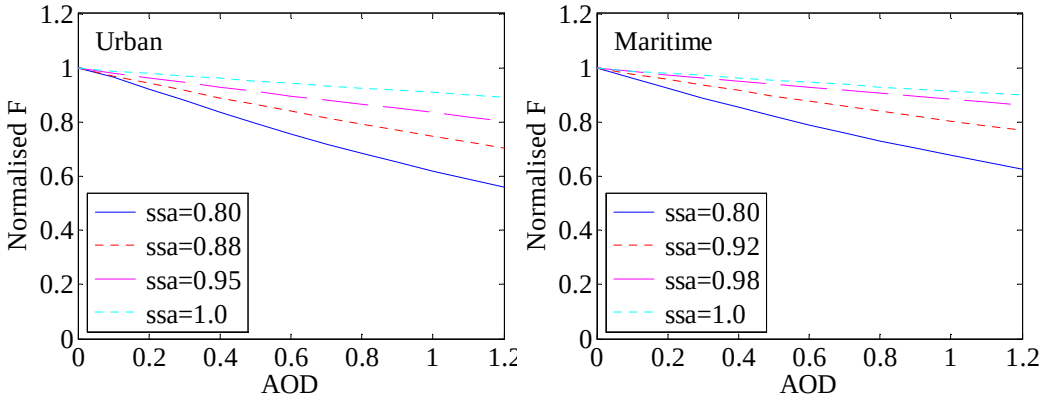

Figure 5.2 Normalised irradiance as a function of AOD and SSA for two aerosol types.

From Figure 5.2, the best fit between the normalised F and AOD is shown in term of an exponential relationship, of the form:

$$F(AOD, SSA) = \exp^{-k(SSA)\cdot AOD} \quad (5.2).$$

The coefficient value (k) is a function of SSA and can be estimated by using a regression method as described by *Stoecker W.F.* [1971], to give the results in Equation 5.3.

$$\begin{aligned} k &= 2.8(1-SSA)^2 + 1.3(1-SSA) + 0.1 \quad \text{for urban} \\ k &= 0.1(1-SSA)^2 + 1.4(1-SSA) + 0.1 \quad \text{for maritime} \end{aligned} \tag{5.3}$$

The semi-empirical method illustrated above (Equations 5.1-5.3), allows the erythemal irradiance retrieved from OMI to be corrected if the aerosol optical depth and single scattering albedo are available.

5.1.2 Validation Based on Ground-Based Aerosol Optical Depth Data

To validate the erythemal irradiance at local solar noon calculated from the empirical model, the data of year 2007 which is independent data from that used to generate the model was used. The daily aerosol optical depth at 320 nm retrieved from Brewer spectrophotometer was used for Reading, and AOD at 340 nm from AERONET was used for the Thai sites. The aerosol single scattering albedo values were set as constant values: 0.89 and 0.97 for the urban and rural Thai sites respectively, and 0.85 for Reading, as described in Chapter 4.

The validation and associated statistical analysis are shown in Figure 5.3 and Table 5.1. These include median and mean of the ratio, $\%W_{10}$, $\%W_{20}$, $\%W_{30}$, %AvgDiff and %Bias. The results also show the comparison between the original OMI data and corrected OMI data.

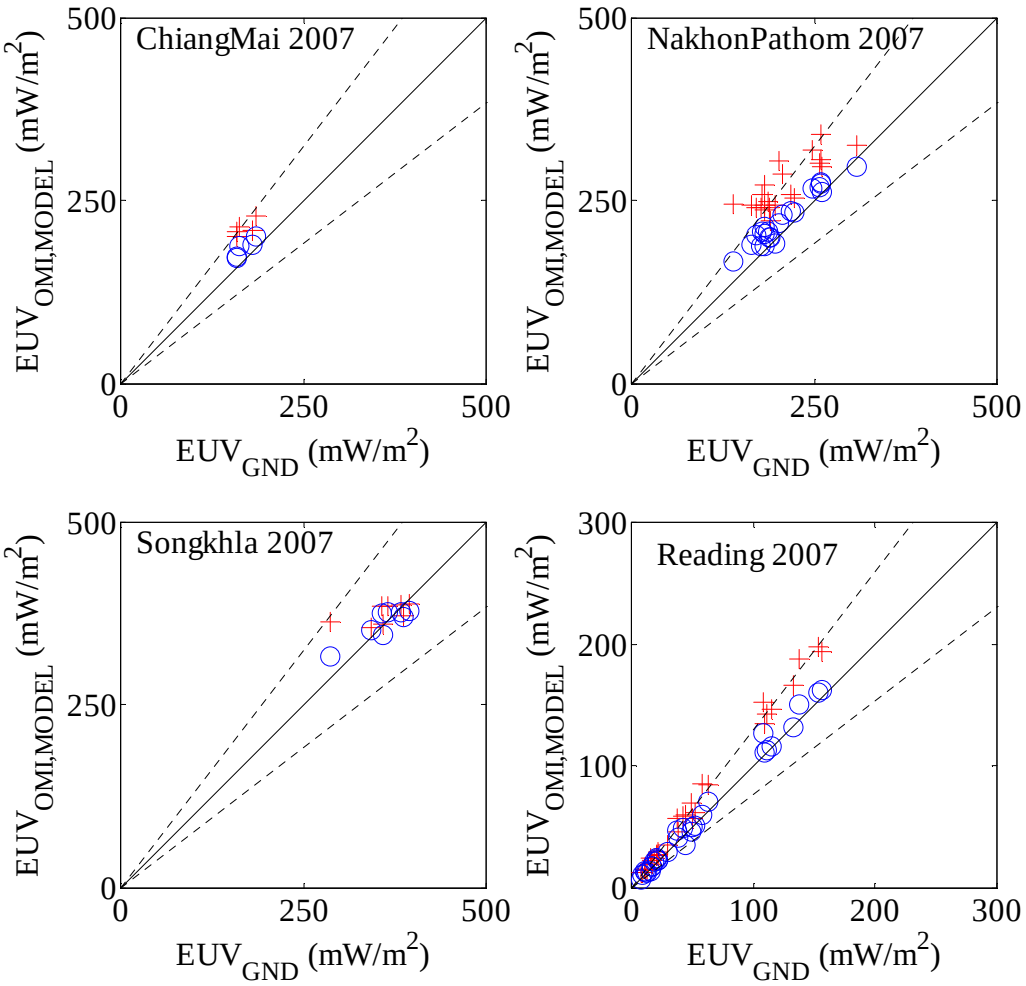

Figure 5.3 Comparison of erythemal irradiance at local solar noon from the original OMI (EUV_{OMI}, +) and the AOD empirical model (EUV_{MODEL}, o) with ground-based measurements (EUV_{GND}) under clear sky conditions using AOD from the ground-based measurement. The 1:1 correlation (—) and ±30% limits (---) are also shown.

Table 5.1 Statistical analysis of the ratio of the original OMI data and the AOD modelled data to ground-based data under cloudless conditions using AOD from independent ground-based measurements.

Sites	Cloudless conditions (Original OMI)								Cloudless conditions (AOD and SSA model)							
	N	Median	Mean	$\%W_{10}$	$\%W_{20}$	$\%W_{30}$	%AvgDiff	%Bias	N	Median	Mean	$\%W_{10}$	$\%W_{20}$	$\%W_{30}$	%AvgDiff	%Bias
Chiang Mai	5	1.28	1.26	0	20	60	23	26	5	1.09	1.10	80	100	100	9	10
Nakhon Pathom	22	1.32	1.32	5	32	45	27	32	22	1.07	1.09	64	95	100	8	9
Songkhla	8	1.02	1.05	88	88	100	4	5	8	1.00	1.01	88	100	100	1	1
Reading (Bentham)	32	1.34	1.34	0	16	44	28	34	32	1.04	1.06	59	91	100	6	6

As can be seen from the above results, after the process of aerosol correction, all of the median ratios were close to one (less than 10% from unity) which were generally better than those from the original OMI data (up to 34%). Most of the empirically corrected data was close to the ground-based data by within ±20%, which was a significant improvement on the uncorrected data. The aerosol correction factor could improve the OMI erythemal data by 2%-30%, with the smaller improvement at the cleanest site, where there is least aerosol.

5.1.3 Validation Based on OMI Aerosol Optical Depth Data

The above validation was based on the ground-based aerosol optical depth which is not always widely available. The OMI aerosol products provide the same coverage, and are spatially matched with the OMI UV products. Therefore the aerosol optical depth at 354 nm taken from the OMI overpass time was considered, as described in Section 3.4.3, to investigate the performance of the empirical model. The single scattering albedo values were assumed as constant values: 0.89 for the urban Thai sites, 0.97 for the maritime site, and 0.85 for the UK sites. Since aerosol information comes from the satellite, all ground-based sites could be used in this evaluation. The noontime erythemal irradiance was calculated using the empirical model (Equations 5.1-5.3) for the four Thai sites and nine UK sites. All data used in this part were from years 2004, 2006 and 2007 for Thai sites, and years 2006 and 2007 for UK sites, which are independent data from the generation of the model (year 2005). Note, that in this study the HPA data is available until April, 2007, except for Snowdon that has no data in year 2007. The empirically corrected data were compared with those from the ground-based measurement as shown in Figure 5.4 and Table 5.2.

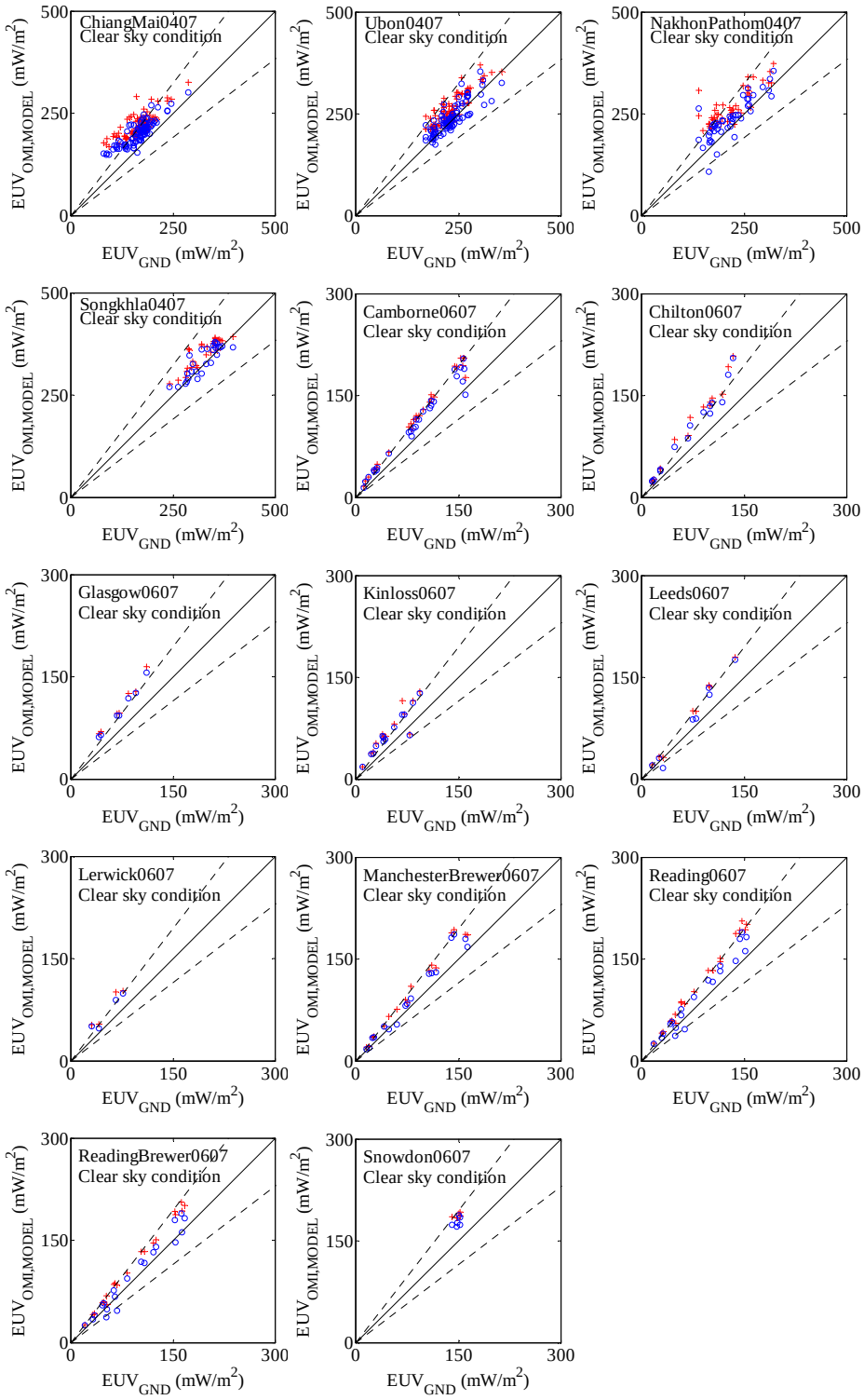

Figure 5.4 Comparison of erythemal irradiance at local solar noon from the original OMI (+) and the AOD empirical model (o) with ground-based measurements under clear sky conditions using AOD from OMAERUV product. The 1:1 correlation (—) and ±30% limits (---) are also shown.

Table 5.2 Statistical analysis of the ratio of the original OMI data and the AOD modelled data to ground-based data under cloudless conditions using AOD from OMAERUV product.

Sites	Cloudless conditions (Original OMI)								Cloudless conditions (AOD and SSA model)							
	N	Median	Mean	$\%W_{10}$	$\%W_{20}$	$\%W_{30}$	%AvgDiff	%Bias	N	Median	Mean	$\%W_{10}$	$\%W_{20}$	$\%W_{30}$	%AvgDiff	%Bias
Chiang Mai	98	1.29	1.37	0	20	54	30	37	98	1.21	1.25	11	49	76	21	25
Ubon Ratchathani	94	1.12	1.13	40	80	93	12	13	94	1.03	1.02	73	93	97	1	2
Nakhon Pathom	45	1.24	1.27	11	44	60	22	27	45	1.10	1.12	42	76	93	10	12
Songkhla	27	1.08	1.09	63	93	100	9	9	27	1.03	1.03	89	100	100	3	3
Camborne	27	1.34	1.38	0	4	19	31	38	27	1.25	1.29	7	15	67	25	29
Chilton	15	1.52	1.50	0	0	7	40	50	15	1.43	1.42	0	7	20	34	42
Glasgow	7	1.48	1.48	0	0	0	38	48	7	1.40	1.41	0	0	0	34	41
Kinloss	14	1.55	1.53	0	7	7	40	53	14	1.40	1.45	0	7	7	35	45
Leeds	8	1.34	1.30	13	13	38	26	30	8	1.25	1.17	0	25	63	13	17
Lerwick	4	1.45	1.47	0	0	25	38	47	4	1.33	1.37	0	25	50	30	37
Manchester	17	1.28	1.27	6	29	59	24	27	17	1.14	1.16	24	65	82	14	16
Reading (Bentham)	20	1.37	1.36	0	5	20	30	36	20	1.21	1.17	15	40	80	14	17
Reading (Brewer)	20	1.25	1.25	5	10	85	22	25	20	1.11	1.07	35	80	95	6	7
Snowdon	6	1.25	1.26	0	0	83	23	26	6	1.20	1.20	0	50	100	18	20

From the results shown in Figure 5.4 and Table 5.2, after the OMI aerosol optical depth correction was applied, the corrected OMI erythemal data at all sites were closer to the ground-based values. The median ratios were reduced by 5%-16%, for example, the median ratio was reduced from 1.08 to 1.03 for Songkhla and from 1.37 to 1.21 for Reading. Most of the corrected data was within ±30% of the ground-based data. The exceptions were the sites at Chilton, Glasgow, Kinloss and Lerwick, but the median values of these sites were still closer to one after the aerosol correction was applied.

When the results in Tables 5.1 and 5.2 were compared for Chiang Mai, Nakhon Pathom, Songkhla and Reading, the results in Table 5.1, using ground-based aerosol optical depth, were better than the results in Table 5.2, using the OMI OMAERUV aerosol optical depth. This may be due to the uncertainty of OMI aerosol optical depth. Comparing aerosol optical depth retrieved from AERONET with that from the OMI product (not shown), it was found that most of the OMI aerosol optical depth data was lower than the AERONET aerosol optical depth, and would therefore produce less correction. Once again this may be a feature of the inability of satellites to probe the lowest levels of the boundary layer [*Tanskanen et al.*, 2006].

From the results, it could be concluded that the empirical model based on the sensitivity study with the uvspec calculation leads to an improvement in the OMI erythemal irradiance at local solar noon for all sites of either tropical or temperate climatologies. As might be expected, the performance of the model strongly depends on the accuracy of aerosol optical depth used in the model, and is most effective where ground-based aerosol optical depth at a particular site is available.

5.2 The Aerosol Absorption Optical Depth Correction

The first method to correct the OMI erythemal data described in Section 5.1 was based on aerosol optical depth and aerosol single scattering albedo. These parameters relate to aerosol absorption optical depth (AAOD), written as $AAOD=AOD\cdot(1-SSA)$. In this section, an aerosol absorption correction factor (F_{AAOD}) is introduced as a function of OMI AAOD at 354 nm. This uses a similar method, but different aerosol inputs, to previous work [*Arola et al.*, 2005; *Arola et al.*, 2009; *Ialongo et*

al., 2010; *Kazadzis et al.*, 2009a; *Krotkov et al.*, 2005]. For example, *Arola et al.* [2009] used a merge of model and AERONET data while *Krotkov et al.* [2005] used UV multifilter rotating shadow band radiometer data.

5.2.1 Modelling

In this section, the ratio of the OMI erythemal irradiances to the ground-based data in year 2005 at Chiang Mai, Ubon Ratchathani, Nakhon Pathom, Songkhla and Reading, were plotted against OMI AAOD values at 354 nm taken at overpass time (OMAERUV, as described in Section 3.4.3) for cloudless cases as illustrated in Figure 5.5. The data of Songkhla was used as a reference maritime site while the combined data of the other four sites represented the urban case; the latter having a correlation coefficient of 0.47 and a standard error in the slope of 0.26.

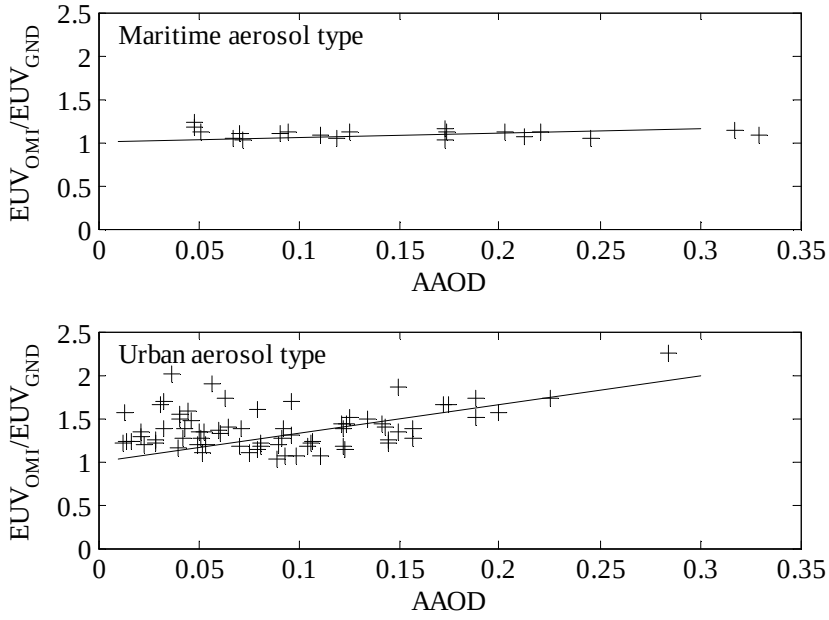

Figure 5.5 The ratio between the erythemal irradiances at local solar noon derived from OMI (EUV_{OMI}) and from ground-based instruments (EUV_{GND}) as a function of OMI aerosol absorption optical depth (AAOD) at 354 nm for urban and maritime areas.

Using Figure 5.5, the OMI data must be divided by the equation for the straight line fit to get the ground-based values. Thus, the aerosol correction factor, F_{AAOD} becomes:

$$F_{AAOD} = [1 + 3.33 \cdot AAOD]^{-1} \quad \text{for urban aerosols}$$
$$\text{and} \quad F_{AAOD} = [1 + 0.50 \cdot AAOD]^{-1} \quad \text{for the maritime case.} \tag{5.4}$$

This can be compared with $F_{AAOD} = [1 + 1.60 \cdot AAOD(320nm)]^{-1}$ as introduced by *Ialongo et al.* [2010] and $F_{AAOD} = [1 + 3 \cdot AAOD(325nm)]^{-1}$ as suggested by *Krotkov et al.* [2005].

To correct the OMI erythemal irradiance for clear sky conditions, these factors were then applied to the equation as follows:

$$E_{CORR} = F_{AAOD} \cdot E_{OMI} \tag{5.5}$$

where E_{CORR} and E_{OMI} are noontime erythemal dose rates corrected for absorbing aerosols and retrieved from OMI product, respectively, and F_{AAOD} is the aerosol absorption correction factor.

5.2.2 Validation Based on Ground-Based Aerosol Absorption Optical Depth Data

The erythemal irradiance at local solar noon in year 2007 calculated from the empirical model was compared with the concurrent ground-based erythemal irradiance at the four sites: Chiang Mai, Nakhon Pathom, Songkhla and Reading. The AAOD values (AAOD=AOD·(1-SSA)) at the four sites were calculated by using AOD and SSA as described in Section 5.1.2. The validation and the same statistical analysis are shown in Figure 5.6 and Table 5.3.

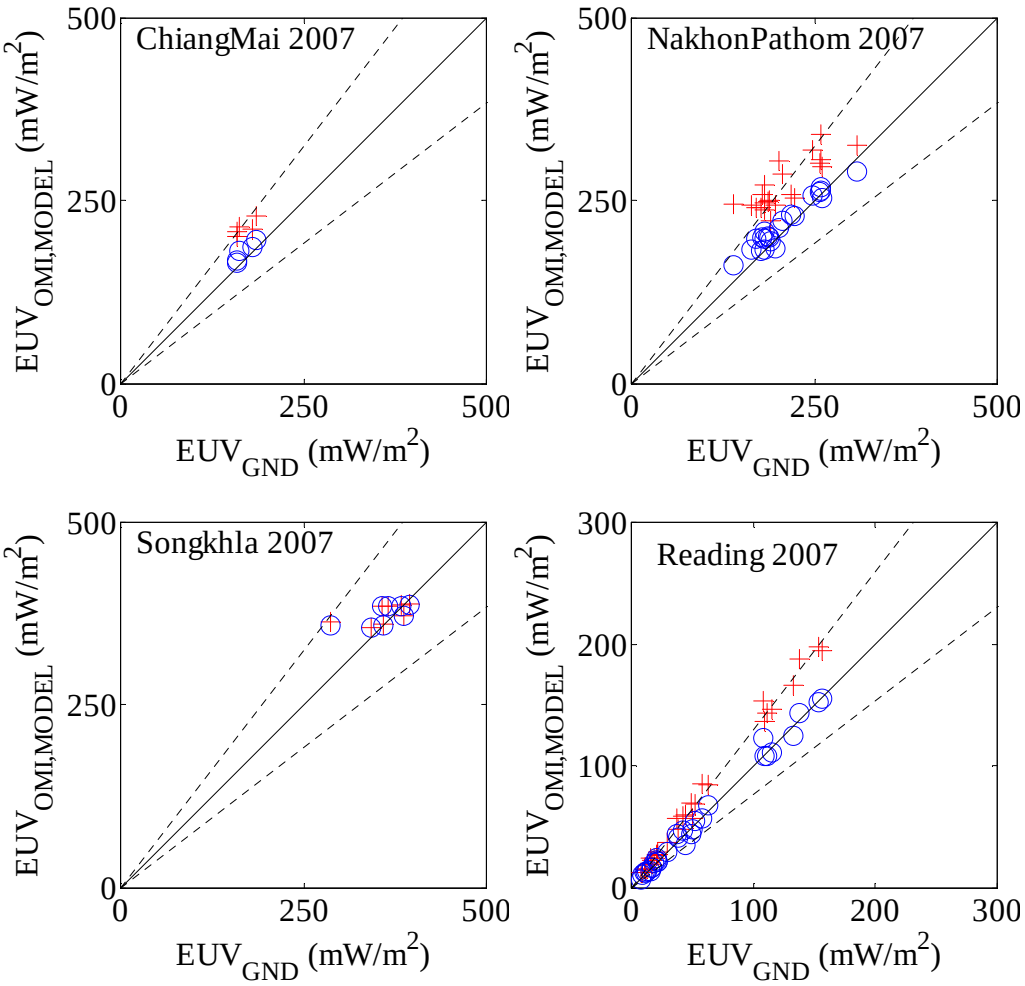

Figure 5.6 Comparison of erythemal irradiance at local solar noon from the original OMI (EUV_{OMI}, +) and the AAOD empirical model (EUV_{MODEL}, o) with ground-based measurements (EUV_{GND}) under clear sky conditions using AAOD from the ground-based measurement. The 1:1 correlation (—) and ±30% limits (---) are also shown.

Table 5.3 Statistical analysis of the ratio of the original OMI data and the AAOD modelled data to ground-based data under cloudless conditions using AAOD from the ground-based measurement.

Sites	Cloudless conditions (Original OMI)								Cloudless conditions (AAOD model)							
	N	Median	Mean	$\%W_{10}$	$\%W_{20}$	$\%W_{30}$	%AvgDiff	%Bias	N	Median	Mean	$\%W_{10}$	$\%W_{20}$	$\%W_{30}$	%AvgDiff	%Bias
Chiang Mai	5	1.28	1.27	0	20	60	23	27	5	1.06	1.07	80	100	100	6	7
Nakhon Pathom	22	1.32	1.32	5	32	41	27	32	22	1.05	1.06	77	100	100	5	6
Songkhla	8	1.02	1.05	88	88	100	4	5	8	1.02	1.05	88	88	100	4	5
Reading (Bentham)	32	1.34	1.35	0	6	41	29	35	32	1.04	1.03	66	91	100	3	3

As can be seen from the results above, when the aerosol correction factor was applied, the corrected OMI data showed an improvement by about 30%. The median values of the corrected OMI data were closer to one (between 1.02 and 1.06) while those of the original OMI data were higher (up to 1.34). Most of the OMI corrected data was within ±20% of the ground-based data.

5.2.3 Validation Based on OMI Aerosol Absorption Optical Depth Data

The AAOD based on ground-based data was used in the above validation. The following validation used AAOD values based on the OMI OMAERUV product taken from OMI overpass time, as described in Section 3.4.3. The noontime erythemal irradiances in this section are the same set that was used in Section 5.1.3. Using the above method (Equations 5.4 and 5.5), the erythemal irradiances corrected for aerosol absorption were validated by comparing with ground-based data for independent years (2004, 2006 and 2007), as shown in Figure 5.7. The mean and median of the ratio between the corrected data and ground-based data, and also the $\%W_{10}$, $\%W_{20}$, $\%W_{30}$, %AvgDiff and %Bias are given in Table 5.4, together with the corresponding values for the original OMI data.

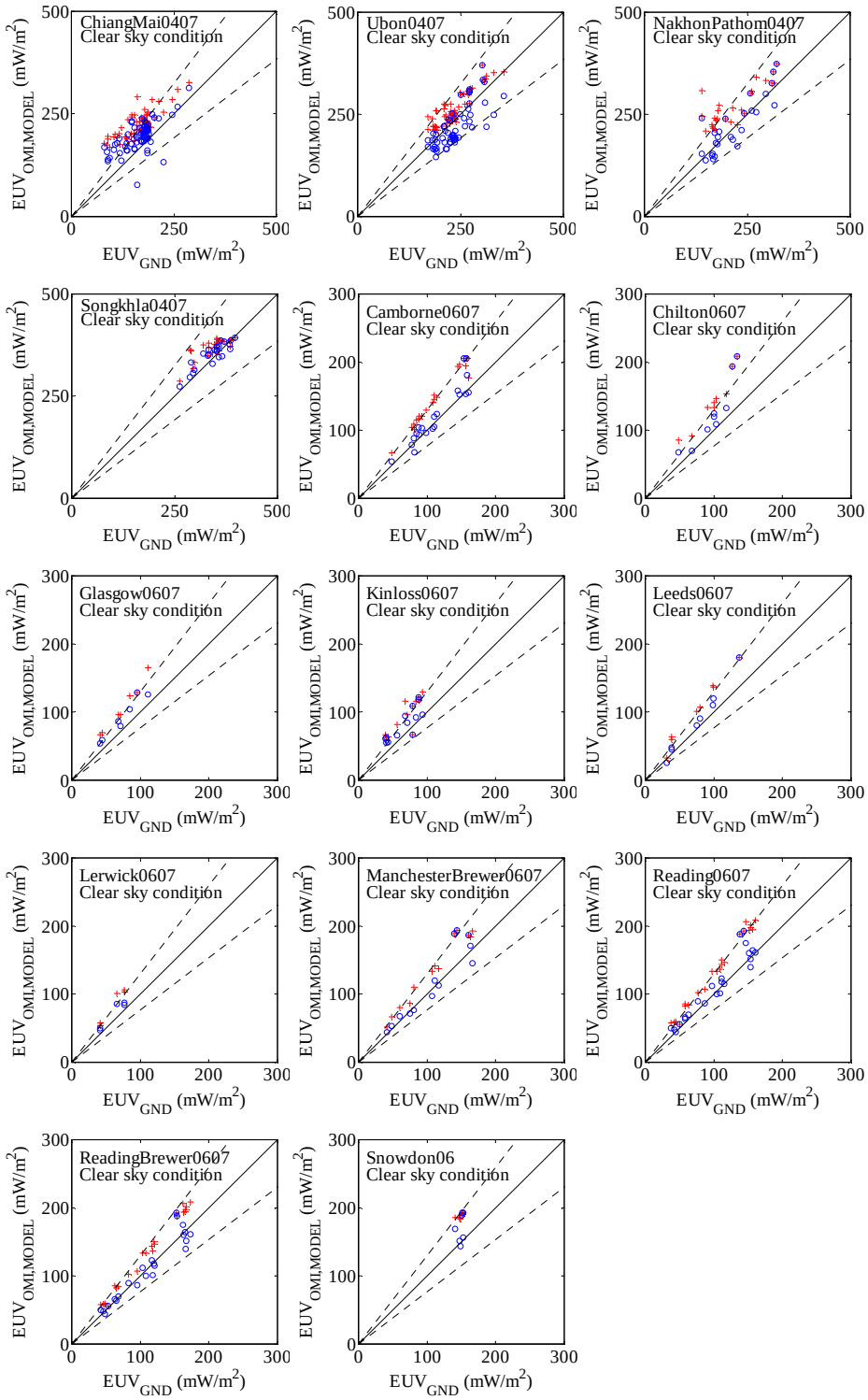

Figure 5.7 Comparison of erythemal irradiance at local solar noon from the original OMI (EUV_{OMI}, +) and the AAOD empirical model (EUV_{MODEL}, o) with ground-based measurements (EUV_{GND}) under clear sky conditions using AAOD from OMAERUV product. The 1:1 correlation (—) and ±30% limits (---) are also shown.

Table 5.4 The ratio of OMI corrected data and the ground-based data and the ratio of original OMI data and the ground-based data statistics under clear sky conditions using AAOD from OMAERUV product.

Sites	Cloudless conditions (Original OMI)								Cloudless conditions (AAOD model)							
	N	Median	Mean	$\%W_{10}$	$\%W_{20}$	$\%W_{30}$	%AvgDiff	%Bias	N	Median	Mean	$\%W_{10}$	$\%W_{20}$	$\%W_{30}$	%AvgDiff	%Bias
Chiang Mai	70	1.30	1.40	0	26	50	31	40	70	1.17	1.21	26	57	71	17	21
Ubon Ratchathani	59	1.11	1.13	42	80	92	12	13	59	0.90	0.93	37	81	100	-8	-7
Nakhon Pathom	26	1.24	1.29	15	42	58	24	29	26	1.01	1.03	46	85	96	2	3
Songkhla	24	1.08	1.08	67	92	100	8	8	24	1.04	1.03	92	100	100	3	3
Camborne	20	1.33	1.32	0	5	25	27	32	20	1.09	1.07	60	90	90	7	7
Chilton	9	1.42	1.46	0	0	11	37	46	9	1.19	1.25	22	56	67	21	25
Glasgow	7	1.46	1.47	0	0	0	38	47	7	1.29	1.26	0	29	57	23	26
Kinloss	13	1.39	1.42	0	8	8	34	42	13	1.34	1.29	8	38	38	24	29
Leeds	8	1.37	1.38	13	13	13	31	38	8	1.15	1.14	13	63	88	12	14
Lerwick	5	1.38	1.39	0	0	20	33	39	5	1.14	1.18	0	60	100	16	18
Manchester	13	1.27	1.26	0	38	62	23	26	13	1.08	1.08	54	85	85	6	8
Reading (Bentham)	23	1.33	1.33	0	4	43	28	33	23	1.10	1.10	52	87	87	9	10
Reading (Brewer)	23	1.24	1.23	4	26	91	21	23	23	0.99	1.02	78	91	100	1	2
Snowdon	7	1.25	1.26	0	0	86	23	26	7	1.21	1.15	43	43	100	13	15

It is apparent from Figure 5.7 and Table 5.4 that after the absorbing aerosol correction was included, all of the corrected erythemal irradiances at local solar noon were closer to the ground-based data especially for the Thai sites. The median ratios were reduced by 4%-24%, for example the median ratio was reduced from 1.08 to 1.04 for Songkhla and from 1.24 to 0.99 for Reading. Most of the corrected OMI UV data were within ±30% of the ground-based data, apart from Chilton, Glasgow and Kinloss. For Ubon Ratchathani, the corrected OMI data was slightly underestimated, which shows that the averaged urban aerosol correction may be slightly too high for this site. It is known that Ubon Ratchathani is cleaner than Chiang Mai, and also not subject to so much biomass burning. The cleanest site, Songkhla, has its own correction factor for maritime aerosol. Even so there is improvement particularly in $\%W_{10}$, with 85% of corrected OMI measurements lying within 10% of the ground-based data.

From the results, it could be concluded that the empirical model using aerosol absorption optical depth can also lead to an improvement in the OMI erythemal irradiance for all sites. The performance of the model depends on accuracy of aerosol absorption optical depth used in the model as can be seen when the ground-based AAOD values were used in the model.

5.3 Summary

In this chapter, two empirical models used for absorbing aerosol correction were introduced. The empirical models were generated using the erythemal irradiances at local solar noon of the year 2005. The corrected OMI erythemal irradiances of the years 2004, 2006 and 2007 for Thai sites, and only 2006 and 2007 for the UK sites were calculated and then compared with the ground-based data. Initially, there was overestimation of UV in the uncorrected OMI data (up to ~47%). After the absorbing aerosol correction factors were applied, for cloudless conditions, the differences between the OMI and ground-based data improved for both the Tropical sites (by up to 28%, site and method dependent) and the temperate sites (by 5%-30%, site and method dependent). These results are comparable to other recent studies taking a similar approach but using different input data for the correction [*Arola et al.*, 2009; *Ialongo et al.*, 2010; *Kazadzis et al.*, 2009a]. For example, a correction for absorbing

aerosol based on ground-based measurements were applied, leading to improvements in the OMI UV retrieval for several locations: 5%-20% at various sites across Europe [*Arola et al.*, 2009], 8%-25% in Rome [*Ialongo et al.*, 2010], and 7%-23% in Thessaloniki [*Kazadzis et al.*, 2009a]. Our results also show that the improvement is much better if the ground-based aerosol data are applied in the empirical models, since they are site specific and expected to represent the boundary layer better than the satellite data. Nonetheless, the correction using widely available satellite data is still significant, particularly when the AAOD correction is used.

Some of the work presented in Chapters 4 and 5 has been published in Journal of Geophysical Research and can be cited as *Buntoung, S., and A.R. Webb* (2010), Comparison of erythemal UV irradiances from Ozone Monitoring Instrument (OMI) and ground-based data at four Thai stations, *J. Geophys. Res.*, 115, D18215, doi:10.1029/2009JD013567, as presented in Appendix 2.

Chapter 6 – Extending Results to Cloudy Conditions

The erythemal irradiance at local solar noon retrieved from OMI under clear sky conditions was investigated and improved as described in Chapter 5. Two empirical models were introduced and used to correct the OMI UV data under clear sky conditions. From the results, it can be seen that after the aerosol correction was applied, the difference between the corrected OMI UV and ground-based UV data was reduced, and at some (but not all) sites the median bias was within the uncertainties of the ground-based data with which the corrected satellite data were compared. However, for all the sites considered, the clear sky case is not the norm and conditions with some degree of cloud cover must also be assessed.

It was shown in Chapter 4 that most of the OMI data overestimated the ground-based data, as it did for clear skies, but for all sky conditions there was considerably more scatter in the data (see, for example, Figure 4.1). This might be due to the fact that the noontime OMI UV and noontime ground-based UV data are not exactly synchronous and cloud is assumed constant in the OMI UV algorithm, which may not be true. In addition, OMI UV data is the averaged value of a large area while ground-based UV data is taken from a specific point, which can cause discrepancies particularly in broken cloud conditions. These mismatches can result in the additional differences (which may be positive or negative) between the two datasets when cloud appears.

In this chapter, an empirical method to improve the OMI erythemal irradiance at local solar noon for cloudy conditions is conducted. The corrected values were validated with ground-based data for cloudy conditions. The correction method was then extended to correct and validate the OMI erythemal data for clear sky conditions. The correction can be split into two requirements: to reduce the bias (as was the case for clear skies) and to reduce the scatter that is a feature of the great variability of cloud in both time and space.

6.1 Cloudy Sky Modelling

Since cloud effects on UV radiation are complex and depend on cloud type and sky coverage, cloud height and depth, and microphysical properties, data that are not available, a simple empirical model to improve the OMI noontime erythemal irradiance for cloudy conditions is introduced in this section. The aim of this is to reduce the bias in the cloudy sky data, while recognising that reduction of the scatter in the data is not possible without significantly more information, which is not routinely available: recall that we aim to improve the UV data available for regions where there is little or no ground-based information and standard satellite products must form the basis of all corrections.

Reducing the bias is essentially the same task as that presented in Chapter 5, and involves accounting for absorbing aerosols – note that the median bias was very similar for both cloudless and all sky conditions (see Chapter 4). However, the correction derived in Chapter 5, for two different aerosol types, rather than location, depends on input aerosol data from the ground or from satellite. In cloudy conditions, this data is not available. Aerosol optical depth measurement from the ground relies on the availability of direct sun, which may be intermittent but unreliable in broken cloud conditions, and absent in overcast conditions. Similarly, aerosol optical thickness, aerosol single scattering albedo and aerosol absorption optical thickness data from OMI can only be derived for cloud free conditions.

In the simplest approach to this problem, the OMI erythemal irradiances at local solar noon for cloudy conditions were plotted against the ground-based erythemal data as shown in Figure 6.1, separated into two cases: Thai and UK sites, for year 2005. The erythemal irradiance used to generate the model was from the OMUVB product that is available at http://avdc.gsfc.nasa.gov/ and ground-based measurement for the four Thai sites and nine UK sites in the year 2005.

While the clear sky corrections were based on aerosol type at the site (i.e., urban or maritime), the all sky data also includes the effect of cloud. Cloud influences can dominate the aerosol dependent effects, and the cloud and aerosol effects can interact, with the end result on radiative transfer depending on both cloud and

aerosol properties. Urban aerosols seem to have similar effects on UV radiative transfer under clear skies in any climate (Chapter 5), but Tropical clouds can be quite different to those experienced in the temperate UK. A typical example would be the comparison of towering Tropical cumulonimbus clouds versus the stratus layer that accompanies a midlatitude warm front. For this reason, and the fact that the correction does not depend directly on aerosol data, the cloudy sky correction was based on sites allocated by region (cloud type) rather than by aerosol type.

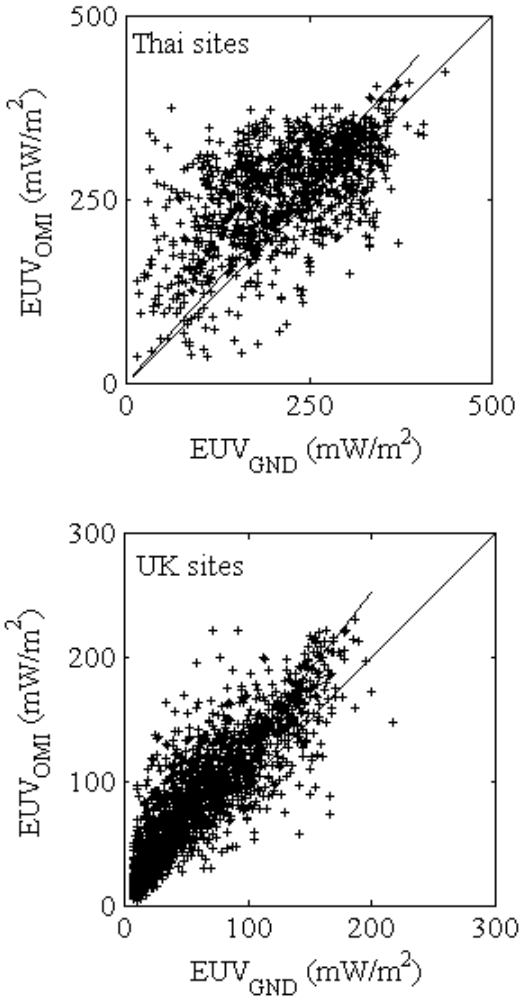

Figure 6.1 Comparison between the noontime OMI erythemal data (EUV_{OMI}) and the noontime ground-based erythemal data (EUV_{GND}) for cloudy conditions of year 2005.

As can be seen in Figure 6.1 most of the OMI erythemal irradiance for UK sites and over half those for Thai sites are higher than the ground-based erythemal data. There

is a great deal more scatter in the Thai data, perhaps due in part to the range of times between OMI overpass and noon, but also to the nature of Tropical cloud. The slope of the Thai graph was lower than that of UK graph, values being 1.12 and 1.26, respectively. Thus, the OMI erythemal data can be adjusted by using the slopes as follows:

$$E_{CORR} = F_{CLOUD} \cdot E_{OMI} \tag{6.1}$$

where E_{CORR} is the corrected OMI erythemal irradiance for cloudy conditions, E_{OMI} is the original OMI erythemal irradiance for cloudy conditions, and F_{CLOUD} is cloud correction factor shown below:

$$F_{CLOUD} = \frac{1}{1.12} \quad \text{for Thai sites}$$

and $$F_{CLOUD} = \frac{1}{1.26} \quad \text{for UK sites.} \tag{6.2}$$

6.2 Validation for Cloudy Sky Conditions

To validate the empirical model for cloudy conditions, the erythemal irradiances at local solar noon in the years 2004, 2006 and 2007 for Thai sites, and 2006 and 2007 for UK sites, which are independent from the model data, were used. Using the empirical model as expressed in Equations 6.1 and 6.2, the corrected OMI erythemal irradiances for cloudy conditions were calculated. Then the modelled erythemal irradiances were compared with the ground-based erythemal irradiances. The comparison results are shown in Figure 6.2 and the statistical analysis such as the median of the ratio, $\%W_{10}$, $\%W_{20}$ and $\%W_{30}$ are also shown in Table 6.1, including the comparison between the original OMI data and corrected OMI data.

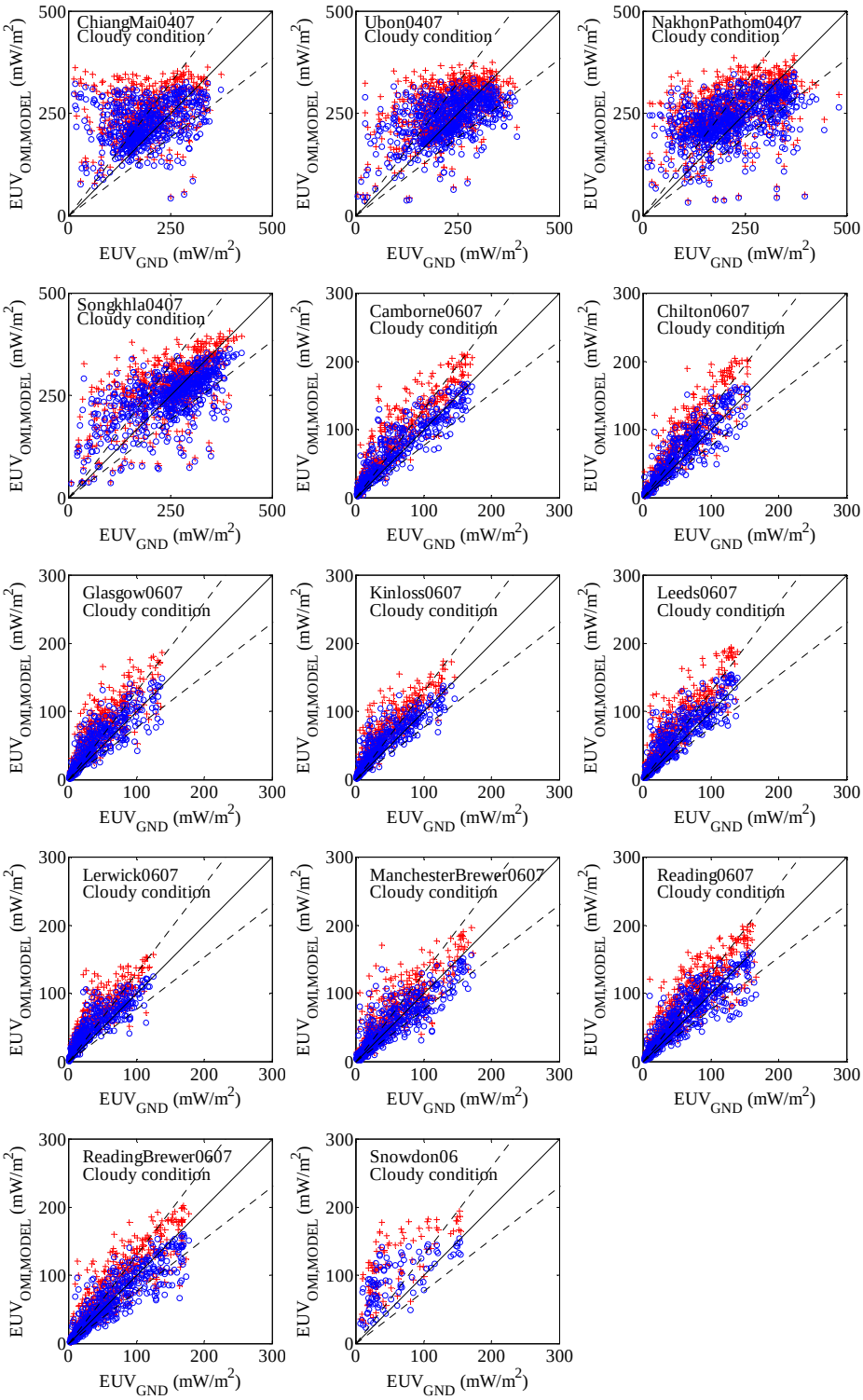

Figure 6.2 Comparison of erythemal irradiance at local solar noon from the original OMI (+) and the empirical (cloudy) model (o) with ground-based measurements under cloudy conditions. The 1:1 correlation (—) and ±30% limits (---) are also shown.

Table 6.1 The ratio of the original OMI data and the modelled data to ground-based data for cloudy conditions.

Sites	Cloudy conditions (Original OMI)								Cloudy conditions (cloudy model)							
	N	Median	Mean	$\%W_{10}$	$\%W_{20}$	$\%W_{30}$	%AvgDiff	%Bias	N	Median	Mean	$\%W_{10}$	$\%W_{20}$	$\%W_{30}$	%AvgDiff	%Bias
Chiang Mai	568	1.28	1.69	17	34	50	30	69	568	1.14	1.51	26	49	65	19	51
Ubon Ratchathani	653	1.13	1.36	30	53	66	19	36	653	1.01	1.21	32	56	73	8	21
Nakhon Pathom	723	1.25	1.48	21	37	51	24	48	723	1.11	1.32	24	45	61	13	32
Songkhla	634	1.08	1.29	38	60	69	14	29	634	0.96	1.16	35	61	72	4	16
Camborne	473	1.56	1.91	8	17	29	50	91	473	1.23	1.51	25	42	55	28	51
Chilton	494	1.49	1.65	7	18	28	40	65	494	1.18	1.31	24	44	62	18	31
Glasgow	487	1.66	1.94	6	13	19	53	94	487	1.32	1.54	14	29	45	32	54
Kinloss	490	1.84	2.16	4	10	18	61	116	490	1.46	1.72	17	30	39	40	72
Leeds	494	1.48	1.83	8	20	30	46	83	494	1.18	1.45	25	47	60	25	45
Lerwick	503	2.09	2.46	3	7	13	70	146	503	1.66	1.95	15	23	30	50	95
Manchester	572	1.26	1.68	18	37	51	30	68	572	1.00	1.34	28	49	65	8	34
Reading (Bentham)	649	1.35	1.55	11	24	42	34	55	649	1.07	1.23	31	52	63	12	23
Reading (Brewer)	619	1.25	1.43	18	38	53	25	43	619	0.99	1.13	30	54	68	3	13
Snowdon	94	2.37	2.82	2	10	19	77	182	94	1.88	2.23	16	22	33	58	123

It can be seen from the results in Figure 6.2 and Table 6.1 that the modelled data were closer to the one-to-one line. The median values of the ratio post-correction were closer to one for all data. Some datasets were slightly over-corrected compared with the ground-based data such as the data of Songkhla, but this was, and remains, close to the ground-based data on average. The average differences between the modelled data and ground-based data were within ±30% for all sites except Glasgow, Kinloss, Lerwick and Snowdon. It is noticeable that these sites can all be described by some combination of high latitude, high altitude and low data availability, where local or seasonal microclimates may influence the observed local UV irradiances (best captured by the ground-based data). Despite this, the UK-wide empirical correction was improved from the OMI correspondence with ground-based data even at these challenging sites. Overall, this method can improve the original OMI erythemal irradiances by about 12%-14% for Thai sites and about 30% for UK sites. As can be seen the correction method can only reduce the bias between the OMI UV data and the ground-based data, but does not much affect on the scatter.

6.3 Validation for Clear Sky Conditions

As it is noted in Chapter 5 that the absorbing aerosol correction for clear sky data depends on the availability of aerosol data, it should be useful if the empirical model for cloudy conditions described above can also be applied for the clear sky data. However, this may result in lowering the original OMI UV data and make it closer to the one-to-one line.

To compare performance of the empirical model in Sections 5.2 and 6.1, the same dataset of the erythemal irradiances at local solar noon under clear sky conditions used in Section 5.2.3 was used in this section. The OMI erythemal data was corrected using the model in Equations 6.1 and 6.2 and then compared to the ground-based data as shown in Figure 6.3 and Table 6.2.

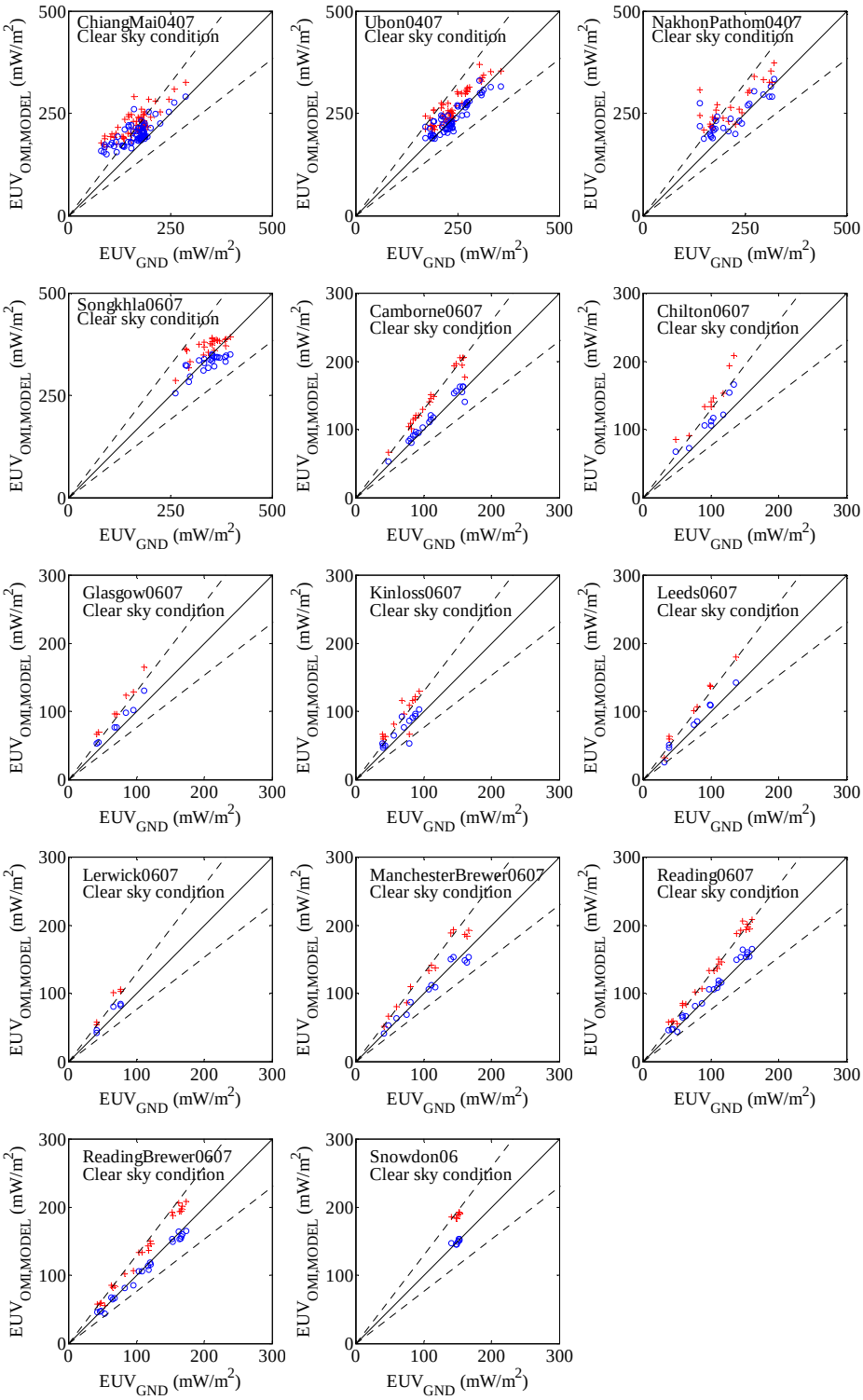

Figure 6.3 Comparison of erythemal irradiance at local solar noon from the original OMI (+) and the empirical (cloudy) model (o) with ground-based measurements under clear sky conditions. The 1:1 correlation (—) and ±30% limits (---) are also shown.

Table 6.2 The ratio of the original OMI data and the modelled data to ground-based data for clear sky conditions.

Sites	Clear sky conditions (Original OMI)								Clear sky conditions (cloudy model)							
	N	Median	Mean	$\%W_{10}$	$\%W_{20}$	$\%W_{30}$	%AvgDiff	%Bias	N	Median	Mean	$\%W_{10}$	$\%W_{20}$	$\%W_{30}$	%AvgDiff	%Bias
Chiang Mai	70	1.30	1.40	0	26	50	31	40	70	1.16	1.25	39	57	73	20	25
Ubon Ratchathani	59	1.11	1.13	42	80	92	12	13	59	0.99	1.01	81	95	100	1	1
Nakhon Pathom	26	1.24	1.29	15	42	58	24	29	26	1.11	1.15	42	65	85	12	15
Songkhla	24	1.08	1.08	67	92	100	8	8	24	0.96	0.97	71	100	100	-4	-3
Camborne	20	1.33	1.32	0	5	25	27	32	20	1.05	1.04	95	100	100	4	4
Chilton	9	1.42	1.46	0	0	11	37	46	9	1.13	1.16	33	67	89	14	16
Glasgow	7	1.46	1.47	0	0	0	38	47	7	1.16	1.17	29	71	100	15	17
Kinloss	13	1.39	1.42	0	8	8	34	42	13	1.10	1.13	23	69	77	11	13
Leeds	8	1.37	1.38	13	13	13	31	38	8	1.09	1.10	50	75	88	8	10
Lerwick	5	1.38	1.39	0	0	20	33	39	5	1.10	1.11	60	80	100	10	11
Manchester	13	1.27	1.26	0	38	62	23	26	13	1.01	1.00	85	100	100	0	0
Reading (Bentham)	23	1.33	1.33	0	4	43	28	33	23	1.06	1.06	74	96	100	5	6
Reading (Brewer)	23	1.24	1.23	4	26	91	21	23	23	0.98	0.98	91	100	100	-2	-2
Snowdon	7	1.25	1.26	0	0	86	23	26	7	1.00	1.00	100	100	100	0	0

It can obviously be seen from the results that all modelled data were closer to the one-to-one line. The median ratios were between 0.96 and 1.16 for the two countries, where the negative biases were shown for the data of the clean aerosol sites such as Songkhla. Over half of the modelled erythemal data were within ±20% compared to the ground-based data. What is interesting is that the improvement by using the cloudy model as described above is slightly better than that using the AAOD or AOD correction methods that are shown in Section 5.2.

6.4 Summary

In this chapter, the empirical method used to improve the OMI noontime erythemal irradiance for cloudy conditions was introduced. After the empirical model was applied, the modelled OMI erythemal irradiances show the better agreement than the original OMI erythemal irradiances, compared with the ground-based data. This method can adjust the OMI data to be closer to ground-based data by about 12%-14% for Thai sites and about 30% for UK sites, but does not solve for cloud variation causing the remaining scatter data. In addition, the empirical model was tested with the clear sky erythemal data. The validation results were slightly better than the results that were described in Chapter 5, where the aerosol correction was applied. This may be due to the uncertainty of the OMI aerosol data. In general, therefore, it seems that the empirical model suggested in Section 6.1 can be used for both cloudy and clear sky conditions, and whether aerosol data is available or not.

As can be seen the empirical method discussed in this chapter can be used to adjust the OMI noontime erythemal irradiance for anywhere, for example, the whole country of Thailand, as far as the OMI erythemal data is available. In addition, this simple empirical method does not depend on aerosol data that is not always available.

Chapter 7 – Extending Results to Generate UV Maps for Thailand

The amount of erythemal irradiance is normally converted (scaled) to UV Index for public dissemination. As described in Chapter 2, the UV Index is a dimensionless number of value between zero and 12 (or more), provided in public broadcasts as an integer number that indicates the sunburning power of the sun at a given time and place. Maps of UV Index have been provided in several countries for example the U.S., Europe and Australia. In Thailand, the UV Index has been presented at only four sites; Chiang Mai, Ubon Ratchathani, Bangkok and Songkhla by Thai Meteorological Department. In a study of *Janjai et al.* [2010], they generated maps of the monthly average erythemal daily dose and the yearly average erythemal daily dose from years 1995 to 2002 over Thailand. Their study used satellite-derived earth-atmospheric albedo (obtained from Geosynchronous Meteorological Satellite-5), total column ozone (retrieved from TOMS) and other ground-based ancillary data (e.g., visibility and aerosol single scattering albedo) as the input parameters. The root mean square difference and mean bias difference between the monthly average erythemal daily doses calculated from the model and ground-based measurements were 12.3% and 0.7%, respectively.

In this study, we have attempted to extend the daily noontime erythemal dose rate and thus the UV Index information to the entire area of Thailand. While the work of *Janjai et al.* [2010] provides climatological data in terms of monthly means and daily doses, the current work indicates the actual noontime (assumed maximum) UV Index for the day in a format with which the public are familiar. This study takes advantage of satellite OMI UV retrievals, and the corrections based on the methods described in Chapter 5 (for clear sky conditions) and Chapter 6 (for cloudy conditions) to generate maps of the noontime erythemal irradiance and then the UV Index over Thailand. Our method needs only two main parameters as the inputs, which are the OMI erythemal dose rate at local solar noon and the OMI aerosol absorption optical depth. Additional information is needed to identify sky conditions either clear or cloudy.

7.1 Operational Approach

In an operational environment, where the aim is to produce corrected daily noontime UV Index on a regular basis, a decision tree is required to adopt the most appropriate correction for each day. This is particularly important at the present time because some satellite data products have not been available for very many years, so this work dealt with incomplete data sets. This is particularly true for AAOD data where in some regions there is not enough information even to provide a monthly mean value. The cloudy correction (Chapter 6) is empirically based and aerosol correction is intrinsic in the overall correction. However, where more precise data for a given location/time are available then the clear sky correction (Chapter 5) is more appropriate.

The initial pragmatic approach has to be based on availability of data. Using this criterion, the data to consider are:

a) Satellite noontime UV data – usually available for every pixel for every day (sometimes a few pixels are missing if the overpass just misses an area. Typically a "*stripe*" of blank pixels occurs across the country, see Figure 7.1)

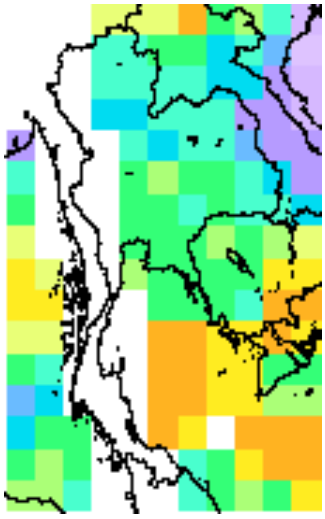

Figure 7.1 An example of a stripe of blank pixels of OMI noontime erythemal data across Thailand on 07/08/2009.

b) Satellite AAOD data – available for most pixels if the area is cloud free (daily basis)

– monthly means for each year have been generated in this work, but still lead to missing pixels (see section 7.3, Figure 7.8)

– monthly means based on all three years available (see section 7.3, Figure 7.9) provide the best estimate that would be available at present. With time, the monthly means will be based on more data until they become true climatological variables.

c) Cloud plus aerosol information – for cloudy conditions, there is no aerosol data available (although this does not define cloud conditions). Thus a correction of satellite UV data under cloudy conditions must use the empirical model which includes, implicitly, effects of aerosol and cloud.

Given this less than ideal access to the data required, the correction applied to the OMI erythemal data would be chosen according to the following criteria:

1) For clear sky conditions, satellite daily erythemal and AAOD data are widely available for the day. Then the clear sky correction is applied.

2) For clear sky conditions, satellite daily erythemal data is widely available, but daily AAOD data is missing. Then the clear sky correction is applied incorporating best available monthly mean data for AAOD. If only a few pixels of data missing, use daily values from adjacent pixels.

3) For cloudy regions or country, satellite daily erythemal data is widely available, but no AAOD data is available. Then the cloudy correction which implicitly includes aerosol is applied.

4) In case of no information on cloud/aerosol, satellite daily erythemal data is only available. Then the cloudy correction, i.e. the default correction that also works reasonably well for clear skies (Chapter 6) is applied.

5) For default case, no satellite daily erythemal data is available. Then the cloudy correction is applied to satellite monthly erythemal data.

The problem then becomes one of identifying clear sky conditions, using only the satellite overpass data. Earlier we used ground-based data to identify clear sky days. This is no longer an option as there are few ground-based stations. The sky

conditions in the examples given in the following work were identified manually from satellite visible images retrieved from Meteorological satellite. However, another method to identify sky conditions, that relies only on OMI data, was used in *Arola et al.* [2009]. This would negate the need to use more than one satellite product, and would be preferable for widespread operational use. Therefore, this method is included in the outline decision making, below. The OMI clear sky erythemal dose rate (EUV_{clr}) and the OMI erythemal dose rate (EUV_{cld}) at local solar noon included in the OMUVBd product were used together. Sky conditions are separated by using OMI cloud modification factor ($CMF=EUV_{cld}/EUV_{clr}$). Clear sky data is determined when the cloud modification factor is higher than 0.95.

Overall approach is summarised as a flow chart shown in Figure 7.2.

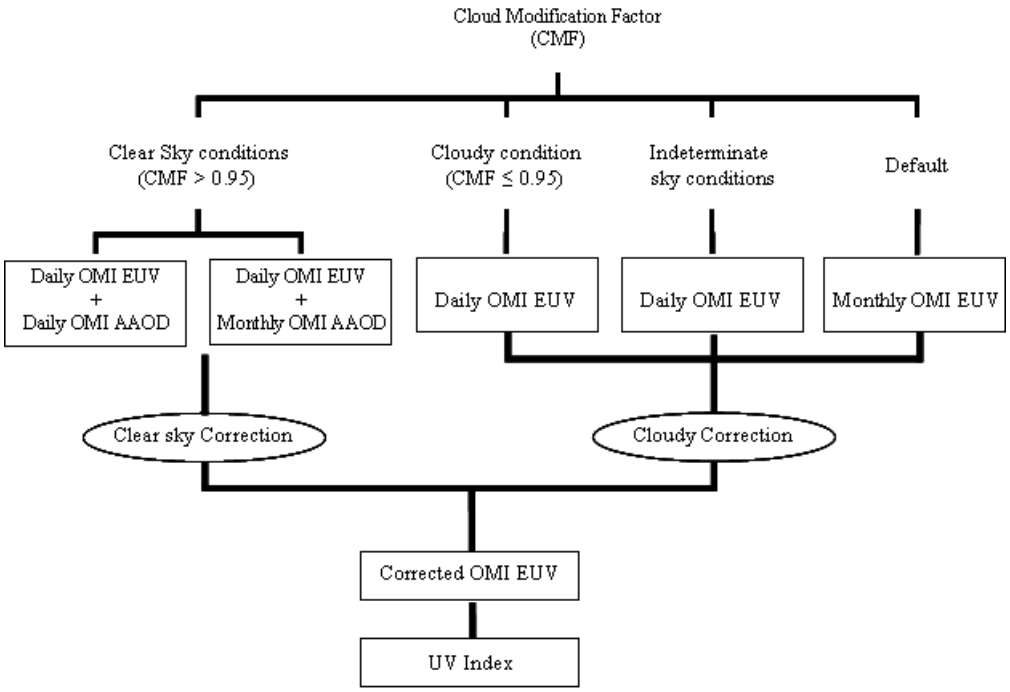

Figure 7.2 Operational approach to correct OMI noontime erythemal dose rate in this thesis.

7.2 Mapping Input Data

For the mapping process, there are two main parameters needed as input data into the empirical models described in earlier chapters. The first parameter is erythemal dose

rate at local solar noon taken from the OMUVBd OMI data product, and the second data is AAOD at 388 nm included in the OMAERUVd OMI data product. Both datasets are in the OMI level 3 data products and can be acquired from the NASA's Goddard Earth Sciences Data and Information Services Centre (GES DISC, data available at http://disc.sci.gsfc.nasa.gov). The data is in the HDF-EOS format.

The OMI level 3 data products contain data for a 1.0 degree by 1.0 degree longitude by latitude grid covering the whole globe [*OMI Team*, 2009]. These products are produced by weighted averages of best pixel data from single orbit level 2 OMUVB swath observations over the fixed grids from latitudes -180° to +180° and longitudes -90° to +90° [*McPeters et al.*, 1998]. The dimensions of the grids are 360 by 180. The centre of the first grid cell is located at longitude -179.5° and latitude -89.5°. The centre of the final grid cell is located at longitude +179.5° and latitude +89.5°. The centre of the grid itself is located at longitude 0.0° and latitude 0.0°, and corresponds to the corners of four grid cells. Examples of the noontime erythemal dose rate and AAOD data are shown in Figure 7.3 and 7.4. Note, the stripes of unavailable data are shown in Figure 7.3, and the paucity of data in Figure 7.4.

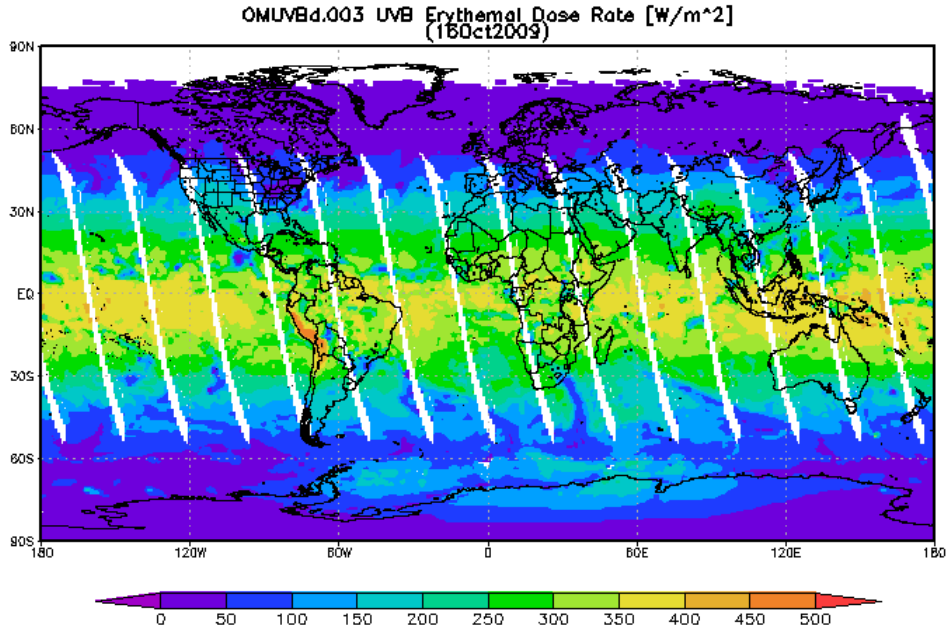

Figure 7.3 An example of noontime erythemal dose rate from OMUVBd data product of 16 October, 2009. This figure was produced with the Giovanni online data system, developed and maintained by the NASA GES DISC.

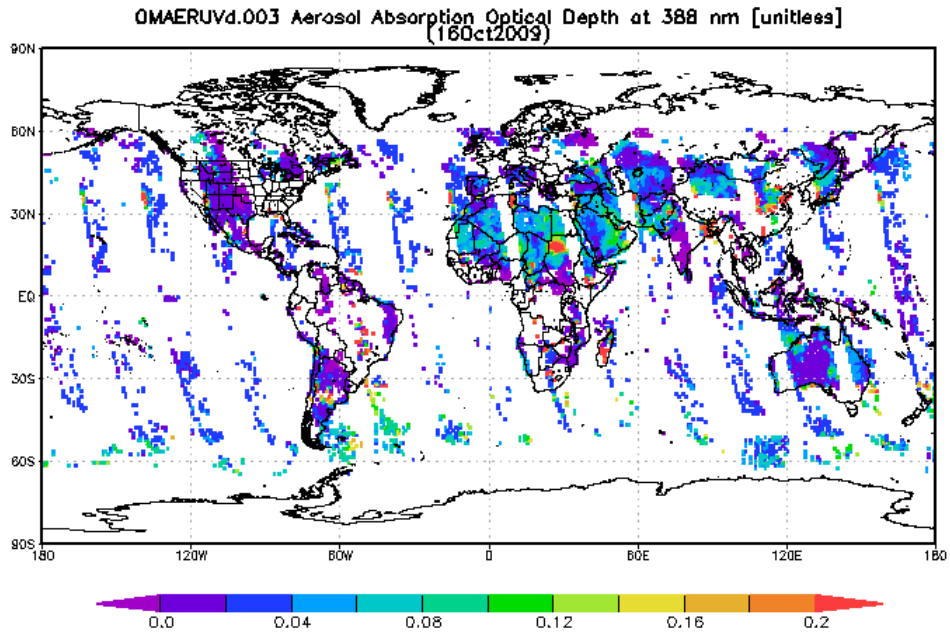

Figure 7.4 An example of AAOD from OMAERUVd data product of 16 October, 2009. This figure was produced with the Giovanni online data system, developed and maintained by the NASA GES DISC.

The OMUVBd product (accessed for this work on 20 July 2010) was available from 2 January, 2007 to 27 February, 2010 and the OMAERUVd product was available from 1 October, 2004 to 18 July, 2010. It is expected that both data sets will be available in the future. In this study, the coincident data during 2 January, 2007 to 31 December, 2009 were used.

In this study, the OMI noontime erythemal dose rate and OMI AAOD data covering Thailand are selected. The original OMUVBd and OMAERUVd products in HDF-EOS format contain data as an array (180×360 pixels) covering the latitudes from 90ºS to 90ºN and the longitudes from 180ºW to 180ºE. The data covering Thailand i.e. the latitudes of 5ºN to 21ºN and the longitudes of 96ºE to 107ºE, were then selected (16×11 pixels) by using a program written in Interactive Data Language program.

7.3 Methodology

As we can see from the examples of the erythemal dose rate at local solar noon and AAOD data in Figures 7.3 and 7.4, the data sets are incomplete, especially for the AAOD data. This is likely due to cloud contamination and algorithm flags (see in README for OMAERUVd available at http://disc.sci.gsfc.nasa.gov/Aura/data-holdings/OMI/, which provides details of conditions when data are not valid).

To overcome this problem for Thailand, first the monthly mean AAOD data by year was calculated to see whether this would provide sufficient data. The results are illustrated in Figures 7.5-7.7. This still leaves blank pixels (white pixels), so the average for all three years was generated (Figure 7.8). If there still are blank pixels, the average value of adjacent pixels is used to give complete monthly AAOD data (Figure 7.9). Note that monthly AAOD data averaged from the three year period is not enough (which is far from ideal ~30 years) but build up to more complete climatology as years pass and data increases. From the figures we can see that AAOD each year are similar in pattern, being high in March/April and again in October, which can result from biomass burning.

The OMI aerosol absorption optical depth is then converted to aerosol correction factor (F_{AAOD}). Since the calculation of F_{AAOD} depends on aerosol types: urban and maritime, as shown in Equation 5.4, we assumed that the pixels higher than the latitude of 13ºN are occupied by urban aerosols while the others are occupied by maritime aerosols [*Janjai et al.*, 2005].

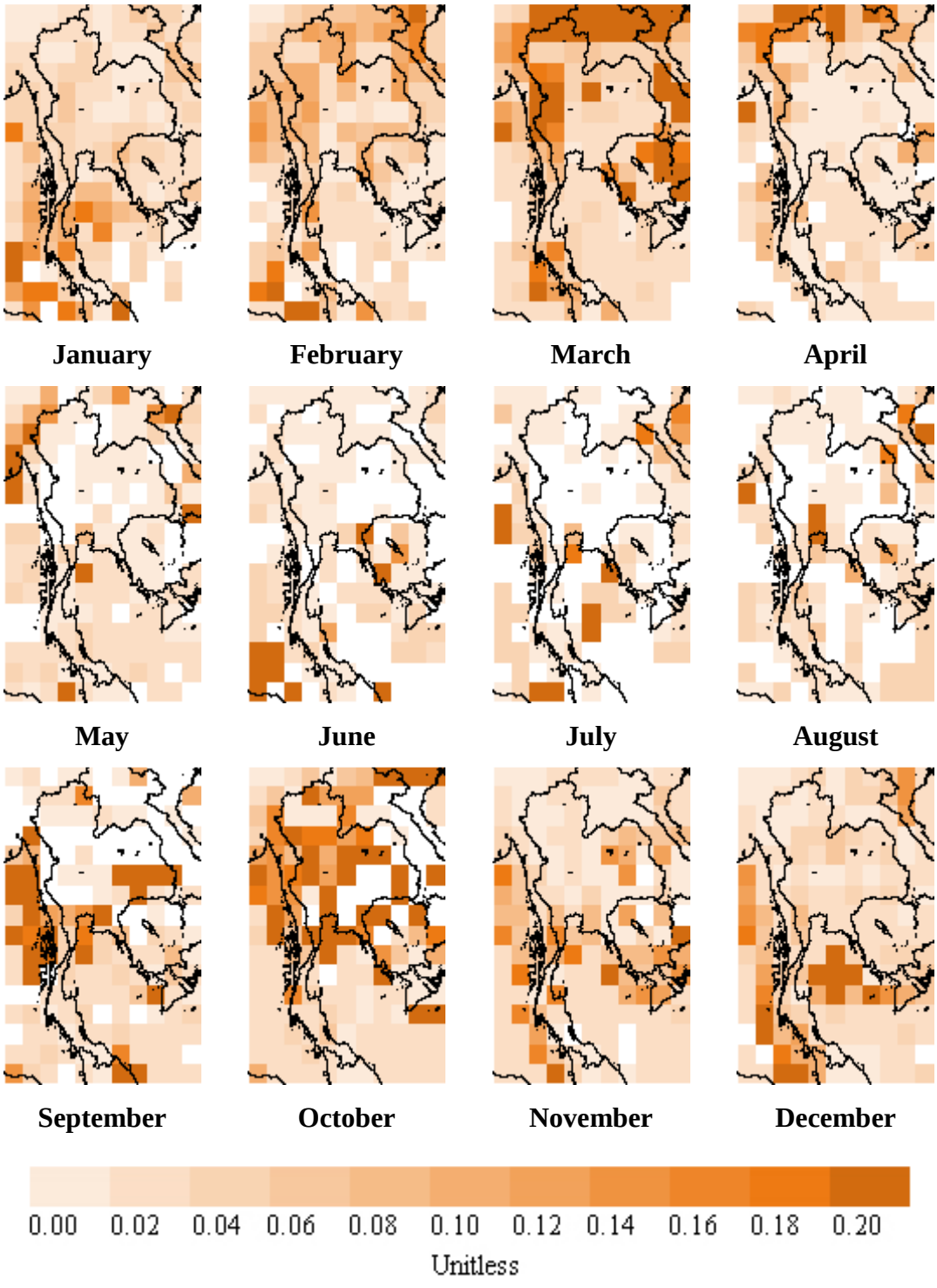

Figure 7.5 The monthly maps of AAOD over Thailand from OMAERUVd product, for year 2007 (white pixels represent no data).

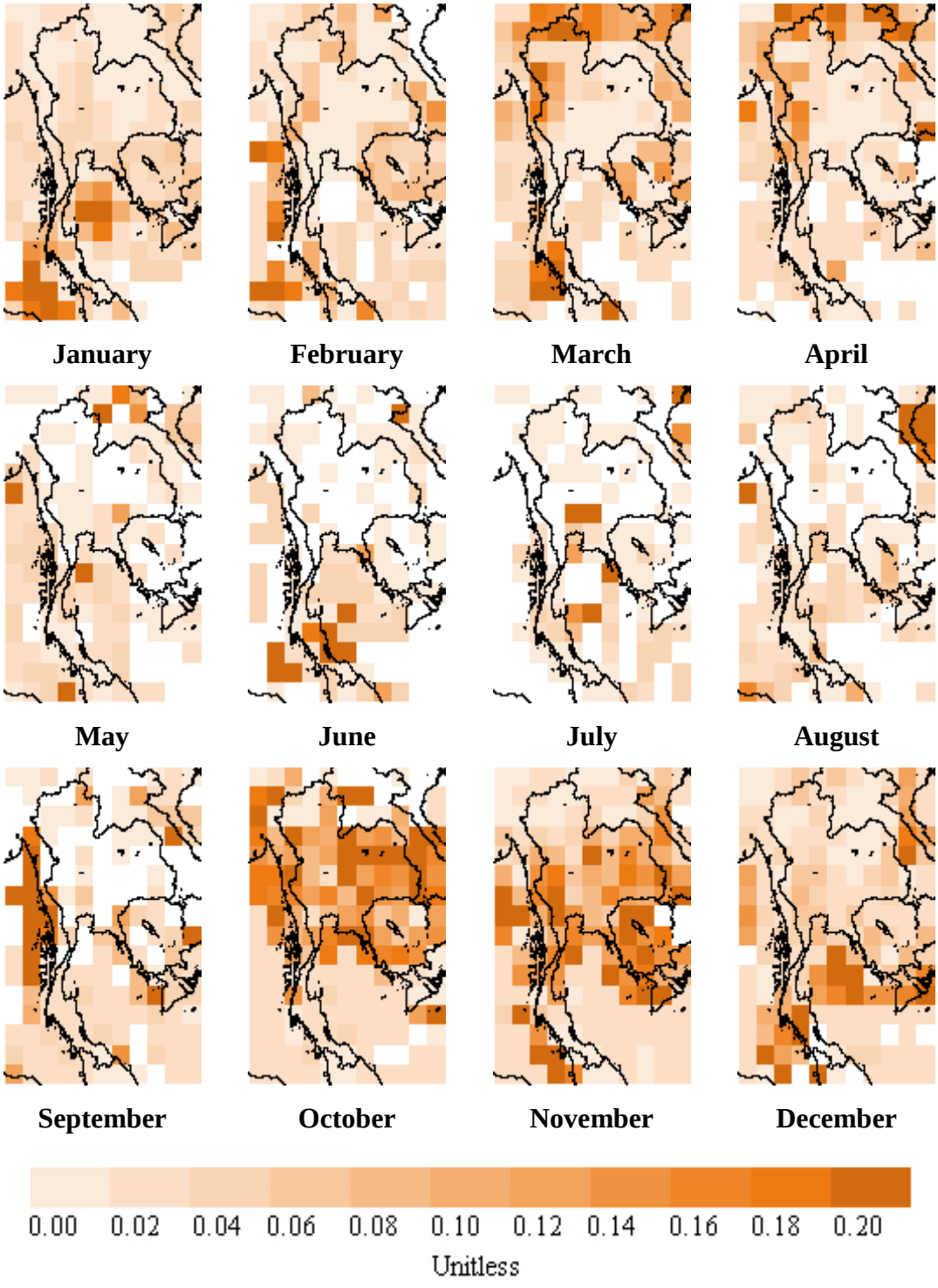

Figure 7.6 The monthly maps of AAOD over Thailand from OMAERUVd product, for year 2008 (white pixels represent no data).

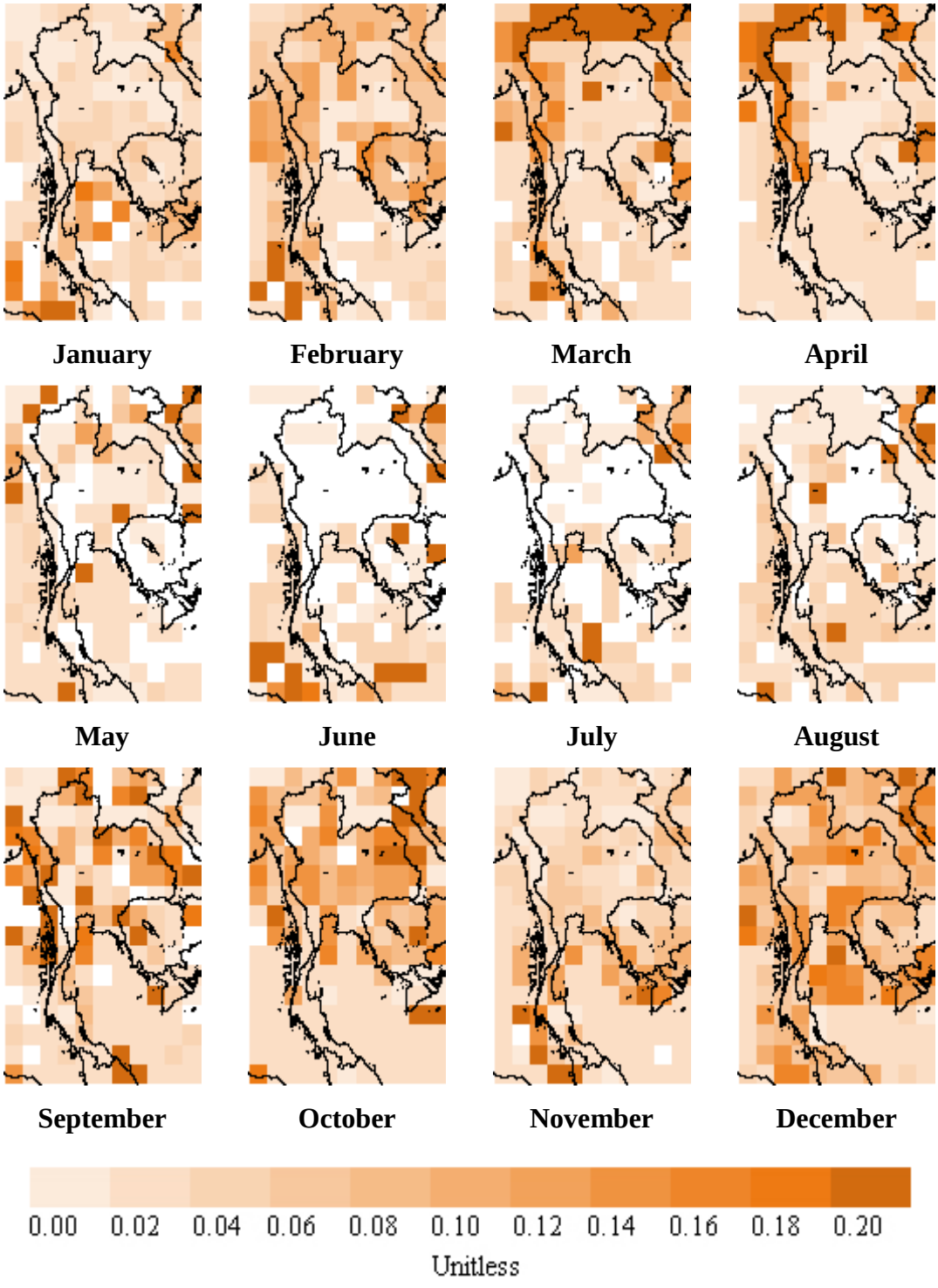

Figure 7.7 The monthly maps of AAOD over Thailand from OMAERUVd product, for year 2009 (white pixels represent no data).

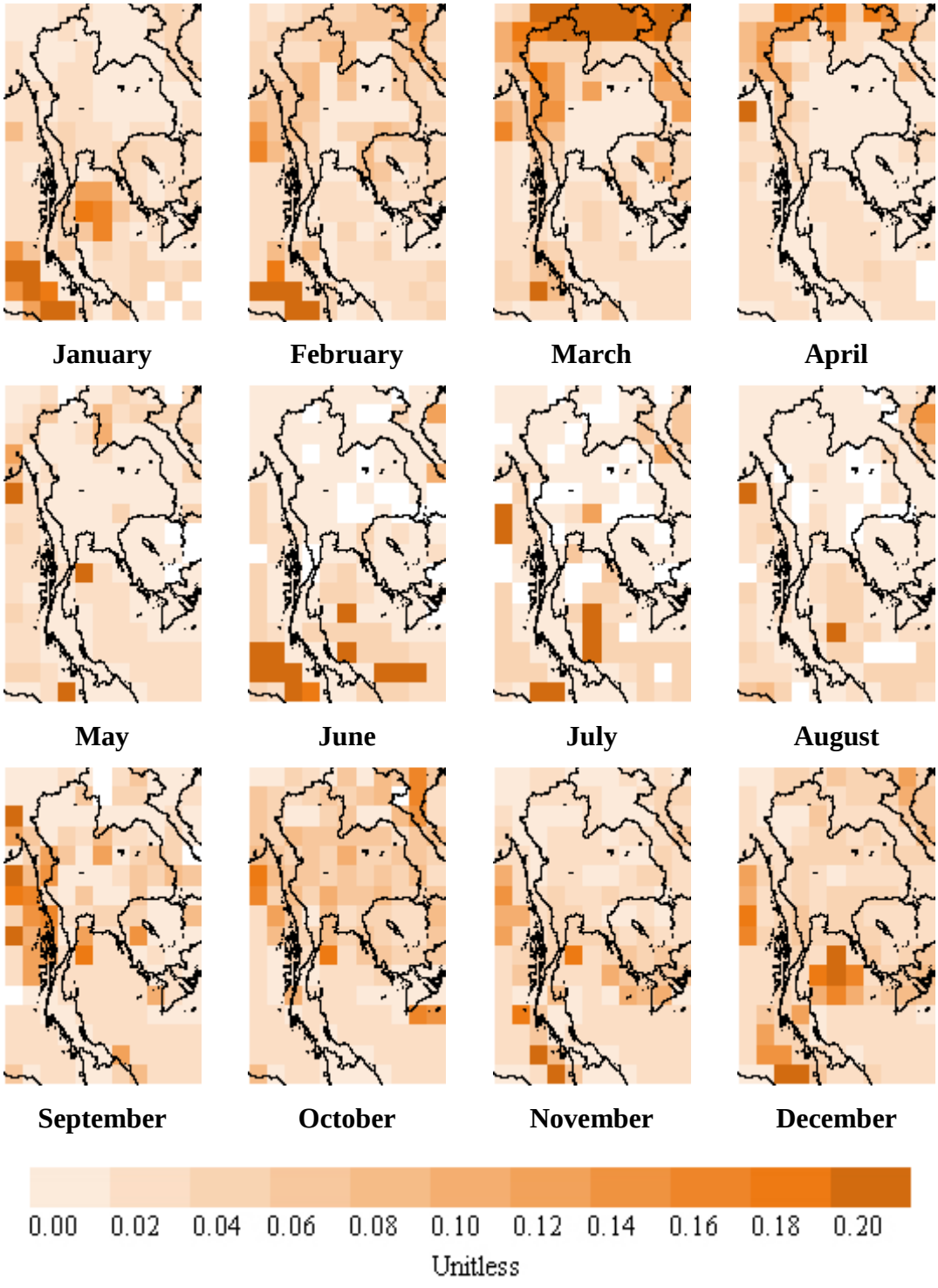

Figure 7.8 The monthly maps of AAOD over Thailand from OMAERUVd product for 3 years (white pixels represent no data).

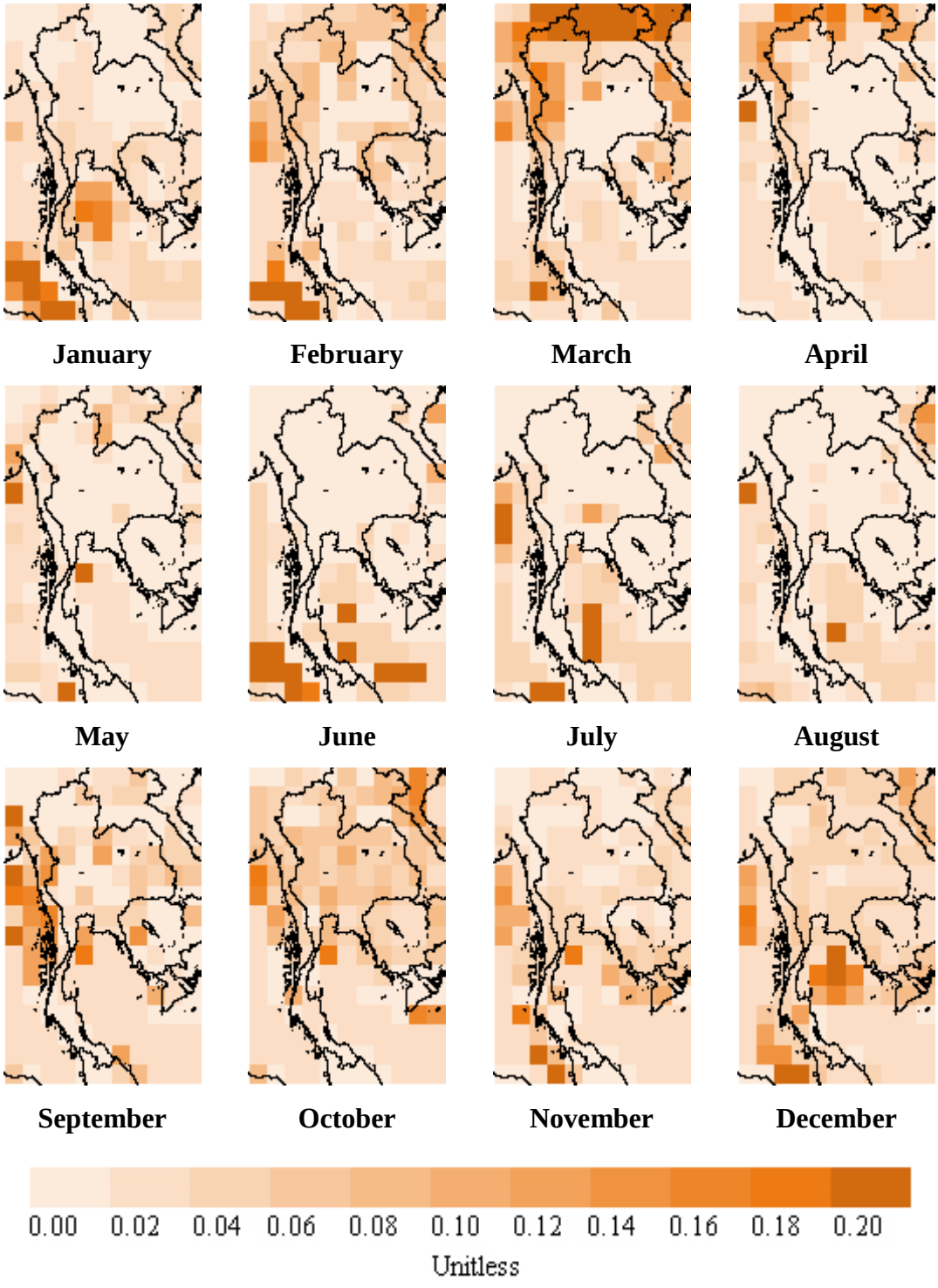

Figure 7.9 The monthly maps of AAOD over Thailand from OMAERUVd product for 3 years with adjacent filling gaps.

The UV data is generally more complete. However, on a daily basis there may still be missing pixels. It is however possible to generate monthly means of erythemal data for each year (see Figures 7.10-7.12), and have a complete data set averaged from the three years data (see Figure 7.13).

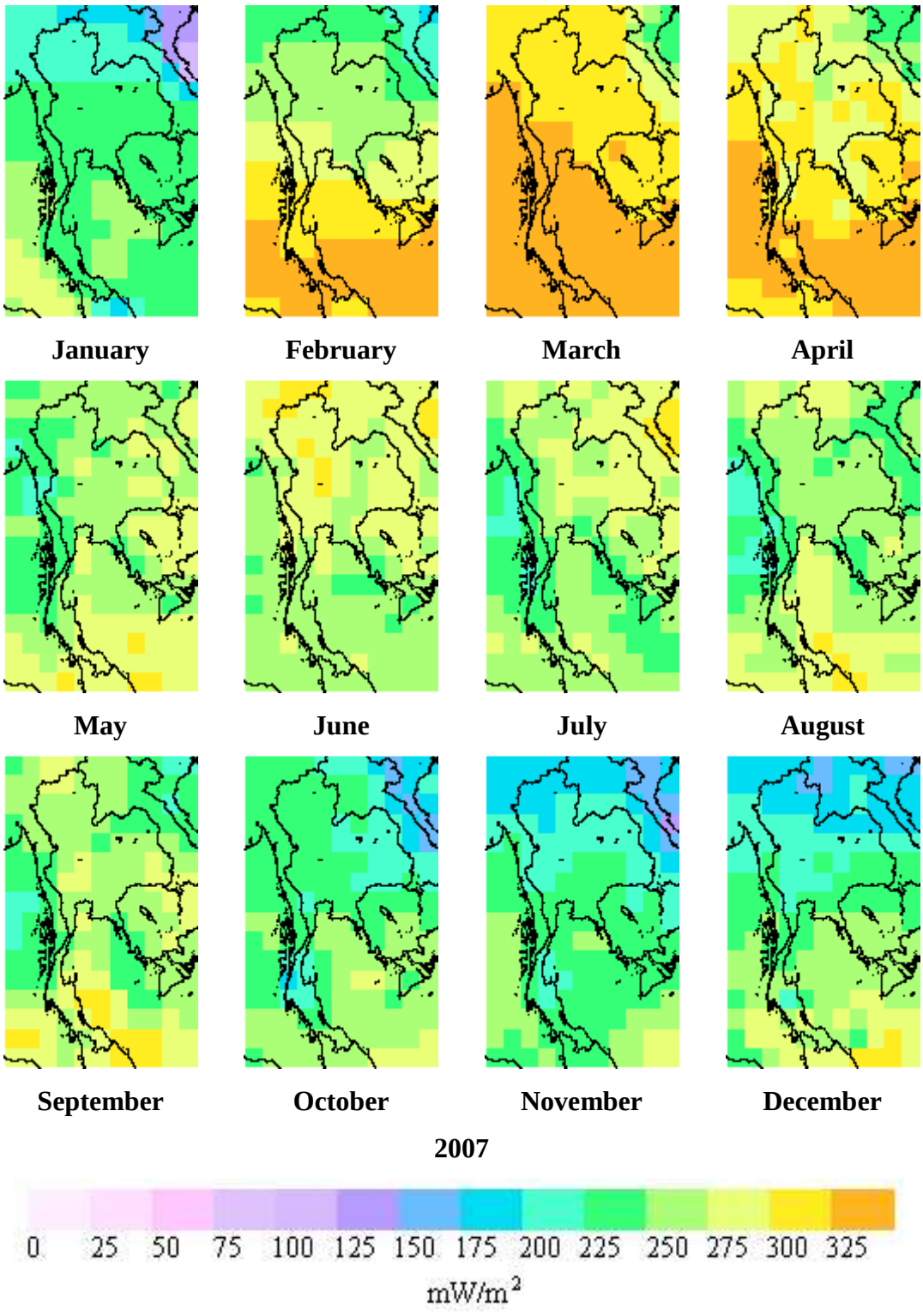

Figure 7.10 The monthly maps of erythemal irradiance at local solar noon over Thailand, for year 2007.

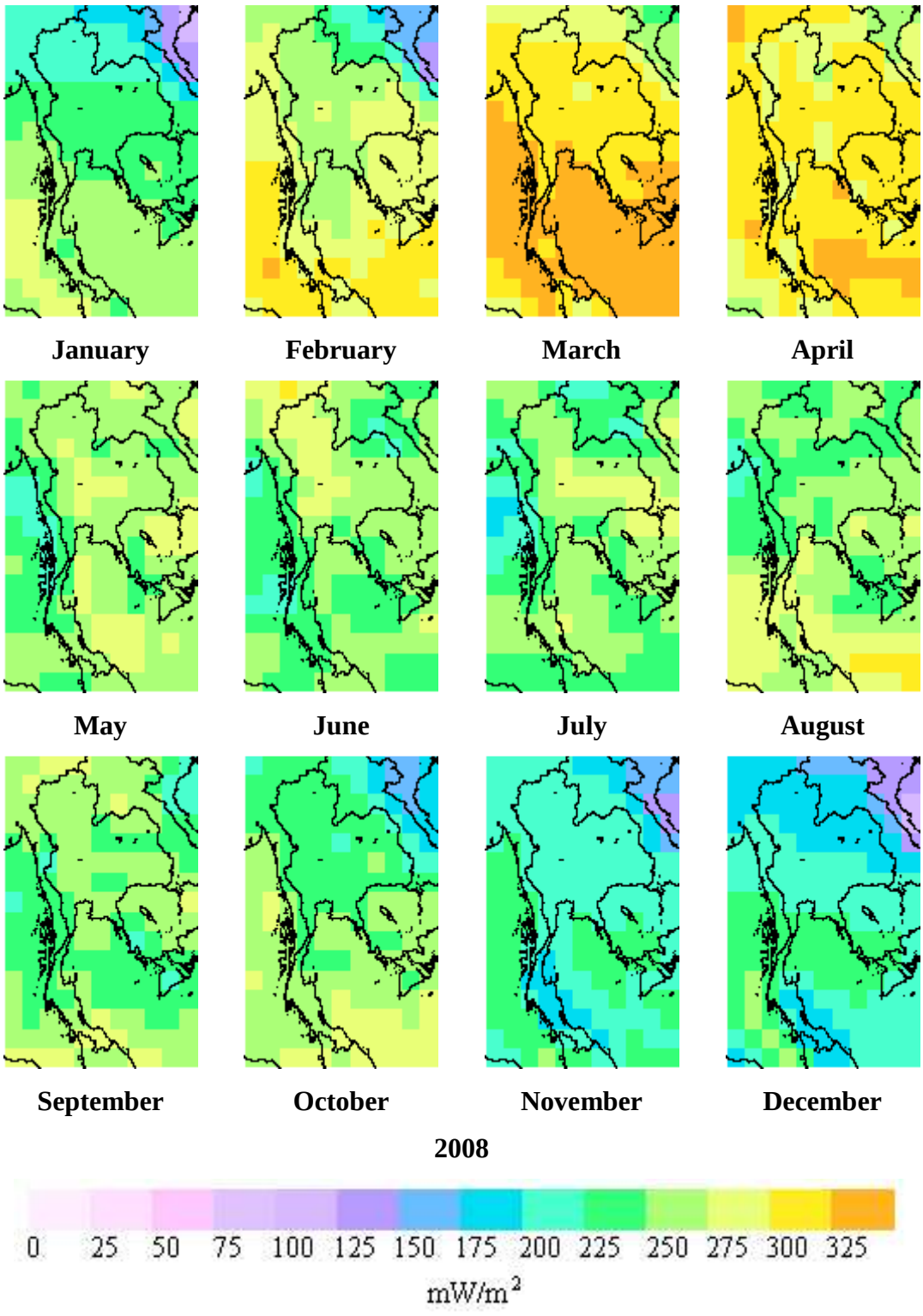

Figure 7.11 The monthly maps of erythemal irradiance at local solar noon over Thailand, for year 2008.

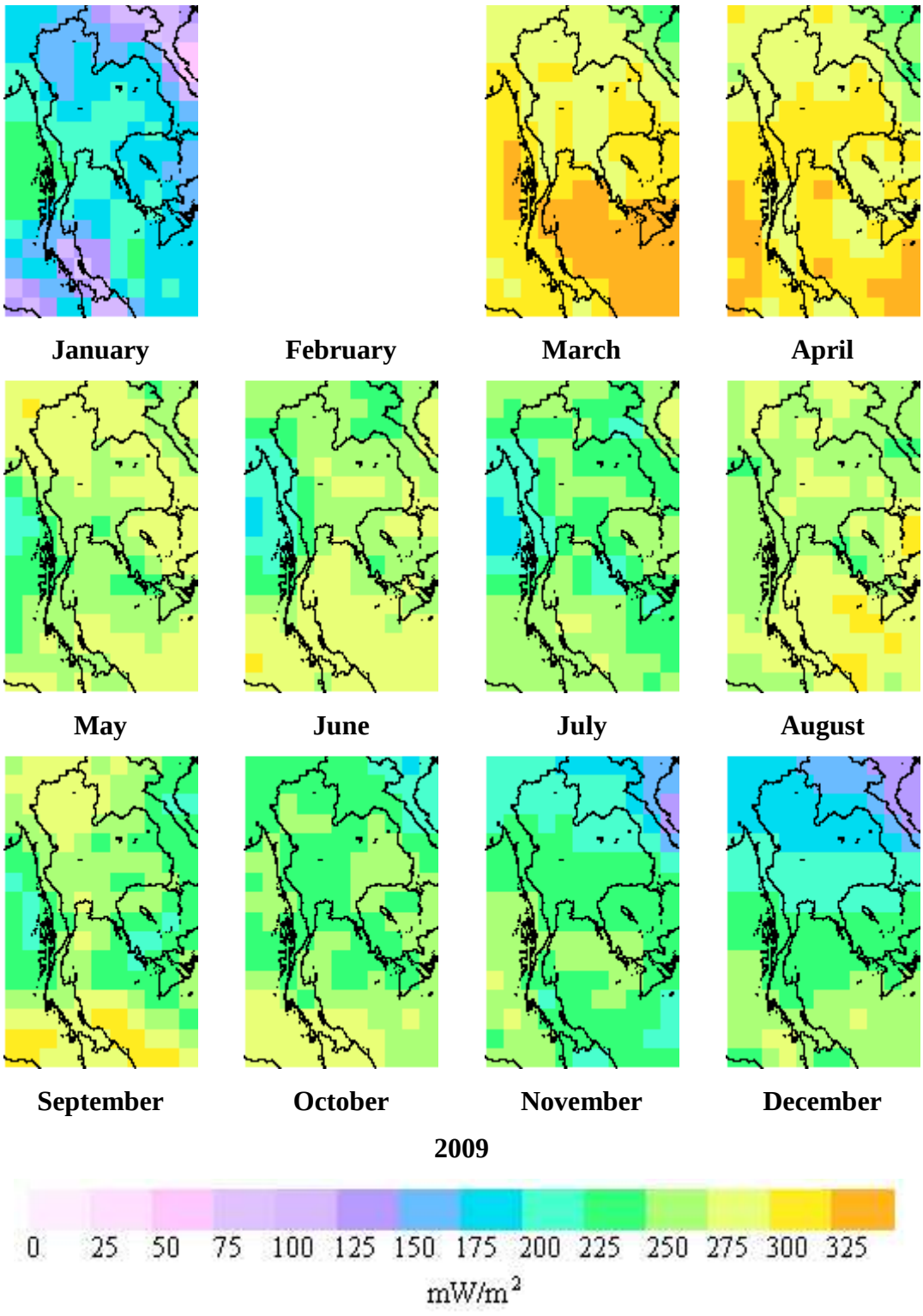

Figure 7.12 The monthly maps of erythemal irradiance at local solar noon from OMUVBd product over Thailand, for year 2009 (no OMUVBd data in February).

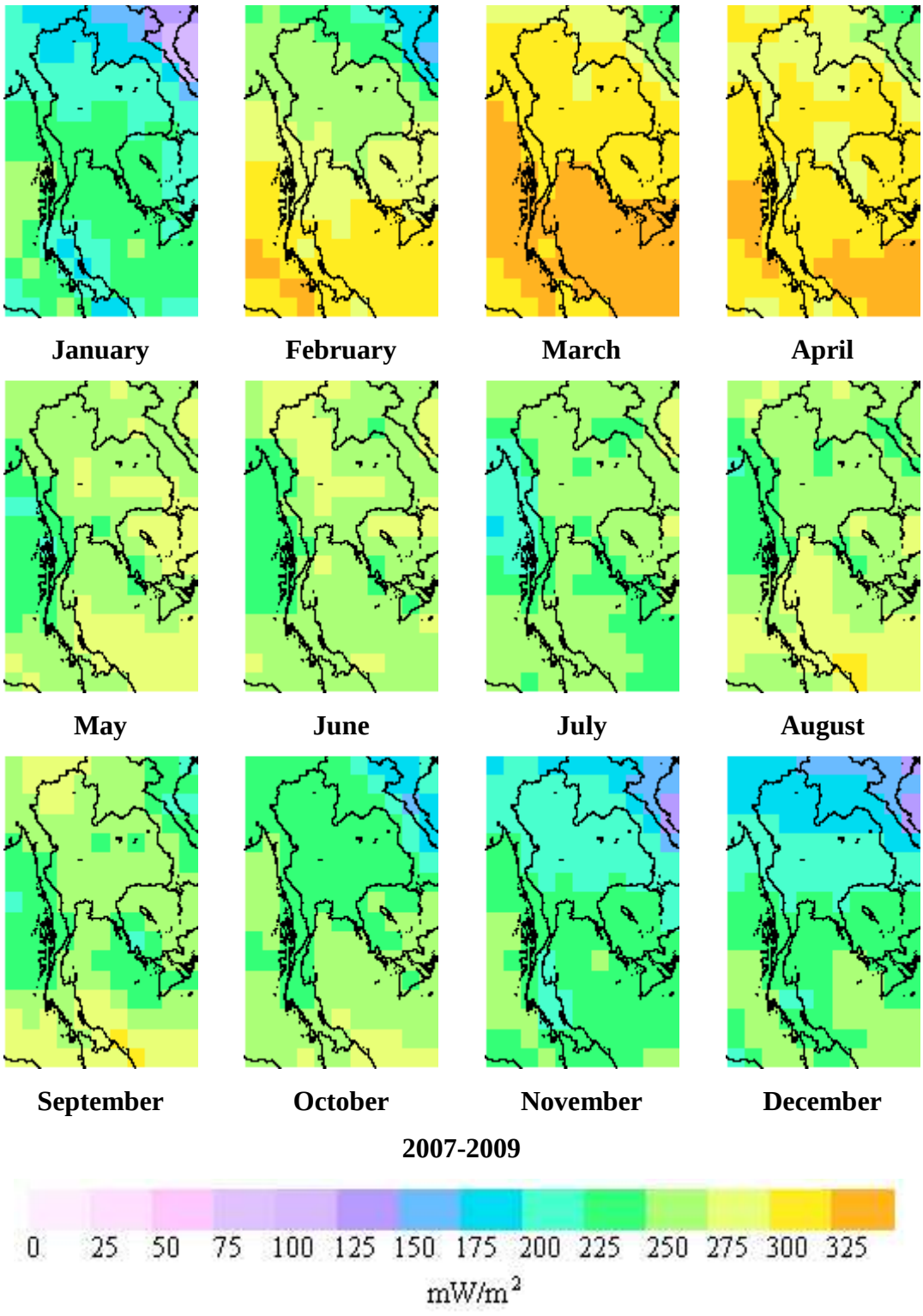

Figure 7.13 The monthly maps of erythemal irradiance at local solar noon from OMUVBd product over Thailand, for three years.

From the maps we can see that the general pattern of the monthly average erythemal dose rates at local solar noon is similar for each year, but details can be variable. There are distinct year to year differences. From January to April, the sun path moves northward from the southern celestial sphere toward the northern celestial sphere. Therefore, high erythemal dose rate areas increase progressively from the South to the North. From mid-May to mid-October, the influence of the South-West monsoon causing rain for the whole country decreases the erythemal dose rate over the country especially the western part of the country. From mid-October to mid-February, the North-East monsoon brings cool and dry air to the northern and north-eastern part but causes rainfall in the eastern part of the South. However, at this period the apparent sun path moves southward from the celestial equator causing low erythemal dose rate in the North, the Northeast and the Centre.

The following figures illustrate, for specific cases, the generation of UV Index maps based on varying amounts of data availability, starting with the worst case (no AAOD and missing UV pixels), and proceeding to the best case (fully available daily data). Since a goal of this thesis is to extend the results for public use, the corrected noontime erythemal dose rate ($mW \cdot m^{-2}$) in each case was divided by 25 in order to calculate the noontime UV Index over the country (see Figures 7.14-7.17, where $\times$ in the UV Index maps represents the position of ground-based sites).

The lowest level default for a UV map of Thailand (e.g. if a data blank covers much of the country for a day), based on the maps generated above and the work of Chapters 5 and 6, would then be the year specific monthly mean UV corrected with the default cloud correction, to give monthly mean corrected UV for year 20XX (see Figure 7.14). This would apply for past data. For near real time data (e.g. yesterday) a year specific monthly mean is not available, and instead the long-term monthly mean data must be used e.g. Figure 7.13 which is the average of years 2007-2009, but can be improved upon as more data becomes available.

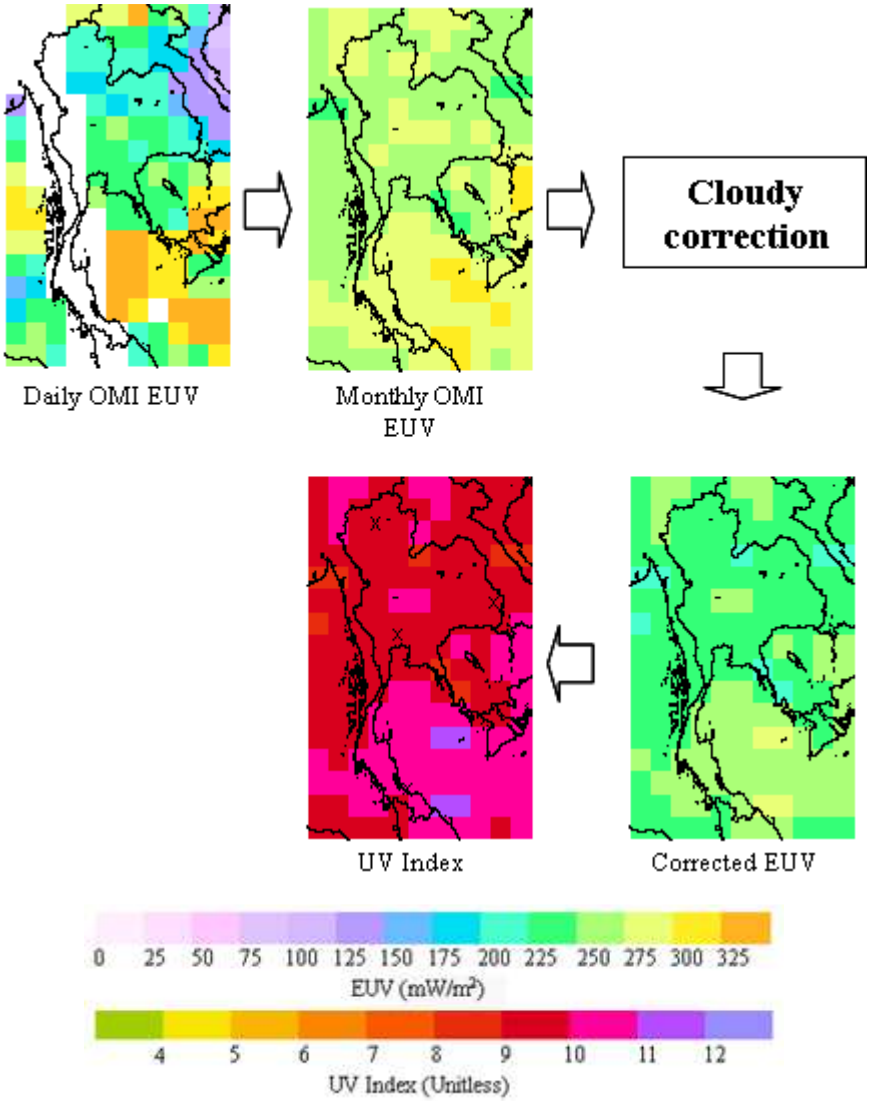

Figure 7.14 An example of noontime erythemal map on 07/08/2009 (white pixels represent no data).

Given that the underlying daily erythemal data is generally available, and a decision can be made about clear or cloudy conditions, it is possible for most days to improve upon this. If the daily UV data is available but it is cloudy or cloud is indeterminate, then the cloud correction is applied to the daily UV data (see Figure 7.15).

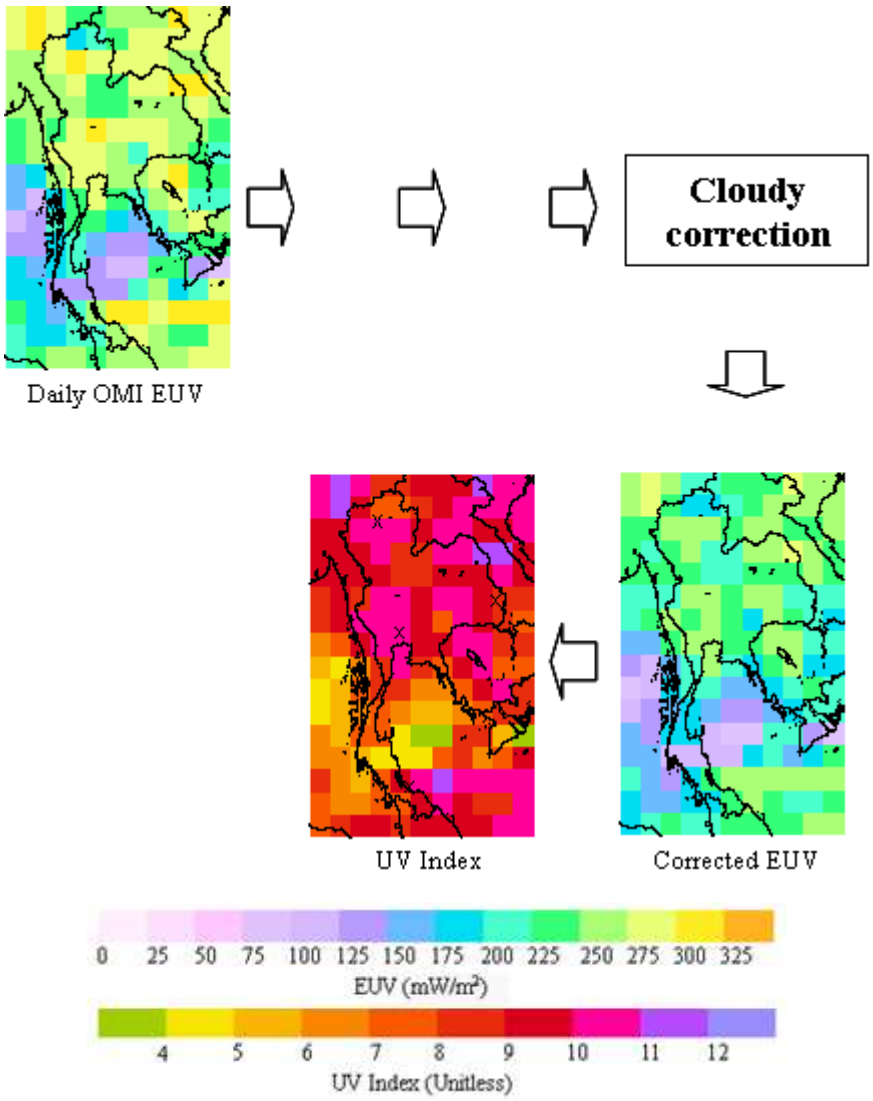

Figure 7.15 An example of noontime erythemal map on cloudy day (03/08/2008).

Where conditions are known to be clear, but full AAOD data is not available, the clear sky correction can be used with the monthly mean AAOD data from Figure 7.9 (see Figure 7.16).

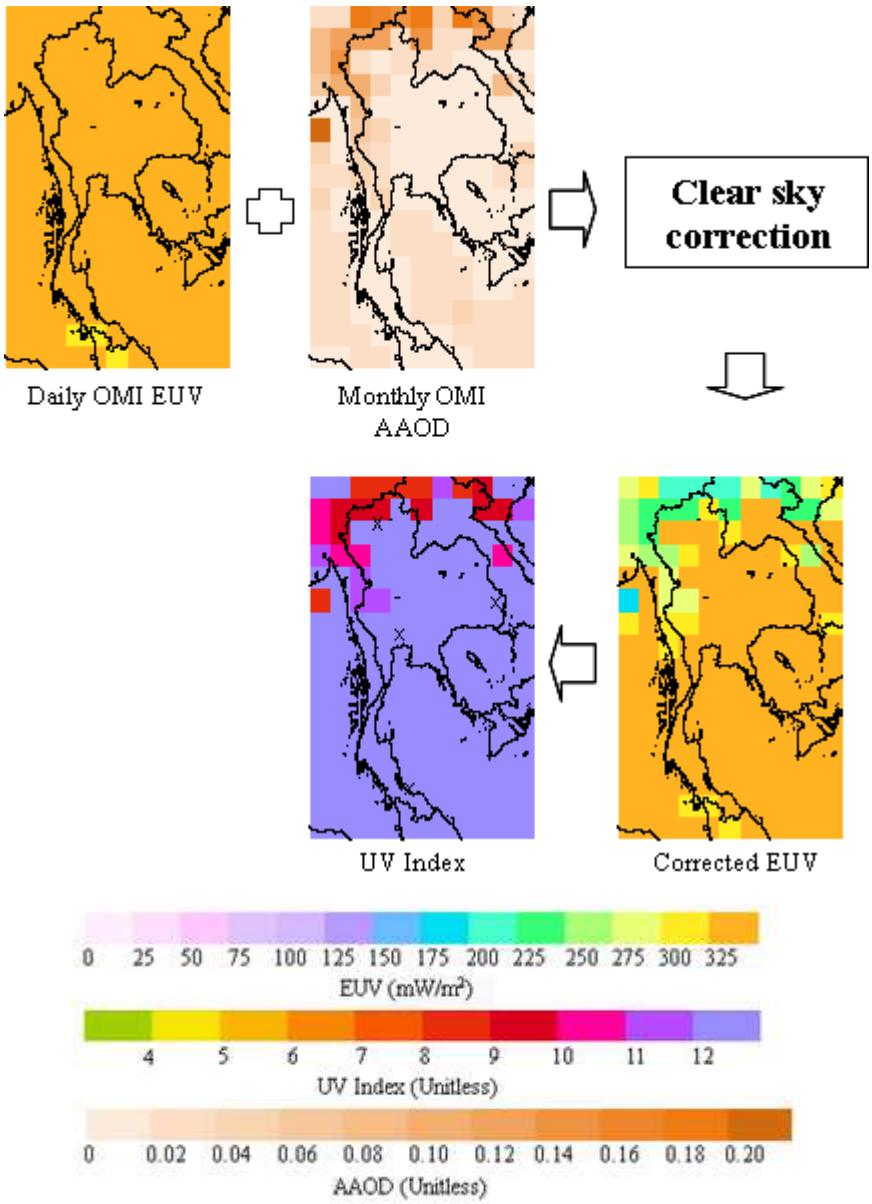

Figure 7.16 An example of noontime erythemal map on clear sky day (02/04/2007) with the monthly AAOD correction.

In the ideal case, both erythemal and AAOD data are fully available and a day specific correction can be applied (see Figure 7.17).

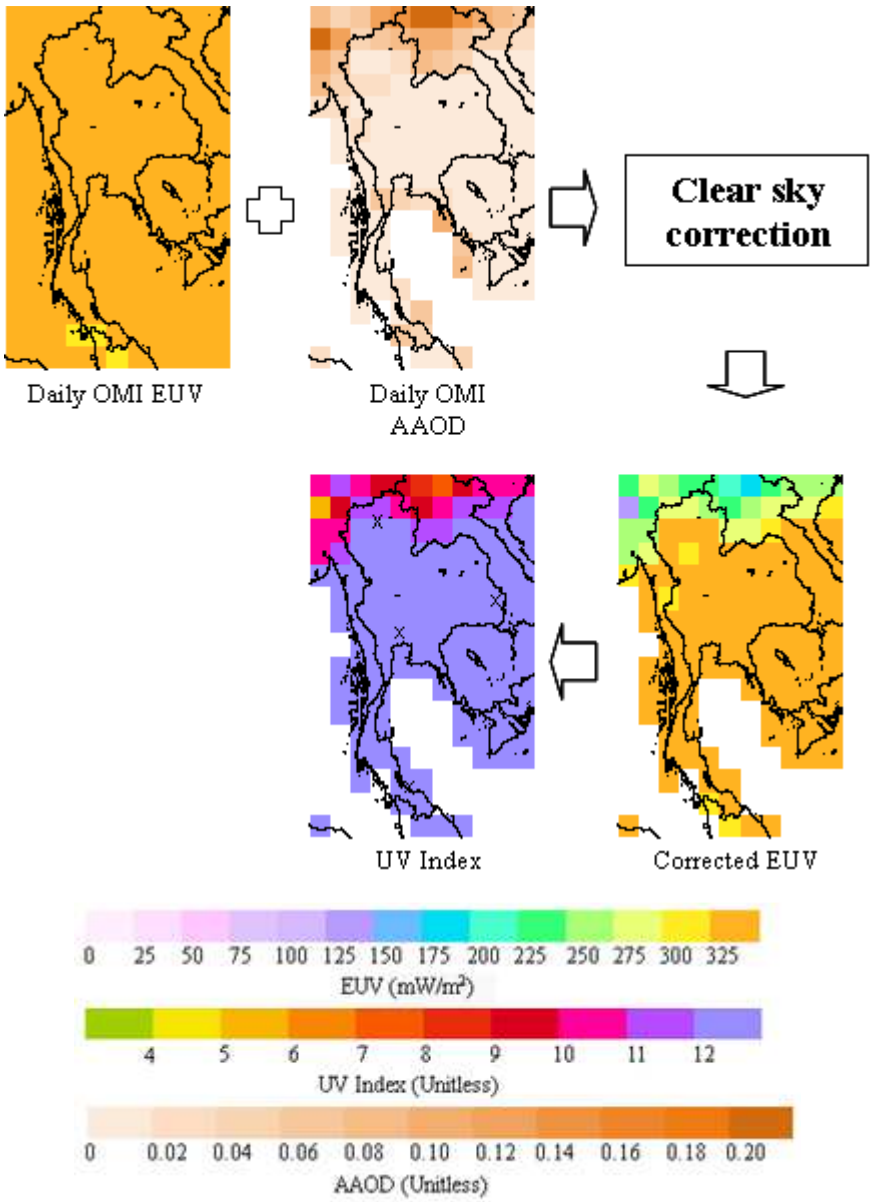

Figure 7.17 An example of noontime erythemal map on clear sky day (02/04/2007) with the daily AAOD correction (white pixels represent no data).

7.4 Validation

To validate the model performance, noontime UV Indices at the four Thai sites: Chiang Mai, Ubon Ratchathani, Nakhon Pathom and Songkhla, were selected from the maps. The comparison results are presented in Table 7.1.

Table 7.1 Validation of the corrected OMI UV Index with respect to ground-based UV Index.

Conditions	UV data	AAOD data	Model	Sites*	Ground-based UVI	Corrected OMI UVI
Undefined (07/08/2009)	Monthly	No	Cloudy correction	CM	2.8	9.9
				UB	4.2	10.9
				NP	4.2	9.5
				SK	11.4	10.4
Cloudy (03/08/2008)	Daily	No	Cloudy correction	CM	14.1	10.6
				UB	9.3	8.1
				NP	9.1	10.3
				SK	10.1	9.6
Clear sky (02/04/2007)	Daily	No	Cloudy correction	CM	10.7	12.7
				UB	13.3	13.3
				NP	11.3	13.0
				SK	No data	13.1
Clear sky (02/04/2007)	Daily	Monthly	Clear sky correction	CM	10.7	13.2
				UB	13.3	13.5
				NP	11.3	14.2
				SK	No data	14.7
Clear sky (02/04/2007)	Daily	Daily	Clear sky correction	CM	10.7	13.8
				UB	13.3	14.8
				NP	11.3	14.2
				SK	No data	14.7
Clear sky (11/01/2008)	Daily	No	Cloudy correction	CM	7.1	8.1
				UB	7.2	8.9
				NP	6.9	8.8
				SK	10.3	10.6
Clear sky (11/01/2008)	Daily	Monthly	Clear sky correction	CM	7.1	8.9
				UB	7.2	9.1
				NP	6.9	8.9
				SK	10.3	11.8
Clear sky (11/01/2008)	Daily	Daily	Clear sky correction	CM	7.1	8.6
				UB	7.2	9.9
				NP	6.9	9.8
				SK	10.3	11.8
Clear sky (12/01/2008)	Daily	No	Cloudy correction	CM	7.0	8.1
				UB	6.8	8.1
				NP	7.4	8.8
				SK	11.6	10.4
Clear sky (12/01/2008)	Daily	Monthly	Clear sky correction	CM	7.0	9.0
				UB	6.8	8.3
				NP	7.4	9.0
				SK	11.6	11.7
Clear sky (12/01/2008)	Daily	Daily	Clear sky correction	CM	7.0	9.1
				UB	6.8	No data
				NP	7.4	9.5
				SK	11.6	No data

*CM = Chiang Mai, UB=Ubon Ratchathani, NP=NakhonPathom, SK=Songkhla

The validation results in Table 7.1 show that for the default case where the monthly erythemal data was used with the cloudy correction, the differences between the corrected OMI and ground-based UV Index are large (within ±7 UVI) as expected. Smaller differences were achieved when the daily OMI UV data was used with either clear sky or cloudy correction. Using the clear sky correction, the corrected OMI UV Index values are similar (±3 UVI) when either the daily or monthly OMI AAOD data were used. Better results (±2 UVI) are shown when the cloud correction was applied. While one might hope that specific aerosol data would provide the best correction, this assumes that the aerosol data fully represent the conditions. It is known that the satellite data do not fully probe the lower boundary layer where much of the aerosol exists, and this is evident in the results. The cloud correction, while empirical, intrinsically accounts for both cloud and aerosol effects through the full depth of the atmosphere. It would appear that until there is an improvement in satellite aerosol products, and broad scale, satellite-based correction for aerosol is not as effective as a simple empirical correction. Where ground-based aerosol optical depth data exists, and accounts for the full depth of the atmosphere, this provides the best corrective option in clear sky conditions.

7.5 Summary

In this chapter, noontime erythemal irradiance calculated from the OMI products (i.e., OMUVBd and OMAERUVd) were corrected over the entire area of Thailand. There are two empirical models used in this study: clear sky correction (see Chapter 5) and cloud correction (see Chapter 6). The use of the correction depends on the availability of input parameters and the sky conditions. The final results were shown in term of the UV Index over the country. The daily corrected satellite data was compared to the daily ground-based data. The differences between the two datasets are within ±3 UVI for the clear sky correction and ±2 UVI for the cloud correction.

The method and results that are shown in this chapter are only some example taken from different sky conditions: clear sky and cloudy days. Attempts to correct the satellite UV data over Thailand were limited by both availability and quality of the input parameters required for the correction, especially the AAOD data. The correction method would be improved if aerosol and cloud information were more

readily available. Ideally, aerosol data that represents the full atmosphere is required – much of the aerosol extinction takes place in the lower boundary layer which is poorly represented in satellite products. It should also be remembered that the satellite product represents an area of 312 km^2 while the ground-based measurement represents a specific point. Localised effects may influence one measurement and not the other, and some uncertainty can be expected from this scaling issue.

Given the lack of high quality AAOD data, the most effective correction for a country wide application is the cloudy sky empirical correction that implicitly includes cloud and aerosol typical of the region. Note that, as with all empirical techniques, the details of this correction may not be directly applicable to other regions and climates.

Chapter 8 – Summary

Solar ultraviolet irradiance has effects on human health, terrestrial and aquatic ecosystems. The erythemal irradiance affecting human skin (sunburning), taken as the focus in this thesis, varies depending on the solar energy output, geographical factors (e.g., sun-earth distance, solar zenith angle and altitude), atmospheric composition (e.g., ozone, aerosols and clouds) and surface properties (e.g., albedo). The amount of irradiance can be measured directly by ground-based measurements; however, ground-based instruments have been installed only at limited sites. Satellite UV estimation techniques based on radiative transfer models and reflectivity measurements have potential to provide UV irradiance on a global basis. However, satellite data represents average conditions over large areas, and is based on model calculations that inevitably include assumptions that sometimes produce errors for all or part of the region concerned. Thus, the validation of satellite data with ground-based data is still required. This thesis attempted to use the benefit of satellite UV retrieval to estimate erythemal irradiance at local solar noon for the whole country of Thailand where ground-based measurements are sparse, and compared the results to similar validation techniques in the UK. This is the first time that such studies have been conducted for the Tropics, previous work has been in midlatitudes where the climate is quite different.

In this study, the erythemal irradiance at local solar noon is investigated for two different climate areas; Tropics and midlatitudes. There are four Thai ground-based sites: Chiang Mai, Ubon Ratchathani, Nakhon Pathom and Songkhla; and nine UK sites: Camborne, Chilton, Glasgow, Kinloss, Leeds, Lerwick, Manchester, Reading, and Snowdon. Most of the sites have been installed with broadband radiometers, but Manchester and Reading have spectroradiometers. Apart from the ground-based measurement, OMI onboard the Aura spacecraft measures solar reflected and backscattered light at UV and visible wavelengths which enable a series of data products to be retrieved: total column ozone, trace gases, aerosols, clouds and hence finally the surface UV irradiance on a global scale.

The comparisons of the noontime erythemal irradiance retrieved from OMI between years 2004 and 2007 with respect to the ground-based data at the various sites were detailed in Chapter 4. There was a general overestimation of UV by the OMI data but with considerable variation that included some instances of underestimation for both Tropics and midlatitudes. The biases between the OMI data and the ground-based data were 9% for cloudless conditions and 32% for all sky conditions at the cleanest site sampled. Biases were much higher (at least about 20% for cloudless conditions) for the urban sites. Further investigation indicated that the positive bias is mainly due to aerosol absorption optical depth that is not accounted for in the OMI UV algorithm.

As a result, two empirical models were derived to account for absorbing aerosol under cloudless conditions (clear sky correction). These were introduced in Chapter 5. One correction uses aerosol optical depth from ground-based instruments and aerosol single scattering albedo, while the other uses aerosol absorption optical depth from the satellite as the input parameters. After the absorbing aerosol correction factors were applied, for cloudless conditions, the differences between the corrected OMI and ground-based data were reduced by up to 28% for the Tropical sites and 5%-30% for the temperate sites. The results also show that the improvement is much better if ground-based aerosol data were applied to the empirical models, since they are site specific and expected to represent the boundary layer better than the satellite data.

Since cloudless conditions are comparatively rare, an empirical method to correct the erythemal irradiance from OMI at local solar noon in cloudy conditions (cloudy correction) was then introduced (see Chapter 6). The corrected OMI erythemal irradiances were closer to the ground-based data than the original OMI erythemal irradiances. This method resulted in an improvement to the OMI data (relative to ground-based) of 12%-14% for Thai sites and about 30% for UK sites. However, this does not solve the issue of considerable scatter in the comparison data due to the vast variations possible in cloud type and characteristics. The cloudy correction was also successfully used with clear sky data.

To extend the correction methods to the whole country of Thailand, the two empirical models (clear sky correction and cloudy correction) were applied depending on the availability of inputs (especially aerosol data) and the sky conditions, as detailed in Chapter 7. The final results were presented in terms of daily noontime UV Index maps which are familiar to public health bodies and the public themselves. The differences between the corrected OMI UV Index and the ground-based UV Index were within ±3 UVI for the clear sky correction when the satellite aerosol data are available. However, there was very little daily aerosol data available so monthly averages had to be used. This situation should improve as more data becomes available and averages can at least be based on a longer term data set. The cloudy correction proved to be the overall most effective in correcting the OMI UV retrieval, and could be applied to the whole country in any conditions, once a decision about maritime and urban sites had been made. The resulting UV Index maps were again tested against ground-based data for independent years and found to be correct to ±2 UVI for all sites and all conditions, compared to the original OMI data which had a positive bias and could overestimate the true UVI by up to 4 units.

Thus, OMI UV retrievals have been tested for the first time in the Tropics. Results were not dissimilar to validations at midlatitudes, and the main cause of discrepancy for clear sky conditions was shown to be missing aerosol effects in the retrieval algorithm. This could be corrected if ground-based aerosol data were available for a site, and was also attempted with satellite-based aerosol data. A paucity in, and lack of quality control for, the aerosol data meant that such corrections could not be applied on broad space and time scales. A simple linear correction proved most effective at correcting the overestimation of satellite UV and could be applied in all conditions. The correction was empirically derived and required only that Thailand be split into a maritime region (clean) and urban regions. While not able to account for subtle differences in aerosol and cloud that generated scatter in the ground-satellite comparison, this method nonetheless provided UVI ±2 for the whole of Thailand, which is deemed valuable as a public health tool.

From the results presented in this thesis it is clear that some uncertainties still remain in the corrected erythemal irradiances and that these need to be addressed. In particular, further work in the following areas is required:

- The aerosol data (AOD, AAOD and SSA) either from ground-based measurements or satellite retrievals should be further investigated. Improved data availability, and data quality, would improve the satellite UV corrections under clear sky conditions, as highlighted in Chapter 5. With time, it is to be hoped that the uncertainties in the aerosol data will be reduced.
- To improve the background climatological data, the noontime erythemal irradiance and aerosol data should be routinely collected at as many sites as possible, allowing climatological expectations to be more firmly established.
- Cloud information from geostationary satellites that can provide data more often (every 30 minute) than the polar orbiting OMI may help to improve the cloud correction since it removes the assumption that cloud conditions stay the same between satellite overpass and noon.
- The noontime UV Index of Thailand can be produced using results obtained from this study and published for public use. Going one step further to produce a UV index nowcast (current conditions) and ultimately a forecast would provide much added value. For a nowcast, the underlying data must be available in real time. Forecasting requires a good understanding of the local climatology and conditions (which would be provided by the continuing data collection mentioned above and the work within this thesis), combined with weather forecasts (cloud/no cloud) and some economic expectations (e.g. biomass burning, or not).

Appendix 1 – The calibration of UV-Biometer (s/n 5809)

In this appendix, the three calibration processes of UV-Biometer (s/n 5809), which are cosine response, spectral response and absolute calibration, operated at the University of Manchester in year 2009 are described. The UV-Biometer of Solar Light Company Inc. was used as a standard instrument for calibration purposes noted in Section 3.1.2.

A1.1 Spectral Response Calibration of UV-Biometer Solar Light Company Inc. (s/n 5809, Thailand) on 26 August 2009

This section details determination of the relative spectral response of the UV-Biometer model 501A. A solar simulator with a 1000 W universal Xenon arc lamp combined with a double monochromator was used as a light source. The double monochromator of Oriel instruments (Model 77200), which has 0.1 nm resolution with narrow slits and a 1200 line/mm grating, allows a spectral output ranging from 200 nm to 24 μm. However, in this study, we set the slits to obtain about 5 nm FWHM to provide enough signal for the UV-Biometer, since closing the slits reduces the throughput of the monochromator. In order to identify the output of the light source, a Bentham DTM300 double monochromator was set to measure spectral irradiance. The optical head of the Bentham was fixed facing the light source. In front of the optical head of the Bentham, the UV-Biometer was mounted and able to rotate about the vertical to allow the light to pass intermittently to the Bentham input optics for verification of the test radiation. The spectral calibration setup is shown in Figure A1.1.

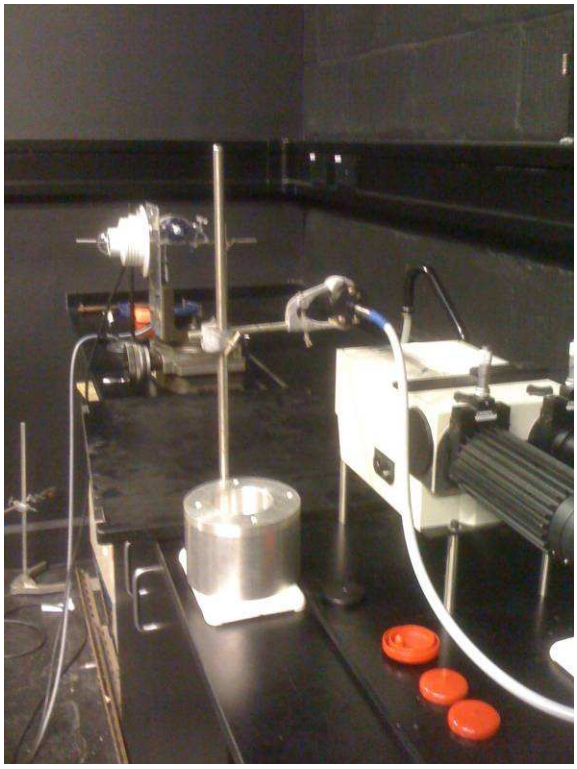

Figure A1.1 Setup of spectral calibration.

The monochromator was set sequentially at wavelengths from 290.00 to 400.00 nm with 2.50 nm step. The output of the UV-Biometer was recorded using the Campbell 21X (TG1), a data recorder of Campbell Scientific Ltd. (UK), averaging over 5 minutes at each wavelength. To measure the spectral irradiance from the light source, the UV-Biometer was rotated 90° to allow the light to pass to the Bentham optical head. The Bentham was set to scan from 290 to 400 nm with the resolution of 0.5 nm. The output of the Bentham is shown in Figure A1.2.

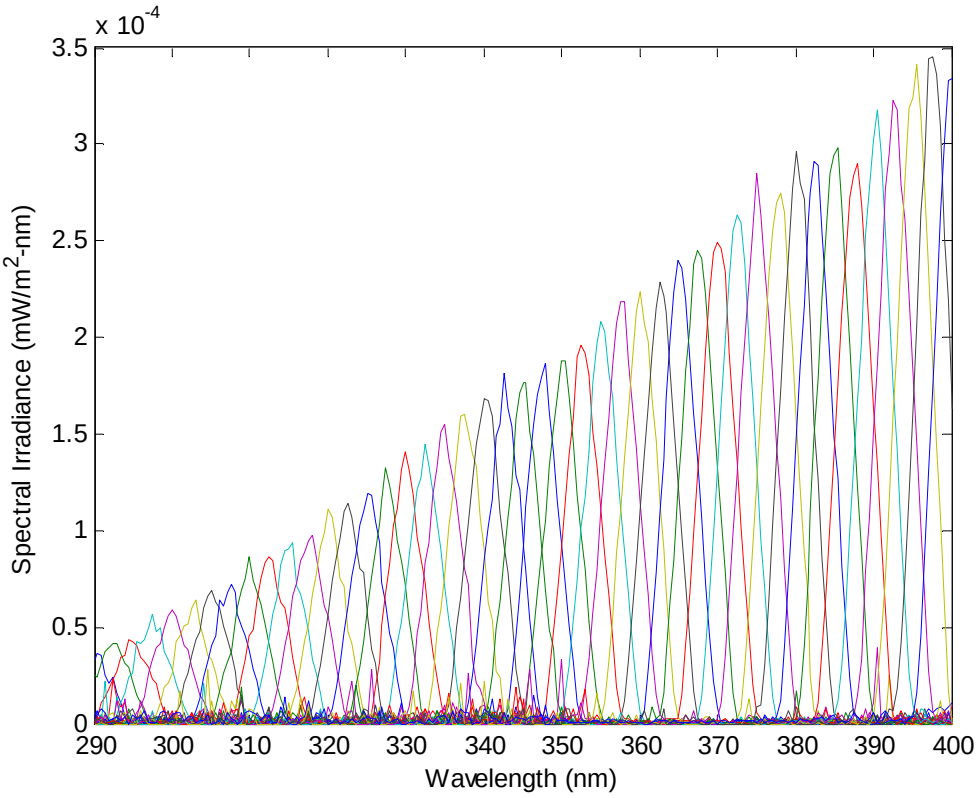

Figure A1.2 The spectral irradiance output from Bentham DTM300.

The relative spectral response of the UV-Biometer was calculated by normalising the ratio of the output from the UV-Biometer (mV) and Bentham (mW/m^2-nm). The relative spectral response function retrieved in this study was compared with the original value from Solar Light Company Inc. from 2003, and the erythema action spectra defined by CIE, which are shown in Figure A1.3. The new relative spectral response values are also shown in Table A1.1.

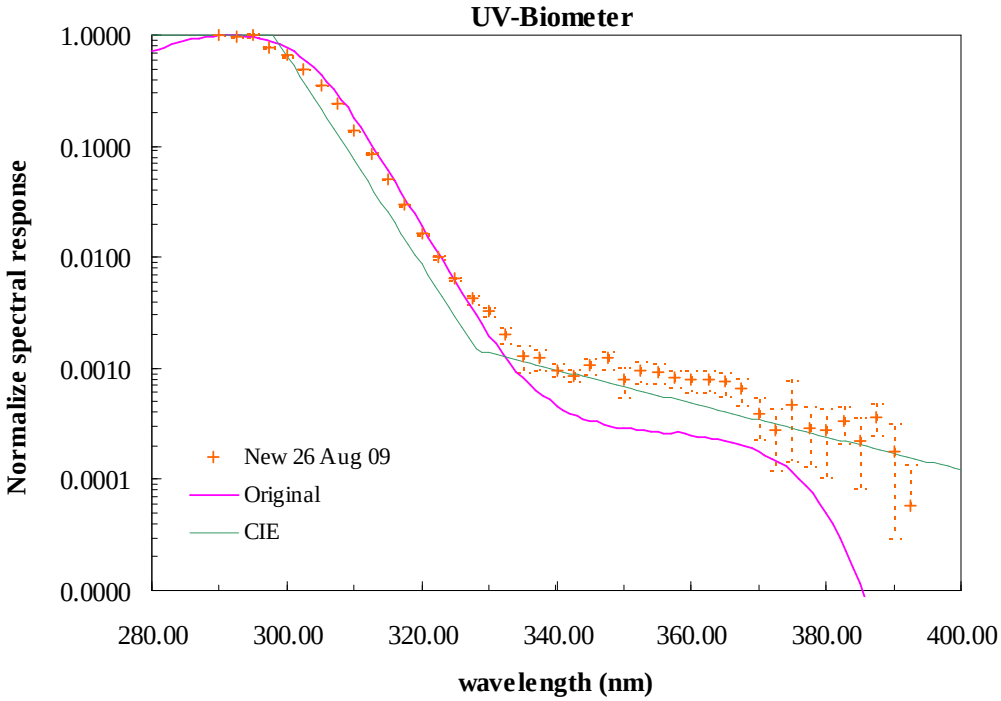

Figure A1.3 The relative spectral response of UV-Biometer.

We can see from Figure A1.3 that the present relative spectral response function is close to the original response for the shorter wavelengths (below 335 nm) but deviates at larger wavelength where there were very low signals recorded by the UV-Biometer. Fortuitously the current spectral response has moved closer to the reference erythemal action spectrum that the instrument is supposed to represent. In order to compare the influence of the two spectral responses on the output of the Biometer, the spectral responses were multiplied by spectral irradiances measured on 1 January, 2008 at 11:00 to calculate erythemal UV irradiances as shown in Figure A1.4. The difference between the erythemal UV irradiances using the present and original spectral response functions was about 8%.

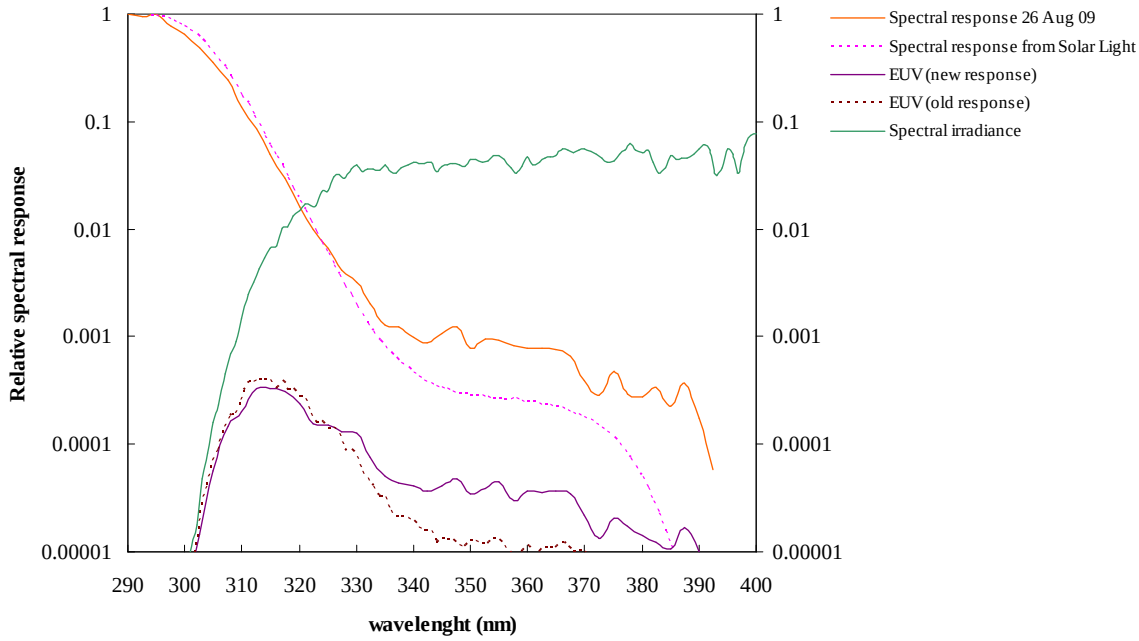

Figure A1.4 Comparison of erythemal UV irradiance using different spectral responses.

Table A1.1 The relative spectral response function of UV-Biometer calibrated on 26 August 2009.

λ (nm)	Normalised spectral response
290.00	1.00E+00
292.50	9.57E-01
295.00	9.98E-01
297.50	7.78E-01
300.00	6.54E-01
302.50	4.89E-01
305.00	3.52E-01
307.50	2.43E-01
310.00	1.38E-01
312.50	8.64E-02
315.00	5.00E-02
317.50	2.93E-02
320.00	1.62E-02
322.50	9.95E-03
325.00	6.51E-03
327.50	4.20E-03
330.00	3.24E-03
332.50	2.00E-03
335.00	1.27E-03
337.50	1.24E-03
340.00	9.71E-04
342.50	8.67E-04
345.00	1.06E-03
347.50	1.23E-03
350.00	7.83E-04
352.50	9.45E-04
355.00	9.28E-04
357.50	8.25E-04
360.00	7.80E-04
362.50	7.83E-04
365.00	7.54E-04
367.50	6.56E-04
370.00	3.92E-04
372.50	2.82E-04
375.00	4.75E-04
377.50	2.94E-04
380.00	2.75E-04
382.50	3.38E-04
385.00	2.23E-04
387.50	3.66E-04
390.00	1.77E-04
392.50	5.80E-05
395.00	0.00E+00
397.50	0.00E+00
400.00	0.00E+00

A1.2 Cosine Calibration of UV-Biometer Solar Light Company Inc. (s/n 5809, Thailand) on 10 March 2009

In general, UV-Biometers have an angular response close to the ideal cosine function. It is difficult to make an instrument with a perfect angular response due to small imperfections in commercial quartz domes. Traditionally, the cosine angular response of these instruments is deemed acceptable if it has less than 5% error for zenith angles less than 60° [*Webb et al.*, 1998].

Regarding this calibration, a FEL 1000W standard lamp (s/n F318) of the Centre of Atmospheric Science, the University of Manchester, was used as a light source. This lamp has a vertical coil and surrounding bulb and is mounted in a holder on an optical rail via two vertical pins at the bottom of the bulb unit. It requires an 8 amp current-stabilised power supply. The Campbell 21X (TG1) was setup to record signals from the UV-Biometer, averaging every 10 seconds. The calibration setup is shown in Figure A1.5. The distance between the centre of the lamp and the UV-Biometer is about 0.65 m. The lamp was mounted at one end of an optical rail while the UV-Biometer was mounted at the other side so that its vertical rotation axis passed through the plane of the receiving surface of the UV-Biometer. A low power laser was used to horizontally align the centre of the UV-Biometer and the light source by passing the beam through the lamp position to the centre of UV-Biometer.

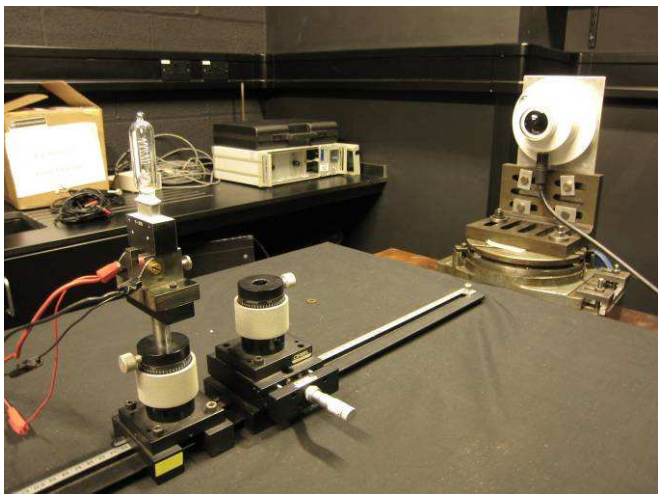

Figure A1.5 Setup of cosine calibration.

The Campbell was set to record the UV and temperature signals in mV every second and average every ten seconds. The cosine response was measured across four quadrants (Q1, Q2, Q3, Q4) at intervals of 90° as can be seen in Figure A1.6. The centre of the UV-Biometer was set at 0° and then the receiving plane was rotated about its vertical axis (also passing through the central point) using a micrometer controlled rotation plate. Rotations went from zero to 88° in 4° steps.

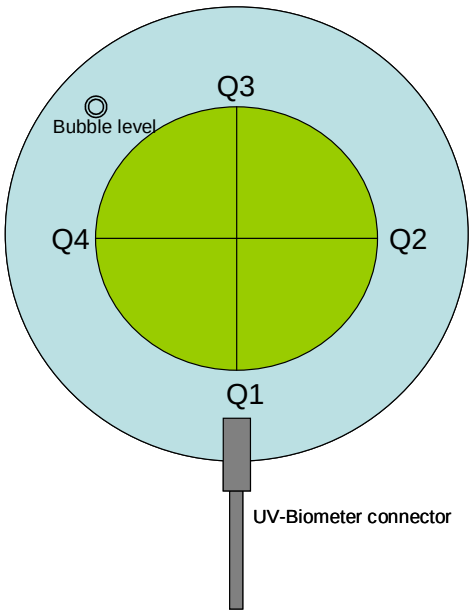

Figure A1.6 The definition of four quadrants using the UV-Biometer connector and the bubble level as referent points.

The signals recorded at each angle for each quadrant were normalised by the reference signals measured at 0°, to give the relative angular response across each quadrant. The result in Figure A1.7 shows the relative angular response of the four quadrants of the UV-Biometer and their average obtained in this study compared with the value from Solar Light and the ideal cosine function.

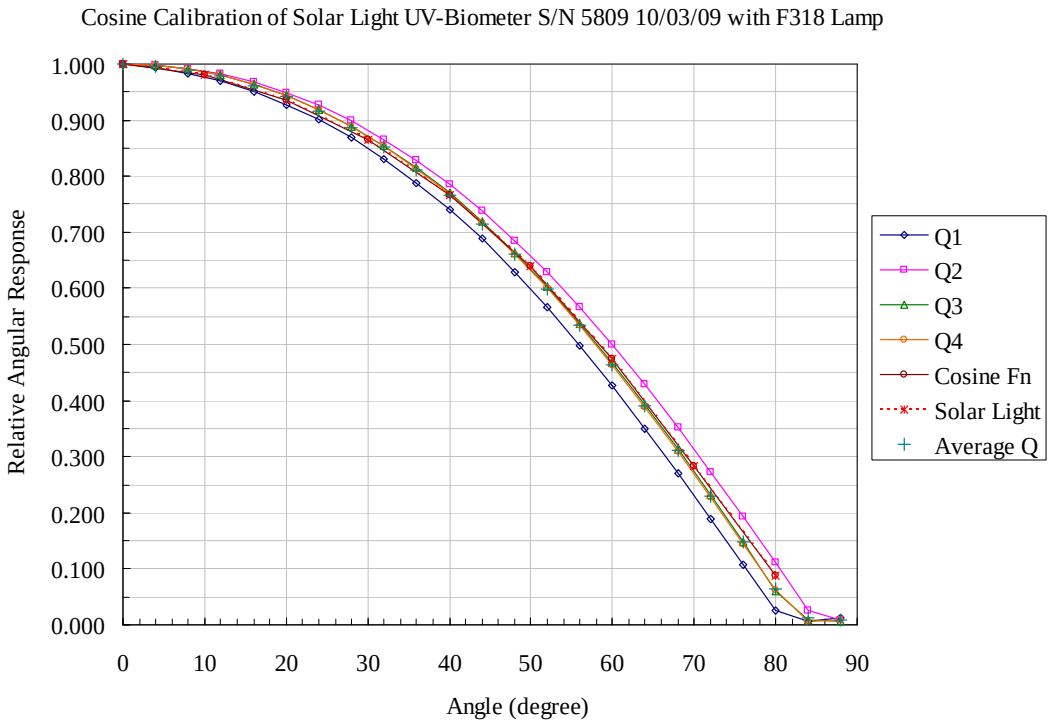

Figure A1.7 Relative angular response of the UV-Biometer.

From the result, we can see that the values of Q1 were lower than the cosine function while those of Q2 were higher. Furthermore, the values of Q3 and Q4 were between those values. This might have resulted from the position of the UV-Biometer centre not being exactly the optical centre of the instrument. However, the average value of the four quadrants was close to the value of the true cosine function and the original relative angular response from Solar Light.

In general, the relative angular response is compared with the ideal cosine function. In this study, relative cosine response, $C(\theta)$, of the UV-Biometer is defined as the ratio of the relative angular response of the UV-Biometer, $A(\theta)$, to the cosine function, $\cos(\theta)$, [*Grainger et al.*, 1993] as follows:

$$C(\theta) = \frac{A(\theta)}{\cos\theta} \qquad \text{(A1.1)}$$

The relative cosine response of the four quadrants of the UV-Biometer was calculated and shown in Figure A1.8. The average value of the relative cosine

response for four quadrants were also calculated and then compared with the original value from Solar Light as shown in Figure A1.9 and Table A1.2.

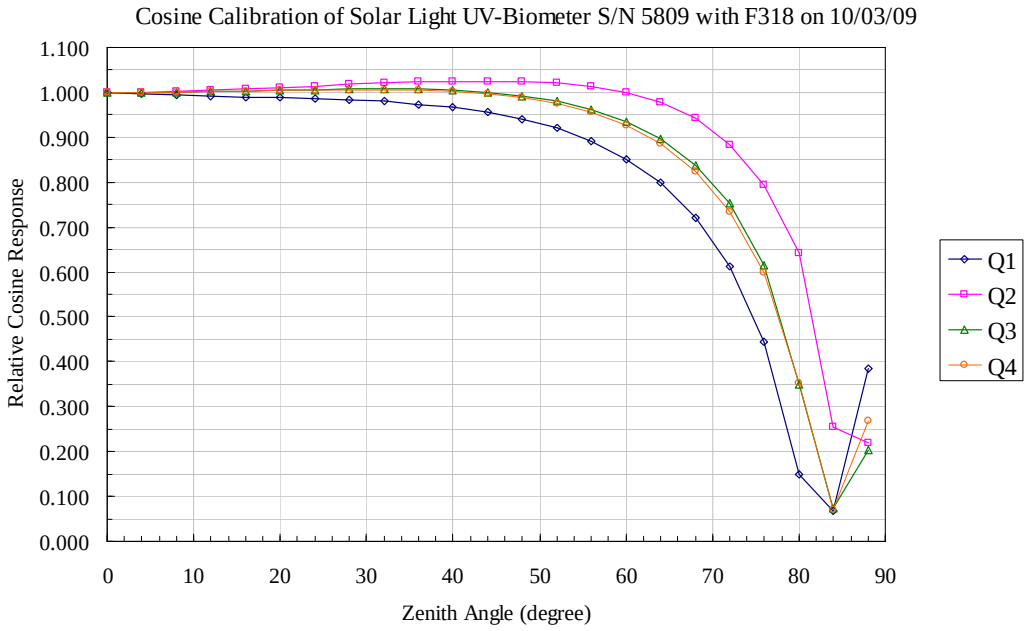

Figure A1.8 The cosine response of the UV-Biometer.

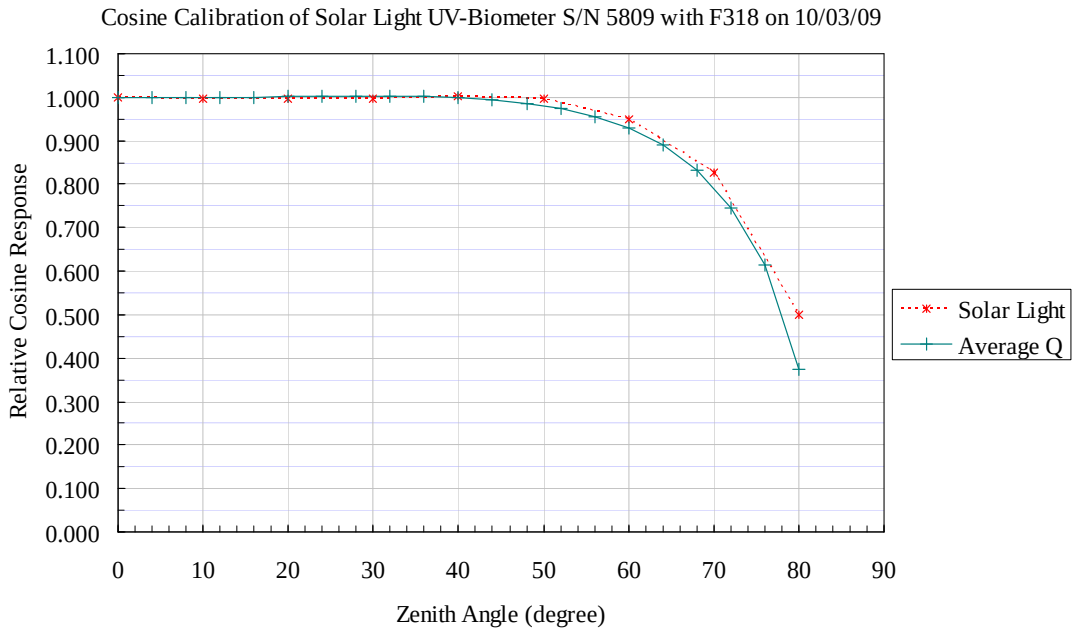

Figure A1.9 The relative cosine response of the UV-Biometer obtained from this study and Solar Light.

Table A1.2 The average value of relative angular response calibrated on 3 March 2009.

Zenith angle	Average angular response
0	1.0000
4	0.9990
8	0.9990
12	0.9997
16	1.0007
20	1.0018
24	1.0029
28	1.0036
32	1.0036
36	1.0023
40	0.9996
44	0.9948
48	0.9868
52	0.9741
56	0.9556
60	0.9285
64	0.8897
68	0.8313
72	0.7453
76	0.6133
80	0.3738
84	0.1168
88	0.2688

Comparing the relative cosine response obtained from this study, and that from Solar Light provided in 2003, shows that the relative cosine response of this UV-Biometer is not appreciably different from a typical cosine response for such instruments. The difference between the two sets of data was less than 2.5% for the zenith angles less than 75° and about 12% for the larger angles.

A1.3 Absolute Calibration of UV-Biometer Solar Light Company Inc. (s/n 5809, Thailand) on 30 May 2009

The purpose of absolute calibration is to determine a conversion factor called sensitivity ($V/(W \cdot m^{-2})$) to convert signals (V) from the UV-Biometer to erythemal irradiances ($W \cdot m^{-2}$). In this study, the UV-Biometer was installed close to the Bentham DTM300 spectroradiometer, used as a reference, on the Pariser building, the University of Manchester as shown in Figure A1.10.

Figure A1.10 Intercomparison between the UV-Biometer and the Bentham spectroradiometer on the Parisor Building in May 2009.

The Bentham scanned every 15 minutes while the UV-Biometer recorded voltage signals every 10 seconds and then averaged every 15 minutes matching with the Bentham scan times. The irradiance spectra from the Bentham were weighted with the CIE erythema action spectrum to produce erythemal irradiances. Then the signals from the UV-Biometer were plotted against the erythemal irradiance from the Bentham as shown in Figure A1.11. The slope of the graph is then the sensitivity of the UV-Biometer which is 3.8526 $V/(W \cdot m^{-2})$ with the standard error values of 0.0119.

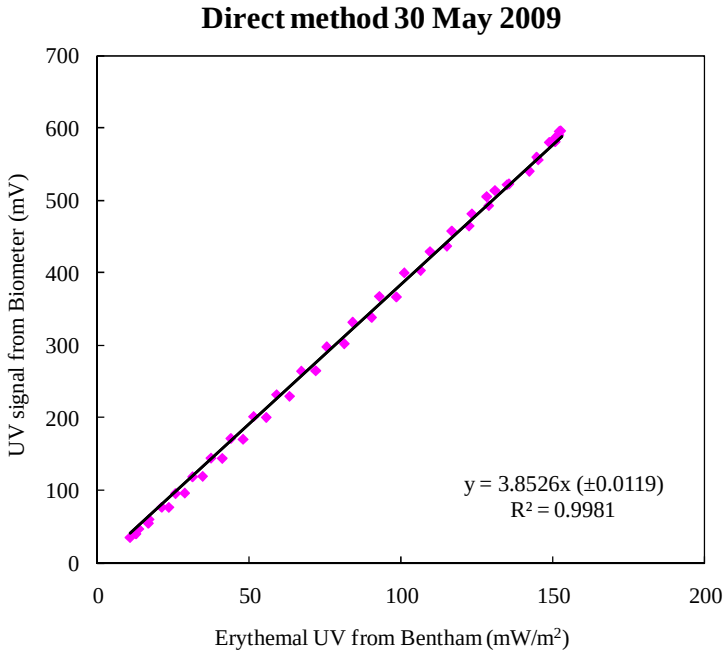

Figure A1.11 Correlation plot between signals from the UV-Biometer and the erythemal UV irradiance from the Bentham spectroradiometer.

The correlation between the two instruments is excellent even at large solar zenith angle where such calibrations tend to become non-linear. This is a result of the now excellent match between the biometer response and the reference erythemal action spectrum.

To compare the new sensitivity (3.8526 V/(W·m^{-2})) with the original value from Solar Light (4.2589 V/(W·m^{-2})) since 2003, the UV-Biometer sensitivity studied in this work has gradually changed about 2% per year which is in the same range as the other UV-Biometers (2%-5%).

In addition, we plotted the sensitivity against solar zenith angles, separated total column ozone measured from a brewer spectroradiometer at Manchester as shown in Figure A1.12. We can see from the result that the sensitivity has changed within 20% from minimum to maximum solar zenith angles. Also, the total column ozone affects the sensitivity at the larger solar zenith angles (more than 60°).

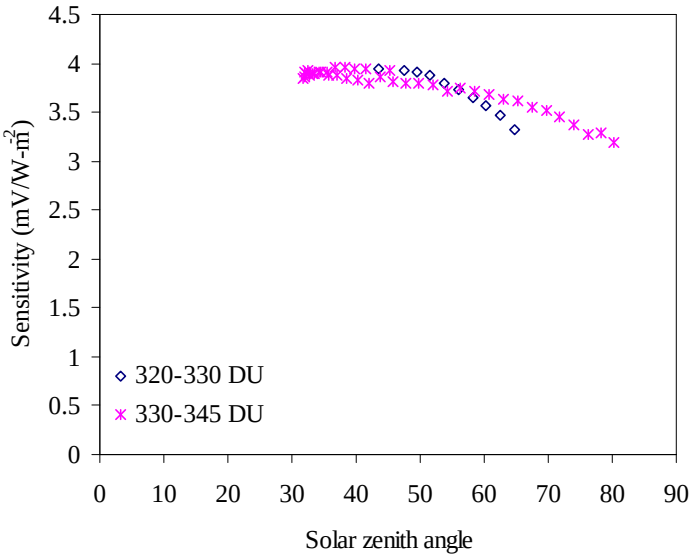

Figure A1.12 Variation of the sensitivity with solar zenith angle and total column ozone.

Appendix 2 – Publication Paper

Presented here is a paper published in the Journal of Geophysical Research, cited as *Buntoung, S., and A.R. Webb* (2010), Comparison of erythemal UV irradiances from Ozone Monitoring Instrument (OMI) and ground-based data at four Thai stations, *J. Geophys. Res.*, 115, D18215, doi:10.1029/2009JD013567.

JOURNAL OF GEOPHYSICAL RESEARCH, VOL. 115, D18215, doi:10.1029/2009JD013567, 2010

Comparison of erythemal UV irradiances from Ozone Monitoring Instrument (OMI) and ground-based data at four Thai stations

S. Buntoung[1] and A. R. Webb[1]

Received 19 November 2009; revised 17 June 2010; accepted 21 June 2010; published 28 September 2010.

[1] The Ozone Monitoring Instrument (OMI), on board the NASA EOS Aura spacecraft since July 2004, provides a global view of surface spectral ultraviolet (UV) irradiance at 305, 310, 324, and 380 nm; erythemal dose rate both at overpass time and local noontime; and erythemal daily dose. Previous studies have shown comparisons of the OMI erythemal UV irradiances and ground-based UV measurements in areas of midlatitude and high latitudes, predominantly in the Northern Hemisphere. In this study the noontime erythemal UV dose rates retrieved from OMI and measured from broadband instruments at four sites in Thailand were compared. The comparisons show a positive bias for the OMI data with respect to the ground-based measurements. The differences between the two data sets were 30%–60% for all data and were 10%–40% for cloudless data. The differences for the cleanest site showed better agreement than those for the more urban sites. Using the Libradtran radiative transfer model, we show that aerosol is responsible for much of the positive bias in polluted areas. Since absorbing aerosol is not taken into account in the OMI surface UV algorithm, aerosol absorption correction factors have been introduced as a function of aerosol absorption optical thickness provided by OMI to improve the OMI UV data for urban and maritime sites. The differences between the corrected erythemal UV data and the ground-based data were reduced to less than 20%.

Citation: Buntoung, S., and A. R. Webb (2010), Comparison of erythemal UV irradiances from Ozone Monitoring Instrument (OMI) and ground-based data at four Thai stations, *J. Geophys. Res.*, *115*, D18215, doi:10.1029/2009JD013567.

1. Introduction

[2] Erythemally weighted UV radiation is strongly affected by atmospheric ozone, cloudiness, and aerosols, as well as the predictable cycles of solar zenith angle. Its effects on human health require an understanding of the global distribution of solar UV [*United Nations Environmental Programme* (*UNEP*), 2007; *World Meteorological Organization* (*WMO*), 2007]. For example, for public health purposes, the UV Index (UVI, 1 unit equals 25 $mW.m^{-2}$) is used to express the level of erythemally effective UV, which can be up to the value of about UVI 12 in the Tropics [*Ilyas et al.*, 1999; *Janjai et al.*, 2009a], whereas at high latitudes, e.g., Southern Ontario, Canada, the value does not exceed about 6 [*Fioletov et al.*, 2004].

[3] Ground-based UV monitoring sites are relatively sparse and unevenly distributed on a global scale [*WMO*, 2007]. Since the 1970s, satellite retrievals combined with radiative transfer models have been used to derive erythemal UV irradiances at the Earth's surface for the entire globe, initially using Total Ozone Mapping Spectrometer (TOMS), operational from 1978. This has been superseded by Ozone Monitoring Instrument (OMI) onboard the NASA Aura spacecraft since 2004. OMI is a nadir viewing spectrometer that measures solar reflected and backscattered light at UV and visible wavelengths and provides a series of data products: total column ozone, trace gases, aerosols, clouds, and surface UV irradiance [*Levelt et al.*, 2006; *Tanskanen et al.*, 2006].

[4] Although satellite retrievals can provide data over a wide geographical distribution, they do so at relatively low spatial resolution, and ground-based validation of satellite data is required in any event. Initial studies compared TOMS UV data with ground-based UV data [*Arola et al.*, 2002; *Fioletov et al.*, 2002; *Kalliskota et al.*, 2000; *Kazantzidis et al.*, 2006; *McKenzie et al.*, 2001]. After the Aura spacecraft was launched, comparisons of the OMI UV data and ground-based data became the focus of attention [*Buchard et al.*, 2008; *Ialongo et al.*, 2008; *Kazadzis et al.*, 2009a; *Tanskanen et al.*, 2007; *Weihs et al.*, 2008]. Many of the studies used UV data from spectrophotometers to calculate spectral UV dose rates and daily doses for the northern high and midlatitudes, but several have used broadband measurements [e.g., *Ialongo et al.*, 2008; *Weihs et al.*, 2008]. The broadband data are often at higher time resolution and thus would allow the effects of rapidly changing conditions to be examined. Overall, results showed overestimation of UV by OMI when compared with ground-based data; however, for some instances of snow-covered surfaces, OMI underestimated measurements compared to ground-based instruments as the bright scene from

[1]School of Earth, Atmospheric and Environmental Science, University of Manchester, Manchester, UK.

0148-0227/10/2009JD013567

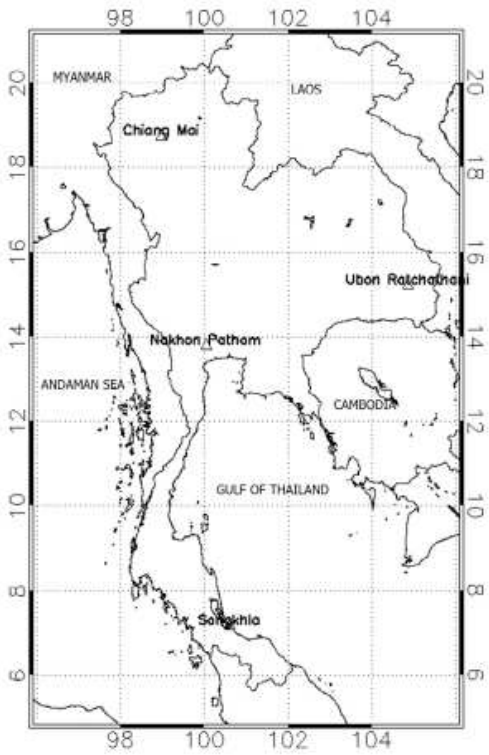

Figure 1. Map of Thailand sites.

the snow-covered surface was misinterpreted as cloud [*Tanskanen et al.*, 2007].

[5] It would appear that the bias mainly results from aerosol absorption that is not accounted for in the satellite UV algorithm and therefore causes the satellite retrieval to overestimate surface UV when significant aerosols are present. Several studies [*Arola et al.*, 2009; *Ialongo et al.*, 2009; *Kazadzis et al.*, 2009a] have introduced various correction procedures to account for aerosol absorption with some success, e.g., the correction method in the study by *Arola et al.* [2009] reduced bias by 5%–20% at midlatitude sites. It should be remembered that aerosols are not the only source of uncertainty in the satellite retrievals. Other sources include problems with defining surface albedo [*Tanskanen et al.*, 2007], cloudiness, and pixel inhomogeneities [*Kazadzis et al.*, 2009b; *Weihs et al.*, 2008]. In addition, the noon UV irradiance product, which we use here as most suitable for public health applications, is calculated from atmospheric parameters at overpass time, giving an additional uncertainty due to the assumption that the noon conditions are the same as those at overpass.

[6] This paper seeks to redress the lack of UV information and satellite validation for the Tropics. In this study, erythemally weighted UV dose rates at local solar noon, derived from OMI products, were compared with ground-based measurements for four sites in Thailand. The Libradtran radiative transfer model has been used to confirm that aerosol is a major cause of positive bias in the OMI UV estimates. Finally, a method to correct satellite data for absorbing aerosols was introduced and validated against the ground-based data.

2. OMI Surface UV Algorithm

[7] The OMI surface UV algorithm is based on the TOMS UV algorithm developed by NASA Goddard Space Flight Center [*Eck et al.*, 1995; *Krotkov et al.*, 1998, 2001; *Tanskanen et al.*, 2006]. However, the OMI UV product has a higher spatial resolution of 13 × 24 km^2 at nadir. The algorithm relies on radiative transfer models and input data such as total column ozone from OMI and climatological surface albedo based on TOMS data [*Tanskanen*, 2004]. Clear-sky UV irradiance is calculated by assuming that the atmosphere has no cloud and no aerosols. Then, the clear-sky irradiance is multiplied by a cloud and nonabsorbing aerosol correction factor (i.e., aerosol scattering that is included in the backscatter measurement) derived from further OMI products, e.g., the measured 360 nm radiance at the overpass time. Note, however, that the backscatter measurements on which this correction is based still do not fully probe the lower boundary layer and the aerosols therein [*McKenzie et al.*, 2008].

[8] The OMI UV irradiance products are provided in terms of surface spectral UV irradiances at 305, 310, 324, and 380 nm; erythemal dose rate both at overpass time and local solar noon; and erythemal daily dose [*Levelt et al.*, 2006; *Tanskanen et al.*, 2006]. These data can be freely accessed from http://avdc.gsfc.nasa.gov/.

3. Ground-Based Data

[9] Thailand is a country in Southeast Asia, covering latitudes from 5°N to 20°N and longitudes from 97°E to 105°E (see Figure 1). The climate of Thailand is classified as tropical wet and dry and characterized by two monsoons: the South-West monsoon (from mid-May to mid-October) causing rain over the whole country, and the North-East monsoon (from mid-October to mid-February) that brings cold and dry air from China to northern and north-eastern parts but causes rain along the eastern side of the country. Between the two monsoons (from mid-February to mid-May) is the period April/May when the Sun is highest in the sky for the country, and temperatures are greatest. The other period of highest Sun coincides with the wet South-West monsoon. The northern part of the country is surrounded by the landmass of Southeast Asia with local industry and traffic, whereas the southern peninsula is surrounded by the Gulf of Thailand in the east and the Andaman Sea in the west, which results in cleaner air than the north.

[10] The four UV measurement stations in Thailand used in this study are at Chiang Mai (18.78°N, 98.98°E, 240 m above sea level, a.s.l.), Ubon Ratchathani (15.25°N, 104.87°E, 122 m a.s.l.), Nakhon Pathom (13.82°N, 100.04°E, 30 m a.s.l.), and Songkhla (7.20°N, 100.60°E, 4 m a.s.l.). These sites cover the four main climatic regions of Thailand and also represent different geographical and environmental conditions from previous studies [*Arola et al.*, 2009; *Ialongo et al.*, 2009; *Kazadzis et al.*, 2009a]. Chiang Mai is a city in

northern Thailand. It has the highest altitude of the four sites with a relatively cool, dry season in winter, and is situated in a natural bowl that tends to trap pollutants. Development within the city drives air pollution to high levels. Nakhon Pathom is a suburb of Bangkok characterized by urban and industrial aerosols with dry season in winter. Ubon Ratchathani is in the northeast of Thailand with a dry season in winter, and the industry is of a more agricultural nature than the other two cities. These cities are also influenced by seasonal biomass burning during January–April as rice straw is burnt after harvesting [*Janjai et al.*, 2009b]. Songkhla is in the southeast of Thailand on the coast of the Gulf of Thailand, which has mild weather and is wet for the whole year. Tourism is the main industry and the aerosols are under a maritime influence.

[11] UV-Biometers (model 501A) from Solar Light Company have been used to monitor broadband radiation at the four sites: Chiang Mai and Nakhon Pathom since 1997 and Ubon Ratchathani and Songkhla since 2000. The response of the sensor is close to erythemal action spectrum defined by Commission Internationale de l'Eclairage [*Diffey and McKinlay*, 1987]. These instruments were originally calibrated to National Institute of Standards and Technology traceable standards via quartz-halogen lamps by the Solar Light facility in Pennsylvania, USA. By using a fifth UV-Biometer purchased in 2003 as a traveling standard, the calibration factors at each site have been reviewed annually by an on-site intercomparison between the standard and each site instrument using the method in the study by *Webb et al.* [2006]. Before 2003, one site instrument per year was sent to Solar Light for characterization and recalibration and then used to check the calibrations at the other sites through intercomparison. The cosine responses showed little change while the spectral responses altered gradually with time causing changes in calibration factors that were within 1.5% over an 8 year period [*Janjai et al.*, 2009a]. The spectral response of the fifth, traveling standard instrument was checked in Thailand in 2008, and both cosine and spectral responses were independently checked in Manchester in 2009: The cosine response showed little change from the original (within the measurement uncertainties ~2%), while there had been a small shift in the spectral response at longer UVA wavelengths. However, the spectral response check in 2008 in Thailand showed no significant change in response. Since we use data up until 2007 only, we take the statement of *Janjai et al.* [2009a] that this traveling instrument was stable for the period of concern. Therefore, the original cosine and spectral responses from the manufacturer have been used throughout since any observed changes during recalibration have been small. The calibration is applied as a matrix dependent on solar zenith angle and ozone [*Webb et al.*, 2006]. The instruments at the four sites are well maintained with daily cleaning of the dome, regular changing of the desiccants, and annual field calibrations under clear-sky conditions. The estimated overall uncertainty of the radiometer is within ±8% [*Janjai et al.*, 2009a].

[12] At each site, signals in voltage have been recorded by a data logger (DC100) from Yokogawa (Japan) that samples every second and then records the averaged values every 10 min. These data are sent to Laboratory of Tropical Atmospheric Physics, Silpakorn University. The voltage signals are then converted to erythemal UV irradiance by using conversion factors in $V/(W.m^{-2})$ from the manufacturer and field calibrations and corrected for spectral and cosine errors.

4. Comparisons of the OMI Erythemal UV Irradiances With Broadband Measurements

[13] In this study the erythemal UV irradiances at local solar noon, when the Sun is highest in the sky, were used. This is a standard OMI data product available for anywhere on the globe and represents the expected maximum UV value for the day under stable conditions. The time difference between the OMI UV overpass and ground-based measurements at local solar noon is up to 3 h for Thailand. The OMI algorithm assumes that atmospheric conditions stay constant between the overpass time and noon, in calculating local noontime UV. This assumption and the time difference can introduce an additional uncertainty into the noon UV data product. This becomes an intrinsic part of the uncertainty in the OMI product. However, the mean ratios at overpass and noon differ by only 2% and the normalized root-mean-square deviations are also similar (0.16 for Songkhla at overpass and 0.18 at noon, with the other sites showing a corresponding result). For a broad application, e.g., one aimed at public health information, noon UV is more easily understood and more applicable, and thus, we use this in the following analysis.

[14] The local noontime erythemal UV irradiances retrieved from OMI at the four Thai sites were compared with those measured from the broadband instruments (solar noon ±6 min). The data used for the comparisons were for the period from August 2004 to December 2007. The results of the comparison are shown as scatterplots for all sky conditions and the subset of cloudless conditions and can be evaluated against the one-to-one line shown in Figure 2. To determine cloudless days, the ground-based UV irradiance (10 min averages) was plotted from sunrise to sunset: Days with an uninterrupted smooth bell curve were manually selected as clear days.

[15] To investigate the level of the agreement between the noontime erythemal UV irradiance retrieved from OMI and the ground-based measurement, the ratios of the OMI data and the ground-based data were calculated and the distribution of the ratio at each site was plotted (not shown). Since most of the distributions were not normal, mean and median of the ratio were calculated [*Tanskanen et al.*, 2007] and shown in Table 1. To distinguish the effect of cloud, the results are shown for all sky conditions and cloudless conditions separately (Figure 2). Furthermore, the percentages of the OMI data that agree within ±10%, ±20%, and ±30% with the ground-based data ($\%W_{10}$, $\%W_{20}$, and $\%W_{30}$, respectively) are presented in Table 1.

[16] We can see from the results in Figure 2 and Table 1 that the noontime erythemal UV irradiances obtained from the OMI data are generally larger than those from ground-based measurements. The ratios for the all sky conditions show greater scatter than for the clear-sky conditions and include instances of underestimation by OMI. Some of this scatter can be due to changing cloud conditions between overpass time and local solar noon. The results for the cleaner air site (Songkhla, mean = 1.32) are in better agreement than the more urban sites (for example, Chiang

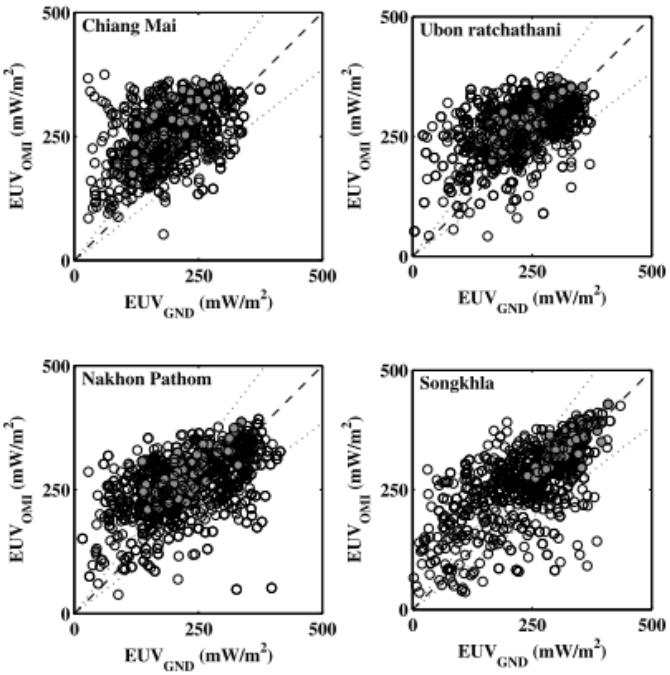

Figure 2. Comparison of the OMI erythemal UV irradiances at local solar noon (EUV_{OMI}) with those measured from ground-based measurements (EUV_{GND}) for all sky condition (open circle) and clear-sky conditions (solid circle) for the years 2004–2007. The 1:1 correlation (dash) and ±30% limits (dots) are also shown.

Mai, mean = 1.62). The ratios for cloudless conditions also show better agreement than for all sky conditions, and most of the OMI measurements for cloudless conditions are within 30% of the ground-based data. The scatter is greater in cloudy conditions, as expected, but the median values are found to be independent of cloudiness as a few large outliers skew the mean values upward in cloudy conditions but do not affect the median. The ratios between the OMI and ground-based data in our study were in general slightly higher than those from the previous studies [*Arola et al.*, 2009; *Kazadzis et al.*, 2009a; *Tanskanen et al.*, 2007]. This may be because the noontime data were used in our study, whereas the overpass time data [*Arola et al.*, 2009; *Kazadzis et al.*, 2009a] and daily doses [*Tanskanen et al.*, 2007] were used for the other studies, but the different environmental and climatological conditions may also have some bearing on the results.

[17] To investigate the effect of aerosol, the Libradtran radiative transfer model [*Mayer and Kylling*, 2005] has been run with and without aerosols for clear-sky days in the years 2005 and 2006 for Chiang Mai, Nakhon Pathom, and Songkhla, where there are Aerosol Robotic Network (AERONET) stations that can provide some indication of aerosol properties. Predefined aerosol types from the Libradtran package were used [*Shettle*, 1989]: urban for Chiang Mai and Nakhon Pathom and maritime for Songkhla. The aerosol optical depth and aerosol single scattering albedo data were taken from level 1.5 (AERONET, data available at http://aeronet.gsfc.nasa.gov) [*Holben et al.*, 1998]. The AERONET stations were not installed until late 2006, and this limited the number of clear-sky days available for use with our ground-based UV dataset. For this reason, we used mean monthly averaged aerosol optical depth data from the years 2006 to 2008, matched to clear-sky UV data from a

Table 1. Ratio of OMI Data and the Ground-Based Data Statistics

	All Data						Cloudless Data					
Sites	*N*	Median	Mean	$\%W_{10}$	$\%W_{20}$	$\%W_{30}$	*N*	Median	Mean	$\%W_{10}$	$\%W_{20}$	$\%W_{30}$
Chiang Mai	1158	1.30	1.62	14	30	48	180	1.30	1.37	1	19	51
Ubon Ratchathani	1203	1.14	1.32	30	53	67	178	1.14	1.19	34	68	82
Nakhon Pathom	1206	1.24	1.44	21	38	52	108	1.29	1.31	7	34	52
Songkhla	1094	1.09	1.32	39	62	70	79	1.09	1.09	52	95	100

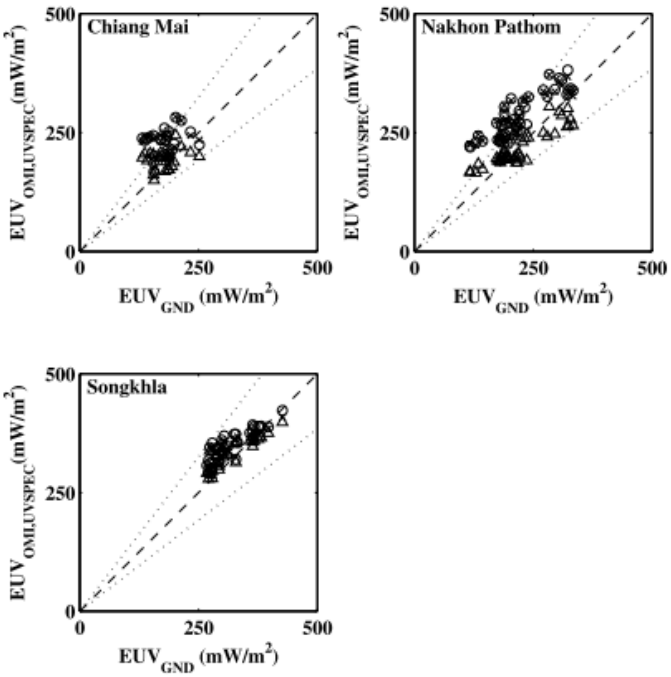

Figure 3. Comparison of erythemal UV retrieved from OMI (EUV_{OMI}, open circle), modeled by Libradtran's UVspec component (EUV_{UVSPEC}) with aerosol (open triangle) and without aerosol (cross), and measured by ground-based instruments under clear-sky conditions. The 1:1 correlation (dash) and ±30% limits (dots) are also shown.

given month. The standard deviation on the monthly mean aerosol optical depth data is about 40% for each site. For the two inland sites (Chiang Mai and Nakhon Pathom), there is a clear seasonal cycle in aerosol optical depth with maximum (up to 1.2) in February–April due to biomass burning [*Kift et al.*, 2006]. This reduces to 0.3–0.6 for the rest of the year. Songkhla in contrast exhibits very little seasonal cycle, having aerosol optical depth values in the range 0.2–0.5 throughout the year. Long-term averaged (years 2006–2008) single scattering albedo values at 440 nm (the shortest wavelength available) were used as constant values; 0.89 for urban sites and 0.97 for the maritime site. The results from the radiative transfer model are shown in Figure 3. As we can see, the values calculated from the Libradtran model with aerosol were closer to the ground-based values than those without aerosol, supporting the hypothesis that a large part of the differences between OMI and ground-based data may be attributed to aerosol. Therefore, to improve the OMI UV data, a correction for the aerosol absorption should be applied as this is not included in the standard OMI UV algorithm (although aerosol scattering has already been included).

5. Empirical Model

[18] Having identified that the OMI UV product requires a correction to account for absorption by aerosols, a broadly applicable method of performing such a correction and a source of aerosol data is needed. AERONET data are not always widely available, but OMI aerosol products provide the same coverage and are spatially matched with the UV products. Therefore, we address a correction of the OMI UV using the corresponding aerosol data from the same satellite. Note, however, that while this addresses the issue of data availability, data quality should still be considered. The data product we used was the aerosol absorption optical thickness (AAOT) at 354 nm taken at overpass time [*Torres et al.*, 2007] (Aura OMI Near-UV Aerosol Data Product level 2 Collection 3, data available at http://avdc.gsfc.nasa.gov/). These data are estimated to have a root-mean-square error about 0.01 [*OMI Team*, 2009].

[19] We introduce an aerosol absorption correction factor (F_A) as a function of OMI AAOT at 354 nm following the method used previously but with different aerosol inputs [*Arola et al.*, 2005, 2009; *Krotkov et al.*, 2005]. For example, *Arola et al.* [2009] used a merge of model and AERONET data, whereas *Krotkov et al.* [2005] used UV-multifilter rotating shadow band radiometer data. More recently, a correction for absorbing aerosol based on ground-based measurements has been applied, leading to improvements in the OMI UV retrieval for several locations: 5%–20% at various sites across Europe [*Arola et al.*, 2009], 8%–25% in Rome [*Ialongo et al.*, 2009], and 7%–23% in Thessaloniki [*Kazadzis et al.*, 2009a].

[20] In this study the erythemal UV irradiances at local solar noon in the year 2005 retrieved from OMI and mea-

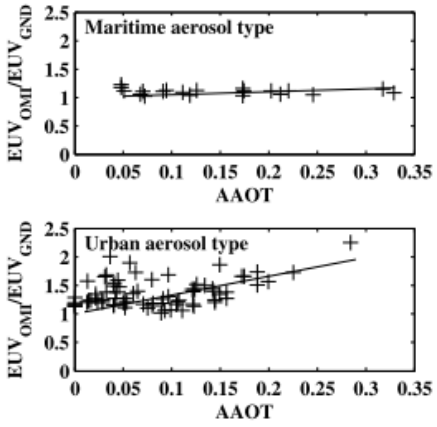

Figure 4. The ratio between the erythemal UV irradiances at local solar noon derived from OMI (EUV_{OMI}) and from ground-based instruments (EUV_{GND}) as a function of OMI aerosol absorption optical thickness (AAOT) for urban and maritime areas.

sured by the broadband instruments have been investigated for cloudless cases. The ratios of the OMI data to the ground-based data were plotted against the OMI AAOT values as shown in Figure 4 for the two different aerosol types (urban and maritime). The data of Songkhla were used as a reference maritime site, whereas the combined data of the other three sites represented the urban case; the latter having a correlation coefficient of 0.50 and a standard error in the slope of 0.27. Using Figure 4, OMI data must be divided by the equation for the straight-line fit to get the ground-based values. Thus, our aerosol correction factor, F_A becomes $[1 + 3.29 \times \text{AAOT}(354\ \text{nm})]^{-1}$ for urban aerosols and $[1 + 0.5 \times \text{AAOT}(354\ \text{nm})]^{-1}$ for the maritime case, compared with $[1 + 1.60 \times \text{AAOT}(320\ \text{nm})]^{-1}$ as introduced by *Ialongo et al.* [2009] and $[1 + 3 \times \text{AAOT}(325\ \text{nm})]^{-1}$ as suggested by *Krotkov et al.* [2005]. These factors were then applied to the equation as follows:

$$E_{CORR} = F_A \times E_{OMI}, \quad (1)$$

where E_{CORR} and E_{OMI} are noontime erythemal UV dose rate corrected for absorbing aerosols and retrieved from the OMI product, respectively.

[21] Using the method above the erythemal UV irradiances corrected for aerosol absorption were validated by comparing with ground-based data for independent years (2004, 2006, and 2007) as shown in Figure 5. We can see that after the absorbing aerosol correction the OMI corrected data are closer to the ground-based data than the original OMI data. The mean and the median of the ratio between the corrected data and ground-based data and also the $\%W_{10}$, %

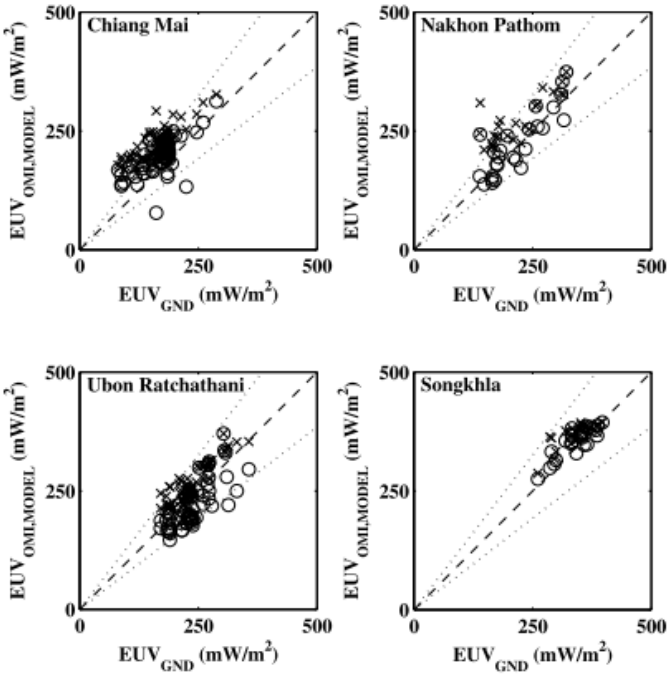

Figure 5. The erythemal UV irradiances at local solar noon retrieved from original OMI data (EUV_{OMI}, cross) and the OMI corrected data (EUV_{MODEL}, open circle) plotted against those measured from the broadband instrument (EUV_{GND}) for cloudless cases. The 1:1 correlation (dash) and ±30% limits (dots) are also shown.

Table 2. Ratio of OMI Corrected Data and the Ground-Based Data and the Ratio of Original OMI Data and the Ground-Based Data Statistics Under Clear-Sky Conditions

	Original OMI Data						Corrected OMI Data					
Sites	*N*	Median	Mean	$\%W_{10}$	$\%W_{20}$	$\%W_{30}$	*N*	Median	Mean	$\%W_{10}$	$\%W_{20}$	$\%W_{30}$
Chiang Mai	79	1.29	1.38	0	29	53	72	1.15	1.20	29	57	75
Ubon Ratchathani	62	1.10	1.13	44	81	92	62	0.91	0.93	39	81	100
Nakhon Pathom	26	1.24	1.29	15	42	58	26	1.01	1.03	46	85	96
Songkhla	26	1.08	1.09	62	92	100	26	1.05	1.04	85	100	100

W_{20}, and $\%W_{30}$ are given in Table 2, together with the corresponding values for the original OMI data.

[22] It is apparent from Table 2 that after the absorbing aerosol correction has been included most of the corrected erythemal UV irradiances at local solar noon are within ±20% of the ground-based data. The biggest improvement is shown at Chiang Mai and Nakhon Pathom, both of which approximately double the number of points within 20% of the ground-based values. These sites have the greatest aerosol levels and largest seasonal variation. In the case of Ubon Ratchathani, the mean data are now slightly underestimated which shows that the averaged urban aerosol correction is slightly too large for this site. It is known that Ubon Ratchathani is cleaner than Chiang Mai and also not subject to so much biomass burning. The cleanest site, Songkhla, has its own correction factor for maritime aerosol. Even so there is improvement particularly in $\%W_{10}$, with 85% of corrected OMI measurements lying within 10% of the ground-based data.

[23] The correction method shown in this study has improved the bias between the OMI and ground-based data for the Tropical sites (5%–26%, site dependent), in a similar way to recent studies at higher latitudes [*Arola et al.*, 2009; *Ialongo et al.*, 2009; *Kazadzis et al.*, 2009a]. Clearly addressing aerosol attenuation in the OMI UV algorithm is a global problem. While we have used the OMI AAOT product, as being available, there are also uncertainties in this product [*Torres et al.*, 2002]. Overcoming the challenges of retrieving aerosol optical properties from the satellite would also help to improve the UV products.

6. Conclusions

[24] In this study noontime erythemal UV irradiance calculated from OMI data from years 2004 to 2007 were compared with those measured by broadband radiometers at four Thai sites. The results showed an overestimation of UV in the OMI product compared with the ground-based data. The differences between the OMI data and the ground-based data under cloudless conditions were generally in the range 10%–40% for urban sites, whereas the value was less than 10% for the cleaner site. After absorbing aerosol correction factors based on OMI AAOT data were applied, for cloudless conditions, the differences between the two data sets were reduced to less than 20% and about 4% for urban and maritime sites, respectively.

[25] The post correction method can be applied to the OMI data under all sky conditions if the aerosol optical properties data are available. However, cloud is likely to be by far the dominant variable in cloudy conditions, and aerosol properties are difficult to quantify in such situations. Thus, the correction is mainly applicable to clear-sky conditions and in these circumstances can improve the UV retrieval.

[26] **Acknowledgments.** The authors are grateful to the OMI and Aura science teams for their efforts in producing the OMI data and to Serm Janjai and the Laboratory of Tropical Atmospheric Physics at Silpakorn University, Thailand, for the ground-based data. We would also like to thank the Royal Thai Government for the Ph.D. financial support.

References

Arola, A., et al. (2002), Assessment of four methods to estimate surface UV radiation using satellite data, by comparison with ground measurements from four stations in Europe, *J. Geophys. Res.*, *107*(D16), 4310, doi:10.1029/2001JD000462.

Arola, A., S. Kazadzis, N. Krotkov, A. Bais, J. Gröbner, and J. R. Herman (2005), Assessment of TOMS UV bias due to absorbing aerosols, *J. Geophys. Res.*, *110*, D23211, doi:10.1029/2005JD005913.

Arola, A., et al. (2009), A new approach to correct for absorbing aerosols in OMI UV, *Geophys. Res. Lett.*, *36*, L22805, doi:10.1029/2009GL041137.

Buchard, V., C. Brogniez, F. Auriol, B. Bonnel, J. Lenoble, A. Tanskanen, B. Bojkov, and P. Veefkind (2008), Comparison of OMI ozone and UV irradiance data with ground-based measurements at two French sites, *Atmos. Chem. Phys.*, *8*, 4517–4528, doi:10.5194/acp-8-4517-2008.

Diffey, B., and A. F. McKinlay (1987), A reference action spectrum for ultraviolet induced erythema in human skin, in *Human Exposure to UV Radiation: Risks and Regulations*, edited by W. F. Passchier and B. F. M. Bosnjakovich, pp. 83–87, Elsevier, New York.

Eck, T. F., P. K. Bhartia, and J. B. Kerr (1995), Satellite estimation of spectral UVB irradiance using TOMS-derived total ozone and UV reflectivity, *Geophys. Res. Lett.*, *22*, 611–614, doi:10.1029/95GL00111.

Fioletov, V. E., J. B. Kerr, D. I. Wardle, N. Krotkov, and J. R. Herman (2002), Comparison of Brewer ultraviolet irradiance measurements with total ozone mapping spectrometer satellite retrievals, *Opt. Eng.*, *41*(12), 3051–3061.

Fioletov, V. E., M. G. Kimlin, N. Krotkov, L. J. B. McArthur, J. B. Kerr, D. I. Wardle, J. R. Herman, R. Meltzer, T. W. Mathews, and J. Kaurola (2004), UV index climatology over the United States and Canada from ground-based and satellite estimates, *J. Geophys. Res.*, *109*, D22308, doi:10.1029/2004JD004820.

Holben, B. N., et al. (1998), AERONET—A federated instrument network and data archive for aerosol characterization, *Remote Sens. Environ.*, *66* (1), 1–16, doi:10.1016/S0034-4257(98)00031-5.

Ialongo, I., G. R. Casale, and A. M. Siani (2008), Comparison of total ozone and erythemal UV data from OMI with ground-based measurements at Rome station, *Atmos. Chem. Phys.*, *8*, 3283–3289, doi:10.5194/acp-8-3283-2008.

Ialongo, I., V. Buchard, C. Brogniez, G. R. Casale, and A. M. Siani (2009), Aerosol single scattering albedo retrieval in the UV range: An application to OMI satellite validation, *Atmos. Chem. Phys.*, *10*, 331–340, doi:10.5194/acp-10-331-2010.

Ilyas, M., A. Pandy, and S. I. S. Hassan (1999), UV-B radiation at Penang, *Atmos. Res.*, *51*(2), 141–152, doi:10.1016/S0169-8095(99)00005-8.

Janjai, S., K. Kirdsiri, I. Masiri, and M. Nunez (2009a), An investigation of solar erythemal ultraviolet radiation in the tropics: A case study at four stations in Thailand, *Int. J. Climatol.*, doi:10.1002/joc.2006.

Janjai, S., S. Suntaropas, and M. Nunez (2009b), Investigation of aerosol optical properties in Bangkok and suburbs, *Theor. Appl. Climatol.*, *96*, 221–233, doi:10.1007/s00704-008-0026-4.

Kalliskota, S., J. Kaurola, P. Taalas, J. R. Herman, E. A. Celarier, and N. A. Krotkov (2000), Comparison of daily UV doses estimated from Nimbus

7/TOMS measurements and ground-based spectroradiometric data, *J. Geophys. Res.*, *105*, 5059–5068, doi:10.1029/1999JD900926.

Kazadzis, S., A. Bais, A. Arola, N. Krotkov, N. Kouremeti, and C. Meleti (2009a), Ozone Monitoring Instrument spectral UV irradiance products: Comparison with ground based measurements at an urban environment, *Atmos. Chem. Phys.*, *9*, 585–594, doi:10.5194/acp-9-585-2009.

Kazadzis, S., A. Bais, D. Balis, N. Kouremeti, M. Zempila, A. Arola, E. Giannakaki, V. Amiridis, and A. Kazantzidis (2009b), Spatial and temporal UV irradiance and aerosol variability within the area of an OMI satellite pixel, *Atmos. Chem. Phys.*, *9*, 4593–4601, doi:10.5194/acp-9-4593-2009.

Kazantzidis, A., et al. (2006), Comparison of satellite-derived UV irradiances with ground-based measurements at four European stations, *J. Geophys. Res.*, *111*, D13207, doi:10.1029/2005JD006672.

Kift, R., A. R. Webb, J. Page, J. Rimmer, and S. Janjai (2006), A Web-based tool for UV irradiance data: Predictions for European and Southeast Asian sites, *Photochem. Photobio.*, *82*, 579–586, doi:10.1562/2005-04-20-ra-494.

Krotkov, N., P. K. Bhartia, J. Herman, J. Slusser, G. Scott, G. Labow, A. P. Vasilkov, T. F. Eck, O. Dubovik, and B. N. Holben (2005), Aerosol ultraviolet absorption experiment (2002 to 2004), part 2: Absorption optical thickness, refractive index, and single scattering albedo, *Opt. Eng.*, *44*, 041005, doi:10.1117/1.1886819.

Krotkov, N. A., P. K. Bhartia, J. R. Herman, V. Fioletov, and J. Kerr (1998), Satellite estimation of spectral surface UV irradiance in the presence of tropospheric aerosols 1. Cloud-free case, *J. Geophys. Res.*, *103*(D8), 8779–8793, doi:10.1029/98JD00233.

Krotkov, N. A., J. R. Herman, P. K. Bhartia, V. Fioletov, and Z. Ahmad (2001), Satellite estimation of spectral surface UV irradiance 2. Effects of homogeneous clouds and snow, *J. Geophys. Res.*, *106*(D11), 11,743–11,759, doi:10.1029/2000JD900721.

Levelt, P. F., G. H. J. van den Oord, M. R. Dobber, A. Malkki, V. Huib, V. Johan de, P. Stammes, J. O. V. Lundell, and H. Saari (2006), The Ozone Monitoring Instrument, *IEEE Trans. Geosci. Remote Sens.*, *44*, 1093–1101.

Mayer, B., and A. Kylling (2005), Technical note: The libRadtran software package for radiative transfer calculations—Description and examples of use, *Atmos. Chem. Phys.*, *5*, 1855–1877, doi:10.5194/acp-5-1855-2005.

McKenzie, R. L., G. Seckmeyer, A. F. Bais, J. B. Kerr, and S. Madronich (2001), Satellite retrievals of erythemal UV dose compared with ground-based measurements at northern and southern midlatitudes, *J. Geophys. Res.*, *106*, 24,051–24,062, doi:10.1029/2001JD000545.

McKenzie, R. L., C. Weinreis, P. V. Johnston, B. Liley, H. Shiona, M. Kotkamp, D. Smale, N. Takegawa, and Y. Kondo (2008), Effects of urban pollution on UV spectral irradiances, *Atmos. Chem. Phys.*, *8*, 5683–5697, doi:10.5194/acp-8-5683-2008.

OMI Team (2009), Ozone Monitoring Instrument (OMI) Data User's Guide, pp. 1–60.

Shettle, E. P. (1989), Models of aerosols, clouds and precipitation for atmospheric propagation studies, in *Atmospheric Propagation in the UV, Visible, IR and mm-Wave Region and Related Systems Aspects*, *AGARD Conf. Proc.*, *454*, 15-11–15-13.

Tanskanen, A. (2004), Lambertian surface albedo climatology at 360 nm from TOMS data using moving time-window technique, in *Proceedings of the XX Quadrennial Ozone Symposium*, pp. 1159–1160, Kos, Greece.

Tanskanen, A., N. A. Krotkov, J. R. Herman, and A. Arola (2006), Surface ultraviolet irradiance from OMI, *IEEE Trans. Geosci. Remote Sens.*, *44*, 1267–1271.

Tanskanen, A., et al. (2007), Validation of daily erythemal doses from Ozone Monitoring Instrument with ground-based UV measurement data, *J. Geophys. Res.*, *112*, D24S44, doi:10.1029/2007JD008830.

Torres, O., R. Decae, J. P. Veefkind, and G. de Leeuw (2002), OMI aerosol retrieval algorithm, in *OMI Algorithm Theoretical Basis Document: Clouds, Aerosols, and Surface UV Irradiance*, edited by P. Stammes, NASA Goddard Space Flight Cent., Greenbelt, Md. (Available at http://eospso.gsfc.nasa.gov/eos_homepage/for_scientist/atbd/docs/OMI/ATBD-OMI-03.pdf)

Torres, O., A. Tanskanen, B. Veihelmann, C. Ahn, R. Braak, P. K. Bhartia, P. Veefkind, and P. Levelt (2007), Aerosols and surface UV products from Ozone Monitoring Instrument observations: An overview, *J. Geophys. Res.*, *112*, D24S47, doi:10.1029/2007JD008809.

UNEP (2007), Environmental effects of ozone depletion and its interactions with climate change, 2006 assessment, *Photochem. Photobio. Sci.*, *6*, 201–332.

Webb, A., J. Gröbner, and M. Blumthaler (2006), *A Practical Guide to Operating Broadband Instruments Measuring Erythemally Weighted Irradiance*, 21 pp., OPOCE.

Weihs, P., M. Blumthaler, H. E. Rieder, A. Kreuter, S. Simic, W. Laube, A. W. Schmalwieser, J. E. Wagner, and A. Tanskanen (2008), Measurements of UV irradiance within the area of one satellite pixel, *Atmos. Chem. Phys.*, *8*, 5615–5626, doi:10.5194/acp-8-5615-2008.

WMO (2007), *Scientific Assessment of Ozone Depletion: 2006, Global Ozone Research and Monitoring Project*, *Rep. 50*, 572 pp., World Meteorological Organization, Geneva, Switzerland.

S. Buntoung and A. R. Webb, School of Earth, Atmospheric and Environmental Science, University of Manchester, Williamson Bldg., Oxford Rd., Manchester M13 9PL, UK. (sumaman.buntoung@postgrad.manchester.ac.uk)

References

Abarca, J. F., C. C. Casiccia, and F. D. Zamorano (2002), Increase in sunburns and photosensitivity disorders at the edge of the Antarctic ozone hole, Southern Chile, 1986-2000, *J. Am. Acad. Dermatol.*, *46*(2), 193-199.

Acosta, L. R., and W. F. J. Evans (2000), Design of the Mexico City UV monitoring network: UV-B measurements at ground level in the urban environment, *J. Geophys. Res.*, *105*(D4), 5017-5026, doi:10.1029/1999JD900250.

Ahn, C., O. Torres, and P. K. Bhartia (2008), Comparison of Ozone Monitoring Instrument UV Aerosol Products with Aqua/Moderate Resolution Imaging Spectroradiometer and Multiangle Imaging Spectroradiometer observations in 2006, *J. Geophys. Res.*, *113*, D16S27, doi:10.1029/2007JD008832.

Al-Bdour, D., and M. Al-Latayfeh (2004), Risk factors for pterygium in an adult Jordanian population, *Acta Ophthalmol. Scand.*, *82*(1), 64-67, doi:10.1046/j.1600-0420.2003.0213.x.

Allaart, M., M. van Weele, P. Fortuin, and H. Kelder (2004), An empirical model to predict the UV-index based on solar zenith angles and total ozone, *Meteorol. Appl.*, *11*(1), 59-65, doi:10.1017/S1350482703001130.

Antón, M., M. L. Cancillo, A. Serrano, and J. A. García (2005), A multiple regression analysis between UV radiation measurements at Badajoz and ozone, reflectivity and aerosols estimated by TOMS, *Physica Scripta*, *T118*, 21-23.

Antón, M., M. López, J. M. Vilaplana, M. Kroon, R. McPeters, M. Bañón, and A. Serrano (2009), Validation of OMI-TOMS and OMI-DOAS total ozone column using five Brewer spectroradiometers at the Iberian peninsula, *J. Geophys. Res.*, *114*, D14307, doi:10.1029/2009JD012003.

Arola, A., S. Kalliskota, P. N. den Outer, K. Edvardsen, G. Hansen, T. Koskela, T. J. Martin, J. Matthijsen, R. Meerkoetter, P. Peeters, G. Seckmeyer, P. C. Simon, H. Slaper, P. Taalas, and J. Verdebout (2002), Assessment of four methods to estimate surface UV radiation using satellite data, by comparison with ground measurements from four stations in Europe, *J. Geophys. Res.*, *107*(4310), doi:10.1029/2001JD000462.

Arola, A., S. Kazadzis, N. Krotkov, A. Bais, J. Gröbner, and J. R. Herman (2005), Assessment of TOMS UV bias due to absorbing aerosols, *J. Geophys. Res.*, *110*, D23211, doi:10.1029/2005JD005913.

Arola, A., S. Kazadzis, A. Lindfors, N. Krotkov, J. Kujanpää, J. Tamminen, A. Bais, A. di Sarra, J. M. Villaplana, C. Brogniez, A. M. Siani, M. Janouch, P. Weihs, A. Webb, T. Koskela, N. Kouremeti, D. Meloni, V. Buchard, F. Auriol, I. Ialongo, M. Staneck, S. Simic, A. Smedley, and S. Kinne (2009), A new approach to correct for absorbing aerosols in OMI UV, *Geophys. Res. Lett.*, *36*, L22805, doi:10.1029/2009GL041137.

Badarinath, K. V. S., K. M. Latha, T. R. K. Chand, and P. K. Gupta (2009), Impact of biomass burning on aerosol properties over tropical wet evergreen forests of Arunachal Pradesh, India, *Atmos. Res.*, *91*(1), 87-93, doi:10.1016/j.atmosres.2008.03.023.

Badosa, J., J.-A. González, J. Calbó, M. van Weele, and R. L. McKenzie (2005), Using a parameterization of a radiative transfer model to build high-resolution maps of typical clear-sky UV Index in Catalonia, Spain, *J. Appl. Meteor.*, *44*(6), 789-803, doi:10.1175/JAM2237.1.

Bais, A. F. (1997), Absolute spectral measurements of direct solar ultraviolet irradiance with a Brewer spectrophotometer, *Appl. Opt.*, *36*(21), 5199-5204, doi:10.1364/AO.36.005199.

Bais, A. F., B. G. Gardiner, H. Slaper, M. Blumthaler, G. Bernhard, R. McKenzie, A. R. Webb, G. Seckmeyer, B. Kjeldstad, T. Koskela, P. J. Kirsch, J. Gröbner, J. B. Kerr, S. Kazadzis, K. Leszczynski, D. Wardle, W. Josefsson, C. Brogniez, D. Gillotay, H. Reinen, P. Weihs, T. Svenoe, P. Eriksen, F. Kuik, and A. Redondas (2001), SUSPEN intercomparison of ultraviolet spectroradiometers, *J. Geophys. Res.*, *106*(D12), 12509-12525, doi:10.1029/2000JD900561.

Bais, A. F., A. Kazantzidis, S. Kazadzis, D. S. Balis, C. S. Zerefos, and C. Meleti (2005), Deriving an effective aerosol single scattering albedo from spectral surface UV irradiance measurements, *Atmos. Environ.*, *39*(6), 1093-1102, doi:10.1016/j.atmosenv.2004.09.080.

Balis, D. S., V. Amiridis, C. Zerefos, A. Kazantzidis, S. Kazadzis, A. F. Bais, C. Meleti, E. Gerasopoulos, A. Papayannis, V. Matthias, H. Dier, and M. O. Andreae (2004), Study of the effect of different type of aerosols on UV-B radiation from measurements during EARLINET, *Atmos. Chem. Phys.*, *4*, 307-321, doi:10.5194/acp-4-307-2004.

Bartlett, L. M., and A. R. Webb (2000), Changes in ultraviolet radiation in the 1990s: Spectral measurements from Reading, England, *J. Geophys. Res.*, *105*(D4), 4889-4893, doi:10.1029/1999JD900493.

Bass, A. M., and R. J. Paur (1985), The ultraviolet cross-sections of ozone, I, Measurements, in Atmospheric ozone, in *Ozone Symposium (1984:Halkidiki, Greece): Atmospheric ozone*, edited by C. Z. Zerefos and A. Ghaz, pp. 606-616, D.Reidel, Hingham, Mass.

Bates, D. R. (1984), Rayleigh scattering by air, *Planet. Space Sci.*, *32*, 785-790.

Bentham, G. (2001), Overview of climate change impacts on human health in the UK: UV Radiation, in *Health effects of climate change in the UK*, edited by UK EGCCH, pp. 70-218, Department of Health.

Bentham Instruments Ltd (1997), A guide to spectroradiometry Instruments and applications for the ultraviolet, edited, p. 27, Reading, UK.

Blumthaler, M., and W. Ambach (1988), Solar UVB-albedo of various surfaces, *Photochem. Photobiol.*, *48*(1), 85-88, doi:10.1111/j.1751-1097.1988.tb02790.x.

Blumthaler, M., W. Ambach, and R. Ellinger (1997), Increase in solar UV radiation with altitude, *J. Photochem. Photobiol. B.*, *39*(2), 130-134, doi:10.1016/S1011-1344(96)00018-8.

Buchard, V., C. Brogniez, F. Auriol, B. Bonnel, J. Lenoble, A. Tanskanen, B. Bojkov, and P. Veefkind (2008), Comparison of OMI ozone and UV irradiance data with ground-based measurements at two French sites, *Atmos. Chem. Phys.*, *8*(16), 4517-4528, doi:10.5194/acp-8-4517-2008.

Burrows, W., R., M. Vallée, D. Wardle, I., J. Kerr, B., L. Wilson, J., and D. Tarasick, W. (1994), The Canadian operational procedure for forecasting total ozone and UV radiation, *Meteor. Appl.*, *1*(3), 247-265, doi:10.1002/met.5060010307.

Calbó, J., D. Pagès, and J.-A. González (2005), Empirical studies of cloud effects on UV radiation: A review, *Rev. Geophys.*, *43*, RG2002, doi:10.1029/2004RG000155.

Cañada, J., G. Pedrós, A. López, and J. V. Boscá (2000), Influences of the clearness index for the whole spectrum and of the relative optical air mass on UV solar irradiance for two locations in the Mediterranean area, Valencia and Cordoba, *J. Geophys. Res.*, *105*(D4), 4759-4766, doi:10.1029/1999JD901106.

Cañada, J., G. Pedros, and J. V. Bosca (2003), Relationships between UV (0.290-0.385 μm) and broad band solar radiation hourly values in Valencia and Córdoba, Spain, *Energy*, *28*(3), 199-217, doi:10.1016/S0360-5442(02)00111-1.

Cebula, R. P., G. O. Thuillier, M. E. VanHoosier, E. Hilsenrath, M. Herse, G. E. Brueckner, and P. C. Simon (1996), Observations of the solar irradiance in the 200-350 nm interval during the ATLAS-1 Mission: A comparison among three sets of measurements-SSBUV, SOLSPEC, and SUSIM, *Geophys. Res. Lett.*, *23*(17), 2289-2292, doi:10.1029/96GL01109.

Cede, A., E. Luccini, L. Nuñez, R. D. Piacentini, and M. Blumthaler (2002), Monitoring of erythemal irradiance in the Argentine ultraviolet network, *J. Geophys. Res.*, *107*, 4165, doi:10.1029/2001JD001206.

Cede, A., E. Luccini, L. Nuñez, R. D. Piacentini, M. Blumthaler, and J. R. Herman (2004), TOMS-derived erythemal irradiance versus measurements at the stations of the Argentine UV Monitoring Network, *J. Geophys. Res.*, *109*, D08109, doi:10.1029/2004JD004519.

Chadyšienė, R., and A. Girgždys (2008), Ultraviolet radiation albedo of natural surfaces, *J. Environ. Eng. Landsc. Manag. Vilnius: Technika 16*(2), 83-88.

Chandrasekhar, S. (1960), *Radiative Transfer*, 393 pp., Dover Publications, Inc., New York.

Chou, M. D., P. H. Lin, P. L. Ma, and H. J. Lin (2006), Effects of aerosols on the surface solar radiation in a tropical urban area, *J. Geophys. Res.*, *111*, D15207, doi:10.1029/2005JD006910.

Chubarova, N. (2006), Role of tropospheric gases in the absorption of UV radiation, *Dokl. Earth Sci.*, *407*(1), 294-297, doi:10.1134/S1028334X06020322.

Chubarova, N. Y. (2008), UV variability in Moscow according to long-term UV measurements and reconstruction model, *Atmos. Chem. Phys.*, *8*(12), 3025-3031, doi:10.5194/acp-8-3025-2008.

Chubarova, N. Y. (2009), Seasonal distribution of aerosol properties over Europe and their impact on UV irradiance, *Atmos. Meas. Tech.*, *2*(2), 593-608, doi:10.5194/amt-2-593-2009.

CIE (1998), Erythema reference spectrum and standard erythema dose, *CIE S 007/E-1998, CIE Central Bureau, Vienna, Austria, pp.4.*

Cordero, R. R., G. Seckmeyer, D. Pissulla, and F. Labbe (2009), Exploitation of spectral direct UV irradiance measurements, *Metrologia*, *46*(1), 19.

Corrêa, M. D. P., and J. C. Ceballos (2008), UVB surface albedo measurements using biometers, *Rev. Bras. Geof.*, *26*(4), 411-416.

Dahlback, A. (1996), Measurements of biologically effective UV doses, total ozone abundances, and cloud effects with multichannel, moderate bandwidth filter instruments, *Appl. Opt.*, *35*(33), 6514-6521, doi:10.1364/AO.35.006514.

Dave, J. V. (1964), Meaning of successive iteration of the auxiliary equation in the theory of radiative transfer, *Astrophys. J.*, *140*, 1292, doi:10.1086/148024.

Davis, A., G. H. W. Deane, and B. L. Diffey (1976), Possible dosimeter for ultraviolet radiation, *Nature*, *261*(5556), 169-170.

Davis, A., B. L. Diffey, and T. K. Tate (1981), A personal dosimeter for biologically effective solar UV-B radiation, *Photochem. Photobiol.*, *34*(2), 283-286, doi:10.1111/j.1751-1097.1981.tb09360.x.

de Gruijl, F. R., J. Longstreth, M. Norval, A. P. Cullen, H. Slaper, M. L. Kripke, Y. Takizawag, and J. C. van der Leunh (2003), Health effects from stratospheric ozone depletion and interactions with climate change, *Photochem. Photobiol. Sci.*, *2*, 16-28, doi:10.1039/b211156j.

DeLuisi, J., D. Theisen, J. Augustine, P. Disterhoft, K. Lantz, E. Weatherhead, G. Hodges, C. Cornwall, I. Petropavlovskikh, A. Stevermer, D. Wellman, and J. Barnett (2003), On the correspondence between surface UV observations and TOMS determinations of surface UV: a potential method for quality evaluating world surface UV observations, *Ann. Geophys.*, *46*(2), 295-308.

Demers, A. A., Z. Nugent, C. Mihalcioiu, M. C. Wiseman, and E. V. Kliewer (2005), Trends of nonmelanoma skin cancer from 1960 through 2000 in a Canadian population, *J. Am. Acad. Dermatol.*, *53*(2), 320-328, doi:10.1016/j.jaad.2005.03.043.

den Outer, P. N., H. Slaper, and R. B. Tax (2005), UV radiation in the Netherlands: Assessing long-term variability and trends in relation to ozone and clouds, *J. Geophys. Res.*, *110*, D02203, doi:10.1029/2004JD004824.

Di Menno, I., M. L. Moriconi, M. Di Menno, G. R. Casale, and A. M. Siani (2002), Spectral ultraviolet measurements by a multichannel monitor and a Brewer spectroradiometer: A field study, *Radiat. Prot. Dosim.*, *102*(3), 259-263.

di Sarra, A., M. Cacciani, P. Chamard, C. Cornwall, J. J. DeLuisi, T. Di Iorio, P. Disterhoft, G. Fiocco, D. Fuá, and F. Monteleone (2002), Effects of desert dust and ozone on the ultraviolet irradiance at the Mediterranean island of Lampedusa during PAUR II, *J. Geophys. Res.*, *107*, 8135, D18, doi:10.1029/2000JD000139.

Diffey, B. L. (1997), Monitoring personal exposure to solar ultraviolet radiation, in *Solar ultraviolet radiation: modelling measurements and effects*, edited by C. S. Zerefos and A. F. Bais, pp. 187-200, Springer-Verlag, Berlin.

Dobber, M. R., R. J. Dirksen, P. F. Levelt, G. H. J. van den Oord, R. H. M. Voors, Q. Kleipool, G. Jaross, M. Kowalewski, E. Hilsenrath, G. W. Leppelmeier, V. Johan de, W. Dierssen, and N. C. Rozemeijer (2006), Ozone monitoring instrument calibration, *IEEE Trans. Geosci. Remote Sens.*, *44*(5), 1209-1238.

Dubrovský, M. (2000), Analysis of UV-B irradiances measured simultaneously at two stations in the Czech Republic, *J. Geophys. Res.*, *105*, 4907-4913, D4, doi:10.1029/1999JD900374.

Dunne, R. P. (1999), Polysulphone film as an underwater dosimeter for solar ultraviolet-B radiation in tropical latitudes, *Mar. Ecol. Prog. Ser.*, *189*, 53-63.

Eck, T. F., P. K. Bhartia, and J. B. Kerr (1995), Satellite estimation of spectral UVB irradiance using TOMS derived total ozone and UV reflectivity, *Geophys. Res. Lett.*, *22*, 611-614, doi:10.1029/95GL00111.

Erlick, C., and J. E. Frederick (1998), Effects of aerosols on the wavelength dependence of atmospheric transmission in the ultraviolet and visible 2. Continental and urban aerosols in clear skies, *J. Geophys. Res.*, *103*(D18), 23275-23285, 10.1029/98jd02119.

Esteve, A. R., J. A. Martínez-Lozano, M. J. Marín, V. Estellés, F. Tena, and M. P. Utrillas (2009), The influence of ozone and aerosols on the experimental values of UV erythemal radiation at ground level in Valencia, *International Journal of Climatology*, *29*(14), 2171-2182.

Farman, J. C., B. G. Gardiner, and J. D. Shanklin (1985), Large losses of total ozone in Antarctica reveal seasonal ClOx/NOx interaction, *Nature*, *315*(6016), 207-210, doi:10.1038/315207a0.

Feister, U., E. Jäkel, and K. Gericke (2002), Parameterization of daily solar global ultraviolet irradiation, *Photochem. Photobiol.*, *76*(3), 281-293.

Fioletov, V. E., J. B. Kerr, D. I. Wardle, N. Krotkov, and J. R. Herman (2002), Comparison of Brewer ultraviolet irradiance measurements with total ozone mapping spectrometer satellite retrievals, *Opt. Eng.*, *41*(12), 3051-3061.

Fioletov, V. E., J. B. Kerr, L. J. B. McArthur, D. I. Wardle, and T. W. Mathews (2003), Estimating UV index climatology over Canada, *J. Appl. Meteor.*, *42*(3), 417-433.

Fioletov, V. E., M. G. Kimlin, N. Krotkov, L. J. B. McArthur, J. B. Kerr, D. I. Wardle, J. R. Herman, R. Meltzer, T. W. Mathews, and J. Kaurola (2004), UV index climatology over the United States and Canada from ground-based and satellite estimates, *J. Geophys. Res.*, *109*, *D22308*, doi:10.1029/2004JD004820.

Fioletov, V. E., L. J. B. McArthur, T. W. Mathews, and L. Marrett (2009), On the relationship between erythemal and vitamin D action spectrum weighted ultraviolet radiation, *J. Photochem. Photobiol. B.*, *95*(1), 9-16, doi:10.1016/j.jphotobiol.2008.11.014.

Forster, P. M. D. F., K. P. Shine, and A. R. Webb (1995), Modeling ultraviolet radiation at the earth's surface. Part II: Model and instrument comparison, *J. Appl. Meteor.*, *34*(11), 2426-2439.

Ganguly, N., and K. Iyer (2006), Long-term trend in ozone and erythemal UV at Indian latitudes, *J. Atmos. Chem.*, *55*(3), 227-239, doi:10.1007/s10874-006-9035-9.

Gao, W., J. Slusser, J. Gibson, G. Scott, D. Bigelow, J. Kerr, and B. McArthur (2001), Direct-sun column ozone retrieval by the ultraviolet multifilter rotating shadow-band radiometer and comparison with those from Brewer and Dobson spectrophotometers, *Appl. Opt.*, *40*(19), 3149-3155.

Garane, K., A. Bais, K. Tourpali, C. Meleti, C. Zerefos, and S. Kazadzis (2005), Variability of spectral UV irradiance at Thessaloniki, Greece, from 15 years of measurements, paper presented at Ultraviolet ground- and space-based measurements, models, and effects V, SPIE5886, San Diego, CA, USA.

Godar, D. E. (2005), UV Doses Worldwide, *Photochem. Photobiol.*, *81*(4), 736-749, doi:10.1562/2004-09-07-ir-308r.1.

Grainger, R. G., R. E. Basher, and R. L. McKenzie (1993), UV-B Robertson-Berger meter characterization and field calibration, *Appl. Opt.*, *32*(3), 343-349.

Gröbner, J., and J. B. Kerr (2001), Ground-based determination of the spectral ultraviolet extraterrestrial solar irradiance: Providing a link between space-based and ground-based solar UV measurements, *J. Geophys. Res.*, *106*(D7), 7211-7217, doi:10.1029/2000JD900756.

Gröbner, J., J. Schreder, S. Kazadzis, A. F. Bais, M. Blumthaler, P. Görts, R. Tax, T. Koskela, G. Seckmeyer, A. R. Webb, and D. Rembges (2005), Traveling reference spectroradiometer for routine quality assurance of spectral solar ultraviolet irradiance measurements, *Appl. Opt.*, *44*(25), 5321-5331.

Gröbner, J., M. Blumthaler, S. Kazadzis, A. Bais, A. Webb, J. Schreder, G. Seckmeyer, and D. Rembges (2006), Quality assurance of spectral solar UV measurements: results from 25 UV monitoring sites in Europe, 2002 to 2004, *Metrologia*(2), S66.

Gróf, P., S. Gáspái, and G. Rontó (1996), Use of uracil thin layer for measuring biologically effective UV dose, *Photochem. Photobiol.*, *64*(5), 800-806, doi:10.1111/j.1751-1097.1996.tb01837.x.

Hayashi, L. C., S. Hayashi, K. Yamaoka, N. Tamiya, M. Chikuda, and E. Yano (2003), Ultraviolet B exposure and type of lens opacity in ophthalmic patients in Japan, *Sci. Total Environ.*, *302*(1-3), 53-62, doi:10.1016/S0048-9697(02)00320-0.

Herman, J. R., P. K. Bhartia, J. Ziemke, Z. Ahmad, and D. Larko (1996), UV-B increases (1979-1992) from decreases in total ozone, *Geophys. Res. Lett.*, *23*, doi:10.1029/96GL01958.

Herman, J. R., N. Krotkov, E. Celarier, D. Larko, and G. Labow (1999a), Distribution of UV radiation at the Earth's surface from TOMS-measured UV-backscattered radiances, *J. Geophys. Res.*, *104*(D10), 12059-12076, doi:10.1029/1999JD900062.

Herman, J. R., R. L. McKenzie, S. B. Diaz, J. B. Kerr, S. Madronich, and G. Seckmeyer (1999b), Ultraviolet radiation at the Earth's surface, in UNEP/WMO Scientific Assessment of the Ozone Layer: 1998, pp 9.1-9.46.

Holben, B. N., T. F. Eck, I. Slutsker, D. Tanré, J. P. Buis, A. Setzer, E. Vermote, J. A. Reagan, Y. J. Kaufman, T. Nakajima, F. Lavenu, I. Jankowiak, and A. Smirnov (1998), AERONET--A federated instrument network and data archive for aerosol characterization, *Remote Sens. Environ.*, *66*(1), 1-16, doi:10.1016/S0034-4257(98)00031-5.

Houghton, J. (2002), *The physics of atmospheres*, 320 pp., Cambridge University Press, New York.

Hülsen, G., and J. Gröbner (2007), Characterization and calibration of ultraviolet broadband radiometers measuring erythemally weighted irradiance, *Appl. Opt.*, *46*(23), 5877-5886.

Ialongo, I., G. R. Casale, and A. M. Siani (2008), Comparison of total ozone and erythemal UV data from OMI with ground-based measurements at Rome station, *Atmos. Chem. Phys.*, *8*(12), 3283-3289, doi:10.5194/acp-8-3283-2008.

Ialongo, I., V. Buchard, C. Brogniez, G. R. Casale, and A. M. Siani (2010), Aerosol single scattering albedo retrieval in the UV range: an application to OMI satellite validation, *Atmos. Chem. Phys.*, *10*(2), 331-340, 10.5194/acp-10-331-2010.

Ilyas, M., A. Pandy, and S. I. S. Hassan (1999), UV-B radiation at Penang, *Atmos. Res.*, *51*(2), 141-152, doi:10.1016/S0169-8095(99)00005-8.

IPCC (2007), Contribution of working group I to the fourth assessment report of the Intergovernmental Panel on Climate Change, 2007, edited by S. Solomon, et al., Cambridge University Press, Cambridge, United Kingdom and New York, USA.

Iqbal, M. (1983), *An introduction to solar radiation*, 390 pp., Academic Press, Toronto, CA.

Janjai, S., J. Laksanaboonsong, M. Nunez, and A. Thongsathitya (2005), Development of a method for generating operational solar radiation maps from satellite data for a tropical environment, *Solar Energy*, *78*(6), 739-751.

Janjai, S., K. Kirdsiri, I. Masiri, and M. Nunez (2009a), An investigation of solar erythemal ultraviolet radiation in the tropics: a case study at four stations in Thailand, *Int. J. Climatol.*, doi:10.1002/joc.2006.

Janjai, S., S. Suntaropas, and M. Nunez (2009b), Investigation of aerosol optical properties in Bangkok and suburbs, *Theor. Appl. Climatol.*, *96*(3), 221-233, doi:10.1007/s00704-008-0026-4.

Janjai, S., S. Buntung, R. Wattan, and I. Masiri (2010), Mapping solar ultraviolet radiation from satellite data in a tropical environment, *Remote Sens. Environ.*, *114*(3), 682-691.

Josefsson, W., and T. Landelius (2000), Effect of clouds on UV irradiance: As estimated from cloud amount, cloud type, precipitation, global radiation and sunshine duration, *J. Geophys. Res.*, *105*(D4), 4927-4935, doi:10.1029/1999JD900255.

Josefsson, W. (2006), *UV-radiation 1983-2003 measured at Norrköping, Sweden*, 18 pp., Springer, Wien, AUTRICHE.

Kalashnikova, V. Olga, Mills, P. Franklin, Eldering, Annmarie, Anderson, and Don (2007), *Application of satellite and ground-based data to investigate the UV radiative effects of Australian aerosols*, 16 pp., Elsevier, New York, NY, ETATS-UNIS.

Kalliskota, S., J. Kaurola, P. Taalas, J. R. Herman, E. A. Celarier, and N. A. Krotkov (2000), Comparison of daily UV doses estimated from Nimbus 7/TOMS measurements and ground-based spectroradiometric data, *J. Geophys. Res.*, *105*(D4), 5059-5067, doi:10.1029/1999JD900926.

Kazadzis, S., A. Bais, A. Arola, N. Krotkov, N. Kouremeti, and C. Meleti (2009a), Ozone Monitoring Instrument spectral UV irradiance products: comparison with ground based measurements at an urban environment, *Atmos. Chem. Phys.*, *9*(2), 585-594, doi:10.5194/acp-9-585-2009.

Kazadzis, S., A. Bais, D. Balis, N. Kouremeti, M. Zempila, A. Arola, E. Giannakaki, V. Amiridis, and A. Kazantzidis (2009b), Spatial and temporal UV irradiance and aerosol variability within the area of an OMI satellite pixel, *Atmos. Chem. Phys.*, *9*(14), doi:10.5194/acp-9-4593-2009.

Kazantzidis, A., A. F. Bais, J. Gröbner, J. R. Herman, S. Kazadzis, N. Krotkov, E. Kyrö, P. N. den Outer, K. Garane, P. Görts, K. Lakkala, C. Meleti, H. Slaper, R. B. Tax, T. Turunen, and C. S. Zerefos (2006), Comparison of satellite-derived UV irradiances with ground-based measurements at four European stations, *J. Geophys. Res.*, *111*, D13207, doi:10.1029/2005JD006672.

Kerr, J. B. (1991), Trends in total ozone at Toronto between 1960 and 1991, *J. Geophys. Res.*, *96*, doi:10.1029/91JD02282.

Kerr, J. B., and C. T. McElroy (1993), Evidence for large upward trends of ultraviolet-B radiation linked to ozone depletion, *Science*, *262*(5136), 1032-1034.

Kerr, J. B. (2005), Understanding the factors that affect surface ultraviolet radiation, *Opt. Eng.*, *44*(4), 041002-041009.

Key, J. R., and A. J. Schweiger (1998), Tools for atmospheric radiative transfer: Streamer and FluxNet, *Comput. & Geosci.*, *24*(5), 443-451, doi:10.1016/S0098-3004(97)00130-1.

Kift, R., A. R. Webb, J. Page, J. Rimmer, and S. Janjai (2006), A web-based tool for UV irradiance data: Predictions for european and southeast Asian sites, *Photochem. Photobiol.*, *82*(2), 579-586, doi:10.1562/2005-04-20-ra-494.

Kimlin, M. G., J. M. Sabburg, A. V. Parisi, and R. S. Meltzer (2003), Comparison of Brewer spectrophotometer ultraviolet data from similar latitudes in the Northern and Southern Hemisphere, *J. Atmos. Sol.-Terr. Phys.*, *65*(16-18), 1401-1410.

Koepke, P., A. Bais, D. Balis, M. Buchwitz, H. De Backer, X. de Cabo, P. Eckert, P. Eriksen, D. Gillotay, A. Heikkilä, T. Koskela, B. Lapeta, Z. Litynska, J. Lorente, B. Mayer, A. Renaud, A. Ruggaber, G. Schauberger, G. Seckmeyer, P. Seifert, A. Schmalwieser, H. Schwander, K. Vanicek, and M. Weber (1998), Comparison of models used for UV index calculations, *Photochem. Photobiol.*, *67*(6), 657-662.

Kroon, M., J. P. Veefkind, M. Sneep, R. D. McPeters, P. K. Bhartia, and P. F. Levelt (2008), Comparing OMI-TOMS and OMI-DOAS total ozone column data, *J. Geophys. Res.*, *113*, D16S28, doi:10.1029/2007JD008798.

Krotkov, N., J. Herman, P. K. Bhartia, C. Seftor, A. Arola, J. Kaurola, S. Kalliskota, P. Taalas, and I. V. Geogdzhaev (2002a), Version 2 total ozone mapping spectrometer ultraviolet algorithm: problems and enhancements, *Opt. Eng.*, *41*(12), 3028-3039.

Krotkov, N., P. K. Bhartia, J. Herman, J. Slusser, G. Scott, G. Labow, A. P. Vasilkov, T. F. Eck, O. Dubovik, and B. N. Holben (2005), Aerosol ultraviolet absorption experiment (2002 to 2004), part 2: absorption optical thickness, refractive index, and single scattering albedo, *Opt. Eng.*, *44*(4), 041005-041017, doi:10.1117/1.1886819.

Krotkov, N. A., P. K. Bhartia, J. R. Herman, V. Fioletov, and J. Kerr (1998), Satellite estimation of spectral surface UV irradiance in the presence of tropospheric aerosols 1. Cloud-free case, *J. Geophys. Res.*, *103*(D8), 8779-8793, doi:10.1029/98JD00233.

Krotkov, N. A., J. R. Herman, P. K. Bhartia, V. Fioletov, and Z. Ahmad (2001), Satellite estimation of spectral surface UV irradiance 2. Effects of homogeneous clouds and snow, *J. Geophys. Res.*, *106*(D11), 11743-11759, doi:10.1029/2000JD900721.

Krotkov, N. A., J. Herman, P. K. Bhartia, Colin Seftor, A. Arola, J. Kaurola, P. Taalas, and A. Vasilkov (2002b), OMI surface UV irradinace algorithm, in *OMI Algorithm Theoretical Basis Document*, edited by P. Stammes, pp. 72-109.

Krzyscin, J. W., and S. Puchalski (1998), Aerosol impact on the surface UV radiation from the ground-based measurements taken at Belsk, Poland, 1980-1996, *J. Geophys. Res.*, *103*(D13), 16175-16181, doi:10.1029/98JD00899.

Kudish, A. I., and E. Evseev (2000), Statistical relationships between solar UVB and UVA radiation and global radiation measurements at two sites in Israel, *Int. J. Climatol.*, *20*(7), 759-770.

Laan, E., D. de Winter, J. de Vries, P. Levelt, G. H. J. van den Oord, A. Maelkki, Leppelmeier, and E. Hilsenrath (2001), Towards the use of the Ozone Monitoring Instrument (OMI), *Proc SPIE 2001*, 4540.

Latha, K. M., K. V. S. Badarinath, P. K. Gupta, A. B. Ghosh, S. L. Jain, B. S. Gera, R. Singh, A. K. Sarkar, N. Singh, R. S. Parmar, S. Koul, R. Kohli, S. Nath, V. K. Ojha, and G. Singh (2004), Impact of biomass burning aerosols on UV erythema-a case study from northeast region of India, *J. Atmos. Sol.-Terr. Phys.*, *66*(11), 981-986, doi:10.1016/j.jastp.2004.03.005.

Lean, J. L., G. J. Rottman, H. L. Kyle, T. N. Woods, J. R. Hickey, and L. C. Puga (1997), Detection and parameterization of variations in solar mid- and near-ultraviolet radiation (200-400 nm), *J. Geophys. Res.*, *102*(D25), 29939-29956, doi:10.1029/97JD02092.

Levelt, P. F., E. Hilsenrath, G. W. Leppelmeier, G. H. J. van den Oord, P. K. Bhartia, J. Tamminen, J. F. de Haan, and J. P. Veefkind (2006a), Science objectives of the ozone monitoring instrument, *IEEE Trans. Geosci. Remote Sens.*, *44*(5), 1199-1208.

Levelt, P. F., G. H. J. van den Oord, M. R. Dobber, A. Malkki, V. Huib, V. Johan de, P. Stammes, J. O. V. Lundell, and H. Saari (2006b), The ozone monitoring instrument, *IEEE Trans. Geosci. Remote Sens.*, *44*(5), 1093-1101.

Li, Z., P. Wang, and J. Cihlar (2000), A simple and efficient method for retrieving surface UV radiation dose rate from satellite, *J. Geophys. Res.*, *105*(D4), 5027-5036, doi:10.1029/1999JD900124.

Lindfors, A., and L. Vuilleumier (2005), Erythemal UV at Davos (Switzerland), 1926–2003, estimated using total ozone, sunshine duration, and snow depth, *J. Geophys. Res.*, *110*, D02104, doi:10.1029/2004jd005231.

Lindfors, A. V., A. Arola, J. Kaurola, P. Taalas, and T. Svenøe (2003), Long-term erythemal UV doses at Sodankylä estimated using total ozone, sunshine duration, and snow depth, *J. Geophys. Res.*, *108*, 4518, doi:10.1029/2002JD003325.

Liou, K. N. (2002), *An Introduction to Atmospheric Radiation*, 2 ed., 583 pp., Academic press, USA.

Livingston, J. M., J. Redemann, P. B. Russell, O. Torres, B. Veihelmann, P. Veefkind, R. Braak, A. Smirnov, L. Remer, R. W. Bergstrom, O. Coddington, K. S. Schmidt, P. Pilewskie, R. Johnson, and Q. Zhang (2009), Comparison of aerosol optical depths from the Ozone Monitoring Instrument (OMI) on Aura with results from airborne sunphotometry, other space and ground measurements during MILAGRO/INTEX-B, *Atmos. Chem. Phys. Discuss.*, *9*(2), 9961-10013.

Longstreth, J., F. R. de Gruijl, M. L. Kripke, S. Abseck, F. Arnold, H. I. Slaper, G. Velders, Y. Takizawa, and J. C. van der Leun (1998), Health risks, *J. Photochem. Photobiol. B.*, *46*(1-3), 20-39.

MacKie, R. M. (2000), Effects of ultraviolet radiation on human health, *Radiat. Prot. Dosim.*, *91*(1-3), 15-18.

Madronich, S., R. L. McKenzie, L. O. Björn, and M. M. Caldwell (1998), Changes in biologically active ultraviolet radiation reaching the Earth's surface, *J. Photochem. Photobiol. B.*, *46*(1-3), 5-19.

Mayer, B., G. Seckmeyer, and A. Kylling (1997), Systematic long-term comparison of spectral UV measurements and UVSPEC modeling results, *J. Geophys. Res.*, *102*(D7), 8755-8767, do:10.1029/97JD00240.

Mayer, B., and A. Kylling (2005), Technical note: The libRadtran software package for radiative transfer calculations - description and examples of use, *Atmos. Chem. Phys.*, *5*(7), 1855-1877, doi:10.5194/acp-5-1855-2005.

Mayer, B., U. Hamann, C. Emde, and A. Kylling (2007), LibRadtran: library for radiative transfer calculations, Edition 1.0 for libradtran version 1.3, edited.

McElroy, M. B., R. J. Salawitch, S. C. Wofsy, and J. A. Logan (1986), Reductions of Antarctic ozone due to synergistic interactions of chlorine and bromine, *Nature*, *321*(6072), 759-762.

McKenzie, R., B. Connor, and G. Bodeker (1999), Increased summertime UV radiation in New Zealand in response to ozone loss, *Science*, *285*(5434), 1709-1711, 10.1126/science.285.5434.1709.

McKenzie, R. L., G. Seckmeyer, A. F. Bais, J. B. Kerr, and S. Madronich (2001), Satellite retrievals of erythemal UV dose compared with ground-based measurements at northern and southern midlatitudes, *J. Geophys. Res.*, *106*(D20), 24051-24062, doi:10.1029/2001JD000545.

McKenzie, R. L., P. J. Aucamp, A. F. Bais, L. O. Bjorn, and M. Ilyas (2007), Changes in biologically-active ultraviolet radiation reaching the Earth's surface, *Photochem. Photobiol. Sci.*, *6*(3), 218-231.

McKenzie, R. L., C. Weinreis, P. V. Johnston, B. Liley, H. Shiona, M. Kotkamp, D. Smale, N. Takegawa, and Y. Kondo (2008), Effects of urban pollution on UV spectral irradiances, *Atmos. Chem. Phys.*, *8*(18), 5683-5697, doi:10.5194/acp-8-5683-2008.

McKinlay, A. F., and B. L. Diffey (1987), A reference action spectrum for ultraviolet induced erythema in human skin, *CIE J.*, *6*(1), 17-22.

McPeters, R. D., P. K. Bhartia, A. J. Krueger, J. R. Herman, C. G. Wellemeyer, C. J. Seftor, G. Jaross, O. Torres, L. Moy, G. Labow, W. Byerly, S. L. Taylor, T. Swissler, and R. P. Cebula (1998), Earth probe total ozone mapping spectrometer (TOMS): data products user's guide. Documentation., National Aeronautics and Space Administration (NASA), Maryland.

Meerkoetter, R., B. Wissinger, and G. Seckmeyer (1997), Surface UV from ERS-2/GOME and NOAA/AVHRR data: A case study, *Geophys. Res. Lett.*, *24*(15), 1939-1942, doi:10.1029/97GL01885.

Meleti, C., A. F. Bais, S. Kazadzis, N. Kouremeti, K. Garane, and C. Zerefos (2009), Factors affecting solar ultraviolet irradiance measured since 1990 at Thessaloniki, Greece, *Int. J. Remote Sens.*, *30*(15), 4167 - 4179.

Meloni, D., A. di Sarra, J. R. Herman, F. Monteleone, and S. Piacentino (2005), Comparison of ground-based and Total Ozone Mapping Spectrometer erythemal UV doses at the island of Lampedusa in the period 1998-2003: Role of tropospheric aerosols, *J. Geophys. Res.*, *110*, D01202, doi:10.1029/2004JD005283.

Met Office (2007), National meteorological library and archive, Fact sheet no. 16: World climates, edited.

Morys, M., and D. Berger (1993), The accurate measurements of biologically effective, paper presented at International Symposium on High Latitude Optics, Tromsö, Norway, July, 1993.

NCAR (National Center for Atmospheric Research) (2006), Tropospheric Ultraviolet and Visible (TUV) radiation model, accessed on 6 November 2006.

Németh, P., Z. Tóth, and Z. Nagy (1996), Effect of weather conditions on UV-B radiation reaching the earth's surface, *J. Photochem. Photobiol. B., 32*(3), 177-181.

Newman, P. A., S. R. Kawa, and E. R. Nash (2004), On the size of the Antarctic ozone hole, *Geophys. Res. Lett., 31*(21), L21104, doi:10.1029/2004GL020596.

Newman, P. A., E. R. Nash, S. R. Kawa, S. A. Montzka, and S. M. Schauffler (2006), When will the Antarctic ozone hole recover?, *Geophys. Res. Lett., 33*(12), L12814, doi:10.1029/2005GL025232.

Norval, M. (2000), The Impact of Ultraviolet Radiation on Immune Responses, *Radiat. Prot. Dosim., 91*(1-3), 51-56.

Norval, M., A. P. Cullen, F. R. de Gruijl, J. Longstreth, Y. Takizawa, R. M. Lucas, F. P. Noonan, and J. C. van der Leun (2007), The effects on human health from stratospheric ozone depletion and its interactions with climate change, *Photochem. Photobiol. Sci., 6*, 232.

NRPB (2002), Health effects from ultraviolet radiation: Report of an advisory group on non-ionising radiation. Doc. NRPB, *13*(1).

Office for National Statistics (2003), Social Trends No. 33, Summerfield C, Editor.2003, Office for National Statistics: London.

OMI Team (2009), Ozone Monitoring Instrument (OMI) Data User's Guide, edited, pp. 1-60.

Parisi, A. V., and M. G. Kimlin (2004), Personal solar UV exposure measurements employing modified polysulphone with an extended dynamic range, *Photochem. Photobiol., 79*(5), 411-415, doi:10.1111/j.1751-1097.2004.tb00028.x.

Pearson, A. J., S. F. Dean, I. E. S. Clark, J. I. Campbell, K. J. Grainger, and C. M. H. Driscoll (2000), NRPB Solar ultraviolet radiation measurement network, *Radiat. Prot. Dosim., 91*(1-3), 169-172.

Pearson, A. J., C. Driscoll, N. Hunter, J. I. Campbell, S. F. Dean, and I. E. Clark (2004), Solar Radiation Measurements at a Network of Seven Sites in the UK, January - December 2003, NRPB-W61.

Pearson, A. J., N. Hunter, J. I. Campbell, and S. F. Dean (2006), Solar radiation measurements in the UK during 2004 and 2005, HPA-RPD-018-HPA.

Pfeifer, M. T., P. Koepke, and J. Reuder (2006), Effects of altitude and aerosol on UV radiation, *J. Geophys. Res., 111*, D01203, doi:10.1029/2005JD006444.

Piacentini, R. D., A. Cede, and H. Bárcena (2003), Extreme solar total and UV irradiances due to cloud effect measured near the summer solstice at the high-altitude desertic plateau Puna of Atacama (Argentina), *J. Atmos. Sol.-Terr. Phys., 65*(6), 727-731, doi:10.1016/S1364-6826(03)00084-1.

Pyle, J. A. (2000), Stratospheric ozone depletion: A discussion of our present understanding, in *Cause and environmental implications of increased UV-B radiation*, edited by R. E. Herter and R. M. Harrison, pp. 1-16, Cambridge: Royal Society Chemistry.

Renaud, A., J. Staehelin, C. Fröhlich, R. Philipona, and A. Heimo (2000), Influence of snow and clouds on erythemal UV radiation: Analysis of Swiss measurements and comparison with models, *J. Geophys. Res., 105*(D4), 4961-4969, doi:10.1029/1999JD900160.

Rettberg, P., R. Sief, and G. Horneck (1999), The DLR-biofilm as personal UV dosimeter, in *Fundamentals for the Assessment of Risks from Environmental Radiation*, edited by C. Baumstark-Khan, et al., pp. 367-370, NATO Science.

Rettberg, P., and C. S. Cockell (2004), Biological UV dosimetry using the DLR-biofilm, *Photochem. Photobiol. Sci., 3*(8), 781-787.

Reuder, J., F. Ghezzi, E. Palenque, R. Torrez, M. Andrade, and F. Zaratti (2007), Investigations on the effect of high surface albedo on erythemally effective UV irradiance: Results of a campaign at the Salar de Uyuni, Bolivia, *J. Photochem. Photobiol. B., 87*(1), 1-8, doi:10.1016/j.jphotobiol.2006.12.002.

Ruggaber, A., R. Dlugi, and T. Nakajima (1994), Modelling radiation quantities and photolysis frequencies in the troposphere, *J. Atmos. Chem., 18*(2), 171-210, doi:10.1007/BF00696813.

Sabburg, J., J. E. Rives, R. S. Meltzer, T. Taylor, G. Schmalzle, S. Zheng, N. Huang, A. Wilson, and P. M. Udelhofen (2002), Comparisons of corrected daily integrated erythemal UVR data from the U.S. EPA/UGA network of Brewer spectroradiometers with model and TOMS-inferred data, *J. Geophys. Res., 107*(4676), doi:10.1029/2001JD001565.

Salby, M. L. (1996), *Fundamentals of Atmospheric Physics*, 627 pp., Academic Press, Inc.

Sasaki, M., S. Takeshita, T. Oyanagi, Y. Miyake, and T. Sakata (2002), Increasing trend of biologically active solar ultraviolet-B irradiance in mid-latitude Japan in the 1990s, *Opt. Eng., 41*(12), 3062-3069.

Schmucki, D. A., and R. Philipona (2002), Ultraviolet radiation in the Alps: the altitude effect, *Opt. Eng., 41*(12), 3090-3095.

Sci-Tec (1995), Brewer MKIV spectrophotometer operator's manual, OM-BA-C01/B Rev J, SCI-TEC Instruments Inc.

Sci-Tec (1996), Brewer spectrophotometer technical papers: section 1 An introduction to the Brewer MKII, MKIII, and MKIV, Courtesy SCI-TEC Instruments Inc.

Sci-Tec (1999), Brewer MKIII spectrophotometer (double spectrometer) operator's manual, OM-BA-C231 Rev B, SCI-TEC Instruments Inc.

Seckmeyer, G., R. Erb, and A. Albold (1996), Transmittance of a cloud is wavelength-dependent in the UV-range, *Geophys. Res. Lett., 23*(20), 2753-2755, doi:10.1029/96GL02614.

Seckmeyer, G., B. Mayer, G. Bernhard, R. Erb, A. Albold, H. Jäger, and W. R. Stockwell (1997), New maximum UV irradiance levels observed in Central Europe, *Atmos. Environ., 31*(18), 2971-2976.

Seckmeyer, G., P. Darius, G. Merle, H. Diamantino, J. Bjorn, W. Ann, S. Anna-Maria, B. Alkis, K. Berit, B. Colette, L. Jacqueline, G. Brian, K. Peter, K. Tapani, K. Jussi, U. Beate, S. Harry, O. Peter den, J. Michal, W. Peter, G. Julian, M. Bernhard, C. Alain de la, S. Stana, and C. Fernanda (2008), Variability of UV irradiance in Europe, *Photochem. Photobiol.*, *84*(1), 172-179.

Seinfeld, J. H., and S. N. Pandis (2006), *Atmospheric chemistry and physics: From air pollution to climate change*, John Wiley & Sons, Inc, Hoboken, New Jersey, Canada.

Shettle, E. P. (1989), Models of aerosols, clouds and precipitation for atmospheric propagation studies, in atmospheric propagation in the UV, visible, IR and mm-wave region and related systems aspects, *AGARD Conf. Proc.*, pp. 15-11 - 15-13.

Siani, A. M., G. R. Casale, and A. Galliani (2002), Investigation on a low ozone episode at the end of November 2000 and its effect on ultraviolet radiation, *Opt. Eng.*, *41*(12), 3082-3089.

Siani, A. M. (2007), Contribution from university of Rome “La Sapienza” (URO), in OMI AO progress report no.4, 75-79 pp.

Siani, A. M., G. R. Casale, H. DiÃ©moz, G. Agnesod, M. G. Kimlin, C. A. Lang, and A. Colosimo (2008), Personal UV exposure in high albedo alpine sites, *Atmos. Chem. Phys.*, *8*(14), 3749-3760, 10.5194/acp-8-3749-2008.

Sinnhuber, B. M., M. P. Chipperfield, S. Davies, J. P. Burrows, K. U. Eichmann, M. Weber, P. von der Gathen, M. Guirlet, G. A. Cahill, A. M. Lee, and J. A. Pyle (2000), Large loss of total ozone during the Arctic winter of 1999/2000, *Geophys. Res. Lett.*, *27*(21), 3473-3476, doi:10.1029/2000GL011772.

Slaper, H., H. A. J. M. Reinen, M. Blumthaler, M. Huber, and F. Kuik (1995), Comparing ground-level spectrally resolved solar UV measurements using various instruments: A technique resolving effects of wavelength shift and slit width, *Geophys. Res. Lett.*, *22*(20), 2721-2724, doi:10.1029/95GL02824.

Stevenson, D., R. Doherty, M. Sanderson, C. Johnson, B. Collins, and D. Derwent (2005), Impacts of climate change and variability on tropospheric ozone and its precursors, *Faraday Discussions*, *130*, 41-57.

Stoecker, W. F. (1971), *Design of Thermal Systems*, 244 pp., McGraw-Hill Companies, New York.

Stolarski, R., R. Bojkov, L. Bishop, C. Zerefos, J. Staehelin, and J. Zawodny (1992), Measured Trends in Stratospheric Ozone, *Science*, *256*(5055), 342-349.

Sudhibrabha, S., R. H. B. Exell, and D. Sukawat (2004), Ultraviolet forecasting in Thailand, *A Thesis Report of the Joint Graduate School of Energy and Environment at King Monghut's University of Technology Thonburl 2nd Semester 2003*.

Tanskanen, A., A. Arola, and J. Kujanpaa (2003), Use of the moving time-window technique to determine surface albedo from TOMS reflectivity data, paper presented at Ultraviolet ground- and space-based measurements, models, and effects II, SPIE4896, Hangzhou, China.

Tanskanen, A. (2004), Lambertian surface albedo climatology at 360 nm from TOMS data using moving time-window technique. In: Proceedings of the XX quadrennial ozone symposium, 1-8 June 2004, Kos, Greece.

Tanskanen, A., N. A. Krotkov, J. R. Herman, and A. Arola (2006), Surface ultraviolet irradiance from OMI, *IEEE Trans. Geosci. Remote Sens.*, *44*(5), 1267-1271.

Tanskanen, A., A. Lindfors, A. Määttä, N. Krotkov, J. Herman, J. Kaurola, T. Koskela, K. Lakkala, V. Fioletov, G. Bernhard, R. McKenzie, Y. Kondo, M. O'Neill, H. Slaper, P. den Outer, A. F. Bais, and J. Tamminen (2007), Validation of daily erythemal doses from Ozone Monitoring Instrument with ground-based UV measurement data, *J. Geophys. Res.*, *112*, D24S44, doi:10.1029/2007JD008830.

Tanskanen, A. (2008), Modelling of surface UV radiation using satellite data, 109 pp, Finnish Meteorological Institute, Helsinki, Finland.

Taylor, H. R. (1980), The environment and the lens, *Brit. J. Ophthalmol.*, *64*(5), 303-310, 10.1136/bjo.64.5.303.

Taylor, H. R., S. K. West, F. S. Rosenthal, B. Muñoz, H. Newland, H. Abbey, and E. A. Emmett (1988), Effect of ultraviolet radiation on cataract formation, *N. Engl. J. Med.*, *319*, 1429-1433.

Threlfall, T. J., and D. R. English (1999), Sun exposure and pterygium of the eye: a dose-response curve, *Am. J. Ophthalmol.*, *128*(3), 280-287.

Torres, O., P. K. Bhartia, J. R. Herman, Z. Ahmad, and J. Gleason (1998), Derivation of aerosol properties from satellite measurements of backscattered ultraviolet radiation: Theoretical basis, *J. Geophys. Res.*, *103*(D14), 17099-17110, doi:10.1029/98JD00900.

Torres, O., P. K. Bhartia, J. R. Herman, A. Sinyuk, P. Ginoux, and B. Holben (2002a), A long-term record of aerosol optical depth from TOMS observations and comparison to AERONET measurements, *J. Atmos. Sci.*, *59*(3), 398-413.

Torres, O., R. Decae, J. P. veefkind, and G. de leeuw (2002b), OMI Aerosol Retrieval Algorithm, in *OMI Algorithm Theoretical Basis Document: Clouds, Aerosols, and Surface UV Irradiance*, edited by P. Stammes, NASA Goddard Space Flight Cent., Greenbelt, Md. (Available at http://eospso.gsfc.nasa.gov/eos_homepage/for_scientist/atbd/docs/OMI/ATBD-OMI-03.pdf).

Torres, O., A. Tanskanen, B. Veihelmann, C. Ahn, R. Braak, P. K. Bhartia, P. Veefkind, and P. Levelt (2007), Aerosols and surface UV products from Ozone Monitoring Instrument observations: An overview, *J. Geophys. Res.*, *112*, D24S47, doi:10.1029/2007JD008809.

Trepte, S., and P. Winkler (2004), Reconstruction of erythemal UV irradiance and dose at Hohenpeissenberg (1968–2001) considering trends of total ozone, cloudiness and turbidity, *Theor. Appl. Climatol.*, *77*(3), 159-171.

Ullrich, S. E. (2005), Mechanisms underlying UV-induced immune suppression, *Mutation Research/Fundamental and Molecular Mechanisms of Mutagenesis*, *571*(1-2), 185-205.

UNEP (2006), Environmental effects of ozone depletion and its interactions with climate change: 2006 Assessment, United Nations Environment Program.

UNEP (2007), Environmental effects of ozone depletion and its interactions with climate change, 2006 assessment, *Photochem. Photobio. Sci.*, *6*(3), 201-332.

van Weele, M., T. J. Martin, M. Blumthaler, C. Brogniez, P. N. d. Outer, O. Engelsen, J. Lenoble, B. Mayer, G. Pfister, A. Ruggaber, B. Walravens, P. Weihs, B. G. Gardiner, D. Gillotay, D. Haferl, A. Kylling, G. Seckmeyer, and W. M. F. Wauben (2000), From model intercomparison toward benchmark UV spectra for six real atmospheric cases, *J. Geophys. Res.*, *105*(D4), 4915-4925, doi:10.1029/1999JD901103.

Vardavas, I. M., and F. W. Taylor (2007), *International series of monographs on physics in Radiation and Climate*, Oxford University Press, Oxford.

Vaughan, G., and J. D. Price (1991), On the relation between total ozone and meteorology, *Q. J. Roy. Meteor. Soc.*, *117*(502), 1281-1298.

Veefkind, J. P., J. F. de Haan, E. J. Brinksma, M. Kroon, and P. F. Levelt (2006), Total ozone from the ozone monitoring instrument (OMI) using the DOAS technique, *IEEE Trans. Geosci. Remote Sens.*, *44*(5), 1239-1244.

Veierod, M. B., E. Weiderpass, M. Thorn, J. Hansson, E. Lund, B. Armstrong, and H.-O. Adami (2003), A prospective study of pigmentation, sun exposure, and risk of cutaneous malignant melanoma in women, *J. Natl. Cancer Inst.*, *95*(20), 1530-1538, doi:10.1093/jnci/djg075.

Verdebout, J. (2000), A method to generate surface UV radiation maps over Europe using GOME, Meteosat, and ancillary geophysical data, *J. Geophys. Res.*, *105*(D4), 5049-5058, doi:10.1029/1999JD900302.

Wang, P., and J. Lenoble (1994), Comparison between measurements and modeling of UV-B irradiance for clear sky: a case study, *Appl. Opt.*, *33*(18), 3964-3971.

Wang, P., Z. Li, J. Cihlar, D. I. Wardle, and J. Kerr (2000), Validation of an UV inversion algorithm using satellite and surface measurements, *J. Geophys. Res.*, *105*(D4), 5037-5048, doi:10.1029/1999JD900403.

Webb, A. (1998), *UVB instrumentations and applications*, 103 pp., Gordon and Breach Science Publishers, Amsterdam, NE.

Webb, A., J. Gröbner, and M. Blumthaler (2006), A practical guide to operating broadband instruments measuring erythemally weighted irradiance, 21 pp, WMO SAG UV and Working Group 4 of COST-726 Action "Long Term Changes and Climatology of UV Radiation over Europe".

Webb, A. R. (1995), Measuring UV radiation: a discussion of dosimeter properties, uses and limitations, *J. Photochem. Photobiol. B.*, *31*(1-2), 9-13.

Webb, A. R. (1997), Advances in solar ultraviolet spectroradiometry in EC air pollution report 63, 238 pp, Office for Official Publication of the European Commission.

Webb, A. R., B. G. Gardiner, T. J. Martin, K. Leszcynski, J. Metxdorf, and V. A. Mohnen (1998), Guidelines for site quality control of UV monitoring. WMO/GAW No.126. World Meteorological Organisation, Geneva, pp.39.

Webb, A. R., P. Weihs, and M. Blumthaler (1999), Spectral UV irradiance on vertical surfaces: A case study, *Photochem. Photobiol.*, *69*(4), 464-470.

Webb, A. R. (2000a), Standardisation of data from ultraviolet radiation detectors, *Radiat. Prot. Dosim.*, *91*(1-3), 123-128.

Webb, A. R. (2000b), Ozone depletion and changes in environmental UV-B radiation, in *Cause and environmental implications of increased UV-B radiation*, edited by R. E. Herter and R. M. Harrison, pp. 17-36, Cambridge: Royal Society Chemistry, Cambridge.

Webb, A. R. (2003), UV instrumentation for field and forest research, *Agricultural and Forest Meteor.*, *120*(1-4), 27-38.

Weihs, P., and S. Simic (2006), Validation of OMI UV products: first results of comparisons with an Austrian ground station, SPIE.

Weihs, P., M. Blumthaler, H. E. Rieder, A. Kreuter, S. Simic, W. Laube, A. W. Schmalwieser, J. E. Wagner, and A. Tanskanen (2008), Measurements of UV irradiance within the area of one satellite pixel, *Atmos. Chem. Phys.*, *8*(18), 5615-5626, doi:10.5194/acp-8-5615-2008.

Wenny, B. N., V. K. Saxena, and J. E. Frederick (2001), Aerosol optical depth measurements and their impact on surface levels of ultraviolet-B radiation, *J. Geophys. Res.*, *106*(D15), 17311-17319, doi:10.1029/2001JD900185.

West, S. K., J. D. Longstreth, B. E. Munoz, H. M. Pitcher, and D. D. Duncan (2005), Model of Risk of Cortical Cataract in the US Population with Exposure to Increased Ultraviolet Radiation due to Stratospheric Ozone Depletion, *Am. J. Epidemiol.*, *162*(11), 1080-1088, 10.1093/aje/kwi329.

WHO (1992), IARC monographs on the evalution of carcinogenic risks to humans.

WHO (2002), Global UV index: A practical guide., World Health Organization: Geneva, Switzerland; WHO/SDE/OEH/O2.2.

WMO (2001), Instruments to measure solar ultraviolet radiation, Part 1: Spectral instruments, *World Meteorological Organisation, Global Atmospheric Watch Report No. 125 (lead author G. Seckmeyer), TD No. 1066*.

WMO (2003), Scientific assessment of ozone depletion: 2002, Global Ozone Research and Monitoring Project - Report No. 47 498 pp, Geneva, Switzerland.

WMO (2007), Scientific assessment of ozone depletion: 2006, Global ozone research and monitoring project - Report No.50 572 pp, World Meteorological Organization, Geneva, Switzerland.

WMO (2008), The ninth biennial WMO consultation on Brewer ozone and UV spectrophotometer operation, Calibration and data reporting 69 pp, Delft, The Netherlands, 31 May - 3 June 2005

Wuttke, S., J. Verdebout, and G. Seckmeyer (2003), An improved algorithm for satellite-derived UV radiation, *Photochem. Photobiol.*, *77*(1), 52-57.

Zeng, G., and J. A. Pyle (2003), Changes in tropospheric ozone between 2000 and 2100 modeled in a chemistry-climate model, *Geophys. Res. Lett.*, *30*(7), 1392, doi:10.1029/2002GL016708.

Zeng, J., R. McKenzie, K. Stamnes, M. Wineland, and J. Rosen (1994), Measured UV spectra compared with discrete ordinate method simulations, *J. Geophys. Res.*, *99*(D11), 23019-23030, doi:10.1029/94JD02145.

Zerefos, C. S., C. Meleti, D. S. Balis, A. F. Bais, and D. Gillotay (2000), On changes of spectral UV-B in the 90's in Europe, *Adv. Space Res.*, *26*(12), 1971-1978, doi:10.1016/S0273-1177(00)00167-8.

Zerefos, C. S. (2002), Long-term ozone and UV variations at Thessaloniki, Greece, *Phys. Chem. Earth*, *27*(6-8), 455-460, doi:10.1016/S1474-7065(02)00026-8.